frontiers | Research Topics

Exploring frontiers: astroparticle, space science and public health for future crewed space missions

Edited by
Alessandro Bartoloni, Nan Ding, Gianluca Cavoto, Cristina Consolandi, Lidia Strigari, F. R. Tang and Christopher D. Porada

Published in
Frontiers in Physiology
Frontiers in Astronomy and Space Sciences
Frontiers in Immunology
Frontiers in Physics
Frontiers in Public Health

ISSN 1664-8714
ISBN 978-2-8325-6482-0
DOI 10.3389/978-2-8325-6482-0

Generative AI statement
Any alternative text (Alt text) provided alongside figures in the articles in this ebook has been generated by Frontiers with the support of artificial intelligence and reasonable efforts have been made to ensure accuracy, including review by the authors wherever possible. If you identify any issues, please contact us.

About Frontiers

Frontiers is more than just an open access publisher of scholarly articles: it is a pioneering approach to the world of academia, radically improving the way scholarly research is managed. The grand vision of Frontiers is a world where all people have an equal opportunity to seek, share and generate knowledge. Frontiers provides immediate and permanent online open access to all its publications, but this alone is not enough to realize our grand goals.

Frontiers journal series

The Frontiers journal series is a multi-tier and interdisciplinary set of open-access, online journals, promising a paradigm shift from the current review, selection and dissemination processes in academic publishing. All Frontiers journals are driven by researchers for researchers; therefore, they constitute a service to the scholarly community. At the same time, the *Frontiers journal series* operates on a revolutionary invention, the tiered publishing system, initially addressing specific communities of scholars, and gradually climbing up to broader public understanding, thus serving the interests of the lay society, too.

Dedication to quality

Each Frontiers article is a landmark of the highest quality, thanks to genuinely collaborative interactions between authors and review editors, who include some of the world's best academicians. Research must be certified by peers before entering a stream of knowledge that may eventually reach the public - and shape society; therefore, Frontiers only applies the most rigorous and unbiased reviews. Frontiers revolutionizes research publishing by freely delivering the most outstanding research, evaluated with no bias from both the academic and social point of view. By applying the most advanced information technologies, Frontiers is catapulting scholarly publishing into a new generation.

What are Frontiers Research Topics?

Frontiers Research Topics are very popular trademarks of the *Frontiers journals series*: they are collections of at least ten articles, all centered on a particular subject. With their unique mix of varied contributions from Original Research to Review Articles, Frontiers Research Topics unify the most influential researchers, the latest key findings and historical advances in a hot research area.

Find out more on how to host your own Frontiers Research Topic or contribute to one as an author by contacting the Frontiers editorial office: frontiersin.org/about/contact

Exploring frontiers: astroparticle, space science and public health for future crewed space missions

Topic editors

Alessandro Bartoloni — National Institute of Nuclear Physics of Rome, Italy
Nan Ding — Institute of Modern Physics, Chinese Academy of Sciences (CAS), China
Gianluca Cavoto — Sapienza University of Rome, Italy
Cristina Consolandi — University of Hawaii at Manoa, United States
Lidia Strigari — IRCCS Azienda Ospedaliero-Universitaria di Bologna, Italy
F. R. Tang — National University of Singapore, Singapore
Christopher D. Porada — Wake Forest University, United States

Citation

Bartoloni, A., Ding, N., Cavoto, G., Consolandi, C., Strigari, L., Tang, F. R., Porada, C. D., eds. (2025). *Exploring frontiers: astroparticle, space science and public health for future crewed space missions*. Lausanne: Frontiers Media SA. doi: 10.3389/978-2-8325-6482-0

Table of contents

frontiers | Frontiers in Astronomy and Space Sciences

TYPE Editorial
PUBLISHED 06 June 2025
DOI 10.3389/fspas.2025.1634483

OPEN ACCESS

EDITED AND REVIEWED BY
Alberto Fairén,
CSIC-INTA, Spain

*CORRESPONDENCE
Alessandro Bartoloni,
alessandro.bartoloni@roma1.infn.it

RECEIVED 24 May 2025
ACCEPTED 26 May 2025
PUBLISHED 06 June 2025

CITATION
Bartoloni A, Cavoto G, Consolandi C, Ding N, Porada CD, Tang FR and Strigari L (2025) Editorial: Exploring frontiers: astroparticle, space science and public health for future crewed space missions.
Front. Astron. Space Sci. 12:1634483.
doi: 10.3389/fspas.2025.1634483

Editorial: Exploring frontiers: astroparticle, space science and public health for future crewed space missions

Alessandro Bartoloni[1]*, Gianluca Cavoto[2], Cristina Consolandi[3], Nan Ding[4], Christopher D. Porada[5], Feng Ru Tang[6] and Lidia Strigari[7]

[1]Roma Division, Istituto Italiano di Fisica Nucleare, Roma, Italy, [2]Physics Department, Università degli Studi di Roma La Sapienza, Roma, Italy, [3]Department of Physics and Astronomy, University of Hawaii at Manoa, Honolulu, HI, United States, [4]Institute of Modern Physics, Chinese Academy of Sciences, Lanzhou, China, [5]School of Medicine, Wake Forest University, Winston-Salem, NC, United States, [6]Singapore Nuclear Research and Safety Institute, Singapore, Singapore, [7]Department of Medical Physics, IRCCS Azienda Ospedaliero-Universitaria di Bologna, Bologna, Italy

KEYWORDS

human space exploration, space medicine, space radiobiology, space radiation, Deep space missions, space physiology, interdiscplinary research, space biomedicine

Editorial on the Research Topic
Exploring frontiers: astroparticle, space science and public health for future crewed space missions

Introduction

As humanity sets its sights on long-duration space travels and permanent outposts on the Moon and Mars to start a life beyond Earth, understanding the radiation-induced effects and underlying mechanisms has never been more critical. The Research Topic *Exploring frontiers: astroparticle, space science and public health for future crewed space missions* brings together pioneering studies that span various disciplines—from radiation biology and toxicology to neurophysiology and mental health. Collectively, these contributions aim to highlight the multifaceted risks of spaceflight and inform countermeasures to protect human health during future crewed missions.

Astronauts are exposed to complex and variable particle radiation in space, while microgravity-induced deconditioning, altered immune responses, and psychological stressors challenge human adaptability. This Research Topic of ten peer-reviewed articles reflects the growing synergy between space science, astroparticle physics, and public health in confronting these challenges with innovative methodologies and translational insights.

Radiation exposure and biological consequences

Radiation remains one of the most significant health threats in space. Several articles in this collection tackle its acute and chronic effects from biological and engineering

perspectives. Cai et al. investigate how the gut microbiome could serve as a predictive biomarker for radiation-induced intestinal injury. It identifies Erysipelatoclostridium and its metabolite ptilosteroid A as potential indicators of intestinal damage. Leung et al. explore the late effects of heavy-ion radiation on immune cell function, specifically splenocyte subpopulations and NK cell cytotoxicity, providing insight into the long-term immunological risks astronauts may face.

In a translational leap, Daiz et al. also assessed the protective effects of curcumin-loaded nanolipoprotein particles (cNLPs) against acute gastrointestinal injury induced by radiation doses equivalent to those of a Mars mission. This study presents a potential countermeasure and highlights the importance of nanotechnology in the field of space radiation medicine.

On a molecular level, Raber et al. present an experimental analysis of the effects of 5-Ion (simplified GCR simulator) beam irradiation, both with and without hindlimb unloading, examining behavioral and metabolic shifts in a rodent model. This reinforces how mechanical unloading can exacerbate the systemic effects of radiation.

Countermeasures and physiological protection

Countermeasures are essential to mitigate the detrimental effects of prolonged microgravity. Arbeille et al. in this collection presents compelling data showing that exercise with artificial gravity, as well as exercise alone, can prevent morphological changes in organs and blood vessels during simulated microgravity (55 days of head-down tilt bed rest). These findings highlight the importance of integrated exercise protocols in maintaining astronaut health during extended missions.

Microgravity also has far-reaching effects on hormonal systems. Cutigni et al., in a narrative review on this topic, discuss how microgravity impairs endocrine signaling and reproductive health in women, emphasizing the need for sex-specific research and countermeasure development to ensure the health of all crew members on future missions.

Lunar dust and environmental toxicology

With renewed interest in lunar exploration, the environmental hazards of the Moon's surface are receiving renewed attention. Crucian et al. characterize pulmonary and systemic immune alterations in rats exposed to airborne lunar dust, while Colorado et al. assess the immunogenicity and allergenicity of lunar dust particles. These findings raise crucial safety considerations for astronauts engaging in extravehicular activities and long-term lunar habitation.

Measurement, modeling, and simulation

Understanding the radiation environment is foundational for mission planning. A key contribution in this area is a study presented by Chicco et al., which uses Bonner sphere spectrometry to measure high-energy neutron spectra from 1 GeV/u 56Fe ion beams and compares the results with Monte Carlo simulations. This work provides critical validation data for radiation transport models and shielding design.

Mental health and evolutionary medicine

Beyond the physiological aspects, the psychological dimensions of space travel demand equal attention. A novel article by Saniotis et al. in this collection advocates for an evolutionary medicine approach to mental health, arguing that the stressors of long-duration missions may evoke mismatches between our evolved biology and the artificial conditions of space. By addressing these mismatches, this work opens new avenues for mitigating psychological risks in space environments.

The role of interdisciplinary research in space exploration-related topics

Addressing the complexities of human spaceflight demands a deeply interdisciplinary research approach. The unique and multifaceted challenges presented by space environments—such as radiation, microgravity, confinement, and isolation—cannot be fully understood or mitigated within the boundaries of a single discipline. A systems-level perspective is essential, one that integrates knowledge from physics, chemistry, biology, medicine, engineering, and behavioral sciences.

For instance, understanding the effects of cosmic radiation involves astroparticle physics and radiation biology, as well as toxicology, microbiome research, and materials science for shielding solutions. Similarly, counteracting microgravity-induced deconditioning requires insights from physiology, biomechanics, exercise science, and even aerospace engineering to design effective countermeasures. Moreover, the psychological and social challenges of long-duration missions highlight the need for contributions from neuroscience, psychiatry, and human factors research. We can only anticipate interactions between physiological systems and environmental stressors by fostering active collaboration across these domains, developing robust predictive models, and creating effective interventions. As space missions extend in duration and distance, particularly toward the Moon, Mars, and beyond, the integration of disciplines becomes advantageous and imperative.

Exploring Frontiers: Astroparticle, Space Science and Public Health for Future Crewed Space Missions

Strategic Domains	Focus Area	Key Research Threads
Radiation Effects	Heavy-Ion Radiation	Immune system modulation (splenocytes, NK function)
		Gut microbiome response (Erysipelatoclostridium, ptilosteroid A)
	SEP/GCR Radiation Exposure	Acute gastrointestinal injury
		Nanoparticle countermeasures (curcumin-loaded cNLPs)
	Ion Beam Exposure & Combined Stressors	Behavioral and metabolic alterations
		Hindlimb unloading as a compounding factor
Mental Health & Evolutionary Medicine	Psychological Stressors	Isolation, confinement, sensory monotony
		Evolutionary Mismatch
		Maladaptation to space environments
		Bioastronautics-informed approaches to resielence
	Endocrine & Reproductive Health	Hormonal disruption in microgravity
		Reproductive implications for women astronauts
Countermeasures & Physiology	Artificial Gravity & Exercise	Protection against vascular and organ morphological changes
		Mitigation of microgravity-induced deconditioning
	Endocrine & Reproductive Health	Hormonal disruption in microgravity
		Reproductive implications for women astronauts
Lunar & Environmental Hazards	Lunar Dust Exposure	Pulmonary and systemic immune effects
		Immunogenicity and allergenicity of regolith particles
Measurement & Simulation	Neutron Spectrometry	High-energy particle measurement
		Monte Carlo modeling validation
		Radiation environment characterization

FIGURE 1
Strategic Domains and Key Research Threads in the Research Topic Collection. This figure presents a structured, table-like representation of a conceptual mind map, outlining the main strategic domains and associated research threads addressed in the collection. It highlights the high degree of interdisciplinarity inherent in this field. It serves as both a synthesis of current research directions and a practical reference for stakeholders, including space agencies, research institutions, academia, and industry, who are committed to advancing knowledge for safe human deep space exploration and long-term habitation.

This Research Topic exemplifies how such integration leads to novel insights and tangible solutions, from nanotherapeutics and exercise protocols to evolutionary perspectives on mental health. Expanding interdisciplinary research activities is crucial for accelerating discovery, translating findings into practice, and safeguarding human health in space. Continued investment in cross-disciplinary platforms and collaborative frameworks will empower the scientific community to overcome existing knowledge gaps and prepare for space exploration's profound physiological and psychological demands. In doing so, we advance space science and catalyze innovations with applications on Earth, reinforcing the mutual benefits of research that transcends traditional boundaries. The diversity of scientific contributions in this Research Topic reflects the increasing convergence of multiple disciplines toward a unified understanding of the challenges associated with human spaceflight. As illustrated in Figure 1, the Research Topic's conceptual framework, presented as a mind map in a table-like format, summarizes the strategic domains and key research threads addressed across the collection. This structure not only demonstrates the wide-ranging interdisciplinary nature of the field but also serves as a practical guide for stakeholders aiming to support safe and sustainable human exploration beyond Earth.

Conclusion

Together, the articles in this Research Topic exhibit how multidisciplinary collaboration can help address one of the most significant challenges in human exploration. From microbial biomarkers and nanotherapeutics to lunar toxicology and psychological resilience, these studies collectively push the frontiers of knowledge required for the next giant leap.

This Research Topic grounds public health within the framework of astroparticle physics and space science, informing the design of

safer, more effective crewed missions. It enriches our understanding of human biology under extreme conditions. We hope this Research Topic serves as a springboard for future studies and stimulates continued cross-disciplinary dialogue as we prepare for a multi-planetary future.

Author contributions

AB: Writing – review and editing, Writing – original draft. GC: Writing – review and editing. CC: Writing – review and editing. ND: Writing – review and editing. CP: Writing – review and editing. FT: Writing – review and editing. LS: Writing – review and editing, Writing – original draft.

Funding

The author(s) declare that no financial support was received for the research and/or publication of this article.

Conflict of interest

The authors declare that the research was conducted in the absence of any commercial or financial relationships that could be construed as a potential conflict of interest.

Generative AI statement

The author(s) declare that no Generative AI was used in the creation of this manuscript.

Publisher's note

frontiers in Public Health

ORIGINAL RESEARCH
published: 28 March 2022
doi: 10.3389/fpubh.2022.862598

Gut Bacteria *Erysipelatoclostridium* and Its Related Metabolite Ptilosteroid A Could Predict Radiation-Induced Intestinal Injury

Shang Cai[1,2,3†], *Yongqiang Yang*[1,2,3†], *Yuehong Kong*[1,2,3†], *Qi Guo*[1,2,3], *Yingying Xu*[1,2,3], *Pengfei Xing*[1,2,3], *Yanze Sun*[1,2,3], *Jianjun Qian*[1,2,3], *Ruizhe Xu*[1,2,3], *Liwei Xie*[1,2,3], *Yijia Hu*[1,2,3], *Min Wang*[4], *Ming Li*[5], *Ye Tian*[1,2,3*] *and Weidong Mao*[1,2,3*]

[1] *Department of Radiotherapy and Oncology, The Second Affiliated Hospital of Soochow University, Suzhou, China,* [2] *Institute of Radiotherapy and Oncology, Soochow University, Suzhou, China,* [3] *Suzhou Key Laboratory for Radiation Oncology, Suzhou, China,* [4] *Department of Clinical Laboratory, The Second Affiliated Hospital of Soochow University, Suzhou, China,* [5] *State Key Laboratory of Radiation Medicine and Protection, School of Radiation Medicine and Protection, Medical College of Soochow University, Collaborative Innovation Center of Radiation Medicine of Jiangsu Higher Education Institutions, Soochow University, Suzhou, China*

OPEN ACCESS

Edited by:
Nan Ding,
Institute of Modern Physics (CAS), China

Reviewed by:
Wei Zhang,
Cleveland Clinic, United States
Wenling Ye,
Henan University, China

***Correspondence:**
Ye Tian
dryetian@126.com
Weidong Mao
mwdsz@sohu.com

[†]*These authors have contributed equally to this work*

Specialty section:
This article was submitted to Radiation and Health, a section of the journal Frontiers in Public Health

Received: *26 January 2022*
Accepted: *28 February 2022*
Published: *28 March 2022*

Citation:
Cai S, Yang Y, Kong Y, Guo Q, Xu Y, Xing P, Sun Y, Qian J, Xu R, Xie L, Hu Y, Wang M, Li M, Tian Y and Mao W (2022) Gut Bacteria Erysipelatoclostridium and Its Related Metabolite Ptilosteroid A Could Predict Radiation-Induced Intestinal Injury. Front. Public Health 10:862598. doi: 10.3389/fpubh.2022.862598

It is difficult to study the intestinal damage induced by space radiation to astronauts directly, and few prediction models exist. However, we can simulate it in patients with pelvic tumor radiotherapy (RT). Radiation-induced intestinal injury (RIII) is common in cancer patients who receieved pelvic and abdominal RT. We dynamically analyzed gut microbiota and metabolites alterations in 17 cervical and endometrial cancer patients after pelvic RT. In patients who later developed grade 2 RIII, dysbiosis of gut microbiota and metabolites were observed. Univariate analysis showed that *Erysipelatoclostridium* and ptilosteroid A were related to the occurrence of grade 2 RIII. Notably, a strong positive correlation between gut bacteria *Erysipelatoclostridium* relative abundance and gut metabolite ptilosteroid A expression was found. Furthermore, combinations of *Erysipelatoclostridium* and ptilosteroid A could provide good diagnostic markers for grade 2 RIII. In conclusion, gut bacteria *Erysipelatoclostridium* and its related metabolite ptilosteroid A may collaboratively predict RIII, and could be diagnostic biomarkers for RIII and space radiation injury.

Keywords: radiation-induced intestinal injury, biomarker, gut bacteria, gut bacteria related metabolite, radiotherapy

INTRODUCTION

Life science in space research is committed to understanding the basic laws of life activities in the space environment, and exploring the natural phenomena and laws of life in the universe. However, the extreme environments such as space radiation can also cause serious damage to astronauts. The space radiation environment is an extreme environment that has not been encountered in the evolution of Earth's organisms, and because of the space environment cannot be simulated on the ground, there are still many problems and key technologies to be overcome in the research in this field. In this paper, we used the intestinal damage caused by pelvic tumor radiotherapy as a model to evaluate the impact of radiation on human intestinal damage and intestinal microbes, hoping to

TABLE 1 | Clinical features of patients.

Characteristics	Values
Age (years)	52 (range 35–77)
Karnofsky performance score	
≥70	17 (100%)
<70	0 (0%)
Radiotherapy	
Radical	6 (35%)
Adjuvant	11 (65%)
Concurrent chemotherapy	
Yes	10 (59%)
None	7 (41%)
Stage (I/II/III)	
I	2 (12%)
II	6 (35%)
III	9 (53%)
Radiation enteritis	
0–1	3 (35%)
>2	11 (65%)

TABLE 2 | Clinical features of grade 2 and grade 0 or 1 RIII patients.

Characteristics	2 RIII	0–1 RIII	*P*-values
	11	**6**	
Age (years)			
≥50	4	2	0.661
<50	7	4	
Radiotherapy			
Radical	3	3	0.339
Adjuvant	8	3	
Concurrent chemotherapy			
Yes	8	2	0.682
None	3	4	
Stage (I/II/III)			
I	1	1	0.898
II	4	2	
III	6	3	

TABLE 3 | Dosimetric parameters of grade 2 and grade 0 or 1 RIII patients.

Characteristics	2 RIII	0–1 RIII	*P*-values
V50 (%, small intestine)	7.67 ± 2.98	6.73 ± 2.45	0.83
V40 (%, small intestine)	28.76 ± 3.83	25.55 ± 4.47	0.6
V30 (%, small intestine)	44.51 ± 4.53	42.68 ± 6.34	0.81
D_{max} (cGy, small intestine)	4,639 ± 581	5,328 ± 200	0.37
D_{mean} (cGy, small intestine)	2,642 ± 187	3,180 ± 259	0.11
V50 (%, rectum)	23.93 ± 10.32	27.05 ± 9.93	0.84
V40 (%, rectum)	88.42 ± 2.89	78.17 ± 7.65	0.27
V30 (%, rectum)	97.35 ± 1.76	96.12 ± 1.87	0.65
D_{max} (cGy, rectum)	5,134 ± 99	5,178 ± 114	0.78
D_{mean} (cGy, rectum)	4,379 ± 206	4,544 ± 180	0.58

provide a research basis for the damage mechanism and protection strategies of space radiation.

Radiotherapy (RT) is an essential modality in multi-disciplinary treatment for pelvic and abdominal malignancies (1). However, the risk of normal tissue toxicities restricts the RT application. Among them, radiation-induced intestinal injury (RIII) is one of the main problems (2–4). Since RIII lacks efficient clinical treatment method (5, 6), development of bio-markers for prediction of RIII risk are in urgent need.

Intestinal microbiota influences a range of physiological and pathological processes *via* generating bioactive compound: microbiota–derived metabolites. Therefore, gut microbiota and their derived metabolites not only reflect local intestinal ecosystem, but also provide information about host homeostasis, and may serve as potential bio-markers of RIII and space radiation injury (7–9).

To the best of our knowledge, this study is one of the first attempts to establish the intestinal microbiota—and metabolite—based prediction model of RIII to space radiation damage. In this prospective, observational clinical study, we dynamically explored gut microbiota and their derived metabolite alterations in response to pelvic RT. Base on that, we further established a 2-variable model that contains gut bacteria and its related metabolite for the prediction of RIII. Our results could provide an easily obtainable clinical biomarkers to aid in early diagnoses of RIII and space radiation damage.

MATERIALS AND METHODS

Patient Recruitment and Characteristics

This study was approved by the ethic committee of The Second Affiliated Hospital of Soochow University (JD-LK-2017-013-02), and was conducted according to the principles of the Declaration of Helsinki. Inclusion criteria were: (1) newly diagnosed and pathologically confirmed stage I to III cervical or endometrial cancer; (2) receive pelvic or abdominal RT for the first time; (3) KPS $\geq$ 70. RT treatments were conducted according to the RTOG or ESTRO guidelines. Stool samples were collected before, 20–30 and 45–50 Gy after RT, respectively. All samples were aliquoted and stored at −80°C until further use.

Follow-Up and Assessment of RIII

Patients were examined at least once before RT and weekly during RT. Then, patients were examined 1 week, 1 month, and 3 months after RT completion, and every 3 months thereafter. RIII was diagnosed and scored according to the RTOG acute radiation morbidity scoring criteria.

DNA Extraction and Sequencing of 16S rRNA Gene

Briefly, bacterial genomic DNA was extracted by using the QIAamp Fast DNA Mini Kit (Qiagen, Hilden, Germany), and

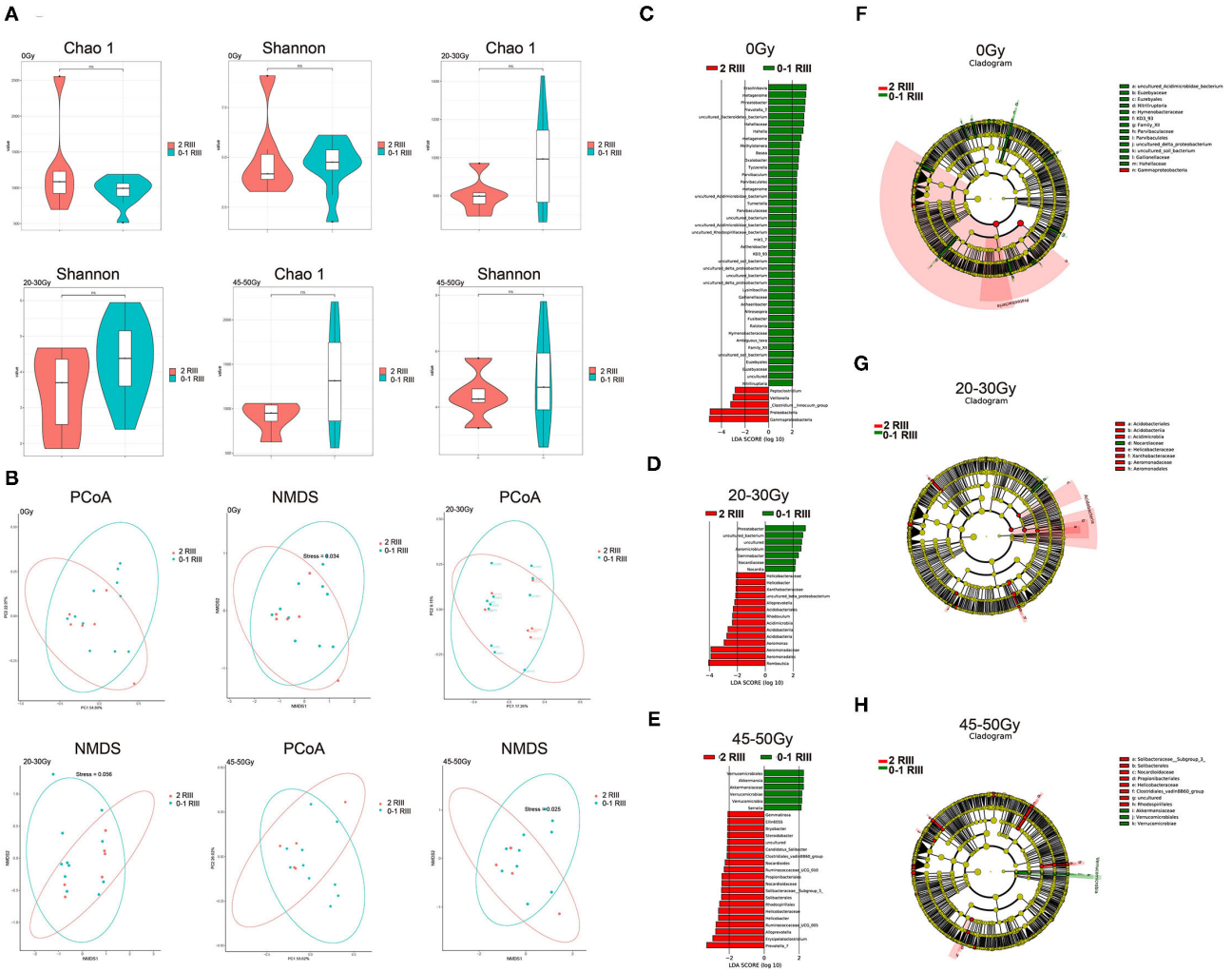

FIGURE 1 | Alterations of gut microbiome between grade 2 and grade 0 or 1 RIII patients at all the three timepoints. **(A)** Box plot of the Chao1 index and Shannon index. **(B)** PCoA and NMDS analysis. **(C–E)** LEfSe analysis based on OTU abundance. **(F–H)** Taxonomic cladograms with LDA score ≥2.

all the operations were conducted following the manufacturer's instructions. Then, the 16S rRNA V3–V4 variable regions were amplified with universal primers (343F and 798R) by PCR. Finally, sequencing was conducted by using the Illumina HiSeq2500 platform.

LC-MS Analysis

LC-MS analysis was performed using ACQUITY UPLC I-Class system (Waters Corporation, Milford, USA) coupled with VION IMS QTOF Mass spectrometer (Waters Corporation, Milford, USA) system with an ACQUITY UPLC BEH C18 column (1.7 μm, 2.1 X 100 mm). Mobile phases A and B were using water and acetonitrile/methanol 2/3(v/v), both containing 0.1% formic acid, respectively. The linear gradient was: 0 min, 1% B; 1 min, 30% B; 2.5 min, 60% B; 6.5 min, 90% B; 8.5 min, 100% B; 10.7 min, 100% B; 10.8 min, 1% B, and 13 min, 1%B. The column temperature was 45°C and the flow rate was 0.4 mL/min.

Statistical Analysis and Bioinformatics

16S rRNA sequencing raw data were firstly preprocessed *via* Trimmomatic software, then converted to generate operational taxonomic units (OTUs) by using Vsearch software with 97% similarity as cutoff value. Next, α-diversity was assessed by Chao1 and Shannon indexes. β-diversity was assessed by PCoA, NMDS, Adonis and Anosim analysis. Further, the differential expressed microbiota were analyzed by ANOVA, Kruskal Wallis, *T*-test, Wilcoxon and LEfSe test.

LC-MS raw data were analyzed by QI software (Waters Corporation, Milford, USA). Partial least squares discrimination analysis (PLS-DA) and orthogonal PLS-DA (OPLS-DA) were performed to visualize the metabolic alterations between different groups. The downstream potential enriched metabolic pathways were acquired by performing KEGG pathway analysis.

Student's *t*-test or Chi-square test were carried out to compare variables between different groups. Univariate logistic regression analysis was used to identify potential

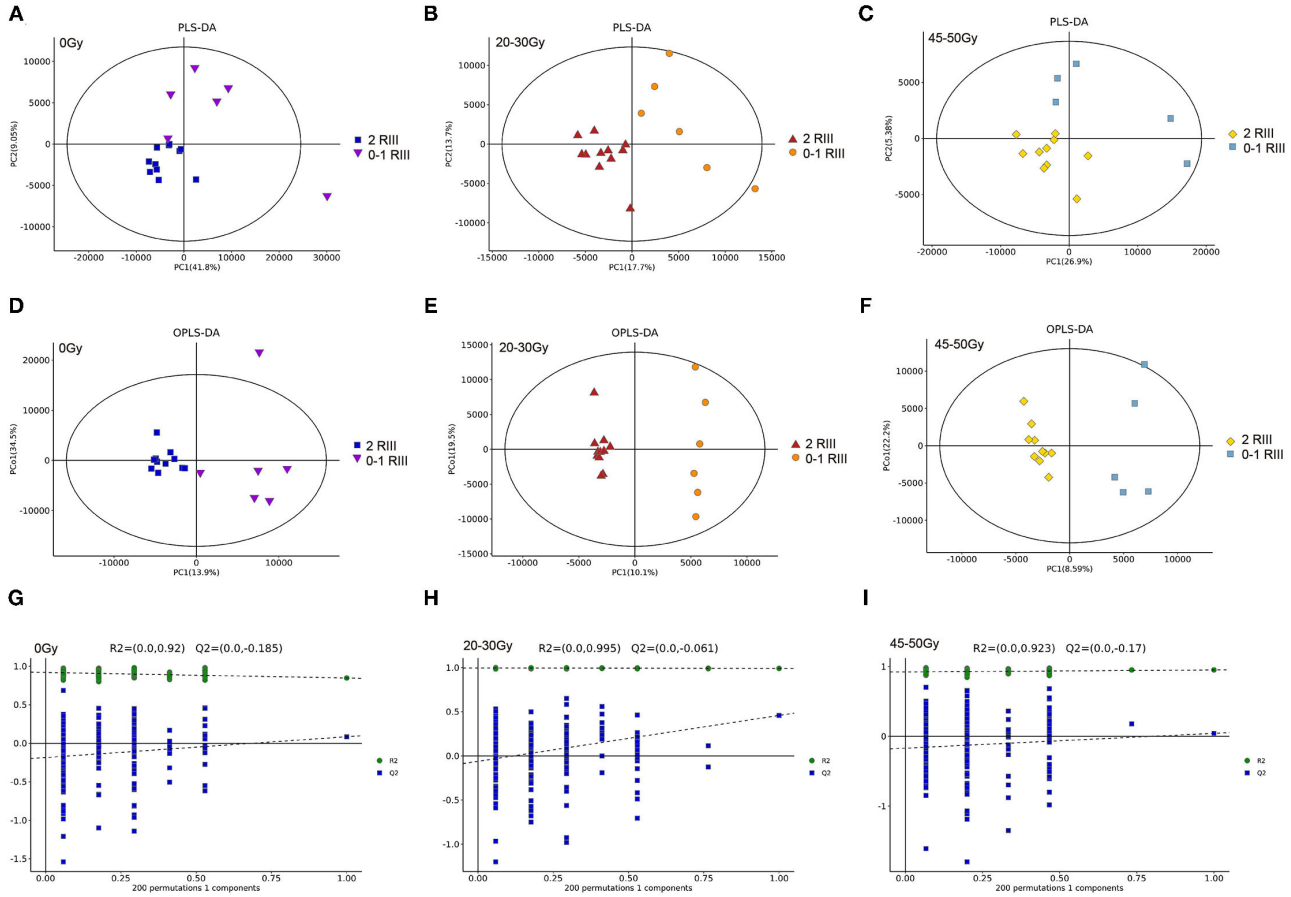

FIGURE 2 | Alterations of gut metabolites between grade 2 and grade 0 or 1 RIII patients at all the three timepoints. **(A–F)** PLS-DA and OPLS-DA score plots. **(G–I)** OPLS-DA score plots.

biomarkers, and receiver operator characteristic (ROC) curves were constructed. Spearman's correlation test was performed to detect the correlation between expression levels of gut *Erysipelatoclostridium* and ptilosteroid A. Statistical analysis was performed using SPSS version 22 software (IBM Corp., Armonk, NY), and p-value < 0.05 was considered significant.

RESULTS

Study Population and Characteristics

Totally, 17 patients (16 cervical cancer and one endometrial cancer) were recruited, and their characteristics are shown in **Table 1**. Among them, 11 (65%) developed grade 2 RIII, 2 (12%) developed grade 1 RIII, and 4 (23%) did not develop any grade of RIII. Since the symptoms of grade 1 RIII is mild and with no need for specific treatment, patients were divided into grade 2 RIII group and grade 0 or 1 RIII group for further analysis. As we can see, no differences in age, RT type, whether acceptance of concurrent chemotherapy or not, tumor stage and dosimetric parameters of gut were found between the two groups (**Tables 2**, **3**).

Differences in Gut Microbiome Between Grade 2 and Grade 0 or 1 RIII Patients

We firstly compared α-diversity and β-diversity between the two groups, respectively. For the α-diversity analysis, we found no significant differences (**Figure 1A**). As for the β-diversity, partial distinction was found (**Figure 1B**), indicating that the heterogeneousness rather than the complexity of gut microbiota community was partly distinct between grade 2 and grade 0 or 1 RIII patients. Next, we try to identify the RIII-related bacterial taxa by LEfSe. As we can see, at genus level, 47, 22, and 26 discriminative features with LDA score ≥ 2 were identified before or after 20–30 and 45–50 Gy, respectively (**Figures 1C–E**). Further, the relationship between taxa at different taxonomic levels of these discriminative features were represented (**Figures 1F–H**).

Gut Metabonomics in Grade 2 RIII Patients Significantly Differed From That in Grade 0 or 1 RIII Patients

For all the three timepoints, both PLS-DA and OPLS-DA analysis identified two distinct metabolite profiles between the

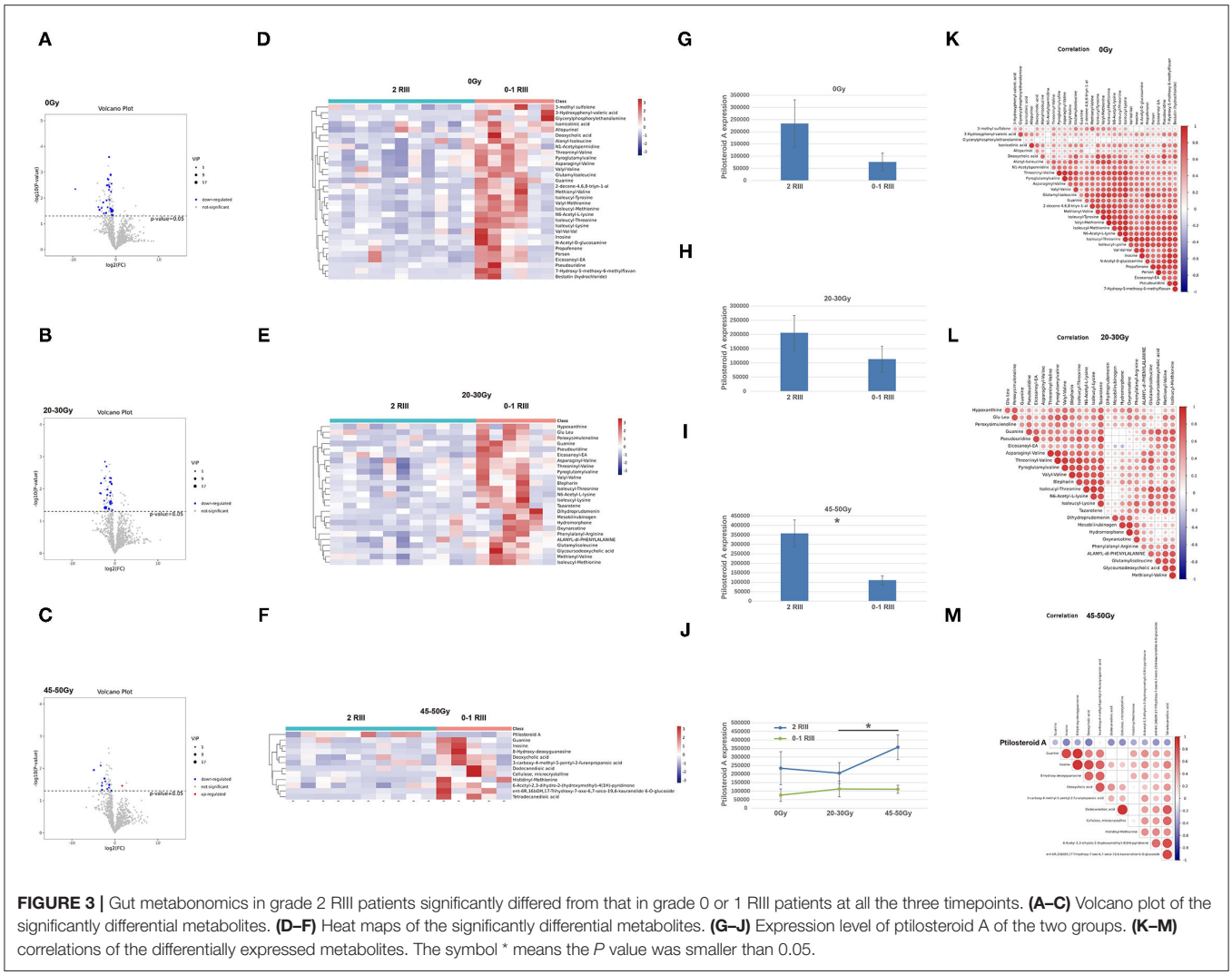

FIGURE 3 | Gut metabonomics in grade 2 RIII patients significantly differed from that in grade 0 or 1 RIII patients at all the three timepoints. **(A–C)** Volcano plot of the significantly differential metabolites. **(D–F)** Heat maps of the significantly differential metabolites. **(G–J)** Expression level of ptilosteroid A of the two groups. **(K–M)** correlations of the differentially expressed metabolites. The symbol * means the *P* value was smaller than 0.05.

two groups (**Figures 2A–F**), indicating that gut metabonomics differed markedly between grade 2 RIII and grade 0 or 1 RIII patients. Further, permutation test was conducted, and the R2 and Q2 values indicated the suitability for subsequent optimization analyses (**Figures 2G–I**).

Gut Metabonomics in Grade 2 RIII Patients Significantly Differed From That in Grade 0 or 1 RIII Patients

As shown in the volcano plot (**Figures 3A–C**), there were 31, 25, and 12 differential metabolites between grade 2 RIII group and grade 0 or 1 RIII group before or after 20–30 and 45–50 Gy, respectively. Heatmap was also presented (**Figures 3D–F**). Among them, ptilosteroid A was the only one that enriched in the grade 2 RIII group (**Figure 3F**). Then we measured gut ptilosteroid A levels between the two groups. We found that before and after 20–30 Gy of RT, the ptilosteroid A levels in the grade 2 RIII group were higher than that of grade 0 or 1 RIII group, but was not significant (**Figures 3G,H**). However, the difference of ptilosteroid A level between the two groups became significant after 45–50 Gy (**Figure 3I**). During the course of RT, for the patients with grade 2 RIII their gut ptilosteroid A level kept increasing and reached the highest level (1.7-fold) after 45–50 Gy, but not for that with grade 0 or 1 RIII patients (**Figure 3J**). Therefore, ptilosteroid A was selected as a potential biomarker for RIII. Next, for these differentially expressed metabolites identified above, their correlations were analyzed by Pearson linear correlation test, and was presented (**Figures 3K–M**).

Identification of Significantly Different Pathways Associated With RIII

Additionally, KEGG pathway analysis was conducted (**Figures 4A–C**), among them the purine metabolism was the only one enriched pathway associated with the occurrence of RIII (**Figures 4D–I**).

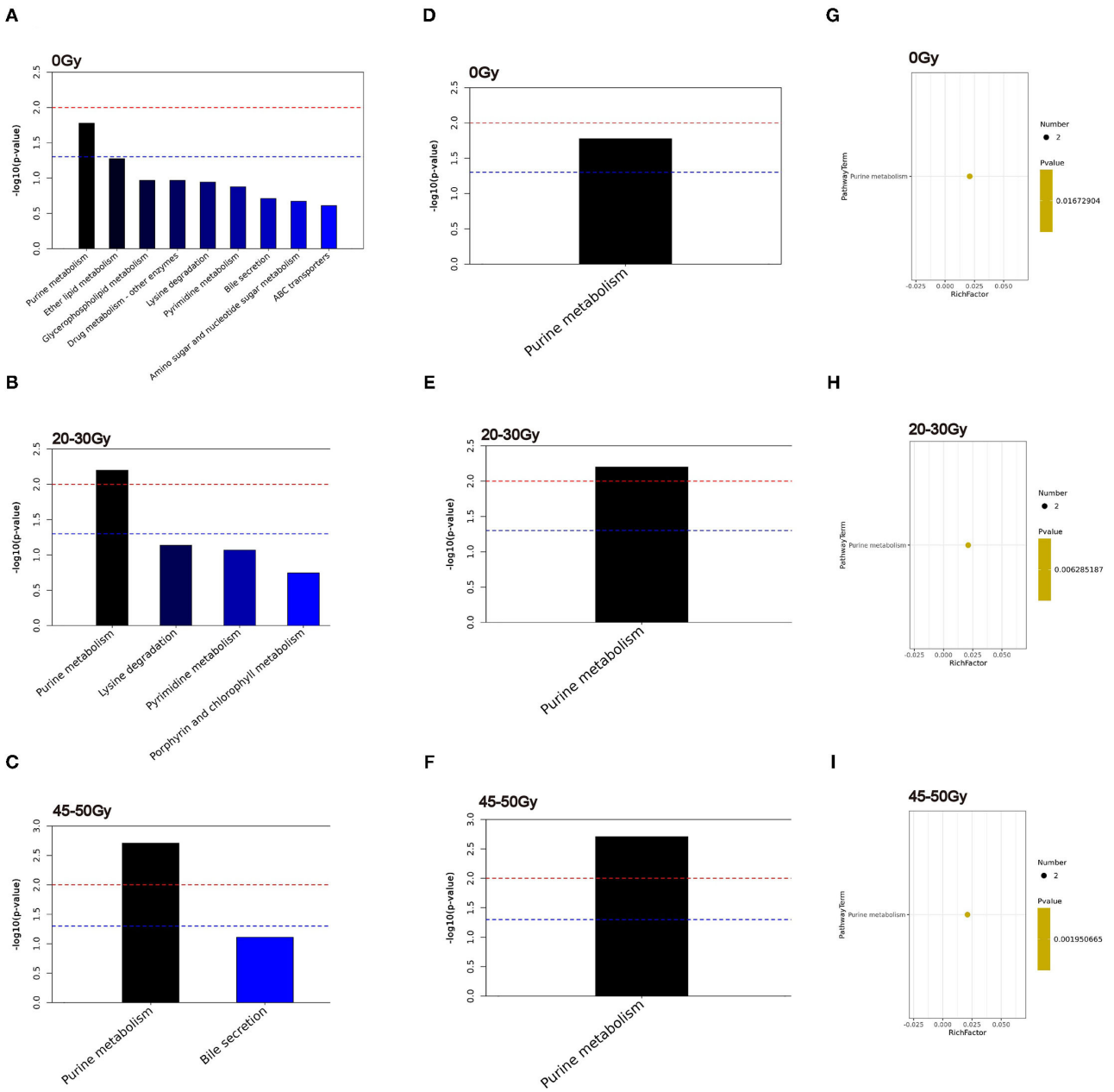

FIGURE 4 | Identification of significantly different pathways associated with RIII. **(A–C)** The top 20 enriched pathways. **(D–F)** Heatmap of enriched metabolic pathway. **(G–I)** bubble plots of enriched metabolic pathway.

Predictive Value of Clinical Characteristics, Gut Microbiome, and Metabolites for Grade 2 RIII

In order to seek out potential bio-markers for RIII, clinical factors gut microbiome and metabolites identified above, were tested by univariate analysis. However, none clinical factors were related to the occurrence of grade 2 RIII (**Table 4**). For the gut microbiome, the relative abundance of *Erysipelatoclostridium* after 45–50 Gy was related to the occurrence of grade 2 RIII. As for the metabolites, the expression level of ptilosteroid A at all the three timepoints were related to the occurrence of grade 2 RIII. Therefore, gut microbial *Erysipelatoclostridium* and metabolite ptilosteroid A were chosen as potential bio-markers for further study. Next, the predictive ability of gut microbial *Erysipelatoclostridium* and metabolite ptilosteroid A for RIII was assessed by ROC analysis. Single variable model containing gut microbial *Erysipelatoclostridium* at 45–50 Gy exhibited AUC value of 0.85 (**Figure 5A**). Meanwhile, single variable model containing gut metabolite ptilosteroid A exhibited ATC value

TABLE 4 | Univariate analysis of predictive factors associated with grade 2 RIII.

Factor	Univariate analysis		
	OR	95% CI	*P*-values
Age	0.877	0.768–1	0.5
RT	0.375	0.047–2.998	0.355
CT	5.333	0.618–45.991	0.128
PCT	1	0.112–8.947	0.206
CRT	1.875	0.15–23.396	0.625
V50 (small intestine)	1.011	0.883–1.156	0.878
V40 (small intestine)	1.009	0.919–1.107	0.857
V30 (small intestine)	0.999	0.926–1.079	0.987
D_{max} (small intestine)	0.375	0.996–1.002	0.456
D_{mean} (small intestine)	0.998	0.995–1	0.106
V50 (rectum)	0.994	0.957–1.032	0.752
V40 (rectum)	1.054	0.964–1.152	0.245
V30 (rectum)	1.066	0.859–1.325	0.561
D_{max} (rectum)	0.999	0.995–1.003	0.734
D_{mean} (rectum)	0.999	0.997–1.002	0.601
Erysipelatoclostridium (0 Gy)	10	0.739–135.27	0.083
Erysipelatoclostridium (25–30 Gy)	2.819	0.229–34.645	0.418
Erysipelatoclostridium (40–50 Gy)	36	1.772–331.02	**0.020***
Ptilosteroid A (0 Gy)	20	1.391–287.6	**0.028***
Ptilosteroid A (25–30 Gy)	13.333	1.069–166.374	**0.044***
Ptilosteroid A (40–50 Gy)	16	1.093–234.248	**0.043***

*The bold values indicate the P value was smaller than 0.05. The * and red highlights indicates these factors were related to the grade 2 RIII.*

of 0.788 (0 Gy), 0.8 (after 20–30 Gy), and 0.8 (after 45–50 Gy), respectively (**Figures 5B–D**). Interestingly, better predictive ability can be obtained by combining ptilosteroid A of all the three timepoints or ptilosteroid A with *Erysipelatoclostridium* (**Figures 5E,F**).

Gut Microbial *Erysipelatoclostridium* Positively Correlates With Gut Metabolite Ptilosteroid A

Next, the correlation between gut microbial *Erysipelatoclostridium* and gut metabolite ptilosteroid A was tested. We found a positive correlation between relative abundance of *Erysipelatoclostridium* and expression levels of ptilosteroid A at all the three timepoints (**Figure 6**), indicating that the gut metabolite ptilosteroid A could be mainly produced by gut microbiota *Erysipelatoclostridium.*

DISCUSSION

Based on the needs of manned return to the moon or Mars, the international aerospace powers focus on how to assess the space radiation risks. NASA summarizes the main research directions organized in recent years related to space radiation risks, which including radiation carcinogenicity, radiation-induced central nervous system damage, radiation-induced heart disease and other degenerative diseases, acute radiation syndrome immune system and radiation caused intestinal damage. After decades of research, a lot of evidence has been obtained about the effects of space radiation and health risks, but the underlying mechanism is still not fully understood, resulting in great uncertainty in space radiation risk assessment. The solution of these problems requires more space flight opportunities, more efficient simulation and monitoring technology of space radiation quality and biomarkers, and real-time on-orbit monitoring; technologies such as big data mining and biophysical modeling are needed to conduct space radiation, etc. Here, we wished to use a model of human radiation-induced intestinal injury to assess markers of space radiation induced damage to the digestive system.

Human intestinal microbiota refers to the microorganisms that live in the gastrointestinal tract, including bacteria, fungi, archaea, eukarya and protozoa, etc. These microorganisms inhabit the epithelial barrier surface of gastrointestinal tract, and exert both local and systemic effects (7–9). Increasing evidence has confirmed that gut microbiota orchestrates key physiological functions (10–12). Meanwhile, the out of balance of gut microbiota can lead to several local and systemic pathological processes, like obesity, cardiovascular diseases, autoimmune diseases, gout, inflammatory bowel disease, and several types of cancer (13–15). As for RIII, the role of gut microbiota in initially driving RIII has become increasingly evident (16, 17). In our study, we observed partly distinction of β-diversity but not α-diversity of intestinal microbiota between patients with grade 2 RIII and without. Then, we found that patients who developed grade 2 RIII had obviously enriched *Erysipelatoclostridium* after 45–50 Gy of RT. Univariate analysis showed that the relative abundance of *Erysipelatoclostridium* after 45–50 Gy of RT was related to the occurrence of grade 2 RIII. Furthermore, we developed a single gut microbial *Erysipelatoclostridium* model that exhibited high discriminative ability of RIII (AUC value of 0.85). Collectively, these available evidence indicated that gut microbiota including *Erysipelatoclostridium* may serve as potential bio-markers for RIII.

Since the 16S rRNA sequencing technology lacks the ability to tell transcriptional genes that each microorganism activates, gut microbiota can provide information on microbial structure rather than their functions (18). To overcome these deficiencies, gut metabonomics is an available option. In the gastrointestinal tract, these metabolites function as messengers, signal to distant organs in the body, and allow communication between local gut microbiota and distant organs (19, 20). For example, Mathewson et al. proved that gut microbiota-derived SCFA can mitigate graft vs. host disease (19). Recently, several studies have attempted to use gut metabonomics as biomarkers for RIII (21). Similarly, in our study, unique gut metabonomics signature of RIII was observed. Meanwhile, ptilosteroid A was more abundant in grade 2 RIII patients, especially after 45–50 Gy of RT. Univariate analysis showed that ptilosteroid A were related to the occurrence of grade 2 RIII. Further, we developed single variable model containing gut metabolite ptilosteroid A at three timepoints that exhibited high discriminative ability of RIII. Interestingly, better predictive ability can be obtained by combining ptilosteroid A of all the 3 timepoints. Ptilosteroid A was firstly isolated in the

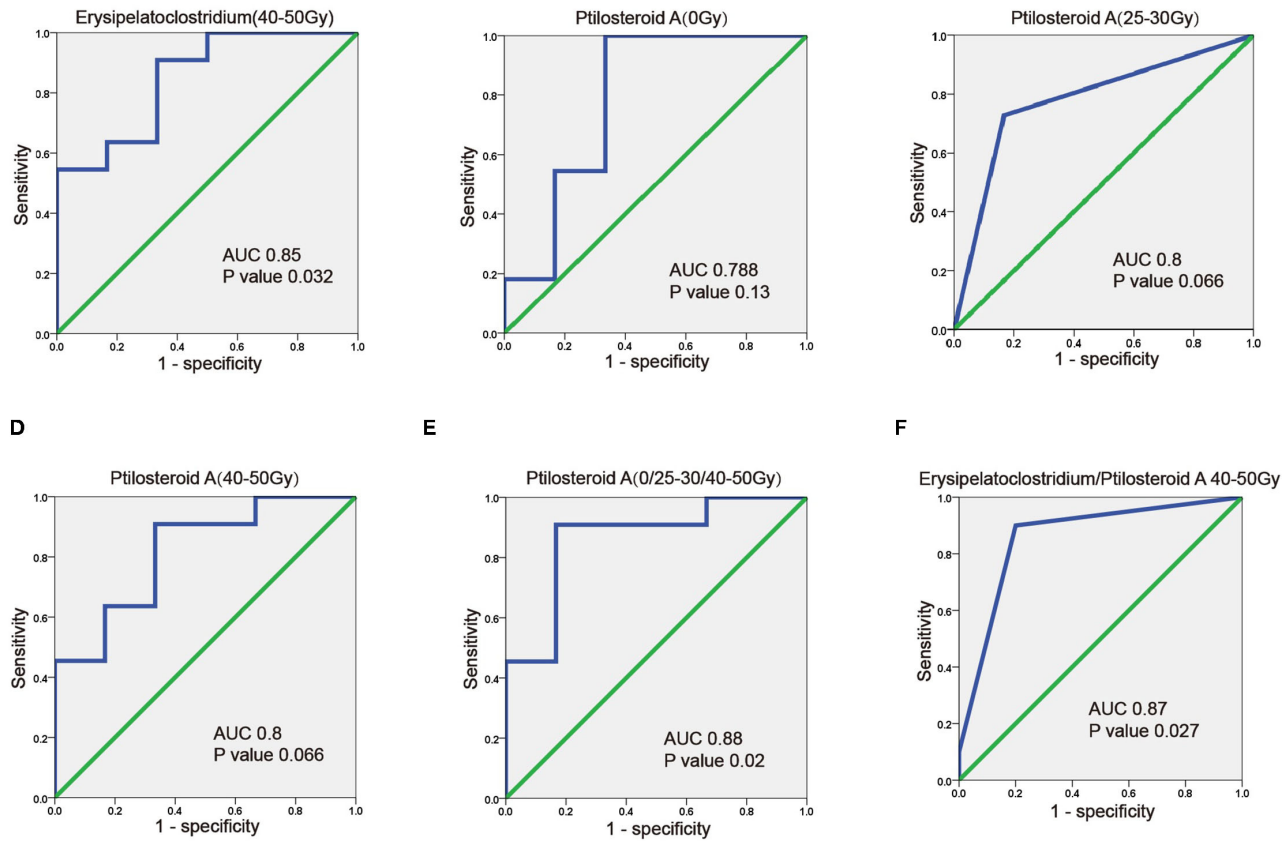

FIGURE 5 | Predictive value of gut microbiome and metabolites for predicting RIII. **(A)** ROC plot for *Erysipelatoclostridium* after 45–50 Gy. **(B–D)** ROC plot for ptilosteroid A at 0 Gy, after 20–30 and 45–50 Gy. **(E)** The ROC analysis of the combination of ptilosteroid A at all the three timepoints. **(F)** The ROC analysis of the combination of *Erysipelatoclostridium* and ptilosteroid A.

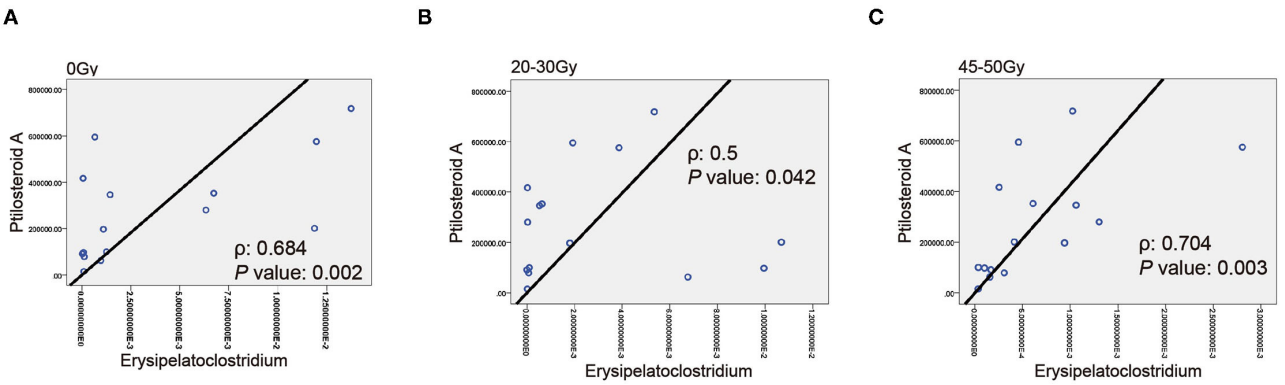

FIGURE 6 | Associations between *Erysipelatoclostridium* and ptilosteroid A. **(A–C)** The correlation between gut *Erysipelatoclostridium* relative abundance and ptilosteroid A expression at all the three timepoints by Spearman's correlation analysis.

Solomon Islands in 2009 (22). Currently few articles about the function of ptilosteroid A has been reported, but the key role that lipids play in maintaining of gut epithelial integrity has been well-investigated. Therefore, gut metabolite ptilosteroid A may contribute to the etiology of RIII, and serve as potential biomarker for RIII.

Further, our study found a positive correlation between relative abundance of *Erysipelatoclostridium* and expression level of ptilosteroid A at all the three timepoints (0 Gy, after 20–30 and 45–50 Gy). As we mentioned above, ptilosteroid A belongs to the superclass of lipids and lipid-like molecules. Wang et al. reported that green tea leaf powder could improve lipid metabolism by modulating gut microbiota including *Erysipelatoclostridium* (23). Meanwhile, Luo et al. found that FuFang Zhenshu TiaoZhi could exert anti-aging effect *via* interference with lipid metabolism and by regulating gut microbiota including *Erysipelatoclostridium* (24). Therefore, gut metabolite ptilosteroid A could be mainly generated by gut microbiota *Erysipelatoclostridium.*

CONCLUSION

In this prospective, observational clinical study, we identified alteration of intestinal microbiota, characterized by enrichment of *Erysipelatoclostridium*, elucidated disorder of gut metabolite, particularly in ptilosteroid A with RIII patients. We further identified *Erysipelatoclostridium* and ptilosteroid A could provide good diagnostic markers for grade 2 RIII. Next, multicenter, larger sample size trials are needed to confirm this.

DATA AVAILABILITY STATEMENT

The datasets presented in this study can be found in online repositories. The names of the repository/repositories and accession number(s) can be found at: https://www.ncbi.nlm.nih.gov/, PRJNA760986.

ETHICS STATEMENT

The studies involving human participants were reviewed and approved by the Ethics Committee of The Second Affiliated Hospital of Soochow University. The patients/participants provided their written informed consent to participate in this study.

AUTHOR CONTRIBUTIONS

WM, YT, MW, and ML designed and supervised this study. SC, YY, YK, QG, YX, and PX recruited patients. YS, JQ, and RX were responsible for the follow-up. SC, LX, and YH conducted sample detection and statistical analysis. All authors contributed to the article and approved the submitted version.

FUNDING

This work was supported by Young Talent Support Project of The Second Affiliated Hospital of Soochow University (XKTJ-RC202007) and Science Foundation of Jiangsu Health Commission (M2021081).

REFERENCES

1. Baumann M, Krause M, Overgaard J, Debus J, Bentzen SM, Daartz J, et al. Radiation oncology in the era of precision medicine. *Nat Rev Cancer.* (2016) 16:234–49. doi: 10.1038/nrc.2016.18
2. Hauer-Jensen M, Denham JW, Andreyev HJ. Radiation enteropathy–pathogenesis, treatment and prevention. *Nat Rev Gastroenterol Hepatol.* (2014) 11:470–9. doi: 10.1038/nrgastro.2014.46
3. Paris F, Fuks Z, Kang A, Capodieci P, Juan G. Ehleiter D, et al. Endothelial apoptosis as the primary lesion initiating intestinal radiation damage in mice. *Science.* (2001) 293:293–7. doi: 10.1126/science.1060191
4. Cao XP. Radiation intestinal injury in the era of precision radiotherapy. *Zhonghua Wei Chang Wai Ke Za Zhi.* (2020) 23:734–6. doi: 10.3760/cma.j.cn.441530-20200505-00254
5. Xie LW, Cai S, Zhao TS, Li M, Tian Y. Green tea derivative (-)-epigallocatechin-3-gallate (EGCG) confers protection against ionizing radiation-induced intestinal epithelial cell death both *in vitro* and *in vivo*. *Free Radic Biol Med.* (2020) 161:175–86. doi: 10.1016/j.freeradbiomed.2020.10.012
6. Singh VK, Newman VL, Romaine PL, Wise SY, Seed TM. Radiation countermeasure agents: an update (2011–2014). *Expert Opin Ther Pat.* (2014) 24:1229–55. doi: 10.1517/13543776.2014.964684
7. Roy S, Trinchieri G. Microbiota: a key orchestrator of cancer therapy. *Nat Rev Cancer.* (2017) 17:271–85. doi: 10.1038/nrc.2017.13
8. David LA, Maurice CF, Carmody RN, Gootenberg DB, Button JE, Wolfe BE, et al. Diet rapidly and reproducibly alters the human gut microbiome. *Nature.* (2014) 505:559–3. doi: 10.1038/nature12820
9. Frias-Lopez J, Shi Y, Tyson GW, Coleman ML, Schuster SC, Chisholm SW, et al. Microbial community gene expression in ocean surface waters. *Proc Natl Acad Sci USA.* (2008) 105:3805–10. doi: 10.1073/pnas.0708897105
10. Medzhitov R. Recognition of microorganisms and activation of the immune response. *Nature.* (2007) 449:819–26. doi: 10.1038/nature06246
11. Cani PD, Amar J, Iglesias MA, Poggi M, Knauf C, Bastelica D, et al. Metabolic endotoxemia initiates obesity and insulin resistance. *Diabetes.* (2007) 56:1761–72. doi: 10.2337/db06-1491
12. Caesar R, Tremaroli V, Kovatcheva-Datchary P, Cani PD, Bäckhed F. Crosstalk between gut microbiota and dietary lipids aggravates WAT inflammation through TLR signaling. *Cell Metab.* (2015) 22:658–68. doi: 10.1016/j.cmet.2015.07.026
13. Luczynski P, Whelan SO, O'Sullivan C, Clarke G, Shanahan F, Dinan TG, et al. Adult microbiota-deficient mice have distinct dendritic morphological changes: differential effects in the amygdala and hippocampus. *Eur J Neurosci.* (2016) 44:2654–66. doi: 10.1111/ejn.13291
14. Arrieta MC, Stiemsma LT, Amenyogbe N, Brown EM, Finlay B. The intestinal microbiome in early life: health and disease. *Front Immunol.* (2014) 5:427. doi: 10.3389/fimmu.2014.00427
15. Crawford PA, Gordon JI. Microbial regulation of intestinal radiosensitivity. *Proc Natl Acad Sci USA.* (2005) 102:13254–9. doi: 10.1073/pnas.0504830102
16. Wang A, Ling Z, Yang Z, Kiela PR, Wang T, Wang C, et al. Gut microbial dysbiosis may predict diarrhea and fatigue in patients undergoing pelvic cancer radiotherapy: a pilot study. *PLoS ONE.* (2015) 10:e0126312. doi: 10.1371/journal.pone.0126312
17. Manichanh C, Varela E, Martinez C, Antolin M, Llopis M, Doré J, et al. The gut microbiota predispose to the pathophysiology of acute postradiotherapy diarrhea. *Am J Gastroenterol.* (2008) 103:1754–61. doi: 10.1111/j.1572-0241.2008.01868.x
18. Cangelosi GA, Meschke JS. Dead or alive: molecular assessment of microbial viability. *Appl Environ Microbiol.* (2014) 80:5884–91. doi: 10.1128/AEM.01763-14
19. Mathewson ND, Jenq R, Mathew AV, Koenigsknecht M, Hanash A, Toubai T, et al. Gut microbiome-derived metabolites modulate intestinal epithelial cell damage and mitigate graft-versus-host disease. *Nat Immunol.* (2016) 17:505–13. doi: 10.1038/ni.3400

20. Zierer J, Jackson MA, Kastenmüller G, Mangino M, Long T, Telenti A, et al. The fecal metabolome as a functional readout of the gut microbiome. *Nat Genet.* (2018) 50:790–5. doi: 10.1038/s41588-018-0135-7
21. Chai Y, Wang J, Wang T, Yang Y, Su J, Shi F, et al. Application of 1H NMR spectroscopy-based metabonomics to feces of cervical cancer patients with radiation-induced acute intestinal symptoms. *Radiother Oncol.* (2015) 117:294–301. doi: 10.1016/j.radonc.2015.07.037
22. Gabant M, Schmitz-Afonso I, Gallard JF, Menou JL, Laurent D, Debitus C, et al. Sulfated steroids: ptilosteroids A-C and ptilosaponosides A and B from the Solomon Islands marine sponge Ptilocaulis spiculifer. *J Nat Prod.* (2009) 72:760–3. doi: 10.1021/np800758c
23. Wang J, Li P, Liu S, Zhang B, Hu Y, Ma H, et al. Green tea leaf powder prevents dyslipidemia in high-fat diet-fed mice by modulating gut microbiota. *Food Nutr Res*. (2020) 64:3672. doi: 10.29219/fnr.v64.3672
24. Luo D, Chen K, Li J, Fang Z, Pang H, Yin Y, et al. Gut microbiota combined with metabolomics reveals the metabolic profile of the normal aging process and the anti-aging effect of FuFang Zhenshu TiaoZhi (FTZ) in mice. *Biomed Pharmacother.* (2020) 121:109550. doi: 10.1016/j.biopha.2019.109550

Conflict of Interest: The authors declare that the research was conducted in the absence of any commercial or financial relationships that could be construed as a potential conflictof interest.

Publisher's Note: All claims expressed in this article are solely those of the authors and do not necessarily represent those of their affiliated organizations, or those of the publisher, the editors and the reviewers. Any product that may be evaluated in this article, or claim that may be made by its manufacturer, is not guaranteed or endorsed by the publisher.

frontiers | Frontiers in Astronomy and Space Sciences

TYPE Original Research
PUBLISHED 07 November 2022
DOI 10.3389/fspas.2022.949432

OPEN ACCESS

EDITED BY
Cristina Consolandi,
University of Hawaii at Manoa,
United States

REVIEWED BY
Pavel Bláha,
National Institute of Nuclear Physics of Naples, Italy
S. M. J. Mortazavi,
Fox Chase Cancer Center, United States

*CORRESPONDENCE
Roger W. Howell,
rhowell@rutgers.edu

SPECIALTY SECTION
This article was submitted to Astrobiology,
a section of the journal
Frontiers in Astronomy and Space Sciences

RECEIVED 20 May 2022
ACCEPTED 24 October 2022
PUBLISHED 07 November 2022

CITATION
Leung CN, Howell DM, De Toledo SM, Azzam EI and Howell RW (2022), Late effects of heavy-ion space radiation on splenocyte subpopulations and NK cytotoxic function.
Front. Astron. Space Sci. 9:949432.
doi: 10.3389/fspas.2022.949432

Late effects of heavy-ion space radiation on splenocyte subpopulations and NK cytotoxic function

Calvin N. Leung[1], Donna M. Howell[1,2], Sonia M. De Toledo[1], Edouard I. Azzam[1,3] and Roger W. Howell [1]*

[1]Department of Radiology, New Jersey Medical School, Rutgers University, Newark, NJ, United States, [2]Natural Sciences Department, Middlesex College, Edison, NJ, United States, [3]Department of Health Sciences, Canadian Nuclear Laboratories, Chalk River, ON, Canada

Introduction: With current goals of increased space exploration and travel to Mars, there has been great interest in understanding the long-term effects of high atomic number, high energy (HZE) ion exposure on various organ systems and the immune system. Little is known about late effects on the immune system after HZE exposure. Therefore, our objective was to determine how natural killer (NK) cell populations were affected in geriatric mice that were exposed to HZE particles during middle-age, thereby representing elderly retired astronauts that undertook deep space missions.

Methods: 10 month old male CBA/CaJ mice were whole-body irradiated: sham (control); 150-cGy gamma-rays (delivered in 1 fraction); 40-cGy 1-GeV/nu $^{28}Si^{14+}$ ions (delivered in 3 fractions); 40-cGy 1-GeV/nu $^{16}O^{8+}$ ions (1 fraction); and 40-cGy 1-GeV/nu $^{16}O^{8+}$ ions (3 fractions). The mice were sacrificed 1–1.5 yr post-exposure, and the spleens harvested. Splenocyte effector (E) cells were harvested and added to ^{51}Cr-labeled Yac-1 target (T) cells in E:T ratios of 12:1, 25:1, 50:1, and 100:1. NK cytotoxicity was measured with ^{51}Cr release. In addition, 2 million splenocytes were aliquoted and stained with a seven-antibody cocktail, and flow cytometry was used to determine the percentage of NK, B lymphocytes, and T lymphocytes in the splenocyte population.

Results: Mice exposed to either a single fraction of 150-cGy gamma rays or 40-cGy $^{16}O^{8+}$ ions in 3 fractions were found to have significant decreases in NK cytotoxicity of approximately 30% and 25%, respectively. No significant differences were observed in NK cytotoxicity for 40-cGy $^{16}O^{8+}$ ions delivered in 1 fraction, or 40-cGy $^{28}Si^{14+}$ ions delivered in 3 fractions. No significant differences were observed in the percentage of spleen cells that were NK (%NK) amongst the groups.

Conclusion: Fractionated HZE ion exposure has the potential to affect the innate arm of the immune system long after exposure, leading to decreases in NK cell function. Therefore, protective countermeasures may need to be considered to decrease the risk of reduced long-term immune function in elderly retired astronauts that undertook deep space missions.

KEYWORDS

heavy ion, ionizing radiation, natural killer cells (NK cells), splenocytes, late effect of radiation

Introduction

The mission to Mars has been a key objective for NASA in recent years. One obstacle in achieving this objective is the high-Z, high-energy (HZE) ion radiation exposure astronauts will face during the voyage duration. Current NASA guidelines allow astronauts a permissible career exposure limit corresponding to 3% risk of radiation-exposure-induced death (REID) for cancer at a 95% confidence level to protect against uncertainties in risk projections (NASA, 2022). The average effective dose an astronaut receives while spending 6 months in the International Space Station is approximately 72 mSv (Cucinotta et al., 2008). An astronaut undergoing a journey to and from Mars is expected to be exposed to approximately 660 mSv (Cucinotta et al., 2012). It has been estimated that during the journey, every cell in the body will be traversed by a low LET proton once every 3–4 days, and an HZE ion every few months (Kerr, 2013). Despite the much lower traversal incidence of HZE particles, their high linear energy transfer (LET) nature produces more complex DNA damage along their trajectory, which is difficult for cellular DNA-repair mechanisms to repair. Potential consequences can include chronic oxidative stress within the cell and surrounding bystander cells (Buonanno et al., 2011), as well as permanent DNA damage which can lead to cell dysregulation and cancer (Bielefeldt-Ohmann et al., 2012).

Exposure to HZE-ions has been demonstrated to have effects in multiple organ systems, including the nervous system and cardiovascular systems (Boerma et al., 2015a; Boerma et al., 2015b; Klein et al., 2021). Another critical organ system that may be potentially affected from heavy ion exposure is the immune system. The immune system is involved in combating invasion from outside sources, such as bacteria, viruses, and parasites, as well as normal surveillance of host cells. Dysregulation of the immune system can lead to a myriad of both acute and chronic issues, including infection, autoimmune disease, and cancer (Ikeda and Togashi, 2022). One component of the immune system is the natural killer (NK) cell. While historically considered part of the innate arm of the immune response, NK cells interact with both the innate and adaptive arms of the immune response (Vivier et al., 2011). In conjunction with $CD8_+$ T lymphocytes, NK cells are involved in the detection and elimination of cancer cells. Where $CD8_+$ T lymphocytes require the expression of antigens on major histocompatibility complex (MHC) Class I receptors to carry out their function, NK cells are able to react to cells avoiding immunodetection through decreased MHC Class I surface expression (Karre et al., 1986). Additionally, NK cells can also recognize NKG2D ligands, a family of ligands that are expressed at low levels in healthy tissues but become elevated under cellular stress conditions, including ULBP1-6 and MICA/B (Zingoni et al., 2018). The NK cell's cytotoxic function is activated upon recognition, causing cell death (Abel et al., 2018). Recent research has also demonstrated that NK cells may possess the ability to "remember," similar to memory T cells (Beaulieu, 2021). When NK cell populations are depressed, both in size and function long-term, there is an elevated risk for viral infections (Orange, 2013; Mace and Orange, 2016) and cancer initiation and progression (Nakajima et al., 1987; Chiossone et al., 2018; Moon and Powis, 2019). In an 11-year study of a Japanese resident cohort, subjects in the lowest tertile for NK cytotoxic function were more likely to develop cancer (Imai et al., 2000). Other studies found that patients with poor NK cell infiltration had worse prognoses for multiple cancer types, highlighting the importance of the NK cell's role in the immune system (Coca et al., 1997; Ishigami et al., 2000a; Ishigami et al., 2000b; Villegas et al., 2002).

It has been well established that cells of the immune system are sensitive to ionizing radiation (Kajioka et al., 2000; Heylmann et al., 2014). Astronauts returning from spaceflight were shown to have considerable decreases in circulating immune cells as early as the 1960s (Crucian et al., 2020). Recovery to pre-flight levels have also been observed to be delayed, as long as 2 months post-return despite the relatively short flight duration. Previous studies in astronauts have shown alterations in the immune system after both short-term (<1 month) (Konstantinova et al., 1995; Crucian et al., 2013) and long-term (≥1 month) spaceflights (Buchheim et al., 2019). More recently, the monozygous twin study conducted by NASA also observed changes in both immune cell number and gene expression after spaceflight, again demonstrating alterations in both immune cell population size and function (Garrett-Bakelman et al., 2019). Studies on the cytotoxic function of NK cells of rat splenocytes after short-duration flights on COSMOS 2044 demonstrated decreased ability to kill target cells (Rykova et al., 1992; Lesnyak et al., 1996). NK cell function in astronauts has also been observed to be decreased upon return from spaceflight (Mehta et al., 2001), with substantial variability in the time required to return to normal function. However, these spaceflights were in low Earth orbit (LEO) where the magnetosphere provides some protection against HZE particles, a protection that will not be available to astronauts traveling to and from Mars. Furthermore, they did not follow NK function over time scales commensurate with an astronaut reaching a geriatric stage of life. Therefore, the present study was conducted to determine the long-term effects of HZE-ion exposure on splenic NK cell population size and function. Ten-month old mice were irradiated in our study to represent

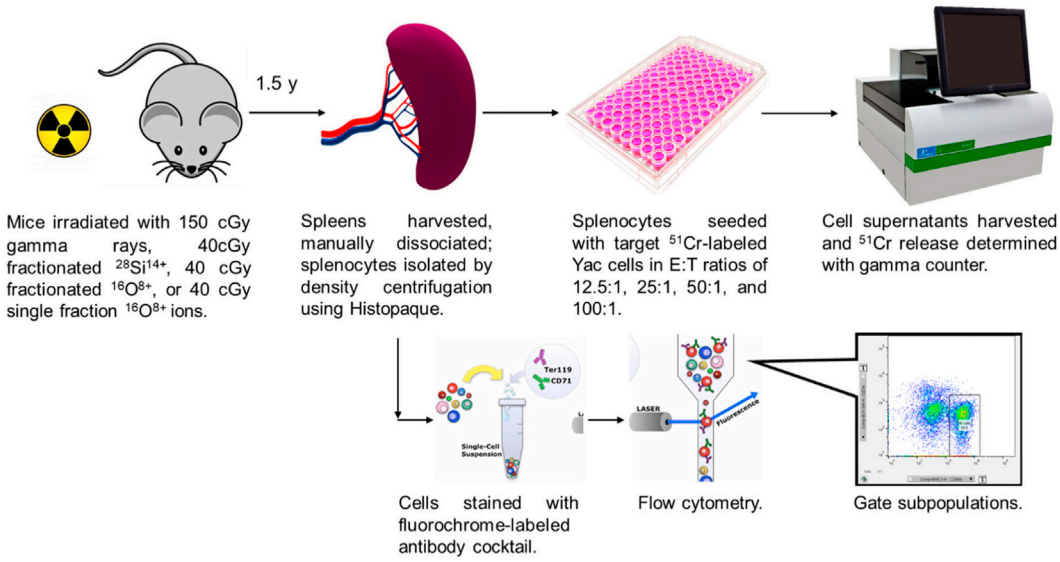

FIGURE 1
Experimental design.

astronauts about 40 years of age. A 1–1.5-year postirradiation period between irradiation and NK assay was undertaken to simulate an elderly retired Mars astronaut.

Materials and methods

The overall experimental approach is depicted in Figure 1. Details regarding the individual steps are described below.

Cell culture

YAC-1 mouse lymphoma cells (kindly provided by Drs. Vincent Tsiagbe and Nicholas Ponzio) were grown in suspension in a 75 cm^2 flask containing 15 ml RPMI media (Sigma-Aldrich) supplemented with 2 mM L-glutamine (Gibco), 200 UI penicillin/200 µg/ml streptomycin (Corning), and 10% fetal bovine serum (Gibco) at 37°C with 5% CO_2. Cells were passaged at a 1:10 ratio every 3 days. Cells used in the NK cytotoxic function assay were split 1:3 the day prior.

Animals

Male CBA/CaJ mice aged 10 months (Jackson Laboratories) were used for this study. They were raised at Jackson Laboratories prior to being shipped directly to the NSRL Animal Facility, where they were acclimated for 7–10 days. Mice were then irradiated as described below, and 4–10 days after irradiation they were shipped to the Rutgers RBHS Animal Facility in Newark, NJ, where they were housed on a 12 h light/dark cycle and given Purina chow and water *ad libitum*.

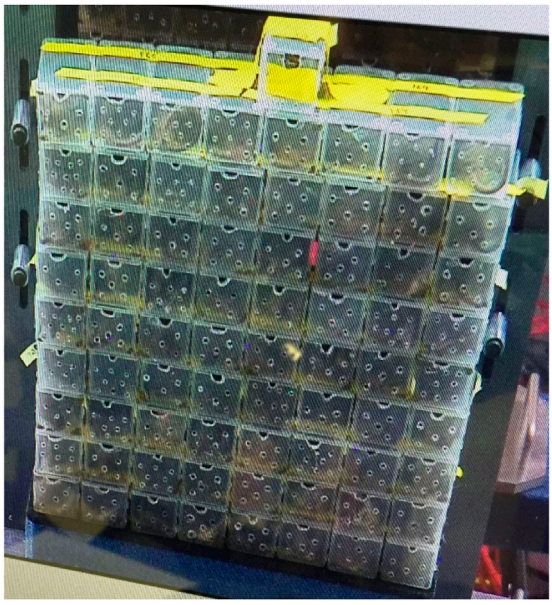

FIGURE 2
Setup for irradiating mice with 1 GeV/u $^{28}Si^{14+}$ or $^{16}O^{8+}$ ions. The 9 × 8 structure holds 72 mice in individual compartments. Ventilation holes and a high-speed fan kept animals at comfortable temperature.

TABLE 1 Animal groups, absorbed doses and irradiation protocols.

Irradiation protocol	Absorbed dose and protocol[b]	Animal ID numbers	Howell UID	Cage ID	Run group irradiation date	Assay date
Control	0 cGy	1792[a] 1793[a] 1794[a] 1807[a] 1808[a] 1809[a] 1992 1993 1994	1-1A 1-1B 1-1C 2-1A 2-1B 2-1C 3-1A 3-1B 3-1C	340 340 340 341 341 341 412 412 412	16B June 15–17, 2016, 17A 13 Feb 2017	10 Jan 2018, 13 Jan 2018, 23 Feb 2018
γ-rays (662 keV)	150 cGy (1F)	1795[a] 1796[a] 1797[a] 1810[a] 1811[a] 1812[a]	1-2A 1-2B 1-2C 2-2A 2-2B 2-2C	316 316 316 316 321 321	16B June 15–17, 2016	10 Jan 2018, January 13, 2018
$^{16}O^{8+}$ (1 GeV/u)	40 cGy (1F)	1804 1805 1806 1819 1820 1821 1986 1987 1988	1-5A 1-5B 1-5C 2-5A 2-5B 2-5C 3-5A 3-5B 3-5C	382 382 382 382 382 378 398 398 398	16C November 1–3, 2016	10 Jan 2018, 13 Jan 2018, 23 Feb 2018
$^{16}O^{8+}$ (1 GeV/u)	40 cGy (3F)	1801[a] 1802[a] 1803[a] 1816[a] 1817[a] 1818[a] 198[a] 1990 1991	1-4A 1-4B 1-4C 2-4A 2-4B 2-4C 3- A 3-4B 3-4C	353 353 353 353 353 354 367 367 367	16C November 1–3, 2016	10 Jan 2018, 13 Jan 2018 , 23 Feb 2018
$^{28}Si^{14+}$ (1 GeV/u)	40 cGy (3F)	1798[a] 1799[a] 1800[a] 181[a] 1814[a] 1815[a]	1-3A 1-3B 1-3C 2-3A 2-3B 2-3C	293 293 293 296 296 296	16B June 15–17, 2016	10 Jan 2018, 13 Jan 2018

[a]Animals underwent Albira PET/CT, in September 2017.
[b](1F) = radiation delivered in 1 fraction, (3F) = radiation delivered in three fractions, separated in time by 1 day.

Irradiation

Irradiations were done at the NASA Space Radiation Laboratory (NSRL) located at Brookhaven National Laboratory (BNL). Groups of mice were placed in a multi-compartment ventilated chamber made of 5-mm thick Lucite (Figure 2). Each chamber held a single mouse and they were arranged one-deep along a rectangular grid containing many chambers. Unsedated mice were loaded quickly into their chambers and whole-body irradiated with 0 cGy (control), 40-cGy 1-GeV/u $^{28}Si^{14+}$ ions (delivered in 3 consecutive fractions (3F), 1 per day), 40-cGy 1-GeV/u $^{16}O^{8+}$ ions (delivered in 1 fraction (1F)), or 40-cGy 1-GeV/u $^{16}O^{8+}$ ions (3F, 1 per day). The isovelocity (1 GeV/u) $^{16}O^{8+}$ and $^{28}Si^{14+}$ ions have LET values of 14 and 44 keV/μm in water, respectively. Calculations using the software application SRIM showed that the LETs of these ions changed by less than 1% and 3%, respectively, upon traversing 5 cm of water. Another group was whole-body irradiated at BNL with 1 fraction of 662-keV gamma rays using a JL Shepherd Mark I irradiator (1 Gy/min) and given an absorbed dose of 150 cGy. Details of the mouse groups are provided in Table 1. All animal studies were approved by the IACUC at both Rutgers and BNL.

Spleen harvest and splenocyte isolation

The spleen plays significant roles in hematopoiesis, red blood cell clearance, and immunological functions. Its immunological functions are conducted primarily be the splenocytes (white blood cells in the spleen). There are many subpopulations of splenocytes such as T cells, B cells, and NK cells, each playing different roles in the immune system. Spleens were harvested from animals 1–1.5 yr after radiation exposure. Animals were given a ketamine/xylazine anesthetic cocktail, followed by cervical dislocation. Splenocytes were manually separated from the spleen by scraping the spleens over a wire mesh in RPMI medium with a rubber policeman, layered onto Histopaque® (Sigma-Aldrich) and centrifuged at 400 g for 30 min. The buffy coat layer containing splenocytes was carefully removed with a pipet, and the cells were washed and centrifuged in culture media twice at 400 g for 10 min and cell concentrations were then determined with a Coulter ZM cell counter.

Natural killer cytotoxic function assay

To assess the NK cell activity, YAC-1 cells were suspended in 1 ml fresh medium and labeled with 9.25 MBq (250 μCi) of ^{51}Cr sodium chromate (Perkin Elmer, NEZ30001MC (185 MBq/mL)) for 1 h at 37°C. Two washes with media were done to remove extracellular activity. After labeling, 5000 YAC-1 cells (targets, T) were seeded into wells of a 96 well plate in 0.1 ml medium. Splenocytes (effectors, E) were then seeded into the wells at effector:target (E:T) ratios of 12.5:1, 25:1, 50:1, and 100:1. The plate was then incubated for 5 h at 37°C and 95% air, 5% CO_2. After incubation, the plate was spun at 500 g for 5 min, and 100 μl aliquots of the supernatant were aliquoted in triplicate to 12 X 75 tubes for ^{51}Cr release measurement with a Cobra gamma counter (Packard). The intracellular ^{51}Cr is released when the NK cells lyse the target YAC-1 cells and therefore ^{51}Cr in the supernatant is used as a measure of cell kill. Accordingly, the ^{51}Cr gamma ray counts per minute (cpm) were recorded for each sample. The % Kill was calculated for each group, *i*, according to the standard chromium release assay as per Eq. 1.

$$\%\,\mathrm{Kill}_i = \frac{\overline{\mathrm{cpm}}_i - \overline{\mathrm{cpm}}_{\text{spontaneous release}}}{\overline{\mathrm{cpm}}_{\text{total release}} - \overline{\mathrm{cpm}}_{\text{spontaneous release}}}, \quad (1)$$

where cpm_i is for the supernatant of the test sample (targets + effectors), $\mathrm{cpm}_{\text{spontaneous release}}$ is for the supernatant of the target cell only sample (no effectors), and $\mathrm{cpm}_{\text{total release}}$ is for the supernatant of lysed sample (targets + effectors).

Splenic cell subpopulation characterization

To characterize radiation-induced changes in the representation of key subpopulations of the splenocytes, two million splenocytes were aliquoted into a 5-ml tube and stained with an antibody cocktail containing the following: BUV395 anti-CD3e (clone 145-2C11 BD Horizon™), Alexa Fluor 700 anti-CD4 (clone RM4-5 BioLegend®), PE/Cy7 anti-CD8a (clone 53–6.7 BioLegend®), FITC anti-CD45R/B220 (clone RA3-6 B2 BioLegend®), PE anti-IgM (clone RMM-1 BioLegend®), and Pacific blue anti-CD49b (clone DX5 BioLegend®). The stained cells were analyzed by flow cytometry using 6 color analysis on a BD LSRFortessa™ X-20 equipped with 5 lasers (355, 405, 488, 561, and 642 nm). Compensation parameters were set using single-stained OneComp® control beads (eBioScience) prior to samples being run. NK cells were identified as being CD4 negative ($CD4^-$), CD8 negative ($CD8^-$), IgM negative (IgM^-), B220R negative ($B220R^-$), CD49b positive ($CD49b^+$), and CD3 negative ($CD3^-$). The resulting FCS files were imported into FlowJo™ (BD) for gating analysis. Identification of splenocyte subpopulations is given in Table 2.

Analysis

Figures and statistical analysis for subpopulation characterization were done in SigmaPlot 14.5. One-way ANOVA using Bonferroni's method was used to determine if subpopulations were significantly affected. When the one-way ANOVA arrived at no significance ($p > 0.05$), then two-tailed t-tests for each treatment relative to control were conducted. Figures for NK cytotoxic function were created in SigmaPlot 14.5. The NK cytotoxicity data was analyzed for statistical significance in OriginPro® (OriginLab®) using F tests that compared unweighted linear least-squares fits for each dataset with that of control.

Results

Changes in $CD4_+$ and natural killer cell populations

The relative number of splenocytes that were harvested from each group is plotted in Figure 3A. The number of splenocytes in the spleens of irradiated mice were not significantly different than controls when tested with the one-way ANOVA. However, t-tests between individual groups and control indicated that the 150-cGy gamma-ray treated mice had significantly more splenocytes compared to unirradiated control ($p = 0.023$, Figure 3A). In contrast, mice exposed to a single fraction or fractionated schedule of the selected ions showed no significant changes in splenocyte number compared to control (Figure 3A).

A one-way ANOVA indicated that the percentages of $CD4^+$ T_h lymphocytes in each group of irradiated animals were not significantly different than in the control group. However, it did give significance when irradiated groups taken together were compared to the control group ($p = 0.026$, Figure 3B). Finally, a one-way ANOVA did give significance when pairwise comparing the $^{16}O^{8+}$ single-fraction treated animals and the gamma-ray treated animals ($p = 0.038$). No significant changes were found among the $CD8^+$ T_c lymphocyte and B lymphocyte populations among any of the groups (Figures 3C,D).

Finally, a one-way ANOVA indicated that the percentages of NK cells in each group of irradiated animals were not significantly different than in the control group. However, a *t*-test indicated that the 150-cGy gamma-ray treated mice demonstrated a decrease in percentage of NK cells when compared to unirradiated control ($p = 0.052$, Figure 3E).

TABLE 2 Cell surface markers used to identify splenocyte subpopulations.

	CD3e	CD4	CD8a	CD45R	IgM	CD49b
Mature B lymphocytes	−	−	−	+	++	−
Immature B lymphocytes	−	−	−	+	+	−
Pro-pre B lymphocytes	−	−	−	+	−	−
$CD4_+$ T_h lymphocytes	+	+	−	−	−	−
$CD8_+$ T_c lymphocytes	+	−	+	−	−	−
NK cells	−	−	−	−	−	+

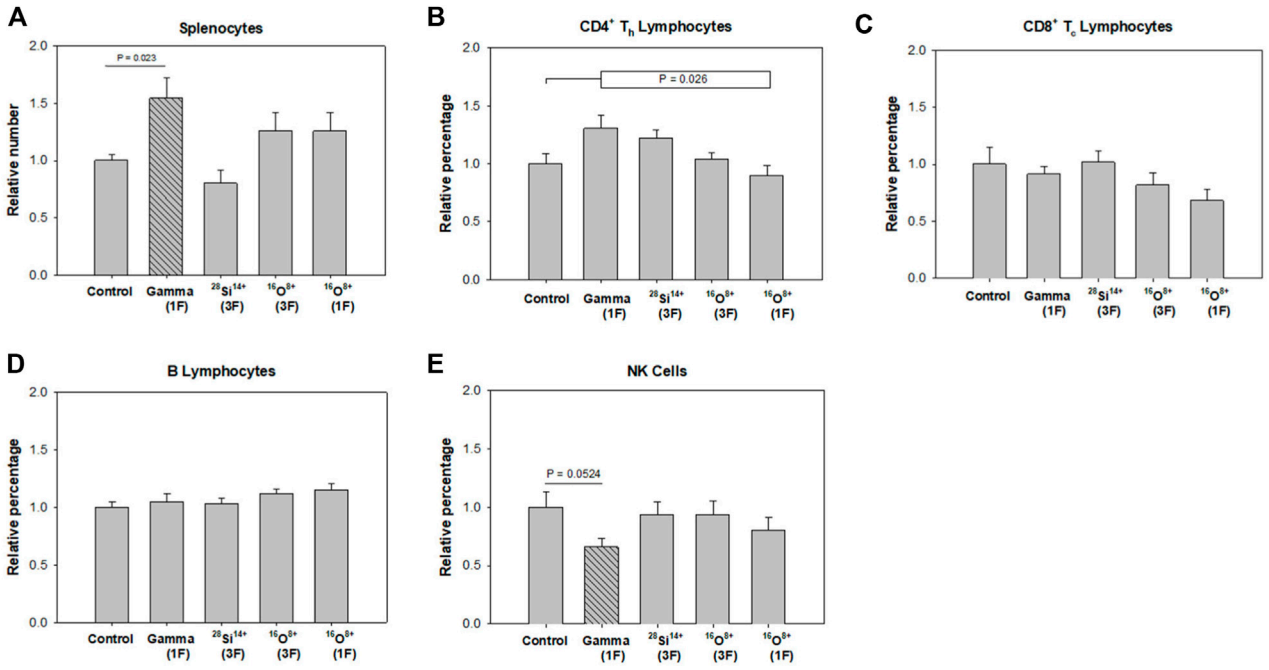

FIGURE 3
Changes in splenocyte numbers and splenocyte subpopulation percentages relative to unirradiated controls at 1–1.5 yr after irradiation of 10-month old mice with 0 cGy (Control, n = 13), 150-cGy gamma-rays in a single fraction [Gamma (1F), n = 6], 40-cGy $^{28}Si^{14+}$ given in three fractions [$^{28}Si^{14+}$ (3F), n = 6], 40-cGy $^{16}O^{8+}$ given in three fractions [$^{16}O^{8+}$ (3F), n = 12], and 40-cGy $^{16}O^{8+}$ given as a single fraction [$^{16}O^{8+}$ (1F), n = 12]. **(A)** splenocytes, **(B)** $CD4_+$ T_h lymphocytes, **(C)** $CD8_+$ Tc lymphocytes, **(D)** B lymphocytes, **(E)** NK cells. Error bars are standard error of the mean. The cross-hatched bars indicate a statistically significant difference ($p < 0.05$) from control.

Cytotoxic function of natural killer cells

The %Kill are plotted as a function of E:T ratios for each irradiation condition (Figure 4). The 150-cGy gamma-ray treated mice were shown to have significantly decreased NK cytotoxic function compared to sham-irradiated control ($p = 7.55 \times 10^{-4}$). The fractionated 40-cGy $^{28}Si^{14+}$ treated mice showed no significant difference (p = 0.74). The single-fraction 40-cGy $^{16}O^{8+}$ treated mice also did not show any significant difference compared to control (p = 0.63), however the fractionated 40-cGy $^{16}O^{8+}$ treated mice showed significant decreases in NK cytotoxic function compared to control (p = 0.0036).

Discussion

Given that alterations in size and function of NK populations can have a significant impact on long-term health, our studies on HZE-radiation-induced changes in NK cells are important for risk assessment for astronauts that conduct extended missions in space. The mice used in this study were 10 months old at irradiation, corresponding to a typical middle-aged adult astronaut, while the 1–1.5 yr assay timepoint was intended to correspond to the time required for a retired astronaut to reach a geriatric stage of life. This timepoint was selected to determine whether an astronaut's radiation exposure during their career would have lasting effects on NK cells, at a stage of life where overall immunity has decreased with age and cancer susceptibility has increased. Our 150-cGy gamma-ray positive control group showed a depressed splenic NK cell population percentage even 1–1.5 yr post-exposure when compared to the sham-irradiated negative control (Figure 3E). Additionally, these mice demonstrated significantly decreased NK cytotoxic function (Figure 4A), which would translate to impaired ability to combat both viral infections as well as precancerous cells. Interestingly, despite an unaltered splenic NK cell population percentage (Figure 3E), the fractionated 40-cGy $^{16}O^{8+}$ treated mice also demonstrated a significant decrease in NK cytotoxic function (Figure 4C). This contrasts the response to single-fraction 40-cGy $^{16}O^{8+}$ (Figure 4D) and fractionated 40-cGy $^{28}Si^{14+}$ treated mice (Figure 4B), which both demonstrated no significant differences in either splenic NK population size or NK cytotoxic function. Curiously, despite their lower LET, fractionated $^{16}O^{8+}$ ions (14 keV/μm) had a greater impact on NK cytotoxic function than $^{28}Si^{14+}$ ions (44 keV/μm). These results suggest that NK cytotoxic function may be altered by exposure to HZE particles on a specific heavy ion basis rather than simply on an LET basis, although it should be noted that the sample size for $^{28}Si^{14+}$ ions is small (n = 6).

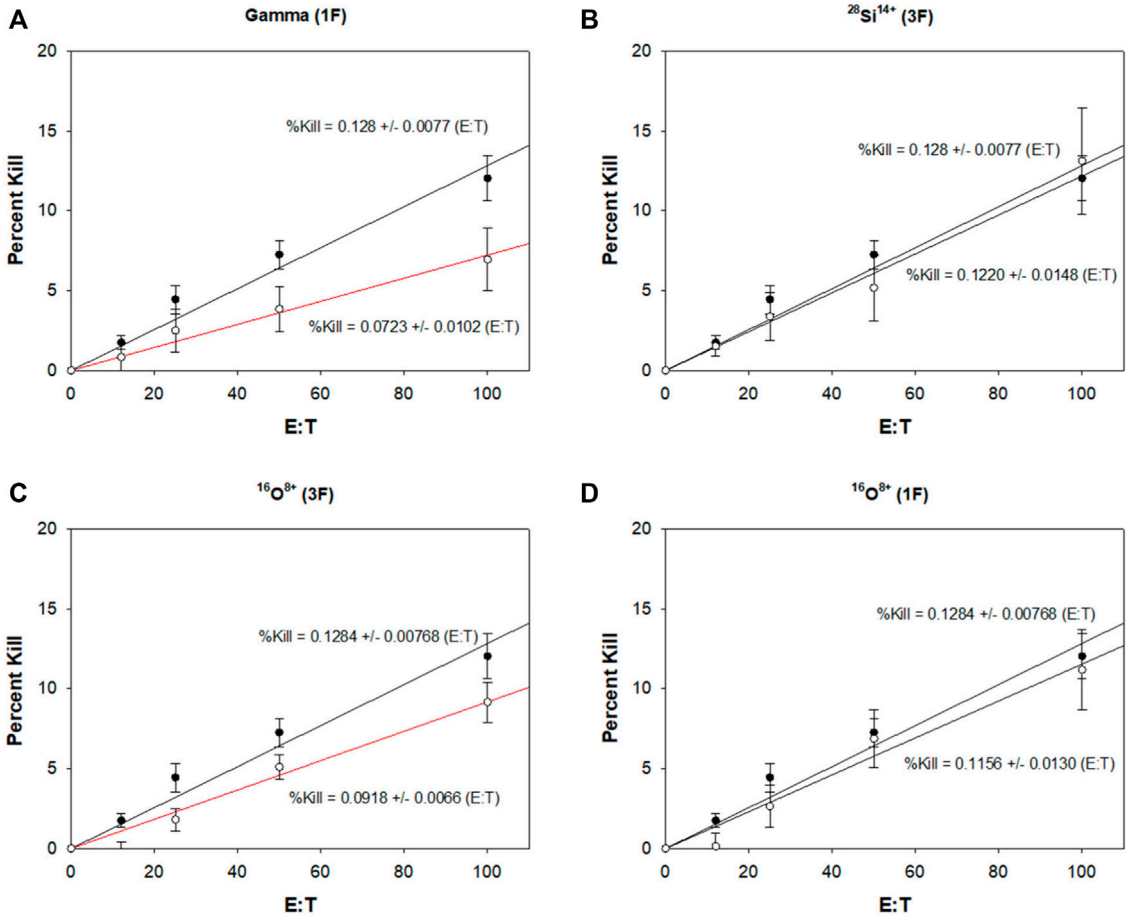

FIGURE 4
Effects of heavy ion exposure on NK cell cytotoxic function 1–1.5 yr after irradiation of 10-month old mice. Unirradiated controls (●, $n = 13$) are shown in each plot. **(A)** 150-cGy gamma rays given in a single fraction [Gamma (1F), $n = 6$], **(B)** 40-cGy $^{28}Si^{14+}$ given in three fractions [$^{28}Si^{14+}$ (3F), $n = 6$], **(C)** 40-cGy $^{16}O^{8+}$ given in three fractions [$^{16}O^{8+}$ (3F), $n = 12$], and **(D)** 40-cGy $^{16}O^{8+}$ given as a single fraction ($^{16}O^{8+}$ (1F), $n = 12$). Linear least squares fits to the data are indicated by the solid lines. The slopes and their standard error are provided for each fit. Significance relative to controls is denoted by the red lines for $p < 0.05$. Both gamma (1F) and $^{16}O^{8+}$ (3F) treatment groups demonstrated decreased NK cytotoxic function compared to control. Error bars are standard error of the mean.

Furthermore, the exposure schedule may also play a role in determining whether NK cell function is impacted. Given that in deep space every cell in the body will be traversed by a low-LET proton once every 3–4 days, and an HZE ion every few months (Kerr, 2013), the fractionated regimens used in this work are more akin to space exposures than the single fraction. Therefore, the fact that NK cytotoxic function was affected long after exposure to fractionated 40-cGy $^{16}O^{8+}$ and not by the single-fraction 40-cGy $^{16}O^{8+}$ is significant and warrants further exploration with this and other HZE particles. Furthermore, it is notable that the NK cell population percentage was similar to control in this case (Figure 3E), yet the NK cells demonstrated impaired cytotoxic function (Figure 4C). When taking into consideration that the radiation exposure will be a fractionated mix of HZE particles during spaceflight, these results suggest long-term overall suppression and decreased function of the NK cells, which in turn may lead to elevated risk to both cancer and viral infections. This conclusion is tempered by the fact that animals were not irradiated with a mixture of protons and HZE ions. As stated above, a given cell in the astronaut's body will be traversed by low-LET protons before being traversed by an HZE ion. It has been demonstrated that pre-exposure with protons can mitigate adverse effects of a subsequent exposure to HZE particles (Buonanno et al., 2015; Fornalski et al., 2022). As summarized in a recent report from the National Aeronautics and Space Agency (NASA), there is considerable experimental evidence for adaptive responses (Huff et al., 2016). Others have discussed the data from astronauts on the International Space Station (ISS) who were tested for chromosome aberrations before, after 1 mission, and then again after a 2nd mission (Chancellor et al., 2014). Aberrations were increased after the first mission but decreased over time to an above pre-mission level, and

then did not increase further after the second mission. The evidence for adaptive responses has prompted proposals to select astronauts for deep space missions based on their intrinsic capacity for robust adaptive responses (Mortazavi et al., 2003; Bevelacqua and Mortazavi, 2017). Their adaptive responses for a variety of biological endpoints could be tested *in vitro* in ground-based studies using tissues from prospective astronauts (Mortazavi et al., 2003). Such an approach could use exposure sequences comprised of protons and HZE ions using the NSRL galactic cosmic ray simulator for rapid sequences of the different radiations, or spaced further in time using protons first, followed by HZE ions.

One area of note is that the mice used in this study were male. Differences in immune response due to sexual dimorphism have been well documented; for instance, females were found to have lower incidences of bacterial, viral, and parasitic infections, but higher incidences of autoimmune diseases when compared to males (Shepherd et al., 2020). A study on NK degranulation activity in response to Hepatitis B viral infection also found higher levels of spontaneous degranulation in female patients compared to their male counterparts, despite identical degranulation capacity (Macek Jilkova et al., 2017). Hirokawa et al. showed greater rate of decline in NK cell number in aging males (Hirokawa et al., 2013). Additionally, better NK cell function was observed in healthy elderly females by Al-Attar et al. (2016). Therefore, additional studies of how NK cell function is affected after space radiation exposure in females must be considered.

Data availability statement

The original contributions presented in the study are included in the article, further inquiries can be directed to the corresponding author.

Ethics statement

The animal study was reviewed and approved by the Rutgers IACUC, Brookhaven National Laboratory IACUC.

Author contributions

CL performed flow cytometry and drafted manuscript. DH conducted NK cytoxicity assays. SD and EA planned and conducted irradiations. RH planned and analyzed NK cytotoxicity experiments, and edited manuscript.

Funding

This study was supported by NASA NNJ13ZSA002N and NIH R01 CA198073.

Acknowledgments

This work benefitted from the technical support of the NJMS Flow Cytometry and Immunology Core Laboratory and the NJMS Confocal Imaging Facility. The authors thank Drs. Jason Domogauer and Nicholas Colangelo for assisting with irradiations, and Dr. Lisamarie Moore, Dr. Jianbo Guo, and Dr. Shravanthi Chidambaram for cataloging and dissections. Also thanks to Adam Rusek's team at the NASA NSRL.

Conflict of interest

The authors declare that the research was conducted in the absence of any commercial or financial relationships that could be construed as a potential conflict of interest.

Publisher's note

References

Abel, A. M., Yang, C., Thakar, M. S., and Malarkannan, S. (2018). Natural killer cells: Development, maturation, and clinical utilization. *Front. Immunol.* 9, 1869. doi:10.3389/fimmu.2018.01869

Al-Attar, A., Presnell, S. R., Peterson, C. A., Thomas, D. T., and Lutz, C. T. (2016). The effect of sex on immune cells in healthy aging: Elderly women have more robust natural killer lymphocytes than do elderly men. *Mech. Ageing Dev.* 156, 25–33. doi:10.1016/j.mad.2016.04.001

Beaulieu, A. M. (2021). Transcriptional and epigenetic regulation of memory NK cell responses. *Immunol. Rev.* 300 (1), 125–133. doi:10.1111/imr.12947

Bevelacqua, J. J., and Mortazavi, S. M. J. (2017). Commentary: Human pathophysiological adaptations to the space environment. *Front. Physiol.* 8, 1116. doi:10.3389/fphys.2017.01116

Bielefeldt-Ohmann, H., Genik, P. C., Fallgren, C. M., Ullrich, R. L., and Weil, M. M. (2012). Animal studies of charged particle-induced carcinogenesis. *Health Phys.* 103 (5), 568–576. doi:10.1097/HP.0b013e318265a257

Boerma, M., Nelson, G. A., Sridharan, V., Mao, X. W., Koturbash, I., and Hauer-Jensen, M. (2015a). Space radiation and cardiovascular disease risk. *World J. Cardiol.* 7 (12), 882–888. doi:10.4330/wjc.v7.i12.882

Boerma, M., Singh, P., Sridharan, V., Tripathi, P., Sharma, S., and Singh, S. P. (2015b). Effects of local heart irradiation in a glutathione S-transferase alpha 4-null mouse model. *Radiat. Res.* 183 (6), 610–619. doi:10.1667/RR13979.1

Buchheim, J. I., Matzel, S., Rykova, M., Vassilieva, G., Ponomarev, S., Nichiporuk, I., et al. (2019). Stress related shift toward inflammaging in cosmonauts after long-duration space flight. *Front. Physiol.* 10, 85. doi:10.3389/fphys.2019.00085

Buonanno, M., de Toledo, S. M., and Azzam, E. I. (2011). Increased frequency of spontaneous neoplastic transformation in progeny of bystander cells from cultures exposed to densely ionizing radiation. *PLoS One* 6 (6), e21540. doi:10.1371/journal.pone.0021540

Buonanno, M., De Toledo, S. M., Howell, R. W., and Azzam, E. I. (2015). Low-dose energetic protons induce adaptive and bystander effects that protect human cells against DNA damage caused by a subsequent exposure to energetic iron ions. *J. Radiat. Res.* 56 (3), 502–508. doi:10.1093/jrr/rrv005

Chancellor, J. C., Scott, G. B., and Sutton, J. P. (2014). Space radiation: The number one risk to astronaut health beyond low Earth orbit. *Life (Basel)* 4 (3), 491–510. doi:10.3390/life4030491

Chiossone, L., Dumas, P. Y., Vienne, M., and Vivier, E. (2018). Natural killer cells and other innate lymphoid cells in cancer. *Nat. Rev. Immunol.* 18 (11), 671–688. doi:10.1038/s41577-018-0061-z

Coca, S., Perez-Piqueras, J., Martinez, D., Colmenarejo, A., Saez, M. A., Vallejo, C., et al. (1997). The prognostic significance of intratumoral natural killer cells in patients with colorectal carcinoma. *Cancer* 79 (12), 2320–2328. -p. doi:10.1002/(sici)1097-0142(19970615)79:12<2320::aid-cncr5>3.0.co;2-p

Crucian, B. E., Makedonas, G., Sams, C. F., Pierson, D. L., Simpson, R., Stowe, R. P., et al. (2020). Countermeasures-based improvements in stress, immune system dysregulation and latent herpesvirus reactivation onboard the international space station - relevance for deep space missions and terrestrial medicine. *Neurosci. Biobehav. Rev.* 115, 68–76. doi:10.1016/j.neubiorev.2020.05.007

Crucian, B., Stowe, R., Mehta, S., Uchakin, P., Quiriarte, H., Pierson, D., et al. (2013). Immune system dysregulation occurs during short duration spaceflight on board the space shuttle. *J. Clin. Immunol.* 33 (2), 456–465. doi:10.1007/s10875-012-9824-7

Cucinotta, F. A., Kim, M.-H. Y., Willingham, V., and George, K. A. (2008). Physical and biological organ dosimetry analysis for international space station astronauts. *Radiat. Res.* 170 (1), 127–138. doi:10.1667/rr1330.1

Cucinotta, F. A., Kim, M. H. Y., and Chappell, L. J. (2012). *Space radiation cancer risk projections and uncertainties*. Springfield, VA: National Technical Information Service. TP-2013-0217375. doi:10.13140/RG.2.1.1413.3528

Fornalski, K. W., Adamowski, L., Dobrzynski, L., Jarmakiewicz, R., Powojska, A., and Reszczynska, J. (2022). The radiation adaptive response and priming dose influence: The quantification of the raper-yonezawa effect and its three-parameter model for postradiation DNA lesions and mutations. *Radiat. Environ. Biophys.* 61 (2), 221–239. doi:10.1007/s00411-022-00963-9

Garrett-Bakelman, F. E., Darshi, M., Green, S. J., Gur, R. C., Lin, L., Macias, B. R., et al. (2019). The NASA twins study: A multidimensional analysis of a year-long human spaceflight. *Science* 364 (6436), eaau8650. doi:10.1126/science.aau8650

Heylmann, D., Rodel, F., Kindler, T., and Kaina, B. (2014). Radiation sensitivity of human and murine peripheral blood lymphocytes, stem and progenitor cells. *Biochimica Biophysica Acta - Rev. Cancer* 1846 (1), 121–129. doi:10.1016/j.bbcan.2014.04.009

Hirokawa, K., Utsuyama, M., Hayashi, Y., Kitagawa, M., Makinodan, T., and Fulop, T. (2013). Slower immune system aging in women versus men in the Japanese population. *Immun. Ageing* 10 (1), 19. doi:10.1186/1742-4933-10-19

Huff, J., Carnell, L., Blattnig, S., Chappell, L., George, K., Lumpkins, S., et al. (2016). *Evidence report: Risk of radiation carcinogenesis*. Springfield, VA: National Technical Information Service. JSC-CN-35748.

Ikeda, H., and Togashi, Y. (2022). Aging, cancer, and antitumor immunity. *Int. J. Clin. Oncol.* 27 (2), 316–322. doi:10.1007/s10147-021-01913-z

Imai, K., Matsuyama, S., Miyake, S., Suga, K., and Nakachi, K. (2000). Natural cytotoxic activity of peripheral-blood lymphocytes and cancer incidence: An 11-year follow-up study of a general population. *Lancet* 356 (9244), 1795–1799. doi:10.1016/S0140-6736(00)03231-1

Ishigami, S., Natsugoe, S., Tokuda, K., Nakajo, A., Che, X., Iwashige, H., et al. (2000a). Prognostic value of intratumoral natural killer cells in gastric carcinoma. *Cancer* 88 (3), 577–583. doi:10.1002/(sici)1097-0142(20000201)88:3<577::aid-cncr13>3.0.co;2-v

Ishigami, S., Natsugoe, S., Tokuda, K., Nakajo, A., Xiangming, C., Iwashige, H., et al. (2000b). Clinical impact of intratumoral natural killer cell and dendritic cell infiltration in gastric cancer. *Cancer Lett.* 159 (1), 103–108. doi:10.1016/s0304-3835(00)00542-5

Kajioka, E. H., Andres, M. L., Li, J., Mao, X. W., Moyers, M. F., Nelson, G. A., et al. (2000). Acute effects of whole-body proton irradiation on the immune system of the mouse. *Radiat. Res.* 153 (5), 587–594. doi:10.1667/0033-7587(2000)153[0587:aeowbp]2.0.co;2

Karre, K., Ljunggren, H. G., Piontek, G., and Kiessling, R. (1986). Selective rejection of H-2-deficient lymphoma variants suggests alternative immune defence strategy. *Nature* 319 (6055), 675–678. doi:10.1038/319675a0

Kerr, R. A. (2013). Radiation will make astronauts' trip to Mars even riskier. *Science* 340 (6136), 1031. doi:10.1126/science.340.6136.1031

Klein, P. M., Parihar, V. K., Szabo, G. G., Zoldi, M., Angulo, M. C., Allen, B. D., et al. (2021). Detrimental impacts of mixed-ion radiation on nervous system function. *Neurobiol. Dis.* 151, 105252. doi:10.1016/j.nbd.2021.105252

Konstantinova, I. V., Rykova, M., Meshkov, D., Peres, C., Husson, D., and Schmitt, D. A. (1995). Natural killer cells after ALTAIR mission. *Acta Astronaut.* 36 (8-12), 713–718. doi:10.1016/0094-5765(95)00161-1

Lesnyak, A., Sonnenfeld, G., Avery, L., Konstantinova, I., Rykova, M., Meshkov, D., et al. (1996). Effect of SLS-2 spaceflight on immunologic parameters of rats. *J. Appl. Physiol. (1985).* 81 (1), 178–182. doi:10.1152/jappl.1996.81.1.178

Mace, E. M., and Orange, J. S. (2016). Genetic causes of human NK cell deficiency and their effect on NK cell subsets. *Front. Immunol.* 7, 545. doi:10.3389/fimmu.2016.00545

Macek Jilkova, Z., Decaens, T., Marlu, A., Marche, H., Jouvin-Marche, E., and Marche, P. N. (2017). Sex differences in spontaneous degranulation activity of intrahepatic natural killer cells during chronic hepatitis B: Association with estradiol levels. *Mediat. Inflamm.* 2017, 1–5. doi:10.1155/2017/3214917

Mehta, S. K., Kaur, I., Grimm, E. A., Smid, C., Feeback, D. L., and Pierson, D. L. (2001 1985). Decreased non-MHC-restricted (CD56+) killer cell cytotoxicity after spaceflight. *J. Appl. Physiol. (1985).* 91 (4), 1814–1818. doi:10.1152/jappl.2001.91.4.1814

Moon, W. Y., and Powis, S. J. (2019). Does natural killer cell deficiency (NKD) increase the risk of cancer? NKD may increase the risk of some virus induced cancer. *Front. Immunol.* 10, 1703. doi:10.3389/fimmu.2019.01703

Mortazavi, S. M., Cameron, J. R., and Niroomand-rad, A. (2003). Adaptive response studies may help choose astronauts for long-term space travel. *Adv. Space Res.* 31 (6), 1543–1551. doi:10.1016/s0273-1177(03)00089-9

Nakajima, T., Mizushima, N., and Kanai, K. (1987). Relationship between natural killer activity and development of hepatocellular carcinoma in patients with cirrhosis of the liver. *Jpn. J. Clin. Oncol.* 17 (4), 327–332.

NASA (2022). *NASA space flight human-system standard: Volume 1: Crew health*. National Aeronautics and Space Administration.Washington, DC, USA.

Orange, J. S. (2013). Natural killer cell deficiency. *J. Allergy Clin. Immunol.* 132 (3), 515–525. doi:10.1016/j.jaci.2013.07.020

Rykova, M. P., Sonnenfeld, G., Lesnyak, A. T., Taylor, G. R., Meshkov, D. O., Mandel, A. D., et al. (1992). Effect of spaceflight on natural killer cell activity. *J. Appl. Physiol. (1985).* 73 (2), 196S–200S. doi:10.1152/jappl.1992.73.2.S196

Shepherd, R., Cheung, A. S., Pang, K., Saffery, R., and Novakovic, B. (2020). Sexual dimorphism in innate immunity: The role of sex hormones and epigenetics. *Front. Immunol.* 11, 604000. doi:10.3389/fimmu.2020.604000

Villegas, F. R., Coca, S., Villarrubia, V. G., Jimenez, R., Chillon, M. J., Jareno, J., et al. (2002). Prognostic significance of tumor infiltrating natural killer cells subset CD57 in patients with squamous cell lung cancer. *Lung Cancer* 35 (1), 23–28. doi:10.1016/s0169-5002(01)00292-6

Vivier, E., Raulet, D. H., Moretta, A., Caligiuri, M. A., Zitvogel, L., Lanier, L. L., et al. (2011). Innate or adaptive immunity? The example of natural killer cells. *Science* 331 (6013), 44–49. doi:10.1126/science.1198687

Zingoni, A., Molfetta, R., Fionda, C., Soriani, A., Paolini, R., Cippitelli, M., et al. (2018). NKG2D and its ligands: "One for all, all for one. *Front. Immunol.* 9, 476. doi:10.3389/fimmu.2018.00476

frontiers | Frontiers in Astronomy and Space Sciences

TYPE Original Research
PUBLISHED 05 May 2023
DOI 10.3389/fspas.2023.1117811

OPEN ACCESS

EDITED BY
Alessandro Bartoloni,
National Institute of Nuclear Physics of Rome, Italy

REVIEWED BY
Charlot Vandevoorde,
Helmholtz Association of German Research Centres (HZ), Germany
Giulia Tomagra,
University of Turin, Italy

*CORRESPONDENCE
Christopher D. Porada,
cporada@wakehealth.edu

†These authors have contributed equally to this work

‡These authors share senior authorship

RECEIVED 06 December 2022
ACCEPTED 21 April 2023
PUBLISHED 05 May 2023

CITATION
Diaz J, Kuhlman BM, Edenhoffer NP, Evans AC, Martin KA, Guida P, Rusek A, Atala A, Coleman MA, Wilson PF, Almeida-Porada G and Porada CD (2023), Immediate effects of acute Mars mission equivalent doses of SEP and GCR radiation on the murine gastrointestinal system-protective effects of curcumin-loaded nanolipoprotein particles (cNLPs). *Front. Astron. Space Sci.* 10:1117811. doi: 10.3389/fspas.2023.1117811

Immediate effects of acute Mars mission equivalent doses of SEP and GCR radiation on the murine gastrointestinal system-protective effects of curcumin-loaded nanolipoprotein particles (cNLPs)

Jonathan Diaz[1†], Bradford M. Kuhlman[1†], Nicholas P. Edenhoffer[1], Angela C. Evans[2,3], Kelly A. Martin[3], Peter Guida[4], Adam Rusek[4], Anthony Atala[1], Matthew A. Coleman[2,3], Paul F. Wilson[2,5‡], Graça Almeida-Porada[1‡] and Christopher D. Porada[1*‡]

[1]Wake Forest Institute for Regenerative Medicine, Winston Salem, NC, United States, [2]Department of Radiation Oncology, University of California Davis School of Medicine, Sacramento, CA, United States, [3]Biosciences and Biotechnology Division, Lawrence Livermore National Laboratory, Livermore, CA, United States, [4]NASA Space Radiation Laboratory, Brookhaven National Laboratory, Upton, NY, United States, [5]Biological Sciences Division, Pacific Northwest National Laboratory, Richland, WA, United States

Introduction: Missions beyond low Earth orbit (LEO) will expose astronauts to ionizing radiation (IR) in the form of solar energetic particles (SEP) and galactic cosmic rays (GCR) including high atomic number and energy (HZE) nuclei. The gastrointestinal (GI) system is documented to be highly radiosensitive with even relatively low dose IR exposures capable of inducing mucosal lesions and disrupting epithelial barrier function. IR is also an established risk factor for colorectal cancer (CRC) with several studies examining long-term GI effects of SEP/GCR exposure using tumor-prone APC mouse models. Studies of acute short-term effects of modeled space radiation exposures in wildtype mouse models are more limited and necessary to better define charged particle-induced GI pathologies and test novel medical countermeasures (MCMs) to promote astronaut safety.

Methods: In this study, we performed ground-based studies where male and female C57BL/6J mice were exposed to γ-rays, 50 MeV protons, or 1 GeV/n Fe-56 ions at the NASA Space Radiation Laboratory (NSRL) with histology and immunohistochemistry endpoints measured in the first 24 h post-irradiation to define immediate SEP/GCR-induced GI alterations.

Results: Our data show that unlike matched γ-ray controls, acute exposures to protons and iron ions disrupts intestinal function and induces mucosal lesions, vascular congestion, epithelial barrier breakdown, and marked enlargement of mucosa-associated lymphoid tissue. We also measured kinetics of DNA double-strand break (DSB) repair using gamma-H2AX- specific antibodies and apoptosis via TUNEL labeling, noting the induction and disappearance of extranuclear cytoplasmic DNA marked by gamma-H2AX only in the charged particle-irradiated samples. We show that 18 h pre-treatment with curcumin-loaded

nanolipoprotein particles (cNLPs) delivered via IV injection reduces DSB-associated foci levels and apoptosis and restore crypt villi lengths.

Discussion: These data improve our understanding of physiological alterations in the GI tract immediately following exposures to modeled space radiations and demonstrates effectiveness of a promising space radiation MCM.

KEYWORDS

space radiation, HZE exposure, gastrointestinal, DNA damage, apoptosis, H2AX foci, curcumin, countermeasure

Introduction

During future missions beyond low Earth orbit (LEO), such as those planned to the Moon, near-Earth asteroids, and Mars, astronauts will face poorly defined health risks as a result of exposure to the complex space ionizing radiation (IR) environment consisting of solar energetic particles (SEP) including protons and light ions and galactic cosmic rays (GCR) ranging from high-energy protons to high atomic number and energy (HZE) charged particles, often referred to as heavy ions. Although heavy ion fluences are orders of magnitude lower than proton and He-4 ions, their associated high linear energy transfer (LET) and correspondingly higher relative biological effectiveness (RBE) values results in them delivering a large portion of the overall dose equivalent that an astronaut will receive during an extended mission. SEP/GCR exposures are chronic, low dose-rate (LDR) on the order of 0.5–1 mGy/day in deep space and ~0.2–0.4 mGy/day on the surfaces of Mars and the Moon with additional dose contributions on these surfaces from albedo neutrons, gamma rays, and other charged particle types (Durante and Cucinotta, 2011; Zeitlin et al., 2013; Hassler et al., 2014; Zhang et al., 2020). Sporadic solar particle events (SPEs) however present a relatively high dose-rate (HDR) exposure scenario whereby an astronaut could potentially receive a dose of ~0.5–1 Gy within minutes to hours capable of generating symptoms of gastrointestinal (GI) syndrome-associated acute radiation sickness (ARS) (Townsend, 2005; Kim et al., 2009; Townsend et al., 2018). Long-duration spaceflight can result in the accumulation of IR exposures that may reach or exceed NASA career exposure limits (600 mSv weighted dose equivalent)—potentially producing both short- and long-term deleterious effects on human physiological systems that may limit mission success and increase risks of central nervous system (CNS) disruption, cardiovascular disease (CVD), and cancer morbidity/mortality in astronauts (Cucinotta et al., 2001; Townsend, 2005; Cucinotta and Durante, 2006; Durante and Cucinotta, 2008; Rodman et al., 2017; Almeida-Porada et al., 2018; Onorato et al., 2020; Simonsen et al., 2020). Physical, biological, and pharmacological-based radiation protection and mitigation strategies will be required to ensure successful mission outcomes, complete with charged particle-specific radiation medical countermeasures (MCMs) that are easily administered, can safely be stored long-term and maintain efficacy, and show beneficial effects in multiple radiosensitive tissue compartments, e.g., the bone marrow (BM) niche and gastrointestinal (GI) tract (Bokhari et al., 2022; DiCarlo et al., 2022).

With research being conducted in this area at ground-based charged particle accelerator facilities and aboard the International Space Station (ISS), our understanding of the biological effects resulting from exposures to this unique/complex radiation environment is still incomplete and complicated by the paucity of human epidemiological studies for these more exotic radiation types. This makes it difficult to accurately extrapolate disease risks from terrestrial radiation exposures from low linear energy transfer (LET) photon radiations and high LET alpha particles from inhaled radon/radon progeny. Accelerated HZE ions can have orders of magnitude higher LET values compared to photons and low dose exposures (≤50 cGy) of both low LET protons and intermediate to high LET heavy ions have been shown to directly induce complex, difficult to repair clusters of double-strand breaks (DSB) and other DNA lesion types in highly-localized DNA regions (Sutherland et al., 2000; Sutherland et al., 2001; Saha et al., 2014; Bennett et al., 2022) whose proper repair is exacerbated in microgravity conditions (Moreno-Villanueva et al., 2017; Hada et al., 2018; Low et al., 2018; Yamanouchi et al., 2020; Beheshti et al., 2021).

It is well documented that the GI system constitutes one of the most radiosensitive tissues of the body, and sensitive to the direct (DNA damaging) and indirect (inflammation-associated) effects of IR exposures. This is due to high turnover rates of the intestinal epithelium, a process fueled by intestinal stem cell (ISC) division and differentiation originating from the base of intestinal crypts up to postmitotic cells at the upper villi positions (Clevers, 2013). Low dose IR exposures have been shown to induce crypt cell apoptosis and lead to mucosal lesions and loss of epithelial barrier function, which increases mucosal permeability, nutrient and fluid loss, and gut pathogen infiltration. The net effect of these insults is the establishment of a state of chronic mucosal inflammation resulting in tissue loss and fibrosis (Shadad et al., 2013; Takiishi et al., 2017; Chen et al., 2021). IR is an established risk factor for colorectal cancer (CRC) (Thompson et al., 1994; Pawel et al., 2008; Grant et al., 2017) and studies by the Fornace group demonstrated acute HDR exposures to accelerated protons and Fe-56 ions delivered at the NASA Space Radiation Laboratory (NSRL) resulted in long-term GI effects in wildtype C57BL/6J mice and significantly enhanced the development and progression of intestinal tumors in mice harboring mutations in the Apc gene (Trani et al., 2010; Datta et al., 2013; Trani et al., 2014; Kumar et al., 2018; Kumar et al., 2019; Suman et al., 2019; Suman et al., 2020; Suman et al., 2021). Fewer studies have investigated immediate short-term (≤24–48 h post-irradiation) acute GI effects following low dose charged particle irradiation using these mouse models. A study by Purgason et al. in BALB/c mice demonstrated decreased crypt cell proliferation, survival, and mucosal surface area along with the induction of apoptosis and

apoptosis-related gene expression for whole-body 250 MeV proton doses as low as 10 cGy (Purgason et al., 2018).

In this report, we performed ground-based studies at the NSRL with male and female 5–6-week-old C57BL/6J mice to better define GI responses immediately (≤24 h) following exposures to doses and ion species typical of the space radiation environment. These experiments were designed to serve as an *in vivo* analog to a series of *in vitro* experiments employing a human "gut-on-a-chip" microfluidic physiological systems (MPS) platform (Shah et al., 2016) used by our co-investigators (manuscript in preparation). We also tested the ability of intravenously delivered curcumin-laden nanolipoprotein particles (cNLPs) that we recently developed (Evans et al., 2022) as a potential medical countermeasure (MCM) to radioprotect the GI tract from the damaging effects of charged particle radiations. A wealth of literature supports curcumin's ability to modulate multiple IR- and cancer-associated pathways involved via its potent antioxidant properties, but its poor solubility and bioavailability has limited its therapeutic use (Weiss and Landauer, 2003; Akpolat et al., 2009; Wang et al., 2017; Kostova et al., 2021). We recently reported that packaging of curcumin in biomimetic nanolipoprotein particles (NLPs) greatly increases its solubility and stability, and pre- or post-IR treatment of human AG05965/MRC-5 fibroblasts with 27 μM cNLPs modulates the expression of multiple genes that regulate DNA repair including CDKN1A and BCL2, and confers both radioprotection and radiomitigation in non-cycling quiescent cultures (Evans et al., 2022). Unfortunately funding and NSRL facility access/cost limitations prevented us from doing longer-term evaluations of low dose-exposed mouse cohorts as well as investigating potential dose-rate effects to better mimic the chronic dose-rates encountered in deep space. The exposures we conducted are consistent with acute doses and dose-rates experienced during sporadic solar particle events (SPE) that can deliver 0.5–1 Gy doses of lower-energy protons and light ions (<100 MeV/n) within minutes to hours. Our results show that exposures to 50 MeV protons and 1 GeV/n Fe-56 ions induces marked structural and functional alterations, DSB-associated foci including extranuclear cytoplasmic DNA fragments marked with gamma-H2AX-specific antibodies, and apoptosis measured by TUNEL staining within intestinal sections recovered and processed from the exposed mice at 15 min to 24 h timepoints. Importantly, we also demonstrate that DSBs and apoptosis induction are reduced in mice pretreated for 18 h with cNLPs delivered intravenously by tail vein injection, with partial restoration of epithelial barrier length, providing evidence for *in vivo* radioprotection by this space radiation MCM candidate. It is our hope that these results will assist NASA in its efforts in space radiation risk assessment modeling and provide a safe nutraceutical-based MCM to promote astronaut safety during extended deep space missions.

Materials and methods

Mice husbandry and irradiations, dosimetry, and harvesting of the small intestine

All animal procedures were performed under protocols approved by the Institutional Animal Care and Use Committees (IACUC) at both Wake Forest University Health Sciences (WFUHS protocol A15-137) and Brookhaven National Laboratory (BNL protocol 500) following the Guide for the Care and Use of Laboratory Animals prepared by the Institute of Laboratory Animal Resources, National Research Council, and U.S. National Academy of Sciences. For this study, we exposed a total of 108 wildtype C57BL/6J mice (male and female) aged 5–6 weeks to the following IR types and doses at the NSRL and using the BNL Biology Department's J.L. Shepherd Mark I Model 68A cesium-137 cabinet irradiator:

1. Sham (0 cGy unirradiated control); n = 24
2. 100 cGy of 662 keV Cs-137 γ-rays (LET = 0.91 keV/μm); n = 24
3. 100 cGy of 50 MeV protons (LET = 1.26 keV/μm); n = 24
4. 50 cGy of 1 GeV/n Fe-56 ions (LET = 151.49 keV/μm); n = 36

Mice were purchased from Jackson Laboratories (Bar Harbor, ME, United States) and shipped directly to the Brookhaven National Laboratory Animal Facility (BLAF) in NY approximately 1 week prior to scheduled beam times to acclimate to the facility. Mice were housed communally 3–6 mice per cage under a 12-h light/dark cycle with standard mouse chow and filtered water provided *ad libitum*. On the mornings of scheduled beam times, all mice (those to be irradiated and the sham controls) were transported by BLAF personnel to the NSRL animal facility. Mice to be irradiated were loaded into individual clean Lucite mouse holders/boxes (3 × 1.5 × 1.5 inches) with pre-drilled air holes and placed in custom 6-box support frames in the NSRL animal facility minutes prior to scheduled beam time, transported into the target room, and exposed (6 mice at a time in a single 6-box support) un-anesthetized at room temperature on the NSRL beamline (≤1–2 min exposure times) after which they were immediately returned to their cages. To control for effects due to handling and/or stress, sham controls were also loaded into Lucite holders for 3 min and were then returned to their cages. To avoid any potential confounding effects caused by residual scattered radiation present in the target room, sham controls were kept in the animal housing room at NSRL, rather than performing "walk-in walk-out" controls by bringing them into the target room. Accelerated 50 MeV proton and 1 GeV/n Fe-56 ion doses were verified by the NSRL physics/dosimetry team using calibrated NIST-traceable ion chambers located upstream and downstream of the target position. Dosimetry of these NSRL mouse irradiations was modeled using the "Digimouse" digital mouse phantom and associated dosimetry calculations provided by Simonsen et al. (Simonsen et al., 2020) with delivered tissue doses within 6% of the prescribed doses. Dose rates ranged from 70.8 to 75.5 cGy/min and 49–50 cGy/min for the proton and iron ion irradiations respectively. Cesium-137 662 keV γ-ray irradiations were conducted as photon reference controls with un-anesthetized mice loaded into clean NSRL mouse holders with pre-drilled air holes and placed in a custom 6-box foam support frame at position #2 perpendicular to the source to ensure uniform dose distribution and irradiated with 100 cGy at a dose-rate of 140.85 cGy/min using the BNL Biology Department's J. L. Shepherd Mark I Model 68A cesium-137 cabinet irradiator. LET values for the IR types are: 1.26 keV/μm (50 MeV protons), 151.49 keV/μm (1 GeV/n Fe-56 ions), and 0.91 keV/μm (Cs-137 γ-ray-induced photoelectrons (ICRP, 2003)); dose to particle fluence conversions were

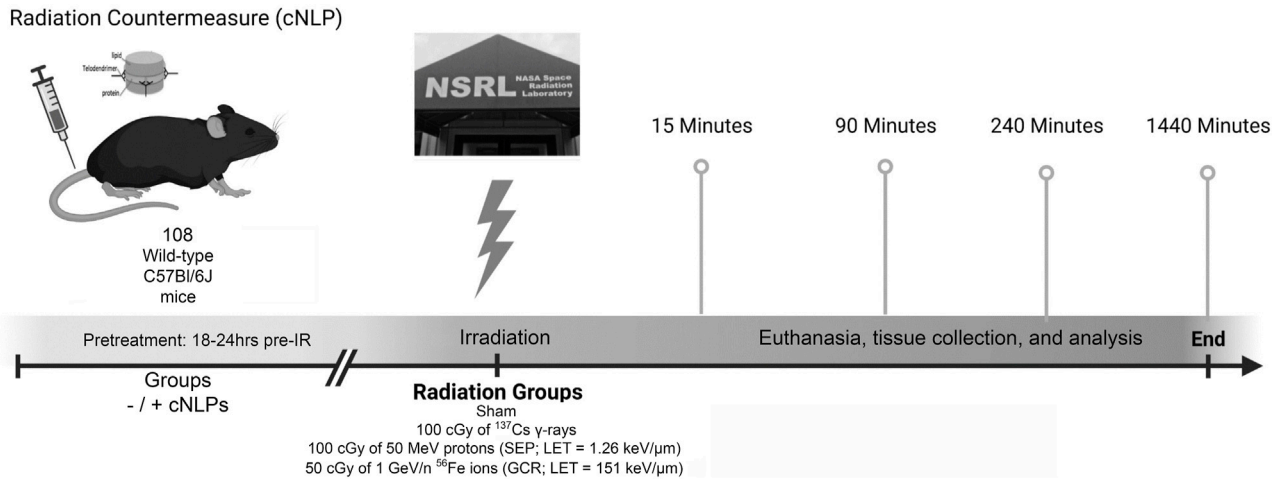

FIGURE 1
Diagrammatic representation of overall experimental design showing IR exposure schemes, pretreatment with cNLP GI MCM (+/−), and euthanasia/tissue collection times post-IR at which mice from each IR cohort were euthanized for analyses. *n* = 108 total C57BL/6J mice; specific IR exposure groups were as follows: sham (0 cGy control) *n* = 24 (18 without cNLPs, 6 with cNLPs); cesium-137 γ-rays (photon reference control) *n* = 24 (18 without cNLPs, 6 with cNLPs); 50 MeV protons (model SEP radiation) *n* = 24 (18 without cNLPs, 6 with cNLPs); 1 GeV/n Fe-56 ions (model GCR radiation) *n* = 36 (24 without cNLPs, 12 with cNLPs).

calculated according to (Schardt et al., 2010). Cohorts from each IR group and corresponding sham controls were euthanized by CO2 asphyxiation and cervical dislocation in either the NSRL or BLAF animal facilities at 15 min, 90 min, 4 h, and 24 h post-irradiation with the GI tract removed and fixed for subsequent immunohistochemical/immunocytochemical processing and staining (see below). Figure 1 shows an overview of the study design.

Curcumin nanolipoprotein particles

18–24 h prior to irradiation, cohorts of C57BL/6J mice from each IR group [6 mice (3M/3F) each from the n = 24 sham, gamma and proton groups and 12 mice (6M/6F) from the n = 36 iron ion groups] were injected with 27 μM (10 μg/mL) curcumin nanolipoprotein particles (cNLPs) in sterile Dulbecco's phosphate-buffered saline (D-PBS) via intravenous (IV) tail vein injection to test its ability to serve as a GI-specific space radiation MCM. Development, production, and characterization of these cNLPs as an *in vitro* radioprotector and radiomitigator in human cells is documented in (Evans et al., 2022). Briefly, cNLP solutions were prepared by resolubilizing lyophilized cNLPs prepared per (Evans et al., 2022) at the Lawrence Livermore National Laboratory (LLNL) in sterile water and subsequently diluting it 1:1 with PBS to 0.1 mg/mL with 100 μL injected into the tail vein under a warming lamp in the BLAF.

Histology, immunofluorescence, and immunohistochemistry

The duodenum of the small intestine was harvested from each mouse at the time of euthanasia (15 min, 90 min, 4 h, and 24 h post-irradiation) and prepared using a standard "Swiss-rolling" technique. Briefly, tissues were gently flushed with ice-cold PBS and fixed overnight in 10% neutral-buffered formalin (Leica Biosystems; 3,800,598). Following fixation, tissues were cut longitudinally, rolled, and placed into tissue cassettes for processing and paraffin embedding. 5-μm tissue sections were prepared via microtome and deposited on positively charged Superfrost® Plus Micro Slides (VWR, Radnor, PA). Slides were then deparaffinized and rehydrated and stained with hematoxylin and eosin using Leica ST5010 Autostainer XL automated processor or antigen retrieval was performed using either citrate buffer (eBioscience™ IHC Antigen Retrieval Solution—Low pH; Invitrogen/ThermoFisher Scientific, Waltham, MA; 00-4955-58) or EDTA buffer (eBioscience™ IHC Antigen Retrieval Solution—High pH; Invitrogen; 00-4956-58) per antigen of interest.

Tight junction length and integrity were assessed following EDTA antigen retrieval using a rabbit primary polyclonal antibody against Claudin-3 (Abcam; ab15102; 1:150 dilution) and AlexaFluor594-conjugated goat anti-rabbit IgG (H + L) secondary antibody (Invitrogen; A-11037; 1:500 dilution). Intestinal stem cells were stained following citrate antigen retrieval and permeabilization with 0.2% Triton X-100 for 5 min. Rat primary monoclonal antibody (Invitrogen; 14-9896-82; 1:200) against the ISC marker Musashi-1 and a rabbit primary polyclonal antibody against PCNA (Abcam; ab18197; 1:1000) were used, detected with Alexa Fluor® 488-conjugated donkey anti-goat IgG (H + L) (Abcam, ab150129) and Alexa Fluor® 594-conjugated goat anti-rabbit IgG secondary antibody secondary antibodies (Invitrogen/ThermoFisher Scientific; A-11037; 1:500 dilution) respectively. Sections were counterstained with 0.2-μg/mL DAPI (ThermoFisher Scientific; 62,248) and cover-slipped using ProLong Gold Antifade Reagent (ThermoFisher Scientific; P10144).

Duodenal samples were also processed at each time point post-IR for analysis of apoptosis via the terminal deoxynucleotidyl dUTP nick end-labeling (TUNEL) assay following the manufacturer's

instructions (Abcam; TUNEL Assay Kit HRP-DAB, ab206386). Each specimen was then counterstained with methyl green for 2 min and coverslipped with Permount (ThermoFisher Scientific). Sections from each duodenum were also subjected to immunofluorescence (IF) analysis using a rabbit primary monoclonal antibody to γ-H2AX pS139 (Abcam; ab81229; 1: 100 dilution) and Alexa Fluor® 488-conjugated goat anti-rabbit IgG (H + L) secondary antibody (Invitrogen/ThermoFisher Scientific, A-11034; 1:500 dilution) to establish levels and repair kinetics of DNA double-strand break (DSB)-associated nuclear foci induced by IR exposure. In brief, sections were permeabilized in Tris-buffered saline containing 0.2% Triton X-100 (TBS-T) followed by 24-h incubation at 4°C with the primary antibody. After 2 h of incubation at RT with the secondary antibody, sections were washed twice in TBS, counterstained with DAPI, and coverslipped using ProLong Gold Antifade Reagent (ThermoFisher Scientific; P10144). For all immunofluorescence assays, following permeabilization, each tissue section was treated with an autofluorescence quencher solution (TrueBlack® Lipofuscin, 23,007) to diminish background autofluorescence present in murine intestinal tissues. All morphological changes were assessed using brightfield microscopy (Leica DM4000B), and fluorescence imaging was performed on an Olympus FV1200 Spectral Laser scanning Confocal Microscope.

Histopathology analysis

Investigators who were blinded to sample identity/treatment group examined all H&E-stained tissue samples to assess GI tissue damage resulting from exposure to each IR dose/type. ImageJ software packages (NIH) were used to perform analysis of the images in this study. Throughout this manuscript, we used ImageJ to create specific macros with multiple functions to automate tasks including normalizing, processing, and analyzing large numbers of images. This included a normalizing step utilizing color deconvolution to separate images into component color channels, and tasks like sharpening and contrast leveling. The macro also included the "Subtract Background" function to isolate and analyze features in images above a uniform background intensity. After background removal, we used auto-thresholding algorithms, a common technique in image processing and analysis, to segment images into different regions based on pixel intensity values. The "Watershed" threshold segmentation algorithm function was used to separate touching or overlapping objects in the images by tracing the boundaries of objects and after normalizing, we used the "Analyze Particles" function to identify and measure features in the image. In some cases, it was necessary for us to fine-tune the image analysis parameters to obtain accurate results by "training" each dataset. We ran the macro multiple times, adjusting parameters as needed to improve overall performance and visually inspecting the results to ensure accuracy. All readings obtained via these custom macros were processed via Excel spreadsheets and were then imported into RStudio using the readxl package. The following GitHub link contains ImageJ algorithms and R scripts that were used for the analyses detailed in this manuscript:

https://github.com/jhd8593/ImageJ_IHC_Java.git

This approach enabled us to obtain unbiased quantitation of apoptotic TUNEL labeling, γ-H2AX foci, and Claudin-3-positive epithelial tight junction spacing within the small intestine of irradiated mice and unirradiated controls. Plots and statistical analysis were performed using RStudio. ANOVA analyses were used to determine significant differences between groups, and we performed pairwise t-tests with a Bonferroni correction to determine specific differences between group means. To assess "normality" of the data, we performed a Shapiro-Wilk test. For all datasets with sufficient "n" to yield a meaningful result via Shapiro-Wilk test (as this test is highly sensitive to sample size), we obtained p-values higher than 0.05, indicating that the null hypothesis cannot be rejected, and the data thus appear to be normally distributed.

Results

Histopathological findings after ionizing radiation exposure

Acute whole-body irradiation with 100 cGy of 50 MeV protons or 50 cGy of 1 GeV/n Fe-56 ions both induced marked swelling/enlargement of local lymph nodes in the duodenum of mice exposed to each of these ions by 24 h post-IR. Such swelling was not observed in either sham-irradiated or 100 cGy γ-ray-irradiated groups. Images of enlarged mucosa-associated lymphoid tissue from representative animals in each IR group are shown in Figure 2. While there was no evidence of mucosal ulcers, inflammation, or crypt epithelial degeneration at these immediate early timepoints post-IR, multiple structural alterations were seen in the animals exposed to the two charged particle types that were not present in the sham-irradiated or γ-ray groups, including vascular congestion (noted in red circles) and edema (noted in green circles) within the villi (Figure 3), as well as disruption of the lymphatics, specifically the lacteal, and occasional splitting of crypts. In addition, focal infiltration of neutrophils/granulocytes was observed in the lymph nodes of three of the mice exposed to Fe-56 ions but not in the other groups. However, as these alterations can occur on rare occasions in sentinel mice housed in animal facilities due to undetected infectious agents and were not present in all animals in each IR group, these findings when considered groupwise were not deemed to be "pathologically important" (although it is interesting that they only occurred in the charged particle-irradiated cohorts).

Epithelial barrier thinning and disruption

To determine modeled SEP/GCR radiation-induced effects on epithelial barrier functionality in the small intestine, we performed immunohistochemical staining with an antibody specific to Claudin-3, a tight junction-associated protein within villi epithelial cells that plays a critical role in the formation and maintenance of the barrier that separates cells of the gut from the intestinal lumen (Van Itallie and Anderson, 2006; Shim et al., 2015). Visual inspection of Claudin-3 staining intensity reveals that proton exposure led to mild disturbance of barrier function, while Fe-56 ion irradiation causes more disruption (Figure 4A). To obtain quantitative data regarding barrier function, we developed and utilized a custom ImageJ

10.3389/fspas.2023.1117811

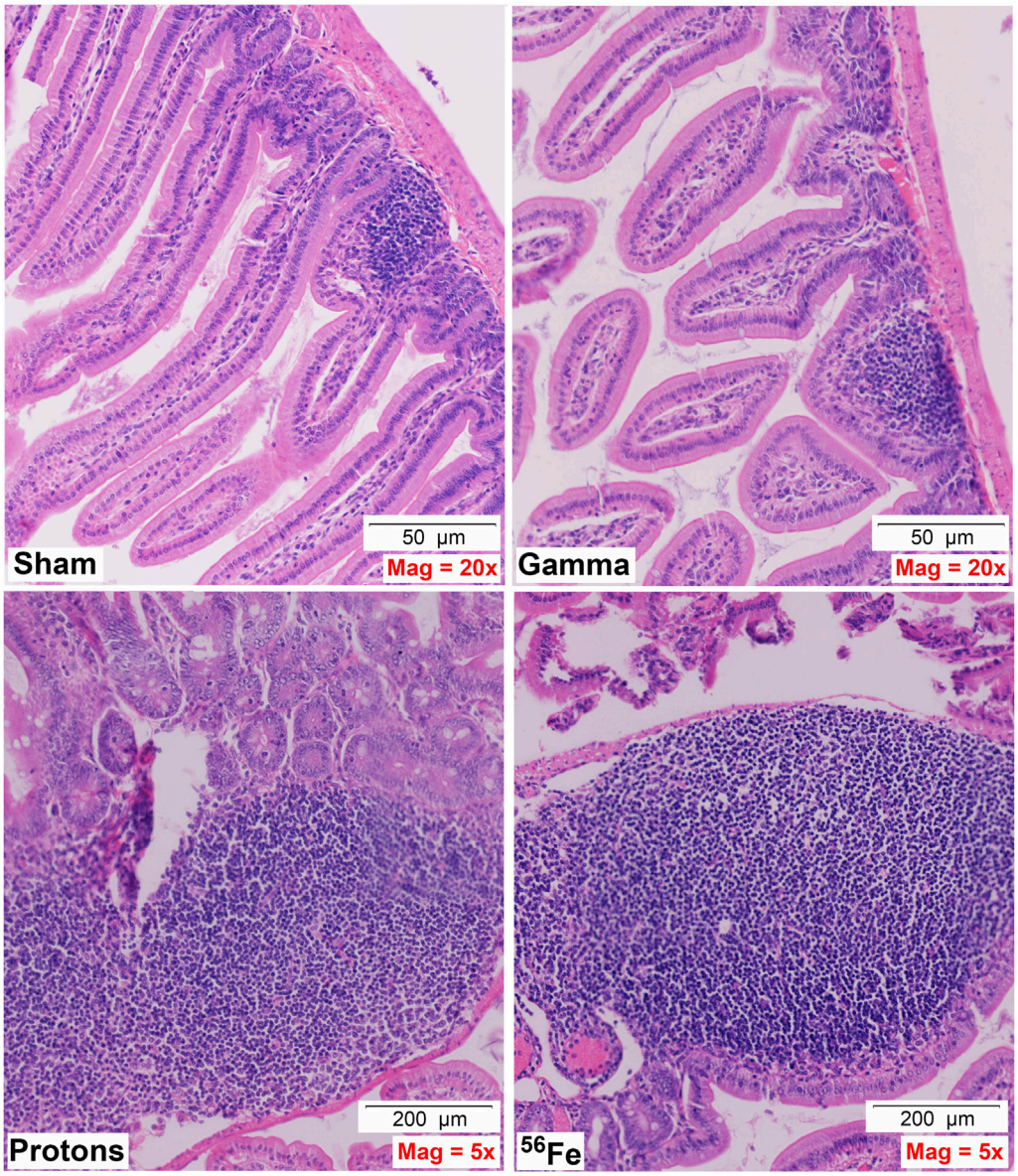

FIGURE 2
Representative H&E-stained sections of duodenal samples collected from C57BL/6J mice exposed to each IR scheme illustrating IR-associated swelling of lymph nodes/MALT (mucosa-associated lymphoid tissue)/Peyer's patches—note magnification for γ-ray exposure is ×20 to allow better visualization of the lymph node, while magnification for protons and Fe-56 ions is ×5 (50- or 200-μm scale bars, as marked).

script to analyze the immunofluorescence images, measuring the tight junctions of each villus with automated two-user polylines (Figure 4B). Multiple "regions of interest" (ROIs) were analyzed per section, and the script computed an average of 30 random μm-based measurements of the narrow junction (n = 3 ROIs per section). This unbiased quantitative approach confirmed our prior visual observations of Claudin-3 staining intensity that the tight epithelial junctions appeared to be reduced in length in duodenum samples of mice exposed to protons and especially in those animals exposed to Fe-56 ions as compared to sham-irradiated or γ-ray controls (Figure 4C).

Effects of SEP/GCR on the intestinal stem cell pool

The epithelium of the small intestine is continually replaced by intestinal stem cells (ISC) that reside within crypts at the base of each villus through carefully orchestrated processes of migration and differentiation. As such, IR-induced killing of ISC cells through accompanying mitotic cell death and apoptosis mechanisms can exert a pronounced deleterious effect on gut physiology and function by disrupting villi functioning and replenishment. To examine whether this occurred following proton or iron ion irradiation,

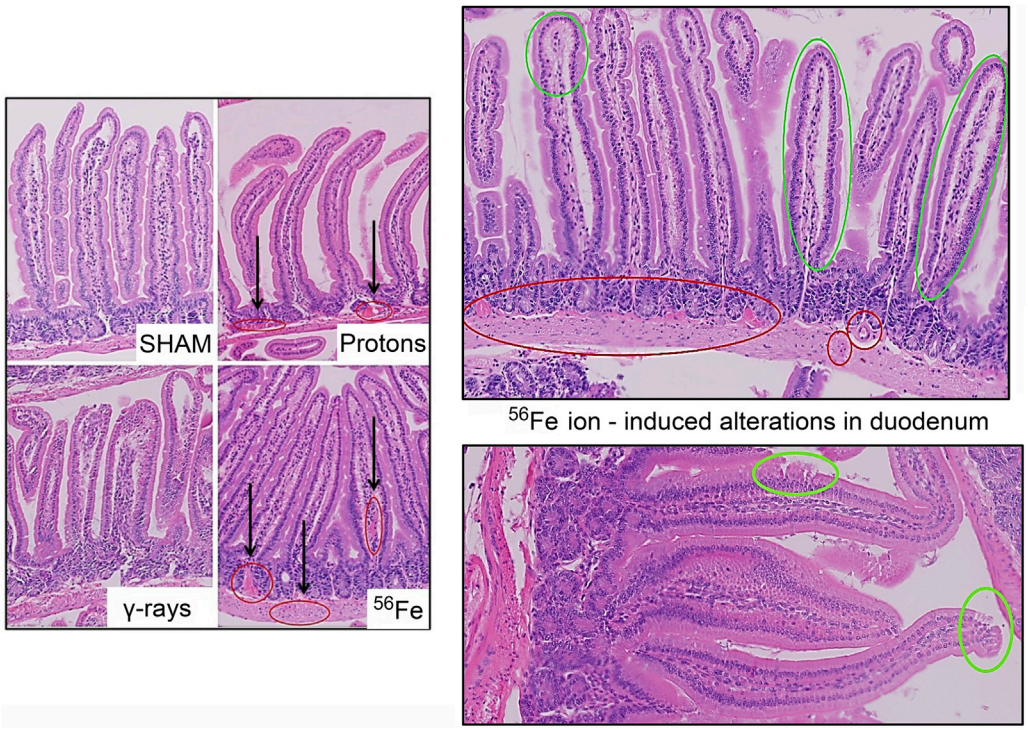

FIGURE 3
Representative H&E-stained sections of duodenal samples collected from C57BL/6J mice exposed to each IR scheme illustrating IR-associated vascular damage/abnormalities. Vascular congestion, dilation, and possible bleeding (red circles); and possible edema and epithelial disruption (green circles) in the duodenum of a mouse exposed to Fe-56 ions.

we next measured how exposures affected the number, position, and cycling status of ISC within the mouse duodenum within 24 h post-irradiation using immunofluorescence-based analyses using antibodies specific to Musashi-1 (Msi-1), a marker of ISC (Potten et al., 2003), and proliferating cell nuclear antigen (PCNA), a marker of actively cycling cells. All 3 IR types led to an increase in the number of Msi-1-positive (red) and PCNA-positive (green) proliferating cells within and around the crypts of the villi (Figures 5, 6), although these changes were not statistically significant ($p \leq 0.05$; Figure 7). Performing ImageJ-based quantitative analyses on these sections also enabled us to assess whether the exposures affected the proliferation status of ISC within the crypts by quantifying the number of Msi-1-positive cells that were likewise positive for PCNA. As seen in Figure 7, the charged particle exposures showed a trend towards reduced numbers of proliferating ISC per crypt, but again these differences did not achieve statistical significance.

IR-induced programmed cell death (apoptosis)

To further examine GI effects of modeled SEP/GCR radiation *in vivo*, TUNEL assays were performed to assess apoptosis induction in response to the different IR types from 15 min to 24 h. All IR types increased levels of TUNEL-positive cells with signal detectable in some samples at 15 min post-IR and steadily increasing over time (representative images shown in Figure 8). To quantitate these levels, we again developed and applied a custom ImageJ script to analyze three regions of interest (ROIs) per mouse. Apoptotic cells in each ROI were quantified as the percent of the area that were TUNEL-positive using the equation: [DAB/Negative Signal * 100]. Each ROI was filtered to remove unwanted artifacts, and size, circulation, and color (DAB/Brown) were then used to identify positive DAB signals. Comparing these sections, we see that exposure to 50 cGy of Fe-56 ions led to a significantly higher TUNEL signal compared to 100 cGy of either protons or cesium-137 γ–rays at both the 15- and 90-min timepoints. Furthermore, the Fe-56 ion-irradiated group had a significantly higher TUNEL signal at both the 4- and 24-h time points compared to protons. Figure 9A shows the quantitative data obtained with the ImageJ script per IR type while Figure 9B presents these same data arranged per timepoint. When analyzing these images, we noted apoptosis-positive cells were typically present at the base of intestinal crypts (notably in mice exposed to the iron ions) indicating that IR exposures resulted in ISC apoptosis (Figure 9A).

Quantification of DNA double-strand breaks (DSBs)

To assess the induction and resolution of DNA double-strand break (DSB)-associated nuclear foci resulting from exposure to each IR scheme, we again utilized a custom ImageJ script to quantify

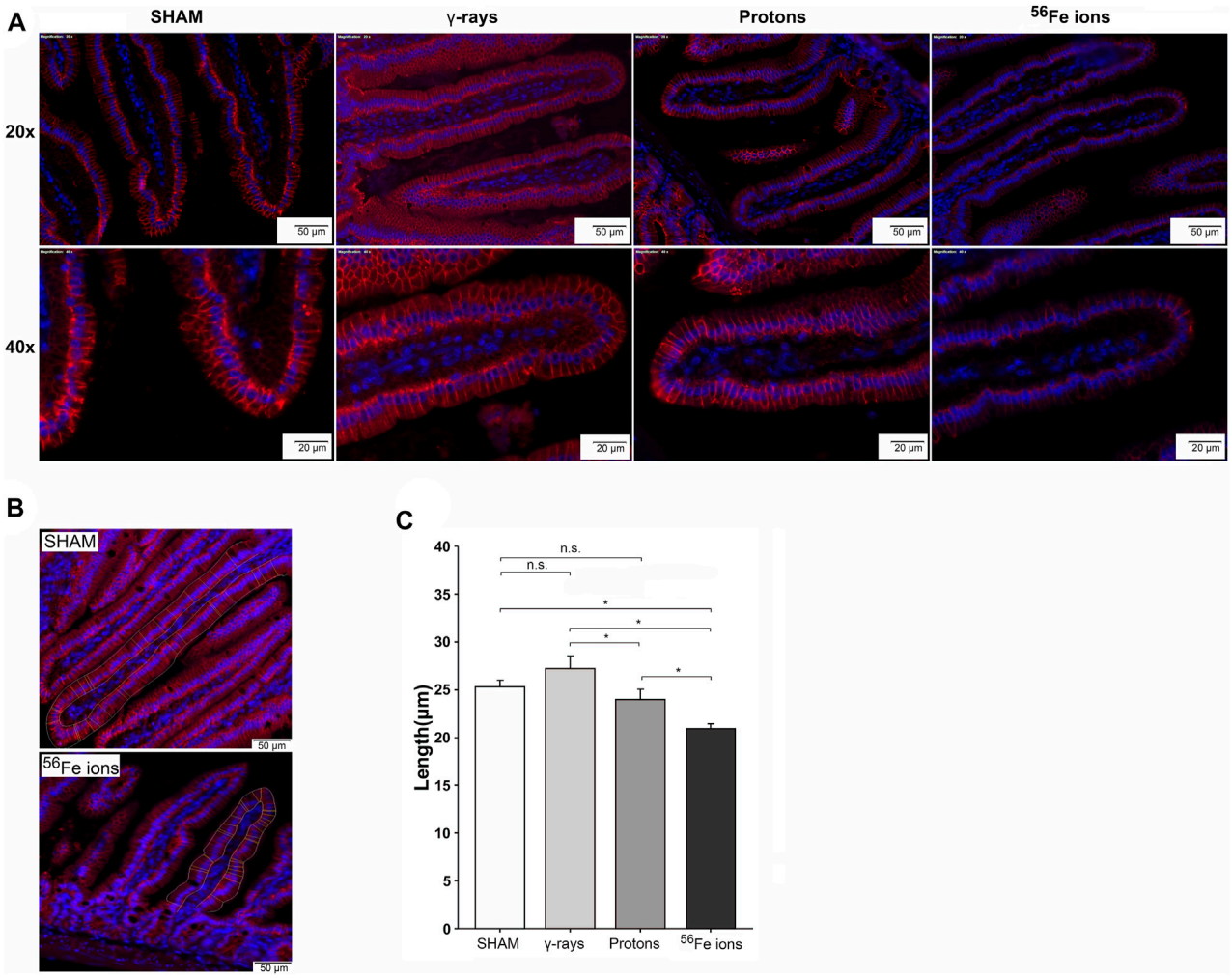

FIGURE 4
Immunofluorescence analysis of tight junction-associated Claudin-3 staining as a measure of epithelial barrier integrity. Panel **(A)** Representative confocal images of duodenal samples from mice exposed to sham (0 cGy), 100 cGy of cesium-137 γ-rays, 100 cGy of 50 MeV protons, or 50 cGy of 1 GeV/n Fe-56 ions stained with an antibody specific to Claudin-3 (red). Top panel shows ×20 magnification (50-μm scale bar); bottom panel shows ×40 magnification (20-μm scale bar). Panel **(B)** Close-up images of Claudin-3 staining in the duodenum of a sham-irradiated (top) and Fe-56 ion-irradiated (bottom) mouse at 24 h post-IR (50-μm scale bar). **(C)** Tight junction length quantified using a custom ImageJ script written to measure the length of the Claudin-3-positive barrier between adjacent epithelial cells. Multiple "regions of interest" (ROIs) were analyzed in each section, and the script computed an average of 30 random measurements (in μm) of the narrow junction (n = 3 ROIs per section); *$p < 0.05$.

intranuclear γ-H2AX pS139 foci/cell in 3 ROIs from each mouse intestinal section. These analyses showed increased foci levels at both 15 min and 4 h post-IR with levels returning to baseline (sham-irradiated control levels) by 24 h post-IR in all of the mice treated with γ-rays or protons. In contrast, the number of γ-H2AX foci were still significantly higher than spontaneous background levels in the duodenum of mice exposed to Fe-56 ions, indicating that DSBs induced by these HZE ions were not fully repaired by this time—consistent with previous reports (Hada and Sutherland, 2006; Asaithamby et al., 2008; Wilson et al., 2010; Mladenov et al., 2018; Bennett et al., 2022). What was more striking was the observation of prominent extranuclear, cytoplasmic DNA fragments that were both DAPI-positive (i.e., DNA-containing) and gamma-H2AX pS139-positive (i.e., containing at least nucleosome-level chromatin) in the charged particle-irradiated samples only. Representative confocal images of γ-H2AX staining appear in Figure 10 and demonstrates the strong intensity and location of these brightly staining cytosolic DNA fragments. The panel at the bottom of Figure 10 shows a high magnification of the area in the red-dashed region, with the individual γ-H2AX (green) and DAPI (blue) channels shown. DAPI (blue) staining of these cytoplasmic γ-H2AX (green) foci confirms that they are composed of DNA fragments. Figure 11A shows a graphical presentation of the quantitative data obtained with the custom ImageJ script, with each panel showing the intranuclear γ-H2AX signal as a result of each IR species; Figure 11B presents these data per time post-IR. It remains to be determined in future studies if the cytoplasmic DNA fragments resulted from charged particle-induced chromothripsis, or chromosomal shattering (Mladenov et al., 2018), with the subsequent egress of small DNA fragments through the

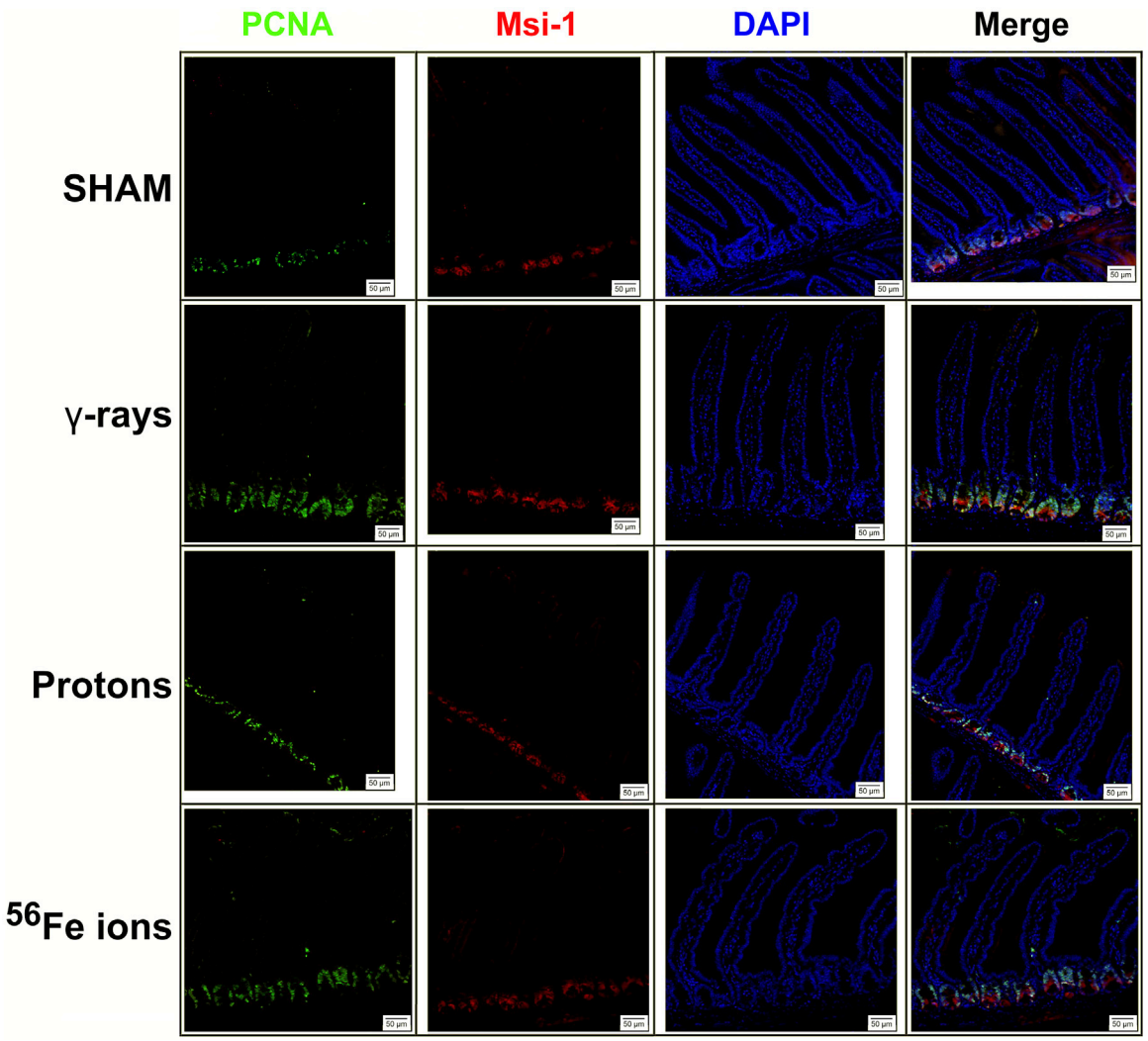

FIGURE 5
Immunohistochemical staining for Musashi-1 (red) and proliferating cell nuclear antigen (PCNA; green) of duodenal sections from mice exposed to various IR schemes collected at 24 h post-irradiation to assess Msi-1-positive intestinal stem cell (ISC) and PCNA-positive proliferating cell numbers and locations. Representative images at ×20 magnification (50-μm scale bar).

damaged/leaky nuclear membrane into the cytosol, and whether this results in activation of cGAS/STING signaling pathways and/or TREX1-mediated degradation of these fragments (Yang et al., 2007; Vanpouille-Box et al., 2017; Durante and Formenti, 2018) given that they are no longer present at 24 h in any of the irradiated samples.

Testing curcumin-laden nanolipoprotein particles (cNLPs) as a GI-specific MCM for SEP/GCR radiation exposures

Our other ongoing functional and multi-omic analyses of space radiation and microgravity effects on human and mouse *in vitro* and *in vivo* model systems have yielded comprehensive datasets on molecular signaling pathways involved in SEP/GCR effects on human hematopoiesis and leukemogenesis and provided targets for developing targeted MCMs (Rodman et al., 2017; Almeida-Porada et al., 2018; Low et al., 2018). These analyses have identified multiple affected signaling cascades that can potentially be modulated by curcumin, a natural bioactive compound derived from turmeric (Curcuma longa) that has been shown to have anti-proliferative and pro-apoptotic effects in a variety of cancer models. Curcumin has also been reported to serve as both a radiosensitizer for cycling cell populations (e.g., tumor cells) and a radioprotector in non-cycling, quiescent cell populations/tissues through its potent antioxidant activities (Sebastia et al., 2014). To overcome curcumin's inherently poor bioavailability, we recently reported on the successful development and characterization of ApoA1-based nanolipoprotein particles (NLPs) loaded with high levels of curcumin (cNLPs) and show this NLP platform markedly increases curcumin's solubility and allows us to lyophilize them for long-term storage and use via injection or oral routes. We also showed that pretreatment of primary human fibroblasts with cNLPs provided significant radioprotection when administered 18–24 h

10.3389/fspas.2023.1117811

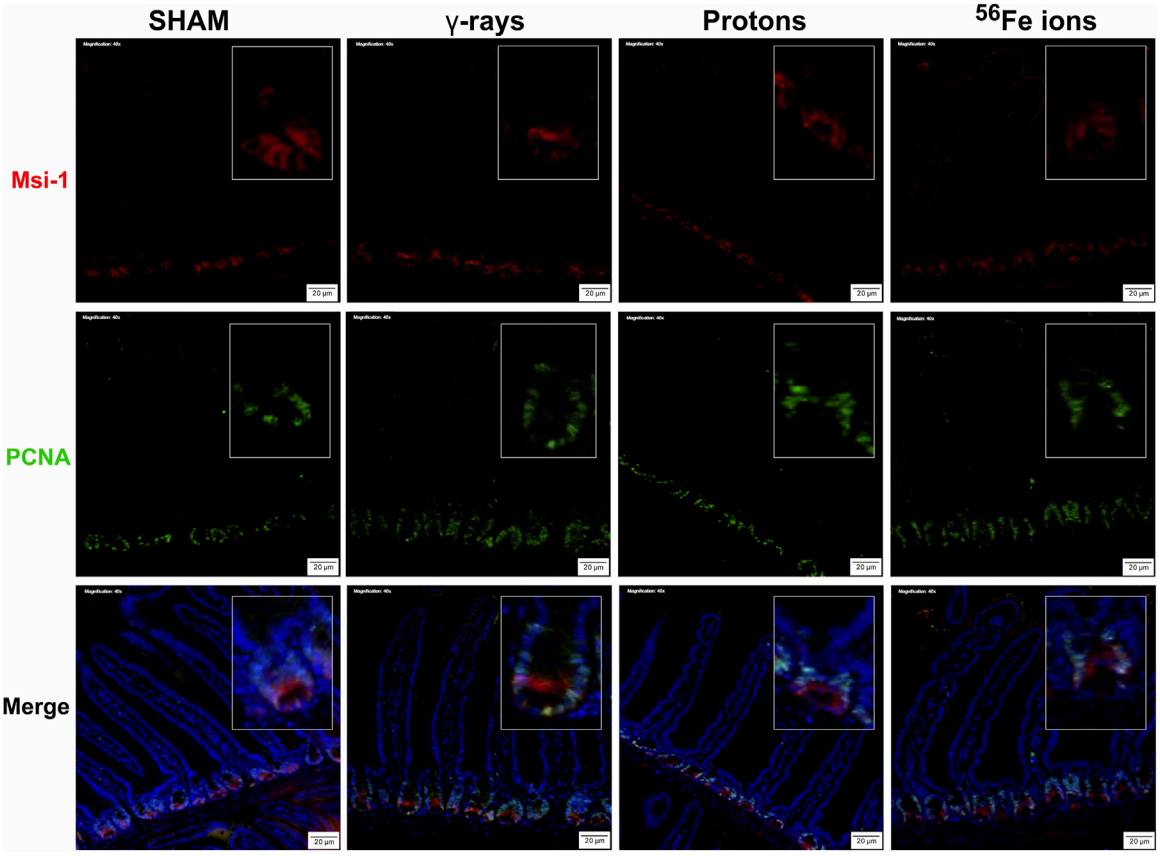

FIGURE 6
Immunohistochemical staining for Musashi-1 (red) and PCNA (green) of duodenal sections from mice exposed to various IR schemes collected at 24 h post-irradiation to assess Msi-1-positive ISC and PCNA-positive proliferating cell numbers and locations. Representative images at ×40 magnification (insets at ×2.5 additional magnification, 20-μm scale bars).

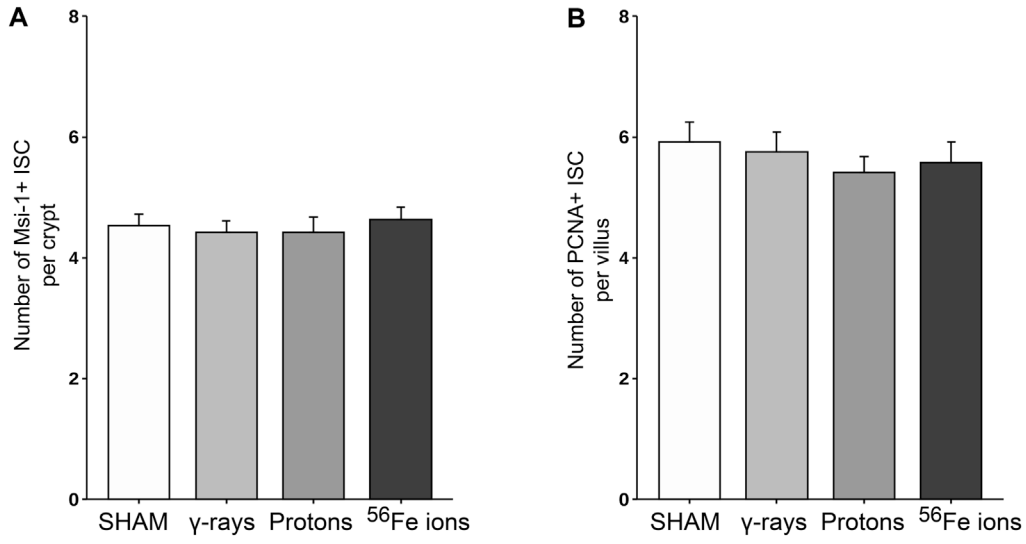

FIGURE 7
Quantification of ISC and proliferating cells within duodenal sections from mice exposed to various IR schemes collected at 24 h post-irradiation, using a custom ImageJ script. Panel **(A)** Plot of Msi-1-positive ISC per crypt quantitated using a custom ImageJ script (n = 3 ROIs per section). Panel **(B)** Plot of PCNA-positive (proliferating) plus Msi-1-positive ISC per crypt quantitated using a custom ImageJ script (n = 3 ROIs per section).

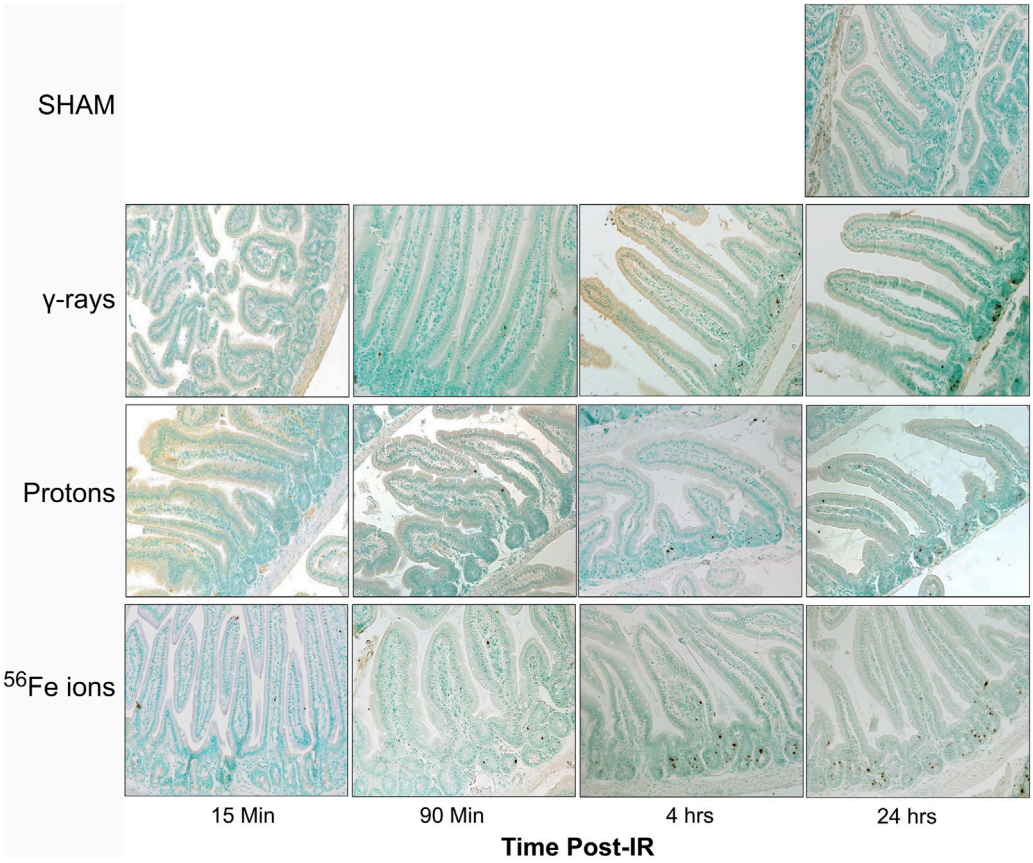

FIGURE 8
Visualization and quantitation of IR-induced apoptosis via TUNEL assay. Representative sections of duodenum collected (at various time points post-IR) from mice exposed to sham (0 cGy), 100 cGy of cesium-137 γ-rays, 100 cGy of 50 MeV protons, or 50 cGy of 1 GeV/n Fe-56 ions stained by terminal deoxynucleotidyl transferase dUTP nick end-labeling (TUNEL) to detect apoptotic DNA fragmentation (x20 magnification; 50-μm scale bar).

pre-irradiation and radiomitigation when administered 15 min post-irradiation, reduced γ-H2AX-positive DSB-associated nuclear foci, and modulated expression of genes involved in the DNA damage response (DDR) following cesium-137 γ-ray irradiation (Evans et al., 2022). In this study, we sought to test whether these cNLPs could serve as a GI-specific MCM against the damaging effects of SEP/GCR radiation *in vivo*. We therefore pretreated C57BL/6J mice with 27 μM (10 μg/mL) cNLPs (the optimum radioprotective concentration derived in our *in vitro* experiments) 18–24 h prior to exposure to 100 cGy of γ-rays or protons, or 50 cGy of Fe-56 ions, and assayed the duodenal samples from the cNLP cohorts identically as described above.

As can be seen in Figure 12, 27 μM cNLP pre-treatment via IV injection reduced the incidence of apoptosis assessed by TUNEL staining using the previously described custom ImageJ script in mice exposed to all 3 radiation types 24 h post-IR, but this decrease only achieved statistical significance in the group exposed to Fe-56 ions. Similarly, radioprotective effects were also seen when we analyzed the incidence of DSB-associated foci via γ-H2AX pS139 staining. As shown in Figure 13, cNLP treatment reduced the number of γ-H2AX foci-positive cells in the duodenum resulting from exposure to γ-rays, protons, and Fe-56 ions at 4 h post-IR (the point of maximal DSB induction in these studies), as well as nearly eliminated the appearance of the gamma-H2AX-positive cytosolic DNA fragments. The panel at the bottom of Figure 13 shows a high magnification of the area in the red-dashed region, with the individual γ-H2AX (green) and DAPI (blue) channels shown. DAPI (blue) staining of these cytoplasmic γ-H2AX (green) foci confirms that they are composed of DNA fragments. Confocal immunofluorescence studies further demonstrated an increase in Claudin 3 staining (Figure 14A) using our ImageJ script, revealing an improvement in the lengths of the epithelial tight junctions in both the proton- and Fe-56 ion-exposed groups. This difference, however, only achieved statistical significance in the proton-exposed group (Figure 14B).

Discussion

It is well appreciated the GI system constitutes one of the most radiosensitive tissues of the body vulnerable to both the direct (DNA damaging) and indirect (inflammation-associated) effects of IR exposure due to the rapid cellular turnover needed

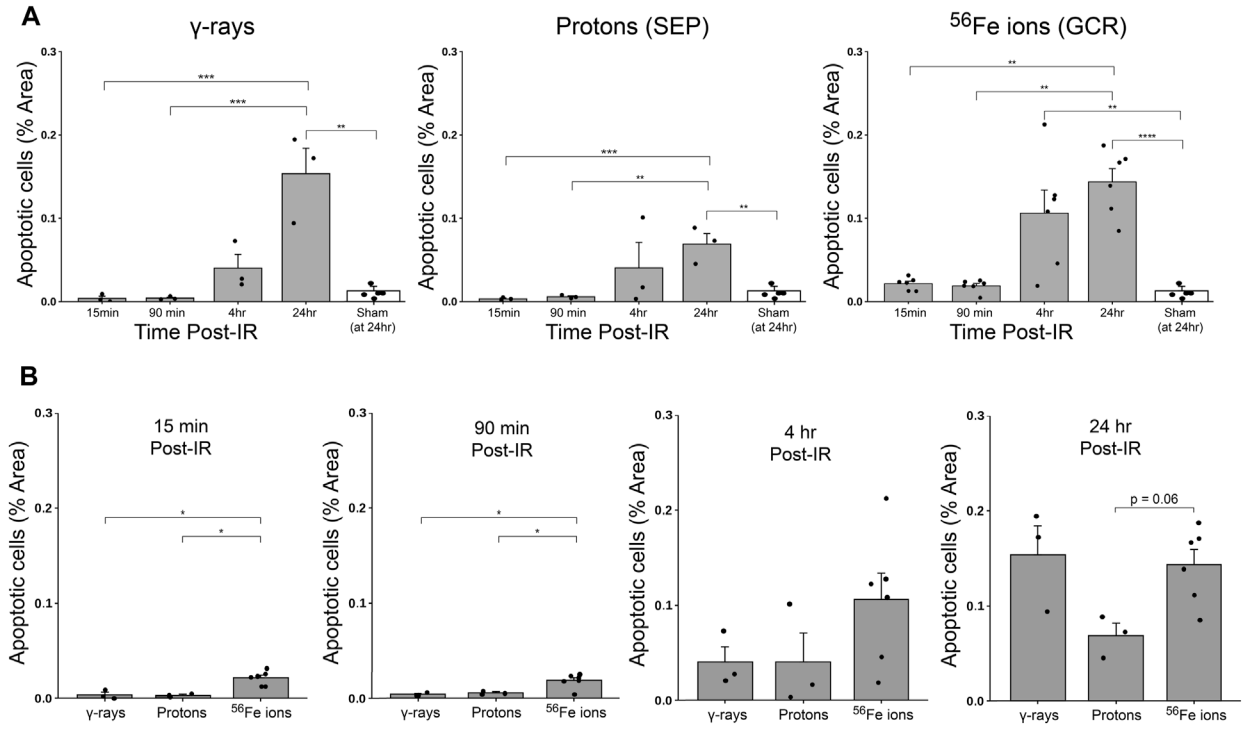

FIGURE 9
Quantification of apoptotic cells within duodenal sections from mice exposed to various IR schemes, using a custom ImageJ script; data presented as a function of IR type in panel **(A)** and by time post-IR in panel **(B)** (n = 3–6 depending upon IR scheme); *p < 0.05; **p < 0.01; ***p < 0.001; ****p < 0.0001.

to continually replenish the epithelial layer of the villi within the small intestine as the epithelial cells at the villi tips are sloughed off as part of normal GI function/wear-and-tear. This process of epithelial replenishment is driven by a small population of intestinal stem cells (ISC) that reside within the crypts at the base of the villi. Even relatively low dose IR exposures can induce crypt cell apoptosis and mucosal lesions, leading to loss of epithelial barrier function and increased mucosal permeability. This increased permeability induces nutrient and fluid loss and allows gut pathogen infiltration. The net effect of these insults is the establishment of a state of chronic mucosal inflammation, which results in tissue loss, fibrosis, and decreased motility (Shadad et al., 2013; Shim et al., 2015; Lee et al., 2019; Chen et al., 2021). With extended deep space missions beyond LEO exposing astronauts to both chronic LDR and sporadic acute HDR charged particles, the higher RBE values for GI-related pathologies documented following low doses exposures presents a major concern for NASA's risk assessment and challenge to astronaut radioprotection and mitigation strategies.

IR is an established risk factor for the development of colorectal cancer (CRC) (Thompson et al., 1994; Pawel et al., 2008; Grant et al., 2017), and NASA-funded studies performed by the Fornace and Datta group demonstrate exposures to low doses (10 and 50 cGy) of protons and 1 GeV/n Fe-56 ions significantly enhances the development and progression of intestinal tumors in mice harboring mutations in the Apc gene due to both direct DNA damage and via increased production of reactive oxygen species (ROS) (Trani et al., 2014; Suman et al., 2016; Suman et al., 2017; Kumar et al., 2018; Kumar et al., 2019; Suman et al., 2020; Suman et al., 2021). The persistent DNA damage resulting from HZE exposures also caused premature senescence and emergence of a senescence-associated secretory phenotype (SASP) within the ISC pool of mice exposed to 50 cGy of Fe-56 ions (Kumar et al., 2018; Kumar et al., 2019), and a recent study from this group highlights the majority impact that exposures to HZE ion components of simulated mixed-field exposures have on GI tumorigenesis (Suman et al., 2022). These studies have primarily focused on the longer-term effects of such exposures, while fewer studies have explored acute/immediate effects of irradiation within the first 24 h post-irradiation (Purgason et al., 2018), a time period in which intervention with an appropriate GI-specific MCM may have the most beneficial effects, especially when considering potential higher dose/dose-rate exposures that may occur if astronauts are exposed to a SPE.

In the present report, we describe the results of ground-based studies performed at NSRL to address these early timepoints in C57BL/6J mice exposed to doses of modeled SEP/GCR radiation designed to approximate the total dose an astronaut will receive during a 3-year Mars mission. Due to time, funding, and facility access/cost restraints, we were limited to

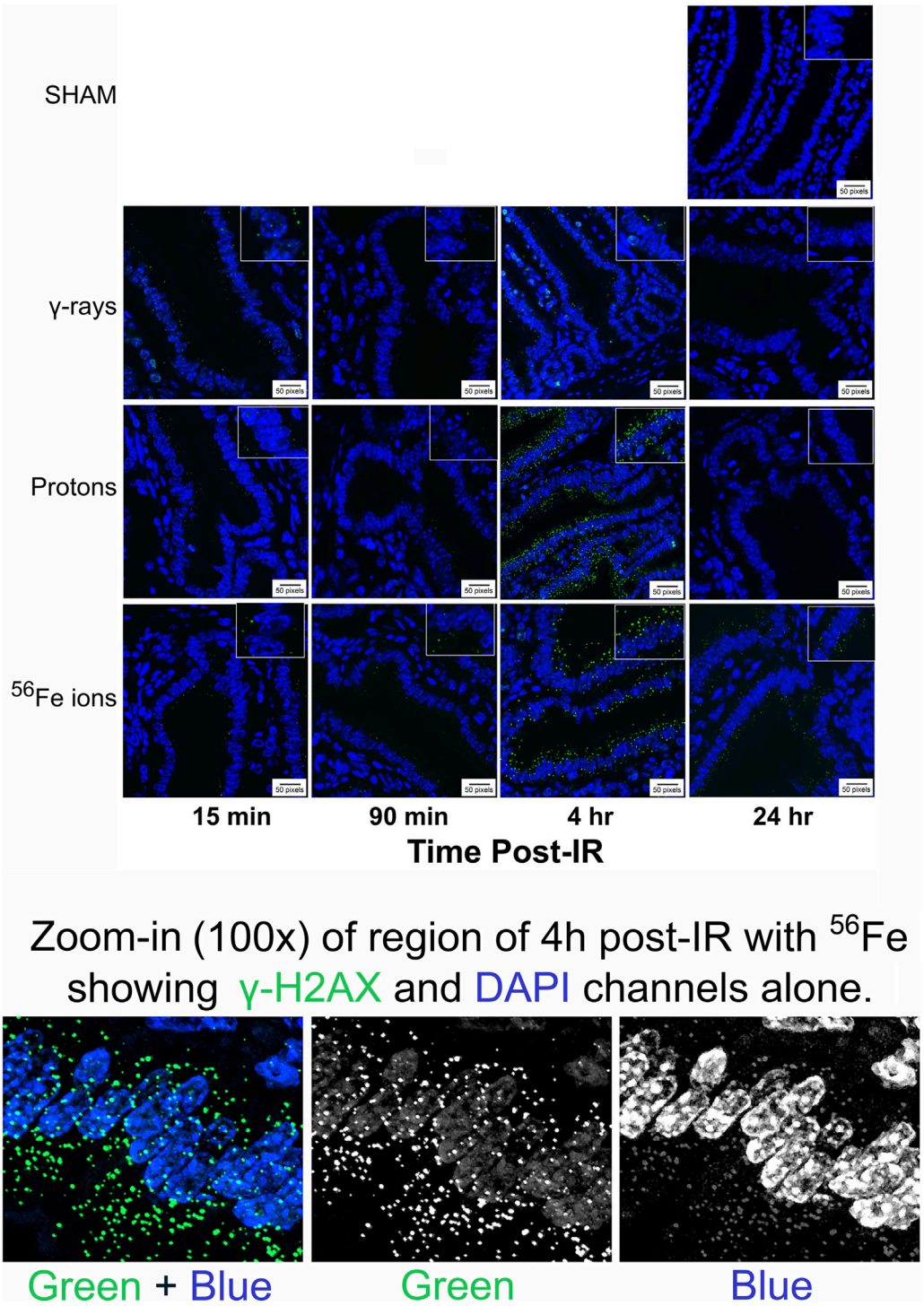

FIGURE 10
Visualization and quantitation of IR-induced DNA double-strand break (DSB)-associated nuclear foci. Panel A) Representative sections of duodenum collected (at various time points post-IR) from mice exposed to sham (0 cGy), 100 cGy of cesium-137 γ-rays, 100 cGy of 50 MeV protons, or 50 cGy of 1 GeV/n Fe-56 ions stained with an antibody specific to γ-H2AX pS139 (green) as a marker of IR-induced DSBs (×40 magnification; 20-μm scale bar). The panel at the bottom of the figure shows a high magnification of the area in the red-dashed region, with the individual γ-H2AX (green) and DAPI (blue) channels shown. DAPI (blue) staining of these cytoplasmic γ-H2AX (green) foci confirms that they are composed of DNA fragments.

conducting acute HDR irradiations and could not explore potential dose-rate effects that may occur if the exposures were extended over several weeks, months or years, though we agree dose-rate is a very critical factor to consider in future studies (Rithidech et al., 2013; Bennett et al., 2022). The mice in this study were euthanized at time points

10.3389/fspas.2023.1117811

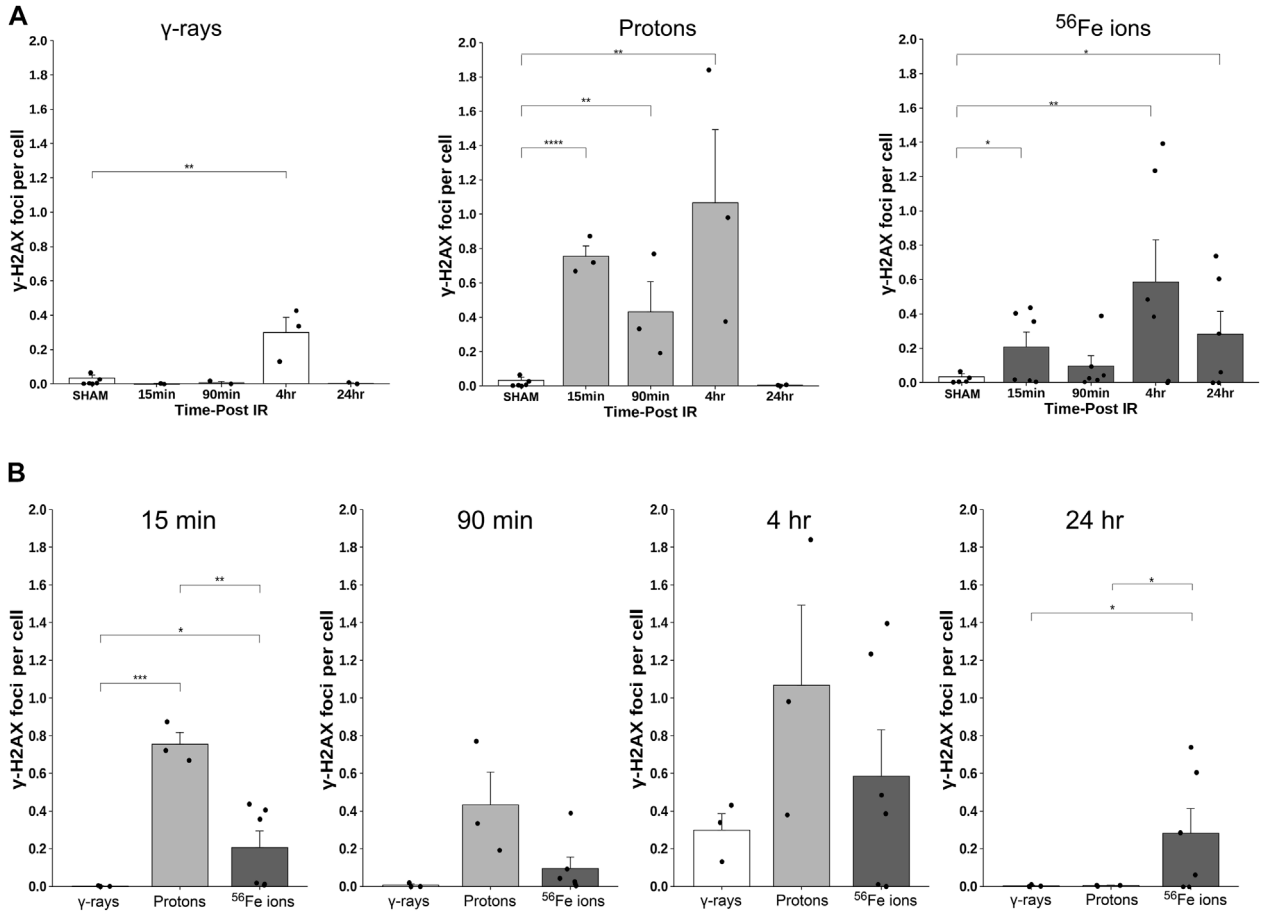

FIGURE 11
Quantification of γ-H2AX foci using a custom ImageJ script; data presented as a function of IR type in panel **(A)** and by time post-IR in panel **(B)** (n = 3–5 depending upon IR scheme); *p < 0.05; **p < 0.01; ***p < 0.001; ****p < 0.0001.

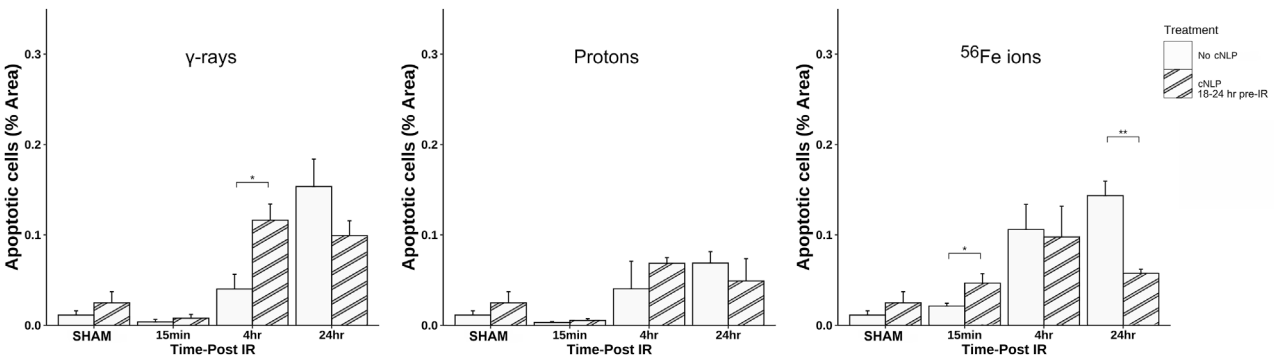

FIGURE 12
Efficacy of cNLPs as a candidate GI MCM for SEP/GCR radiation. Quantification of apoptotic cells via TUNEL assay as above using a custom ImageJ script; data presented as a function of IR type in each panel. Open bars are data from mice that did not receive cNLPs; striped bars are data from mice that received 27 μM cNLPs via IV tail-vein injection 18–24 h pre-IR (n = 3–6 mice depending upon IR scheme); *p < 0.05; **p < 0.01.

ranging from 15 min to 24 h post-irradiation, with their small intestines collected to characterize GI-related effects and test the ability of curcumin-laden nanolipoprotein particles (cNLPs) we recently developed and characterized (Evans et al., 2022) to serve as a much-needed MCM to protect the GI tract of astronauts from the damaging effects of SEP/GCR radiation.

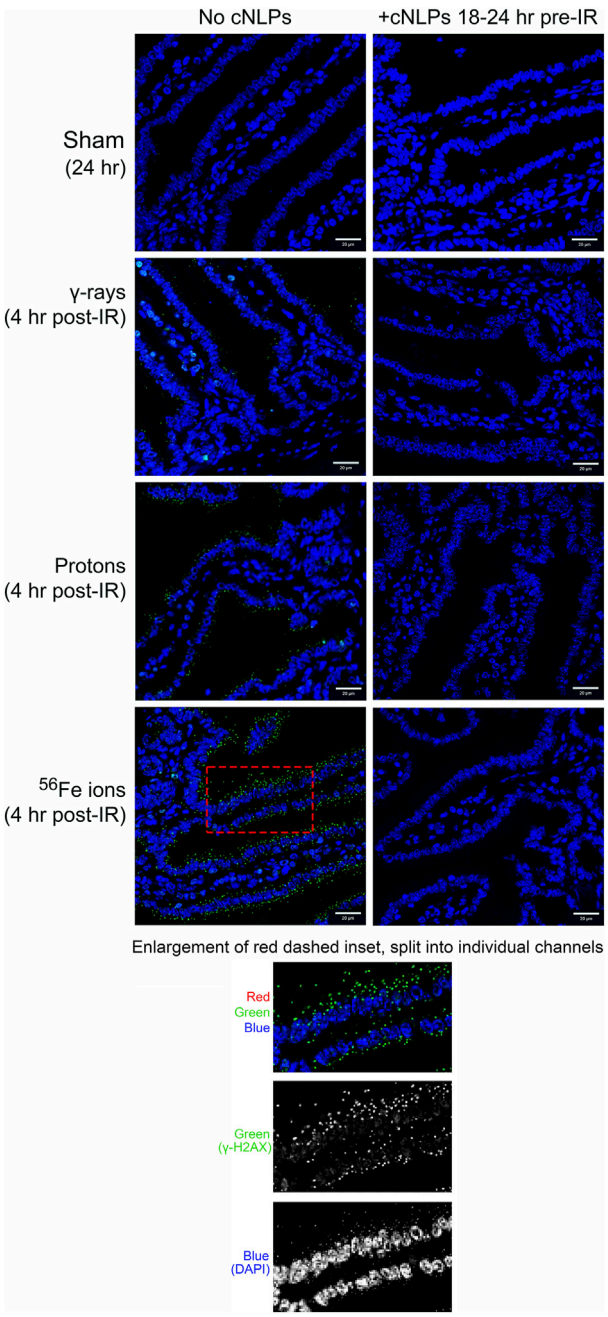

FIGURE 13
Efficacy of cNLPs as a candidate GI MCM for SEP/GCR radiation. Representative sections of duodenum collected 4 h post-irradiation following 100 cGy of cesium-137 γ-rays, 100 cGy of 50 MeV protons, or 50 cGy of 1 GeV/n Fe-56 ions and sham controls collected at 24 h time point stained with a γ-H2AX pS139-specific antibody (green) to detect DSB-associated nuclear foci. Left column shows samples from mice that did not receive cNLPs; right columns are samples from mice that received cNLPs (×40 magnification; 20-μm scale bar). The panel at the bottom of the figure shows a higher magnification (×100) of an area from the duodenum of a Fe-56 ion-exposed mouse collected at 4 h post-IR, with individual γ-H2AX (green) and DAPI (blue) channels shown, confirming they are DNA fragments.

Our results show that both SEP and GCR radiation induces immediate histological and functional alterations within the GI tract of C57BL/6J mice, disrupting epithelial tight junctions and triggering an inflammatory response, leading to dramatic enlargement/swelling of the lymph nodes/MALT (mucosa-associated lymphoid tissue/Payer's patches)—a finding that was unique to some mice exposed to protons and Fe-56 ions. The findings of these alterations in the lymphoid tissue only in mice exposed to protons and Fe-56 ions is likely a result of the differing effects charged particle radiations have been reported to exert on the immune system (Gridley et al., 2002; Schmid and Multhoff, 2012; Hoehn et al., 2019). Exposure to Fe-56 ions also led to marked vascular congestion and edema within the villi in some of the mice, as well as a trend towards a decrease in villi height and evidence suggestive of possible epithelial loss. An important caveat to our findings is that these alterations were only seen in some of the tissue sections from specific mice within the Fe-56 ion-exposed group, which may be the result of mouse-to-mouse variations in handling, diet, etc.

Our conclusions regarding disruption of the intestinal epithelial barrier were based upon quantitative measures of duodenal sections stained with an antibody specific to Claudin-3 and analyzed with a custom script in ImageJ to measure junction lengths between adjacent epithelial cells in an unbiased manner. If SEP/GCR-induced reduction in Claudin-3 junction length translates into epithelial disruption, such exposures would be predicted to lead to increased gut barrier permeability, i.e., leaky gut, which can allow passage of bacteria and toxins into the bloodstream (Fukui, 2016; Kumagai et al., 2018), producing symptoms including fatigue, joint pain, rashes, and food sensitivity and placing the immune system in a hyperactivated state. Astronauts on long duration missions may thus be at risk of chronic digestive issues, e.g., bloating, gas, diarrhea, constipation, and food sensitives/intolerance (Camilleri, 2019) as a result of SEP/GCR-induced damage to their GI tract. We also evaluated the effects of SEP/GCR and how exposure can disrupt tissue homeostasis by depleting intestinal stem cells (ISC), the pool of which is maintained by a delicate balance between cell division and cell death/turnover (Prise and Saran, 2011). While quantitative analyses using antibodies to PCNA and the ISC marker Msi-1 (Potten et al., 2003) did not reveal statistically significant changes in the rate of ISC proliferation, qualitative changes were readily evident based upon visual evaluation of some of the sections by confocal microscopy, with a trend towards an increase in proliferating cells localized within the crypts as a result of IR exposure. Additional studies are underway to examine this issue in more detail, as IR-induced DNA damage to the ISC, combined with enhanced proliferation could lead to the propagation of ISC harboring mutations that could lead to tumor development within the GI tract. Further studies are also planned using machine learning (ML) approaches to examine the duodenal sections at higher resolution to answer the important question of whether SEP/GCR exposure leads to alterations in ISC positioning within the crypt/villi.

Apoptosis/programmed cell death is a normal part of GI homeostasis that ensures aged/damaged cells are safely and efficiently removed and replaced to maintain tissue function (Wan et al., 2022). However, excessive apoptosis within the villi can lead to villous atrophy (Schuller et al., 2006; Hauer-Jensen et al., 2014), as occurs in celiac disease, and can lead to erosion and blunting of the villous tips, resulting in malabsorption of nutrients, diarrhea, and weight loss (Potten, 2004; Williams et al., 2010;

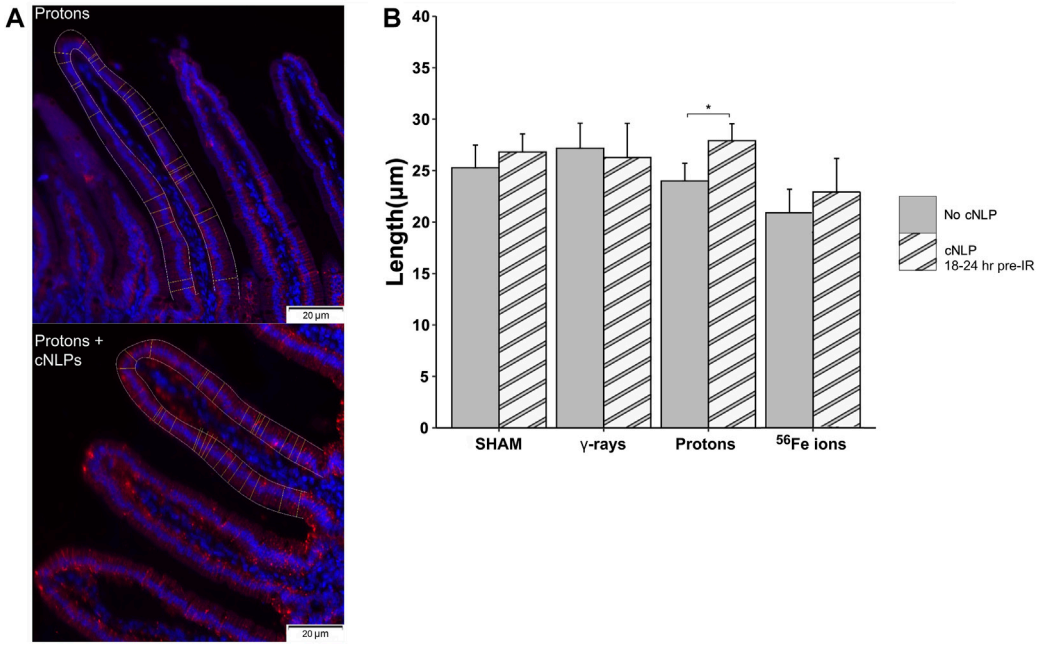

FIGURE 14
Ability of cNLPs to restore epithelial barrier function. Panel **(A)** Representative sections of duodenum collected 24 h post-IR from mice exposed to 50 MeV protons without (top panel) or with cNLP pretreatment (bottom panel) stained with an antibody to tight junction-associated Claudin-3 (red, ×40 magnification; 20-µm scale bars). Panel **(B)** Quantification of Claudin-3 barrier length assessed by custom ImageJ script; data presented as a function of IR type (n = 3–6 depending upon IR scheme); *$p < 0.05$.

Martins et al., 2016). To assess the presence and incidence of IR-induced apoptosis within the duodenum of mice exposed to γ-rays, protons, or Fe-56 ions, quantitative analysis of duodenal sections stained with a chromogenic TUNEL assay and a custom ImageJ script. These analyses demonstrated that mice exposed to a 50 cGy dose of Fe-56 ions had greater TUNEL signal at 4 h post-exposure compared to 1 Gy of γ-rays, reflecting the higher relative biological effectiveness of these HZE ions. Visual inspection of TUNEL-stained duodenal sections revealed the presence of TUNEL-positive cells within the crypts where ISC reside, in agreement with prior studies with mice exposed to high doses (15 Gy) of γ-rays (Hornsey, 1973; Potten, 2004).

One of the primary mechanisms by which IR, especially high LET HZE ions, causes cellular/tissue injury and triggers apoptosis is via DNA double-strand breaks (DSB) induction, can lead to chromosomal aberrations and mitotic cell death and/or apoptosis depending on cell/tissue type. Due to considerations of the track structure and energy deposition patterns of both protons and HZE ions, they are more effective per unit dose than gamma-ray-induced photoelectrons at generating higher levels as well as denser clustering of DSBs and other oxidative base lesions that is more difficult for the cellular DDR machinery to recognize and repair (Sutherland et al., 2001; Hada and Sutherland, 2006; Asaithamby et al., 2008; Mladenov et al., 2018). Phosphorylation of the histone variant H2AX on serine 139 to generate γ-H2AX plays a key role in rapidly recruiting DDR signaling repair proteins to DSB sites (Rogakou et al., 1999; Paull et al., 2000) which are typically resolved back to spontaneous background levels by 24 h post-irradiation in most normal human and rodent cell lines/strains following low LET photon and proton irradiation, with higher levels of residual foci above background levels observed after exposures intermediate to high LET HZE ions (Saha et al., 2014; Bennett et al., 2022). We observed intranuclear γ-H2AX foci post-irradiation in all IR groups with peak γ-H2AX focus formation observed 4 h post-IR.

Surprisingly, our studies also demonstrated the accumulation of cytoplasmic DAPI-positive and γ-H2AX-positive signals in the cytosol of cells within duodenal samples from mice exposed to protons and Fe-56 ions only, suggesting that this response may be specific to charged particle irradiations. Whether these charged particles have the ability to trigger chromothripsis ("shatter" chromosomes (Mladenov et al., 2018)), with subsequent leakage of small DNA fragments through the damaged nuclear membrane is an important observation that will require additional studies. Cytoplasmic DNA has been shown to activate cGAS/STING-mediated extranuclear DNA sensing/signaling pathways (Durante and Formenti, 2018) and activate TREX1-dependent cytosolic DNA cleavage. These may become important candidate pathways to potentially target for charged particle-specific MCMs that would find application for both space radiation and hadron radiotherapy-associated normal tissue radioprotection. It is also important to consider the microdosimetry of these exposures as related to their

relative fluences in the deep space and/or Mars/lunar radiation environments. For the IR types and doses used in these studies, the mean numbers of particle traversals per cell nucleus equates to 265 protons/nucleus for the 100 cGy dose of 50 MeV protons compared to only ~1.1 iron ions/nucleus for 50 cGy dose of 1 GeV/n Fe-56 ions, assuming a mean nuclear surface area of ~50 μm2 (determined from our image analyses).

In addition to characterizing responses of the murine GI system to SEP/GCR radiation, we also performed studied to assess the ability of our candidate curcumin-based nanoparticle MCM (Evans et al., 2022)—cNLPs—to provide GI radioprotection for low to intermediate dose SEP/GCR exposures (including those typical of a SPE), based upon the promising results we recently reported with this MCM in human fibroblasts (Evans et al., 2022). We tested the efficacy of cNLPs when administered intravenously 18–24 h prior to IR exposure in this *in vivo* mouse model to ascertain whether such pretreatment could provide radioprotection from SEP/GCR to the GI system *in vivo*. Our data on IR-induced levels of apoptosis, DSB-associated nuclear foci induction, and epithelial barrier integrity by Claudin-3 staining provides compelling evidence that cNLPs afforded a promising degree of radioprotection in the normal murine small intestine, reducing the incidence of apoptosis and diminishing γ-H2AX foci levels at 4 h post-exposure to protons and to Fe-56 ions. Pretreatment with cNLPs also led to an increase in Claudin-3 signal and some lengthening of the tight junctions between neighboring epithelial cells within the villi of the duodenum was observed, but this effect only achieved statistical significance in the group exposed to protons. We expect that the radioprotective effects of the cNLPs are being mediated, at least in part, by curcumin's established ability to decrease ROS/RNS production by decreasing inducible nitric oxide synthase (iNOS), increasing glutathione peroxidase, as well as increasing the transcription of antioxidant gene response elements through the Nrf2-Keap1 pathway (Aggarwal et al., 2007).

In conclusion, these studies have identified immediate changes in the GI tract caused by low to intermediate dose SEP/GCR-relevant charged particle exposures, giving us a better understanding of potential acute space radiation-induced physiological and molecular changes within the GI system which are relevant when considering the potential for a higher dose/dose-rate SPE during extended missions. With further research and optimization, we envision the cNLPs we have tested herein (and the oral and liquid formulations we have since developed) will yield a viable MCM and contribute to a successful radioprotection strategy that can promote astronaut safety and mission success during prolonged deep space explorations beyond LEO.

Data availability statement

The original contributions presented in the study are included in the article/supplementary material, further inquiries can be directed to the corresponding author.

Ethics statement

The animal study was reviewed and approved by Wake Forest University Health Sciences IACUC and Brookhaven National Laboratory IACUC.

Author contributions

CP, GA-P, MC, and PW were responsible for conception and experimental design, supervising and troubleshooting experiments, and securing funding. JD drafted the manuscript and CP, GA-P, and PW edited and approved the final version of the manuscript. PW provided experimental oversight for work performed at BNL and dosimetry calculations for charged particle irradiations conducted at NSRL and gamma ray irradiations in the BNL Biology Department gamma facility. CP and BK collected and processed all duodenal samples from mice at post-IR timepoints. BK performed the immunofluorescence-based studies examining expression of Claudin-3, Musashi-1, and PCNA. JD performed all TUNEL and γ-H2AX studies. JD and NE designed and wrote the custom scripts in ImageJ to enable unbiased quantitation of staining in tissues sections representing, analyzing, and plotting the data. MC, AE, KM, and PW engineered and optimized the cNLPs to enable their use as a GI MCM. PG and AR provided all necessary logistical support for the studies performed at NSRL and BNL. All authors contributed to the manuscript and approved the submitted version.

Funding

This work was supported by the NASA Translational Research Institute for Space Health (TRISH) through Cooperative Agreement NNX16AO69A. Work was also performed under the auspices of the U.S. Department of Energy by Lawrence Livermore National Laboratory under contract DE-AC52-07NA27344 and supported with funding from the LLNL Laboratory Directed Research and Development program (LDRD-19-SI-003) at LLNL and by Pacific Northwest National Laboratory under contract DE-AC05-76RL01830.

Conflict of interest

The authors declare that the research was conducted in the absence of any commercial or financial relationships that could be construed as a potential conflict of interest.

Publisher's note

References

Aggarwal, B. B., Surh, Y.-J., and Shishodia, S. (2007)"The molecular targets and therapeutic uses of curcumin in health and disease," in *Advances in Experimental Medicine and Biology*. 1st Edn (New York, NY: Springer). 490. doi:10.1007/978-0-387-46401-5

Akpolat, M., Kanter, M., and Uzal, M. C. (2009). Protective effects of curcumin against gamma radiation-induced ileal mucosal damage. *Arch. Toxicol.* 83 (6), 609–617. doi:10.1007/s00204-008-0352-4

Almeida-Porada, G., Rodman, C., Kuhlman, B., Brudvik, E., Moon, J., George, S., et al. (2018). Exposure of the bone marrow microenvironment to simulated solar and galactic cosmic radiation induces biological bystander effects on human hematopoiesis. *Stem Cells Dev.* 27 (18), 1237–1256. doi:10.1089/scd.2018.0005

Asaithamby, A., Uematsu, N., Chatterjee, A., Story, M. D., Burma, S., and Chen, D. J. (2008). Repair of HZE-particle-induced DNA double-strand breaks in normal human fibroblasts. *Radiat. Res.* 169 (4), 437–446. doi:10.1667/rr1165.1

Beheshti, A., McDonald, J. T., Hada, M., Takahashi, A., Mason, C. E., and Mognato, M. (2021). Genomic changes driven by radiation-induced DNA damage and microgravity in human cells. *Int. J. Mol. Sci.* 22 (19), 10507–10530. doi:10.3390/ijms221910507

Bennett, P. V., Johnson, A. M., Ackerman, S. E., Chaudhary, P., Keszenman, D. J., and Wilson, P. F. (2022). Dose-rate effects of protons and light ions for DNA damage induction, survival and transformation in apparently normal primary human fibroblasts. *Radiat. Res.* 197 (3), 298–313. doi:10.1667/rade-21-00138.1

Bokhari, R. S., Beheshti, A., Blutt, S. E., Bowles, D. E., Brenner, D., Britton, R., et al. (2022). Looking on the horizon; potential and unique approaches to developing radiation countermeasures for deep space travel. *Life Sci. Space Res. (Amst)* 35, 105–112. doi:10.1016/j.lssr.2022.08.003

Camilleri, M. (2019). Leaky gut: Mechanisms, measurement and clinical implications in humans. *Gut* 68 (8), 1516–1526. doi:10.1136/gutjnl-2019-318427

Chen, G., Han, Y., Zhang, H., Tu, W., and Zhang, S. (2021). Radiotherapy-induced digestive injury: Diagnosis, treatment and mechanisms. *Front. Oncol.* 11, 757973–757990. doi:10.3389/fonc.2021.757973

Clevers, H. (2013). The intestinal crypt, a prototype stem cell compartment. *Cell* 154 (2), 274–284. doi:10.1016/j.cell.2013.07.004

Cucinotta, F. A., and Durante, M. (2006). Cancer risk from exposure to galactic cosmic rays: Implications for space exploration by human beings. *Lancet Oncol.* 7 (5), 431–435. doi:10.1016/s1470-2045(06)70695-7

Cucinotta, F. A., Schimmerling, W., Wilson, J. W., Peterson, L. E., Badhwar, G. D., Saganti, P. B., et al. (2001). Space radiation cancer risks and uncertainties for Mars missions. *Radiat. Res.* 156 (5), 682–688. doi:10.1667/0033-7587(2001)156[0682:srcrau]2.0.co;2

Datta, K., Suman, S., Kallakury, B. V. S., and Fornace, A. J. (2013). Heavy ion radiation exposure triggered higher intestinal tumor frequency and greater beta-catenin activation than gamma radiation in APC(Min/+) mice. *PLoS One* 8 (3), e59295. doi:10.1371/journal.pone.0059295

DiCarlo, A. L., Carnell, L. S., Rios, C. I., and Prasanna, P. G. (2022). Inter-agency perspective: Translating advances in biomarker discovery and medical countermeasures development between terrestrial and space radiation environments. *Life Sci. Space Res. (Amst)* 35, 9–19. doi:10.1016/j.lssr.2022.06.004

Durante, M., and Cucinotta, F. A. (2008). Heavy ion carcinogenesis and human space exploration. *Nat. Rev. Cancer* 8 (6), 465–472. doi:10.1038/nrc2391

Durante, M., and Cucinotta, F. A. (2011). Physical basis of radiation protection in space travel. *Rev. Mod. Phys.* 83 (4), 1245–1281. doi:10.1103/revmodphys.83.1245

Durante, M., and Formenti, S. C. (2018). Radiation-induced chromosomal aberrations and immunotherapy: Micronuclei, cytosolic DNA, and interferon-production pathway. *Front. Oncol.* 8, 192. doi:10.3389/fonc.2018.00192

Evans, A. C., Martin, K. A., Saxena, M., Bicher, S., Wheeler, E., Cordova, E. J., et al. (2022). Curcumin nanodiscs improve solubility and serve as radiological protectants against ionizing radiation exposures in a cell-cycle dependent manner. *Nanomater. (Basel)* 12 (20), 3619–3633. doi:10.3390/nano12203619

Fukui, H. (2016). Increased intestinal permeability and decreased barrier function: Does it really influence the risk of inflammation? *Inflamm. Intest. Dis.* 1 (3), 135–145. doi:10.1159/000447252

Grant, E. J., Brenner, A., Sugiyama, H., Sakata, R., Sadakane, A., Utada, M., et al. (2017). Solid cancer incidence among the life span study of atomic bomb survivors: 1958-2009. *Radiat. Res.* 187 (5), 513–537. doi:10.1667/rr14492.1

Gridley, D. S., Pecaut, M. J., and Nelson, G. A. (2002). Total-body irradiation with high-LET particles: Acute and chronic effects on the immune system. *Am. J. Physiol. Regul. Integr. Comp. Physiol.* 282 (3), R677–R688. doi:10.1152/ajpregu.00435.2001

Hada, M., Ikeda, H., Rhone, J., Beitman, A., Plante, I., Souda, H., et al. (2018). Increased chromosome aberrations in cells exposed simultaneously to simulated microgravity and radiation. *Int. J. Mol. Sci.* 20 (1), 43. doi:10.3390/ijms20010043

Hada, M., and Sutherland, B. M. (2006). Spectrum of complex DNA damages depends on the incident radiation. *Radiat. Res.* 165 (2), 223–230. doi:10.1667/rr3498.1

Hassler, D. M., Zeitlin, C., Wimmer-Schweingruber, R. F., Ehresmann, B., Rafkin, S., Eigenbrode, J. L., et al. (2014). Mars' surface radiation environment measured with the Mars Science Laboratory's Curiosity rover. *Science* 343 (6169), 1244797. doi:10.1126/science.1244797

Hauer-Jensen, M., Denham, J. W., and Andreyev, H. J. (2014). Radiation enteropathy--pathogenesis, treatment and prevention. *Nat. Rev. Gastroenterol. Hepatol.* 11 (8), 470–479. doi:10.1038/nrgastro.2014.46

Hoehn, D., Pujol-Canadell, M., Young, E. F., Serban, G., Shuryak, I., Maerki, J., et al. (2019). Effects of high- and low-LET radiation on human hematopoietic system reconstituted in immunodeficient mice. *Radiat. Res.* 191 (2), 162–175. doi:10.1667/rr15148.1

Hornsey, S. (1973). The effectiveness of fast neutrons compared with low LET radiation on cell survival measured in the mouse jejunum. *Radiat. Res.* 55 (1), 58–68. doi:10.2307/3573811

ICRP (2003). Relative biological effectiveness (RBE), quality factor (Q), and radiation weighting factor (w(R)). A report of the International Commission on Radiological Protection. *Ann. ICRP* 33 (4), 1–117. doi:10.1016/s0146-6453(03)00024-1

Kim, M. H., Hayat, M. J., Feiveson, A. H., and Cucinotta, F. A. (2009). Prediction of frequency and exposure level of solar particle events. *Health Phys.* 97 (1), 68–81. doi:10.1097/01.hp.0000346799.65001.9c

Kostova, N., Staynova, A., Popova-Hadjiiska, L., Georgieva, D., Ivanova, I., and Hristova, R. (2021). Radioprotective effect of curcumin on DNA double strand breaks in human blood lymphocytes after *in vitro* γ-irradiation. *Int. J. Bioautomation* 25, 159–168. doi:10.7546/ijba.2021.25.2.000794

Kumagai, T., Rahman, F., and Smith, A. M. (2018). The microbiome and radiation induced-bowel injury: Evidence for potential mechanistic role in disease pathogenesis. *Nutrients* 10 (10), 1405–1420. doi:10.3390/nu10101405

Kumar, S., Suman, S., Fornace, A. J., and Datta, K. (2019). Intestinal stem cells acquire premature senescence and senescence associated secretory phenotype concurrent with persistent DNA damage after heavy ion radiation in mice. *Aging (Albany NY)* 11 (12), 4145–4158. doi:10.18632/aging.102043

Kumar, S., Suman, S., Fornace, A. J., and Datta, K. (2018). Space radiation triggers persistent stress response, increases senescent signaling, and decreases cell migration in mouse intestine. *Proc. Natl. Acad. Sci. U. S. A.* 115 (42), E9832–E9841. doi:10.1073/pnas.1807522115

Lee, C. L., Daniel, A. R., Holbrook, M., Brownstein, J., Silva Campos, L. D., Hasapis, S., et al. (2019). Sensitization of vascular endothelial cells to ionizing radiation promotes the development of delayed intestinal injury in mice. *Radiat. Res.* 192 (3), 258–266. doi:10.1667/rr15371.1

Low, E. K., Brudvik, E., Kuhlman, B., Wilson, P. F., Almeida-Porada, G., and Porada, C. D. (2018). Microgravity impairs DNA damage repair in human hematopoietic stem/progenitor cells and inhibits their differentiation into dendritic cells. *Stem Cells Dev.* 27 (18), 1257–1267. doi:10.1089/scd.2018.0052

Martins, C., Teixeira, C., Ribeiro, S., Trabulo, D., Cardoso, C., Mangualde, J., et al. (2016). Seronegative intestinal villous atrophy: A diagnostic challenge. *Case Rep. Gastrointest. Med.* 2016, 1–4. doi:10.1155/2016/6392028

Mladenov, E., Saha, J., and Iliakis, G. (2018). Processing-challenges generated by clusters of DNA double-strand breaks underpin increased effectiveness of high-LET radiation and chromothripsis. *Adv. Exp. Med. Biol.* 1044, 149–168. doi:10.1007/978-981-13-0593-1_10

Moreno-Villanueva, M., Wong, M., Lu, T., Zhang, Y., and Wu, H. (2017). Interplay of space radiation and microgravity in DNA damage and DNA damage response. *npj Microgravity* 3 (1), 14–21. doi:10.1038/s41526-017-0019-7

Onorato, G., Di Schiavi, E., and Di Cunto, F. (2020). Understanding the effects of deep space radiation on nervous system: The role of genetically tractable experimental models. *Front. Phys.* 8, 1–11. doi:10.3389/fphy.2020.00362

Paull, T. T., Rogakou, E. P., Yamazaki, V., Kirchgessner, C. U., Gellert, M., and Bonner, W. M. (2000). A critical role for histone H2AX in recruitment of repair factors to nuclear foci after DNA damage. *Curr. Biol.* 10 (15), 886–895. doi:10.1016/s0960-9822(00)00610-2

Pawel, D., Preston, D., Pierce, D., and Cologne, J. (2008). Improved estimates of cancer site-specific risks for A-bomb survivors. *Radiat. Res.* 169 (1), 87–98. doi:10.1667/rr1092.1

Potten, C. S., Booth, C., Tudor, G. L., Booth, D., Brady, G., Hurley, P., et al. (2003). Identification of a putative intestinal stem cell and early lineage marker; musashi-1. *Differentiation* 71 (1), 28–41. doi:10.1046/j.1432-0436.2003.700603.x

Potten, C. S. (2004). Radiation, the ideal cytotoxic agent for studying the cell biology of tissues such as the small intestine. *Radiat. Res.* 161 (2), 123–136. doi:10.1667/rr3104

Prise, K. M., and Saran, A. (2011). Concise review: Stem cell effects in radiation risk. *Stem Cells* 29 (9), 1315–1321. doi:10.1002/stem.690

Purgason, A., Zhang, Y., Hamilton, S. R., Gridley, D. S., Sodipe, A., Jejelowo, O., et al. (2018). Apoptosis and expression of apoptosis-related genes in mouse intestinal tissue after whole-body proton exposure. *Mol. Cell Biochem.* 442 (1-2), 155–168. doi:10.1007/s11010-017-3200-0

Rithidech, K. N., Honikel, L. M., Reungpatthanaphong, P., Tungjai, M., Golightly, M., and Whorton, E. B. (2013). Effects of 100MeV protons delivered at 0.5 or 1cGy/min on the *in vivo* induction of early and delayed chromosomal damage. *Mutat. Res.* 756 (1-2), 127–140. doi:10.1016/j.mrgentox.2013.06.001

Rodman, C., Almeida-Porada, G., George, S. K., Moon, J., Soker, S., Pardee, T., et al. (2017). *In vitro* and *in vivo* assessment of direct effects of simulated solar and galactic cosmic radiation on human hematopoietic stem/progenitor cells. *Leukemia* 31 (6), 1398–1407. doi:10.1038/leu.2016.344

Rogakou, E. P., Boon, C., Redon, C., and Bonner, W. M. (1999). Megabase chromatin domains involved in DNA double-strand breaks *in vivo*. *J. Cell Biol.* 146 (5), 905–916. doi:10.1083/jcb.146.5.905

Saha, J., Wilson, P., Thieberger, P., Lowenstein, D., Wang, M., and Cucinotta, F. A. (2014). Biological characterization of low-energy ions with high-energy deposition on human cells. *Radiat. Res.* 182 (3), 282–291. doi:10.1667/rr13747.1

Schardt, D., Elsässer, T., and Schulz-Ertner, D. (2010). Heavy-ion tumor therapy: Physical and radiobiological benefits. *Rev. Mod. Phys.* 82 (1), 383–425. doi:10.1103/revmodphys.82.383

Schmid, T. E., and Multhoff, G. (2012). Non-targeted effects of photon and particle irradiation and the interaction with the immune system. *Front. Oncol.* 2, 80. doi:10.3389/fonc.2012.00080

Schuller, B. W., Binns, P. J., Riley, K. J., Ma, L., Hawthorne, M. F., and Coderre, J. A. (2006). Selective irradiation of the vascular endothelium has no effect on the survival of murine intestinal crypt stem cells. *Proc. Natl. Acad. Sci. U. S. A.* 103 (10), 3787–3792. doi:10.1073/pnas.0600133103

Sebastia, N., Montoro, A., Hervás, D., Pantelias, G., Hatzi, V., Soriano, J., et al. (2014). Curcumin and trans-resveratrol exert cell cycle-dependent radioprotective or radiosensitizing effects as elucidated by the PCC and G2-assay. *Mutat. Res.* 766-767, 49–55. doi:10.1016/j.mrfmmm.2014.05.006

Shadad, A. K., et al. (2013). Gastrointestinal radiation injury: Symptoms, risk factors and mechanisms. *World J. Gastroenterol.* 19 (2), 185–198. doi:10.3748/wjg.v19.i2.185

Shah, P., Fritz, J. V., Glaab, E., Desai, M. S., Greenhalgh, K., Frachet, A., et al. (2016). A microfluidics-based *in vitro* model of the gastrointestinal human-microbe interface. *Nat. Commun.* 7, 11535. doi:10.1038/ncomms11535

Shim, S., Lee, J. g., Bae, C. h., Lee, S. B., Jang, W. S., Lee, S. J., et al. (2015). Claudin-3 expression in radiation-exposed rat models: A potential marker for radiation-induced intestinal barrier failure. *Biochem. Biophys. Res. Commun.* 456 (1), 351–354. doi:10.1016/j.bbrc.2014.11.084

Simonsen, L. C., Slaba, T. C., Guida, P., and Rusek, A. (2020). NASA's first ground-based Galactic Cosmic Ray Simulator: Enabling a new era in space radiobiology research. *PLoS Biol.* 18 (5), e3000669. doi:10.1371/journal.pbio.3000669

Suman, S., Jaruga, P., Dizdaroglu, M., Fornace, A. J., and Datta, K. (2020). Heavy ion space radiation triggers ongoing DNA base damage by downregulating DNA repair pathways. *Life Sci. Space Res. (Amst)* 27, 27–32. doi:10.1016/j.lssr.2020.07.001

Suman, S., Kallakury, B. V., Fornace, A. J., and Datta, K. (2019). Fractionated and acute proton radiation show differential intestinal tumorigenesis and DNA damage and repair pathway response in apc(min/+) mice. *Int. J. Radiat. Oncol. Biol. Phys.* 105 (3), 525–536. doi:10.1016/j.ijrobp.2019.06.2532

Suman, S., Kumar, S., Kallakury, B. V. S., Moon, B. H., Angdisen, J., Datta, K., et al. (2022). Predominant contribution of the dose received from constituent heavy-ions in the induction of gastrointestinal tumorigenesis after simulated space radiation exposure. *Radiat. Environ. Biophys.* 61 (4), 631–637. doi:10.1007/s00411-022-00997-z

Suman, S., Kumar, S., Moon, B. H., Angdisen, J., Kallakury, B. V., Datta, K., et al. (2021). Effects of dietary aspirin on high-LET radiation-induced prostaglandin E2 levels and gastrointestinal tumorigenesis in Apc mice. *Life Sci. Space Res. (Amst)* 31, 85–91. doi:10.1016/j.lssr.2021.09.001

Suman, S., Kumar, S., Moon, B. H., Fornace, A. J., and Datta, K. (2017). Low and high dose rate heavy ion radiation-induced intestinal and colonic tumorigenesis in APC(1638N/+) mice. *Life Sci. Space Res. (Amst)* 13, 45–50. doi:10.1016/j.lssr.2017.04.003

Suman, S., Kumar, S., Moon, B. H., Strawn, S. J., Thakor, H., Fan, Z., et al. (2016). Relative biological effectiveness of energetic heavy ions for intestinal tumorigenesis shows male preponderance and radiation type and energy dependence in APC(1638N/+) mice. *Int. J. Radiat. Oncol. Biol. Phys.* 95 (1), 131–138. doi:10.1016/j.ijrobp.2015.10.057

Sutherland, B. M., Bennett, P. V., Schenk, H., Sidorkina, O., Laval, J., Trunk, J., et al. (2001). Clustered DNA damages induced by high and low LET radiation, including heavy ions. *Phys. Med.* 17 (1), 202–204.

Sutherland, B. M., Bennett, P. V., Sidorkina, O., and Laval, J. (2000). Clustered DNA damages induced in isolated DNA and in human cells by low doses of ionizing radiation. *Proc. Natl. Acad. Sci. U. S. A.* 97 (1), 103–108. doi:10.1073/pnas.97.1.103

Takiishi, T., Fenero, C. I. M., and Câmara, N. O. S. (2017). Intestinal barrier and gut microbiota: Shaping our immune responses throughout life. *Tissue Barriers* 5 (4), e1373208. doi:10.1080/21688370.2017.1373208

Thompson, D. E., Mabuchi, K., Ron, E., Soda, M., Tokunaga, M., Ochikubo, S., et al. (1994). Cancer incidence in atomic bomb survivors. Part II: Solid tumors, 1958-1987. *Radiat. Res.* 137 (2), S17–S67. doi:10.2307/3578892

Townsend, L. W., Adams, J., Blattnig, S., Clowdsley, M., Fry, D., Jun, I., et al. (2018). Solar particle event storm shelter requirements for missions beyond low Earth orbit. *Life Sci. Space Res. (Amst)* 17, 32–39. doi:10.1016/j.lssr.2018.02.002

Townsend, L. W. (2005). Implications of the space radiation environment for human exploration in deep space. *Radiat. Prot. Dosim.* 115 (1-4), 44–50. doi:10.1093/rpd/nci141

Trani, D., Datta, K., Doiron, K., Kallakury, B., and Fornace, A. J. (2010). Enhanced intestinal tumor multiplicity and grade *in vivo* after HZE exposure: Mouse models for space radiation risk estimates. *Radiat. Environ. Biophys.* 49 (3), 389–396. doi:10.1007/s00411-010-0292-2

Trani, D., Nelson, S. A., Moon, B. H., Swedlow, J. J., Williams, E. M., Strawn, S. J., et al. (2014). High-energy particle-induced tumorigenesis throughout the gastrointestinal tract. *Radiat. Res.* 181 (2), 162–171. doi:10.1667/rr13502.1

Van Itallie, C. M., and Anderson, J. M. (2006). Claudins and epithelial paracellular transport. *Annu. Rev. Physiol.* 68, 403–429. doi:10.1146/annurev.physiol.68.040104.131404

Vanpouille-Box, C., Alard, A., Aryankalayil, M. J., Sarfraz, Y., Diamond, J. M., Schneider, R. J., et al. (2017). DNA exonuclease Trex1 regulates radiotherapy-induced tumour immunogenicity. *Nat. Commun.* 8, 15618. doi:10.1038/ncomms15618

Wan, Y., Yang, L., Jiang, S., Qian, D., and Duan, J. (2022). Excessive apoptosis in ulcerative colitis: Crosstalk between apoptosis, ROS, ER stress, and intestinal homeostasis. *Inflamm. Bowel Dis.* 28 (4), 639–648. doi:10.1093/ibd/izab277

Wang, J., Ghosh, S. S., and Ghosh, S. (2017). Curcumin improves intestinal barrier function: Modulation of intracellular signaling, and organization of tight junctions. *Am. J. Physiol. Cell Physiol.* 312 (4), C438–c445. doi:10.1152/ajpcell.00235.2016

Weiss, J. F., and Landauer, M. R. (2003). Protection against ionizing radiation by antioxidant nutrients and phytochemicals. *Toxicology* 189 (1-2), 1–20. doi:10.1016/s0300-483x(03)00149-5

Williams, J. P., Brown, S. L., Georges, G. E., Hauer-Jensen, M., Hill, R. P., Huser, A. K., et al. (2010). Animal models for medical countermeasures to radiation exposure. *Radiat. Res.* 173 (4), 557–578. doi:10.1667/rr1880.1

Wilson, P. F., Nham, P. B., Urbin, S. S., Hinz, J. M., Jones, I. M., and Thompson, L. H. (2010). Inter-individual variation in DNA double-strand break repair in human fibroblasts before and after exposure to low doses of ionizing radiation. *Mutat. Res.* 683 (1-2), 91–97. doi:10.1016/j.mrfmmm.2009.10.013

Yamanouchi, S., Rhone, J., Mao, J. H., Fujiwara, K., Saganti, P. B., Takahashi, A., et al. (2020). Simultaneous exposure of cultured human lymphoblastic cells to simulated microgravity and radiation increases chromosome aberrations. *Life (Basel)* 10 (9), 187. doi:10.3390/life10090187

Yang, Y. G., Lindahl, T., and Barnes, D. E. (2007). Trex1 exonuclease degrades ssDNA to prevent chronic checkpoint activation and autoimmune disease. *Cell* 131 (5), 873–886. doi:10.1016/j.cell.2007.10.017

Zeitlin, C., Hassler, D. M., Cucinotta, F. A., Ehresmann, B., Wimmer-Schweingruber, R. F., Brinza, D. E., et al. (2013). Measurements of energetic particle radiation in transit to Mars on the Mars science laboratory. *Science* 340 (6136), 1080–1084. doi:10.1126/science.1235989

Zhang, S., Wimmer-Schweingruber, R. F., Yu, J., Wang, C., Fu, Q., Zou, Y., et al. (2020). First measurements of the radiation dose on the lunar surface. *Sci. Adv.* 6 (39), eaaz1334. doi:10.1126/sciadv.aaz1334

frontiers | Frontiers in Physics

TYPE Original Research
PUBLISHED 18 September 2024
DOI 10.3389/fphy.2024.1456472

OPEN ACCESS

EDITED BY
Alessandro Bartoloni,
National Institute of Nuclear Physics of Rome, Italy

REVIEWED BY
Canel Eke,
Akdeniz University, Türkiye
Mustafa Mohammad Rafiei,
Shahid Bahonar University of Kerman, Iran

*CORRESPONDENCE
Augusto Di Chicco,
augusto.di-chicco@ptb.de

†PRESENT ADDRESS
Felix Horst,
OncoRay—National Center for Radiation Research in Oncology, Faculty of Medicine, Dresden, Germany.

RECEIVED 28 June 2024
ACCEPTED 30 August 2024
PUBLISHED 18 September 2024

CITATION
Di Chicco A, Horst F, Boscolo D, Schuy C, Weber U and Zboril M (2024) Bonner sphere measurements of high-energy neutron spectra from a 1 GeV/u ^{56}Fe ion beam on an aluminum target and comparison to spectra obtained by Monte Carlo simulations.
Front. Phys. 12:1456472.
doi: 10.3389/fphy.2024.1456472

Bonner sphere measurements of high-energy neutron spectra from a 1 GeV/u ^{56}Fe ion beam on an aluminum target and comparison to spectra obtained by Monte Carlo simulations

Augusto Di Chicco[1]*, Felix Horst[2†], Daria Boscolo[2], Christoph Schuy[2], Uli Weber[2] and Miroslav Zboril[1]

[1]Physikalisch-Technische Bundesanstalt, Braunschweig, Germany, [2]Biophysics Department, GSI Helmholtzzentrum für Schwerionenforschung GmbH, Darmstadt, Germany

The goal of this work is to characterize the secondary neutron spectra produced by 1 GeV/u^{56}Fe beam colliding with a thick cylindric aluminum target and to perform a quantitative comparison with simulated results obtained with Monte Carlo codes. The measurements were performed using extended-range Bonner sphere spectrometers at two positions (15° and 40°) with respect to the beam direction. The secondary radiation field was simulated using four Monte Carlo codes (FLUKA, MCNP6, Geant4 and PHITS) and several physical models of nuclei transport and interaction. Neutron and proton energy distributions were simulated for the experimental measurement positions. The simulated neutron spectra, together with data measured with Bonner sphere spectrometers, after carrying out the correction of the contributions induced by the secondary protons, were used as input for the MAXED spectrum unfolding code to obtain the measured neutron spectra. Unfolded neutron spectra were compared with simulated ones to carry out a quantitative analysis of the performance of the chosen Monte Carlo codes and their corresponding physical models. This comparison showed that, because of experimental uncertainties and physical models, there are no unique solutions for each measurement location, but a range of solutions where the true experimental neutron spectra probably lie. The results showed deviations between 4.23% and 8.42% for some simulated spectra. Regarding the total integral values of neutron fluence and ambient equivalent dose, the unfolded neutron spectra showed deviations lower than 2%.

KEYWORDS

space radiation shielding, nuclear fragmentation, neutron spectrum, Monte Carlo, bonner sphere, spectra unfolding, MAXED

1 Introduction

Space exploration with semi-permanent and/or permanent settlements represents one of humanity's greatest and most ambitious challenges. One of the main risks for missions beyond Low Earth Orbit (LEO), without the protection of the Earth's atmosphere and its magnetic field, is related to acute and prolonged exposure to radiation [1]. Galactic cosmic radiation (GCR), consisting of a spectrum of highly energetic (up to several TeV/u) particles ranging from protons to heavy ions (up to ^{58}Ni), is a very important category of radiation to consider because of its isotropic and ubiquitous distribution which is highly penetrating and modulated only by the solar activity [2]. GCRs interact with spacecraft shielding material (aluminum alloys) by producing, through nuclear spallation or fragmentation reactions, high energy secondary particles such as light charged fragments and neutrons. Consequently, during the spacecraft and habitat design, it is crucial to consider not only the primary GCR, but also the secondary radiation field [3]. Neutrons especially, being neutral particles, can penetrate thick shields and deep into organic tissues before interacting with nuclei inducing the production of ionizing secondary radiation which would induce direct biological damage. The quality factor of neutrons, which is a measure of their harmfulness for radiation protection purposes, is strongly energy dependent [4, 5]. Recent studies have shown that neutrons contribute significantly to the ambient dose equivalent of the crew on the International Space Station (ISS) in different locations [6, 7].

Many studies on the impact of the thickness of spacecraft aluminum alloys for GCR shielding, have shown that secondary neutrons and light ions are major contributors to the total equivalent dose inside the scoring area protected by the shielding material [8–11]. However, these comparative studies show large discrepancies because nuclear fragmentation processes are simulated using semi-empirical physical models. These large uncertainties have a negative impact on both the design phase of spacecraft, shelters on the Moon and Mars, and on predictions of possible biological damage. To overcome these problems, simulation codes must take advantage of experimental reaction cross sections to correctly reproduce the secondary radiation field. However, the information of energy-dependent reaction cross sections is partial and in many cases absent [12–14]. The scarcity of experimental data is due to the small number of facilities where ground-based experiments can be performed to measure the secondary radiation field induced by high energy (up to 1 GeV/u) heavy ion beams. Such facilitates are for instance the Heavy Ion Medical Accelerator in Chiba (HIMAC) of the National Institute of Radiological Sciences in Japan, NASA Space Radiation Lab (NSRL) of Brookhaven National Laboratory in United States and Helmholtzzentrum für Schwerionenforschung GmbH (GSI) in Germany. Recent studies have compared experimental neutron yields from thick target with simulated ones, the results showed that no physical model implemented in the various Monte Carlo codes fit perfectly for all energies and measurement angles [15–18].

The work presented in this paper is part of a larger multidisciplinary study funded by the ESA-IBER-2021 program with the aim of studying the physical characteristics and radiobiological effects of the secondary radiation field produced by a 1 GeV/u ^{56}Fe ion beam bombarding a cylindrical aluminum target [19–21]. ^{56}Fe was chosen for this study because among the various high charge (Z) and energy (E) (HZE) nuclei, it is one of the most abundant [22]. The 1 GeV/u energy was chosen because at that energy the iron beam is considered a reasonable approximation for the GCR, making the largest contribution to the equivalent dose, and near the solar cycle maximum, about half of the iron flux is found at energies of 1 GeV/u and above [23]. In addition, most radiobiological experiments on cells, tissues and animals have been performed at this energy [24]. Finally, only the 1 GeV/u energy was chosen because of experimental limitations.

Different from previous works [19–21], which focused only on neutron dosimetry, this work focuses on spectrometry with the complete characterization of the secondary neutron spectra measured with the Bonner Sphere-based system of the Physikalisch-Technische Bundesanstalt (PTB), called NEMUS, measured in the Cave A of the GSI for two representative measurement angles and on the comparison and validation of the simulations obtained with four Monte Carlo codes commonly used int the field of radiation protection in space. The first part of the article describes the working principle of the NEMUS system for neutron measurement, the experimental setup used in Cave A and finally the four Monte Carlo codes and corresponding physical models considered for the simulation of the secondary radiation field. The second part presents the simulation results of the secondary radiation field, the comparison between measured and simulated NEMUS readings. Finally, the simulated neutron experimental spectra are compared with the experimental spectra obtained through the MAXED unfolding code, analyzing the deviations of the integral quantities of fluence and ambient equivalent dose.

2 Materials and methods

2.1 Multiple bonner sphere spectrometer system

Bonner sphere spectrometers (BSS) are the most commonly used method for neutron field characterization in the broad energy range between thermal up to GeV. A BSS consists of central thermal neutron sensors (CTNS) placed in the center of a spheres of moderating material (typically high-density polyethylene) with a variable diameter [25]. Neutrons entering the sphere undergo various elastic scattering reactions with the hydrogen nuclei contained in the polyethylene. They can either escape from the sphere, undergo capture or thermalize and reach the thermal sensor allowing in this last case the neutron detection. The probability of one of these reactions occurring depends mainly on the energy of the incident neutron and the size of the sphere [26]. When a Bonner sphere of diameter (or type) d is subjected to a given neutron flux, for this study produced by a ^{56}Fe particle beam, with an energy spectrum $\phi(E)$ (in neutron/cm^2 ^{56}Fe particle), its reading (or count rate) C_d (in neutron/^{56}Fe particle) can be described by a first-order Fredholm integral equation [27]:

$$C_d = \int_0^\infty R_d(E)\phi(E)dE \tag{1}$$

where $R_d(E)$ (in cm^2) is the Bonner sphere response function. The spherical shape of the moderator ensures an isotropic response;

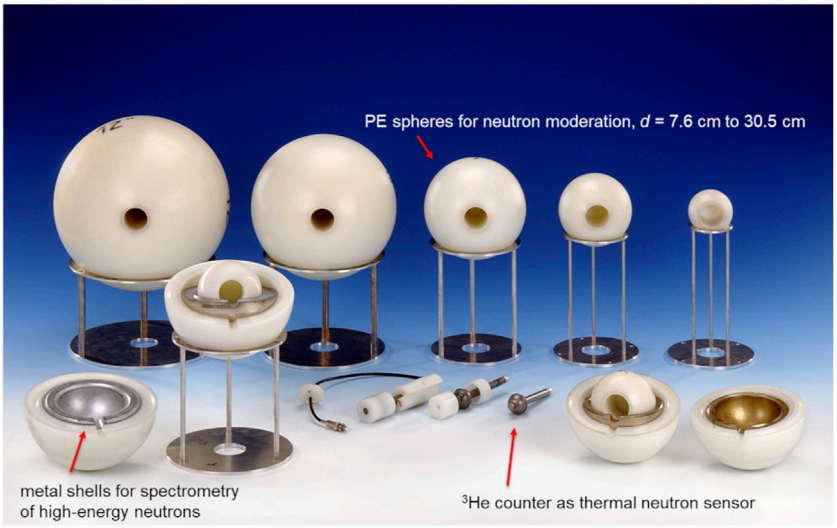

FIGURE 1
Photo of some Bonner spheres from NEMUS (photo taken and modified from [30]). Behind, there are five polyethylene spheres, in front on the right side is a modified open sphere with the metal shell of copper, in front on the left side is a modified open sphere with the metal shell of lead. Front in the center, there are three SP-9 counters with the various polyethylene components to assemble the sphere.

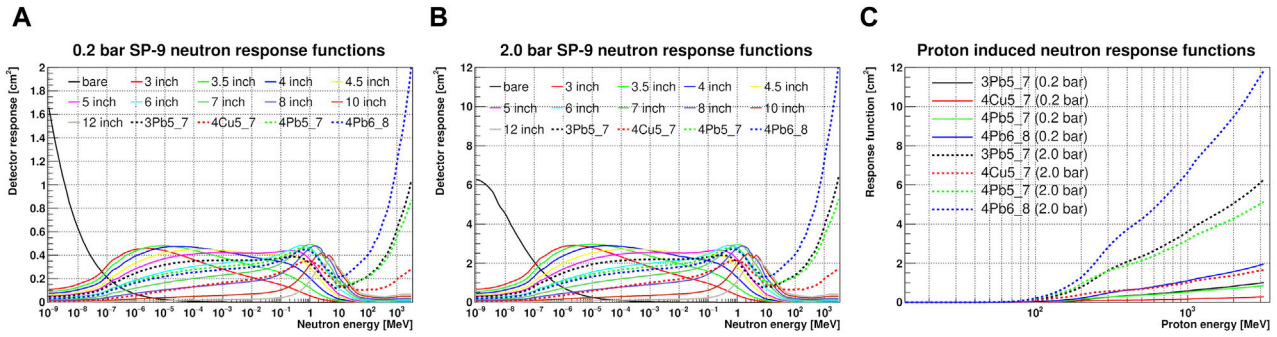

FIGURE 2
Neutron response functions of the NEMUS system of the **(A)** 0.2 bar, **(B)** 2.0 bar SP-9 and **(C)** proton induced for the modified spheres. The detector response functions with diameters between 3 and 12 inch indicate the neutron response functions for full polyethylene spheres (solid lines). The acronyms of the modified sphere response functions (dashed lines) indicate the various combinations of polyethylene inner sphere diameter (ISp), metal shell material and diameter (MeSh) and polyethylene outer shell diameter (OuSh), e.g., for 3Pb5_7, ISp = 3 inch, MeSh = lead (Pb) of 5 inch, OuSh = 7 inch.

however, the use of polyethylene alone as moderating material has limited the measurement to neutrons having energy below 20 MeV. To overcome this problem, modified spheres were designed by adding metallic shells (lead, tungsten, copper etc.), in order to exploit the high (n,xn) reaction cross sections for high energy neutrons [28]. The neutrons produced in the metal shells can thermalize in the inner polyethylene sphere reaching the CTNS, indirectly allowing the detection of the high-energy neutron incident on the sphere.

In this work, the PTB Neutron Multisphere Spectrometer (NEMUS) was used for neutron spectrum measurements [29], see Figure 1. It consists of a set of ten polyethylene spheres with diameters from 3 inch (7.62 cm) to 12 inch (30.48 cm) and four modified spheres with polyethylene and lead or copper inlets. Three sets of CTNSs were used. The first two are spherical ^{3}He-filled proportional counters (type SP-9, manufactured by Centronic Ltd., UK) with an approximate gas pressure of 200 kPa (2.0 bar) and 20 kPa (0.2 bar). The third thermal neutron sensor consists of a ^{235}U-coated fission chamber (type 307719, manufactured by LND Inc., United States). For the last thermal sensor, there are no modified sphere response functions because such spheres have not yet been developed.

Figure 2 shows the neutron response functions of the bare, full polyethylene and modified sphere for the 0.2 bar (A), 2.0 bar (B) ^{3}He-filled proportional counters. The neutron responses of the various detector configurations show that in order to detect neutrons having higher and higher energy, it is necessary to increase the diameter of the polyethylene spheres, because neutrons need more scattering events in order to thermalize and be detected by the CTNS. While for detecting neutrons with energy

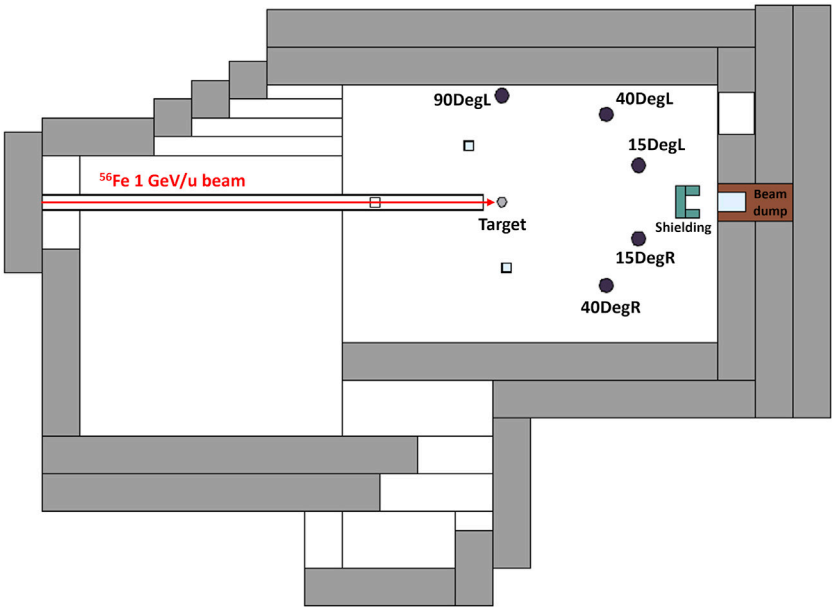

FIGURE 3
Sketch of GSI Cave A experimental setup with the measurement positions.

higher than 30 MeV, modified Bonner spheres need to be used. In addition, the two figures show that the 2.0 bar proportional counter, for the same type of Bonner Sphere, has a higher neutron sensitivity than the 0.2 bar counter. Regarding the data acquisition system used for this work, see reference [31] for more details.

An issue with modified Bonner spheres, in measurement conditions where high-energy charged particles (e.g., protons) are present, is that when these charged particles interact with the metal shell, they induce the production of further neutrons which by thermalizing can be detected by the neutron sensor. Consequently, these contributions must be subtracted from the total sphere reading C_d because they would induce an erroneous overestimation of the neutron spectrum under study [19, 20, 32]. Figure 2C shows the proton-induced neutron response functions of the modified spheres for the 0.2 bar (solid lines) and 2.0 bar (dashed lines) ^{3}He-filled proportional counters.

2.2 GSI cave A and experimental setup

The NEMUS system was used to carry out neutron measurements in GSI Cave A. The secondary radiation field was produced by a 1 GeV/u ^{56}Fe beam, interacting with a cylindrical aluminum target 20 cm in diameter and 20 cm high at 30 cm from the beam window. The ion beam was delivered into Cave A by the SIS18 synchrotron [33] in the form of pencil beam with a Gaussian shape (with a full-width-half-maximum of 1.2 cm) and spills of duration of ≈2.5 s. For constant monitoring of the ion beam, an Ionization Chamber (IC), placed in front of the beam exit window, produces signals as the particles pass through. Then, these signals are converted into digital pulses by a current-to-frequency converter (IFC) and collected by the NEMUS acquisition system. Each pulse corresponds to a certain number of primary ^{56}Fe particles (≈87 ^{56}Fe particle/IFC); this information was fundamental for obtaining absolute neutron yields in addition to the spectral information by the Bonner Spheres (see Section 3.2). For more information on the IC calibration procedure, see [34].

The experimental setup chosen in this work is similar to the one adopted by Boscolo et al. [19] and Sokolov et al. [20], Figure 3 shows a sketch of the implemented experiment with the labelled measurements positions for the Bonner Spheres; information concerning the angle and distance from the target, type of thermal sensor, and purpose are summarized in Table 1. For the 15DegL (Deg = degree, L = left) and 40DegL positions, neutron spectrometry measurements were performed by collecting the count rates produced by the various spheres, while the 15DegR (R = right), 90DegL and 40DegR positions were used only for neutron monitoring. For the measurement position at 15DegL, where the intensity of neutron and proton fluence is higher, the SP-9 0.2 bar thermal sensor was chosen because of its low neutron sensitivity which limits the count rate in the sensor so that there is no need to apply dead time correction.

2.3 Monte Carlo simulation codes

In this work, the simulation of the secondary radiation field measured in the GSI Cave A was done using the Monte Carlo codes FLUKA, MCNP, Geant4, and PHITS.

2.3.1 FLUKA

FLUKA (FLUktuierende KAskade in German, i.e., fluctuating cascade) version 4.2.2 [35, 36] is a general multipurpose Monte Carlo code for the calculation of particle transport and interaction with matter, it is used combined with the graphical user interface FLAIR (FLUKA Advanced Interface) version 3.2 [37]. The RQMD

TABLE 1 Information on the measurement positions of Bonner Spheres implemented in Cave A.

Measurement position label	Angle [°]	Distance from the target [cm]	CTNS	Purpose
15DegL	15	302	SP-9 (0.2 bar)	Spectrometry
40DegL	40	291	SP-9 (2.0 bar)	Spectrometry
90DegL	90	227	SP-9 (0.2 bar)	Monitoring
15DegR	−15	301	^{235}U FC	Monitoring
40DegR	−40	266	SP-9 (2.0 bar)	Monitoring

(Relativistic Quantum Molecular Dynamic) model [38] is used to simulate the nucleus-nucleus interactions in the energy range between 0.125 GeV/u and 5 GeV/u, for lower energies the Boltzmann Master Equation (BME) model is used. The neutron cross sections of the materials defined in FLUKA come from various data libraries (see the reference manual for more information). FLUKA has been used for the study of the secondary radiation field induced by proton beam [39–42], heavy ions [19, 20, 33, 40, 43–45] and by GCR [11, 46–48] with different material targets.

The Cave A geometric model takes into account the dimensions and material compositions of both the shielding elements that define the experimental room (such as the concrete walls and roof) and the materials inside the experimental room itself (experimental table where the target is placed, beam dump, etc.). Table 2 lists the properties of materials implemented in the geometric model of Cave A for all Monte Carlo simulations. This geometric model has already been widely used for previous studies to simulate the secondary radiation field produced by the interaction of various ion beams with different targets [19, 20, 33, 49]. The geometric model was modified to be consistent with the experimental setup described in Section 2.2. For the scoring of neutrons and protons at the measurement points, the USRTRACK card was used; it allows the extraction in the selected regions of the differential distribution of fluence in energy [dΦ/dE (particle/cm^2 GeV•^{56}Fe particle)] using a logarithmic binning from 100 GeV down to 0.1 meV.

2.3.2 MCNP 6.1

MCNP6 (Monte Carlo N-Particle) version 6.1 [50], is a general multipurpose Monte Carlo radiation transport code developed by Los Alamos National Laboratory (LANL) which resulted from the fusion of MCNPX and MCNP5 codes. The Cave A geometric model used for the simulations with the FLUKA code was exported into a format readable and executable by MCNP using the FLAIR interface. In the input file, it is possible to set the importance of the particles in the cells that define the geometry of the problem. For this study, all particles were considered (and not just heavy ions, neutrons, and protons) because light ions and other particles could trigger further nuclear reactions by inducing in turn the production of further neutrons [51]. The simulation of neutron transport having energies up to 20 MeV was done using the ENDF/B-VII (Evaluated Nuclear Data File) [52] cross section library, while for protons the selected library was ENDF70prot [53]. For proper thermal neutron transport, below 4 eV, the S (α,β) library was used. For energy ranges where there are no cross-section data libraries, particle transport is calculated by the use of nuclear models. These models, for neutron and proton transport, are based on the combination of intra-nuclear cascade (INC) models and evaporation (EV) models. In this work, the Cascade-Exciton Model (CEM3.03) was chosen, which includes both INC and EV models. For the transport of all other particles, the Los Alamos Quark-Gluon String model (LAQGSM) was used. MCNP has been used for the study of the secondary radiation field induced by proton beam [39, 51], heavy ions [15, 54–56] and cosmic radiation [57–59] with different material targets. The energy distribution of the neutron and proton fluence [Φ (particle/cm^2 ^{56}Fe particle)] in the measurement points was scored using the averaged cell fluence tally F4.

2.3.3 GEANT4

Geant4 (GEometry ANd Tracking 4) version 11.0 [60] is a toolkit to simulate the passage and interaction of particles with the matter. The FLUKA geometric model of the Cave A experimental room was converted into a GDML (Geometry Description Markup Language) file, readable by Geant4, using the python library PyG4ometry [61]. Material neutron properties are defined by the G4NDL4.6 neutron library, based on the data library JEFF-3.3 [62]. For the hadron inelastic physics, the predefined QGSP_BIC_HP physics list was considered, where the acronym "HP" refers to the data driven high precision neutron package (NeutronHP), this option enables the use of neutron cross sections for energies below 20 MeV. In order to take into account thermal neutron scattering events (below 0.4 eV), the G4NeutronHPThermalScattering option was enabled. In addition to this option, certain materials were defined with the labels "TS_H_Water" or "TS_C_of_Graphite" to properly activate the scattering cross sections in the thermal energy range and thus the thermal neutron scattering events. In Geant4 we focused on physical models that simulate nuclear fragmentation of ions. All three available sets of physical models were chosen [58, 63, 64]. The first one is the Binary Intra-Nuclear cascade (BIC), the second one is the Quantum Molecular Dynamics (QMD) and the last is the Liege Intranuclear Cascade (INCLXX). Geant4 has been used for the study of the secondary radiation field induced by proton beam [42, 44, 65–67], heavy ions [18, 44, 54] and cosmic radiation [48, 58, 68, 69] with different material targets. Within the code, geometric volumes indicating the measurement points were set as Sensitive Detectors. In this way it is possible to choose and extract the type of information within the selected cell such as the nature of the particle, its energy and its track length. The data were processed to extract the energy distributions of neutron and proton fluences [Φ (particle/cm^2 ^{56}Fe particle)] like how it is done by MCNP6 F4 tally, recording the particle track length (in particle cm/^{56}Fe particle) entering the Sensitive Detector and dividing its value by the volume of the Sensitive Detector (in cm^3).

TABLE 2 GSI Cave A material proprieties implemented in Monte Carlo calculations using element Mass Fractions (MF) or Weight Fractions (WF). (Other components such as the Beam tube and the Beam dump were defined as pure iron).

Aluminum target (2.65 g/cm^3)		Concrete walls (2.35 g/cm^3)		Air (1.29 10^{-3} g/cm^3)		Polyethylene in beam shielding (0.94 g/cm^3)	
Element	MF	Element	WF	Element	WF	Element	WF
Al	94.45	H	0.006	N	0.74379	H	0.66667
Si	0.4	O	0.511	C	0.00012	C	0.33333
Fe	0.4	Fe	0.012	H	0.00177	-	-
Cu	0.1	Si	0.358	O	0.24169	-	-
Mn	0.6	C	0.004	Ar	0.01263	-	-
Mg	3.0	Al	0.02	-	-	-	-
Cr	0.5	Ca	0.086	-	-	-	-
Zn	0.2	Na	0.003	-	-	-	-
Sn	0.15	-	-	-	-	-	-

2.3.4 PHITS

PHITS (Particle and Heavy Ion Transport code System) version 3.32 [70, 71] is a general-purpose Monte Carlo particle transport simulation code developed by the Japan Atomic Energy Agency (JAEA). The language adopted by PHITS to describe the geometric model of Cave A experimental room and the definition of material properties is the same as that used in MCNP6. For neutron energies between 20 MeV down to thermal energies, the JENDL-4.0 [72] cross section library was used. For energies between 20 MeV and 200 MeV, the JENDL-4/HE [73] data library was used which contains the cross sections for neutron and proton induced reactions for some materials. For neutron energies above 200 MeV or in the absence of the cross sections, the INCL4.6 physics model combined with the generalized evaporation model (GEM) was used. This model was also used for reactions induced by protons, deuterons, tritium, ^{3}He and alpha particles. For the simulation of nuclear fragmentation processes of heavy ions, the JQMD2.0 (Quantum Molecular Dynamics version 2) model was chosen and coupled with Kurotama model for calculating the total cross sections of nucleus-nucleus reaction. PHITS has been used extensively for the simulation of the secondary neutron field produced by protons [39, 55], heavy ions [15, 45, 55, 74, 75] and cosmic radiation [76–79] with different material targets. The energy distribution of the neutron and proton fluence [Φ (particle/cm^2 ^{56}Fe particle)] in the measurement points was scored using the cell fluence tally T-Track.

For all simulations, no variance reduction techniques were employed and the number of primary particles simulated was 10^7, so that the relative error was of the order of 0.09% for the measurement positions at 15DegL and 40DegL. Geant4 and PHITS simulations were run using a computing cluster which uses two 14-core Intel Xeon E5-2690v4 2.6 GHz and two 14-cores Intel Xeon Gold 6,132 2.6 GHz processors. MCNP6 simulations were run with a desktop PC with 8-core AMD Ryzen 7 Pro 5750G 3.8 GHz, while FLUKA simulations were run with a desktop PC with 8-core Intel Core i7-3770 3.4 GHz.

All results calculated with the four Monte Carlo codes considered as well as all other results obtained in this work were processed and analyzed using the ROOT (version 6.26) framework [80].

3 Results and discussion

3.1 Calculated secondary radiation field

The first information extracted through Monte Carlo codes is the spatial distribution of neutron and proton fluence within the Cave A experimental room. Figure 4 shows the bidimensional (xz plane) distribution of the total neutron (A), photon (B) and proton (C) fluence obtained with MCNP using the CEM3.03 physical model. Like the FLUKA USRBIN card, these distributions were obtained using MCNP TMESH and RMESH tallies. The results showed that for the measurement positions at 15DegL, 40DegL and 90DegL, neutrons represent an important contribution of the total fluence with fractions ranging between ≈43% and ≈45%. While photons exhibit fractions relative to the total fluence for the 15DegL, 40DegL and 90DegL measurement positions of ≈37%, ≈44%, and ≈51%, respectively. These photons can result from various processes, such as neutron capture and de-excitation of excited nuclei generated by both the primary beam or the target nuclear fragments [81]. Despite their ubiquitous presence during the processes of heavy ion interaction with a target, secondary gamma rays will not be further investigated, as they are beyond the scope of this work. Finally, protons have fractions relative to the total fluence at the 15DegL, 40DegL, and 90DegL measurement points of ≈11%, ≈3%, and ≈0.3%, respectively. As mentioned in Section 2.1, high-energy protons can interact with the metal shells of the modified Bonner spheres and induce the production of spallation neutrons that would be added to the primary neutrons. Consequently, such parasitic contributions must be eliminated especially for small scattering angles relative to the beam direction where proton contributions are more significant. It is possible to experimentally characterize the protons and/or other products of nuclear fragmentation induced by the iron beam with the target, through the use of ΔE-E telescopes [82–84]. In a previous

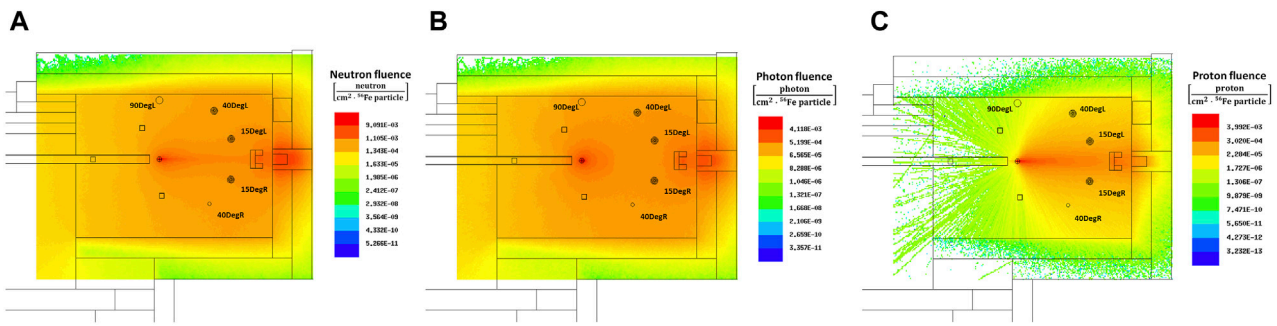

FIGURE 4
2D neutron **(A)** gamma ray **(B)**, and proton **(C)** fluence distribution in the Cave A experimental room obtained with MCNP6.1 using the CEM3.03 model.

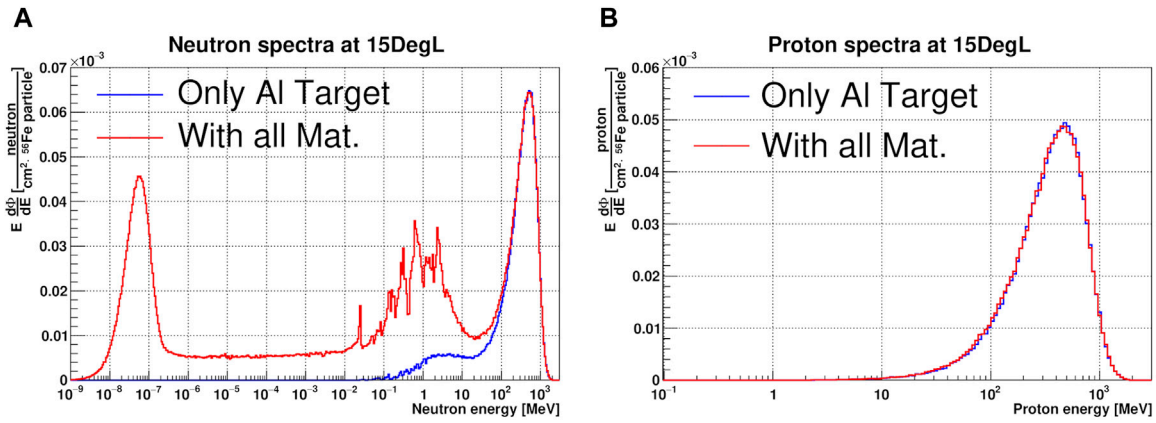

FIGURE 5
Comparison between neutron **(A)** and proton **(B)** fluences in lethargy units and normalized per ^{56}Fe particle at the 15DegL measurement point obtained with MCNP- CEM3.03 by defining only the material properties of the aluminum target (blue solid line) and all materials in Cave A (red solid line).

IBPER-17 campaign, such detectors were used and data analysis is still in progress. In this work, the proton contributions are obtained from Monte Carlo simulations, however these predictions are also biased by uncertainties of the nuclear models.

Another study concerns the shape and contributions of the energy distributions of the simulated neutron and proton fluences. Figure 5A shows the comparison of neutron (A) and proton (B) fluences extracted from the 15DegL position by MCNP-CEM3.03 considering only the aluminum target (blue solid line) and defining all material properties present in Cave A (red solid line). From the ideal case, the direct peak, having a mean energy of (558.5 ± 3.1) MeV, is produced by the fragmentation interactions of the ion beam with the target [85], while the tail of the neutron spectrum for energies below 30 MeV should be induced by inelastic collisions of fragmentation products and other secondary particles interacting with the target. In the case where the material properties of Cave A are defined, the spectrum is divided into four specific zones, the direct peak (energies above 20 MeV), evaporation peak (energies between 100 keV and 20 MeV), the epithermal zone (energies between 0.4 eV and 100 keV) and the thermal peak (energies below 0.4 eV). The evaporation peaks are produced by excited fragment of heavy ions and by the excitation of nuclei induced by high-energy protons and neutrons; the excited nuclei subsequently produce isotropic evaporation neutrons [86]. The structure of the evaporation peak depends mainly on the nuclear resonances of the nuclei which define the Cave A material composition. In the epithermal zone, neutrons interact mainly though elastic scattering with hydrogen nuclei in the concrete walls. During these collisions, neutrons gradually lose their energies until they reach thermal equilibrium (≈25 meV) with the surrounding nuclei and are finally absorbed [87]. This comparison showed how the geometric model implemented in the simulations affects the shape of the neutron energy spectrum, underscoring the need to have a sufficiently accurate geometric model to compare simulated results with experimental ones.

Concerning the proton spectrum, see Figure 5B, no significant differences are seen between the two configurations, both spectra have a mean energy of (490 ± 3) MeV. This means that the proton contributions are exclusively related to the direct production of the collision reactions of ^{56}Fe ions with the aluminum target.

Figure 6 shows the comparison between calculated neutron and proton spectra in lethargy units at the 15DegL (A,B), 40DegL (C,D)

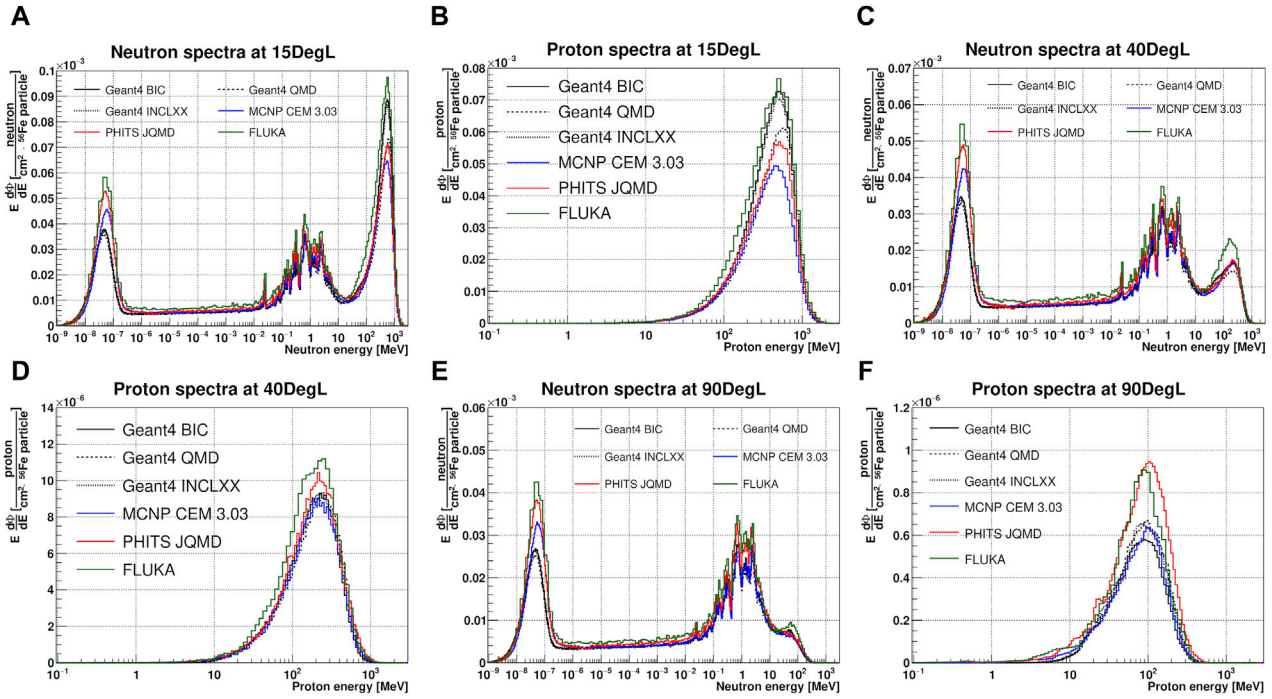

FIGURE 6
Comparison between calculated neutron and proton spectra in lethargy units and normalized per ^{56}Fe particle at the 15DegL **(A, B)**, 40DegL **(C, D)** and 90DegL **(E, F)** measurement points obtained with four Monte Carlo codes and physical models.

TABLE 3 Calculated neutron fluences [neutron/cm^2 ^{56}Fe particle] extracted from the 15DegL, 40DegL and 90DegL measurement points as a function of the neutron energy range (Thermal: E < 0.4 eV, Epithermal: 0.4 eV < E < 100 keV, Evaporation: 100 keV < E < 20 MeV and Direct: E > 20 MeV).

Pos	Energy range	GEANT4 QMD	GEANT 4 INCLXX	GEANT4 BIC	MCNP CEM	PHITS JQMD	FLUKA
15DEGL	Thermal	7.36 10^{-5}	7.65 10^{-5}	7.78 10^{-5}	8.83 10^{-5}	1.04 10^{-4}	1.17 10^{-4}
	Epithermal	6.74 10^{-5}	6.91 10^{-5}	7.04 10^{-5}	7.33 10^{-5}	8.24 10^{-5}	9.90 10^{-5}
	Evaporation	9.46 10^{-5}	9.88 10^{-5}	1.00 10^{-4}	1.04 10^{-4}	1.19 10^{-4}	1.33 10^{-4}
	Direct	1.25 10^{-4}	1.47 10^{-4}	1.48 10^{-4}	1.21 10^{-4}	1.36 10^{-4}	1.86 10^{-4}
	Total	3.61 10^{-4}	3.91 10^{-4}	3.97 10^{-4}	3.86 10^{-4}	4.41 10^{-4}	5.35 10^{-4}
40DEGL	Thermal	6.78 10^{-5}	7.06 10^{-5}	7.17 10^{-5}	8.21 10^{-5}	9.65 10^{-5}	1.09 10^{-4}
	Epithermal	6.31 10^{-5}	6.48 10^{-5}	6.60 10^{-5}	6.78 10^{-5}	7.67 10^{-5}	9.19 10^{-5}
	Evaporation	8.72 10^{-5}	9.16 10^{-5}	9.24 10^{-5}	9.22 10^{-5}	1.07 10^{-4}	1.19 10^{-4}
	Direct	3.69 10^{-5}	4.05 10^{-5}	4.08 10^{-5}	3.91 10^{-5}	4.14 10^{-5}	5.33 10^{-5}
	Total	2.55 10^{-4}	2.68 10^{-4}	2.71 10^{-4}	2.81 10^{-4}	3.22 10^{-4}	3.73 10^{-4}
90DEGL	Thermal	5.39 10^{-5}	5.66 10^{-5}	5.71 10^{-5}	6.58 10^{-5}	7.57 10^{-5}	8.50 10^{-5}
	Epithermal	5.05 10^{-5}	5.31 10^{-5}	5.35 10^{-5}	5.40 10^{-5}	6.07 10^{-5}	7.10 10^{-5}
	Evaporation	7.99 10^{-5}	8.59 10^{-5}	8.59 10^{-5}	8.36 10^{-5}	9.98 10^{-5}	1.08 10^{-4}
	Direct	1.32 10^{-5}	1.32 10^{-5}	1.32 10^{-5}	1.22 10^{-5}	1.35 10^{-5}	1.61 10^{-5}
	Total	1.98 10^{-4}	2.09 10^{-4}	2.10 10^{-4}	2.16 10^{-4}	2.50 10^{-4}	2.80 10^{-4}

and 90DegL (E,F) measurement points obtained with all four Monte Carlo codes and physical models described in Section 2.3. The integral values of total fluence and as a function of the energy range are summarized in Table 3 for neutrons and Table 4 for protons. Globally, both FLUKA neutron and proton spectra are consistent with those obtained by Boscolo et al [19] and Sokolov

TABLE 4 Calculated total proton fluences [proton/cm^2 ^{56}Fe particle] extracted from the 15DegL, 40DegL and 90DegL measurement points.

Pos	GEANT4 QMD	GEANT4 INCLXX	GEANT4 BIC	MCNP CEM	PHITS JQMD	FLUKA
15DEGL	9.38 10^{-5}	1.10 10^{-4}	1.11 10^{-4}	8.31 10^{-5}	9.49 10^{-5}	1.28 10^{-4}
40DEGL	1.67 10^{-5}	1.70 10^{-5}	1.67 10^{-5}	1.63 10^{-5}	1.86 10^{-5}	2.13 10^{-5}
90DEGL	1.24 10^{-6}	1.19 10^{-6}	1.09 10^{-6}	1.16 10^{-6}	1.78 10^{-6}	1.59 10^{-6}

et al. [20]. As for the simulated results obtained on the right side with respect to the beam line, they will not be shown in this paper because they are symmetrical to those obtained in the left side with deviations of less than 2%.

Neutron spectra at the 15DegL position, show a direct peak with average energy of 559.4 ± 6.5 MeV. FLUKA shows the highest integral fluence in the energy range of the direct peak followed by Geant4-BIC and Geant4-INCLXX, while for MCNP-CEM it is the lowest. The total integral neutron fluence is highest for FLUKA and lowest for Geant4-QMD. While the proton spectra show a direct peak with average energy of (488.2 ± 8.5) MeV, the total fluence is highest for FLUKA and lowest for MCNP-CEM simulations.

Neutron spectra at the 40DegL position show a direct peak with average energy of (252.2 ± 2.4) MeV. The highest value of integral fluence on the direct peak is obtained by FLUKA followed by PHITS-JQMD, while the lowest value is obtained with Geant4-QMD. FLUKA and PHITS-JQMD have the highest total neutron fluence integral value, while the lowest value was found with Geant4-QMD. The proton spectra show a direct peak with average energy of (217.1 ± 18.6) MeV, the total fluence is highest for FLUKA followed by PHITS-JQMD, while the other simulations are equivalent. Neutron spectra at the 90DegL position show a direct peak with average energy of (60.3 ± 14.5) MeV. The trend of the fluence integrals is similar to that found at the 40DegL position except in the range of the direct peak where the fluence integral is minimal with MCNP-CEM. The proton spectra show a direct peak with average energy of (101.4 ± 22.3) MeV, the total fluence is highest for PHITS-JQMD and lowest for Geant4-BIC.

3.2 Measured NEMUS readings

As mentioned in Section 2.2, the various readings of the NEMUS system are obtained by repeating the measurements and changing the sphere diameter and type. Each reading consists of a number that is equivalent to the number of neutrons detected by the thermal sensor, normalized by dividing by the total number of primary ^{56}Fe particles generated by the accelerator. Table 5 lists the normalized readings for the measurement positions at 15DegL and 40DegL as a function of the sphere dimension and type. Table 5 also lists the relative uncertainties of the various readings associated with the statistical uncertainty of the experimental data. Readings of the 3Pb5_7 and 4Pb6_8 spheres for the 15DegL and 40DegL measurement positions, respectively, are missing due to the instability of the ion beam, which made the experimental data unusable. In addition, there are the readings of the modified spheres with and without the proton contributions correction. Since protons generate neutrons rather uniformly inside the spheres [19], Equation 1 can be used to estimate the amount of proton-induced neutron contributions. Depending on the sphere type and the physical model of the Monte Carlo simulation, it has been estimated that protons contribute between 11% and 26% of the total reading with a standard deviation of ≈2% for the 15DegL position, while for the 40DegL position, they contribute between 2% and 5% with a standard deviation of ≈0.24%.

Figure 7 shows the comparison between experimental readings measured with NEMUS and those calculated with Monte Carlo codes using Equation 1 for the 15DegL measurement position. The comparison shows that for the bare detector all simulations are higher suggesting that the thermal neutron peak in the simulations is overestimated. For spheres between 4″ and 12″, the calculated readings are underestimated suggesting that the real neutron spectrum in the energy range between the epithermal and evaporative zones has a higher fluence that caused by the oversimplified geometric model of GSI Cave A used for the simulations. Finally, for the modified spheres (BS number between 22 and 25) the calculated readings are underestimated compared with the experimental ones. However, it is difficult to estimate the impact of the neutron direct peak since the modified sphere response functions also includes the evaporation and epithermal energy ranges (see Figures 2A, B). The only way to estimate the real deviations is to reconstruct the measured neutron spectrum; an unfolding procedure is thus required to achieve this goal.

3.3 Neutron spectra unfolding and ambient dose equivalent analysis

The unfolding, or deconvolution, procedure consists of solving the inverse problem associated with Equation 1 in order to estimate the neutron spectrum $\phi(E)$ that has generated the detector reading C_d. In the case of neutron spectrometry with Bonner Spheres, although there is a limited number M of spheres by size and type, it is necessary to estimate the neutron spectrum with a sufficiently fine energy binning N. Equation 1 can be written in the following discretized formula [88]:

$$C_d + \varepsilon_d = \sum_i^N R_{d,i}\phi_i \tag{2}$$

where ε_d is the difference between the predicted and measured values. In this case, where $N \gg M$, the solution of Equation 2 is not unique and an appropriate unfolding procedure must be used in order to have a realistic estimation of the neutron spectrum. In this work, the MAXED [88] code based on the maximum entropy method (see the reference for more details on the working

TABLE 5 Experimental NEMUS readings C_d [neutron/^{56}Fe particle] with and without the proton correction (p. c.) and the associated relative uncertainties as a function of Bonner Sphere (BS) type for measurement positions at 15DegL and 40DegL.

BS type	BS number	15DegL (SP-9 0.2 bar)			40DegL (SP-9 2.0 bar)		
		C_d	C_d (p. c.)	Rel. Unc. [%]	C_d	C_d (p. c.)	Rel. Unc. [%]
Bare	0	$2.27\ 10^{-5}$	$2.27\ 10^{-5}$	0.61	$1.58\ 10^{-4}$	$1.58\ 10^{-4}$	0.28
3 inch	3	$5.78\ 10^{-5}$	$5.78\ 10^{-5}$	0.34	$3.15\ 10^{-4}$	$3.15\ 10^{-4}$	0.17
4 inch	4	$8.68\ 10^{-5}$	$8.68\ 10^{-5}$	0.49	$4.54\ 10^{-4}$	$4.54\ 10^{-4}$	0.22
5 inch	5	$1.01\ 10^{-4}$	$1.01\ 10^{-4}$	0.29	$5.12\ 10^{-4}$	$5.12\ 10^{-4}$	0.16
6 inch	6	$1.04\ 10^{-4}$	$1.04\ 10^{-4}$	0.34	$5.04\ 10^{-4}$	$5.04\ 10^{-4}$	0.13
8 inch	8	$8.57\ 10^{-5}$	$8.57\ 10^{-5}$	0.32	$3.96\ 10^{-4}$	$3.96\ 10^{-4}$	0.13
10 inch	10	$6.32\ 10^{-5}$	$6.32\ 10^{-5}$	0.33	$2.75\ 10^{-4}$	$2.75\ 10^{-4}$	0.17
12 inch	12	$4.78\ 10^{-5}$	$4.78\ 10^{-5}$	0.69	$1.86\ 10^{-4}$	$1.86\ 10^{-4}$	0.34
3Pb5_7	22	-	-	-	$5.84\ 10^{-4}$	$5.61\ 10^{-4}$	0.16
4Cu5_7	23	$9.82\ 10^{-5}$	$8.50\ 10^{-5}$	0.31	$3.73\ 10^{-4}$	$3.65\ 10^{-4}$	0.14
4Pb5_7	24	$1.84\ 10^{-4}$	$1.47\ 10^{-4}$	0.32	$5.63\ 10^{-4}$	$5.42\ 10^{-4}$	0.13
4Pb6_8	25	$2.67\ 10^{-4}$	$1.98\ 10^{-4}$	0.30	-	-	-

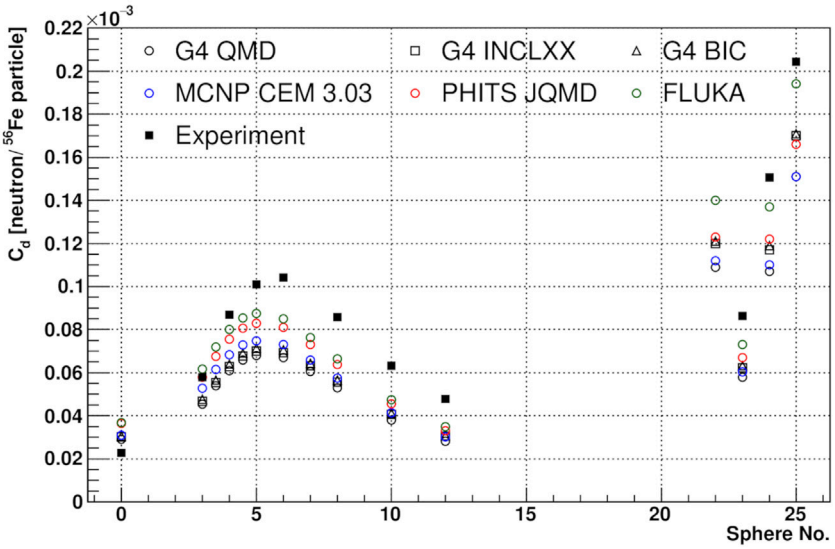

FIGURE 7
Comparison between measured and simulated NEMUS readings at position 15DegL as a function of the BS sphere number, both data sets are normalized per ^{56}Fe particle.

principle of the code) was chosen for the neutron spectra unfolding. MAXED solved the problem of non-uniqueness of the solution of Equation 2 by introducing *a priori* information, i.e., starting from an initial default spectrum that is physically realistic, it is possible to obtain a unique unfolded spectrum that is consistent with the experimental data. The default spectrum that is used as input for the MAXED algorithm can be derived, as in the case of this work, from Monte Carlo simulations. The characteristic peaks of the default spectrum are preserved in the solution even though the energy resolution of Bonner Spheres cannot actually recognize them [89]. MAXED has been widely used and validated for the spectra unfolding produced by cosmic neutrons [90, 91], neutrons induced by carbon [49] and proton beams [92–94] and by photons [95].

To be initialized MAXED needs the measured readings of the Bonner Spheres with uncertainties, the matrix with the neutron response functions, a default energy spectrum and a χ^2 target value for the unfolded readings. Estimated uncertainties from external sources were added by quadrature to the experimental uncertainties,

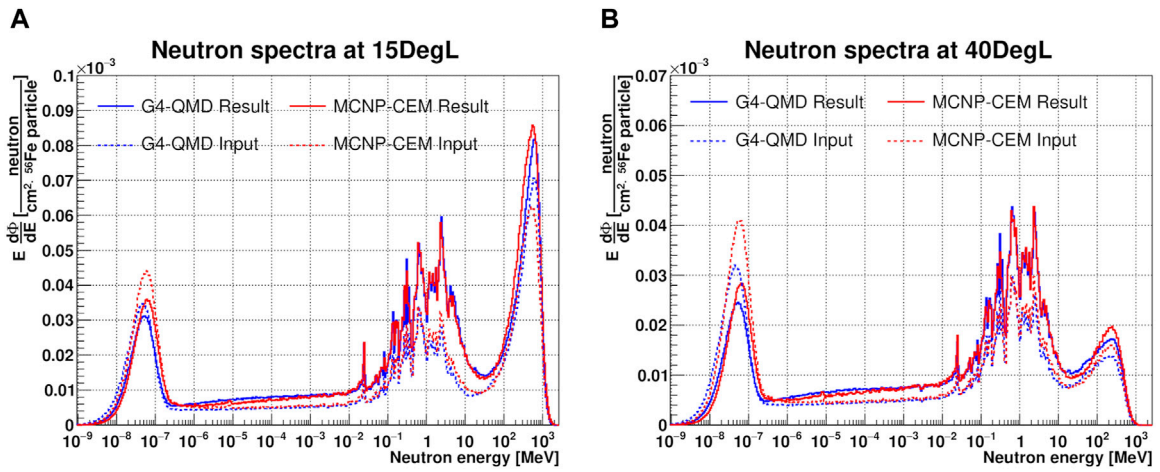

FIGURE 8
Comparison between unfolded (solid line) and corresponding simulated (dashed line) neutron spectra in lethargy units and normalized per ^{56}Fe particle using G4-QMD (blue lines) and MCNP-CEM (red lines) for the 15DegL **(A)** and 40DegL **(B)** measurement positions.

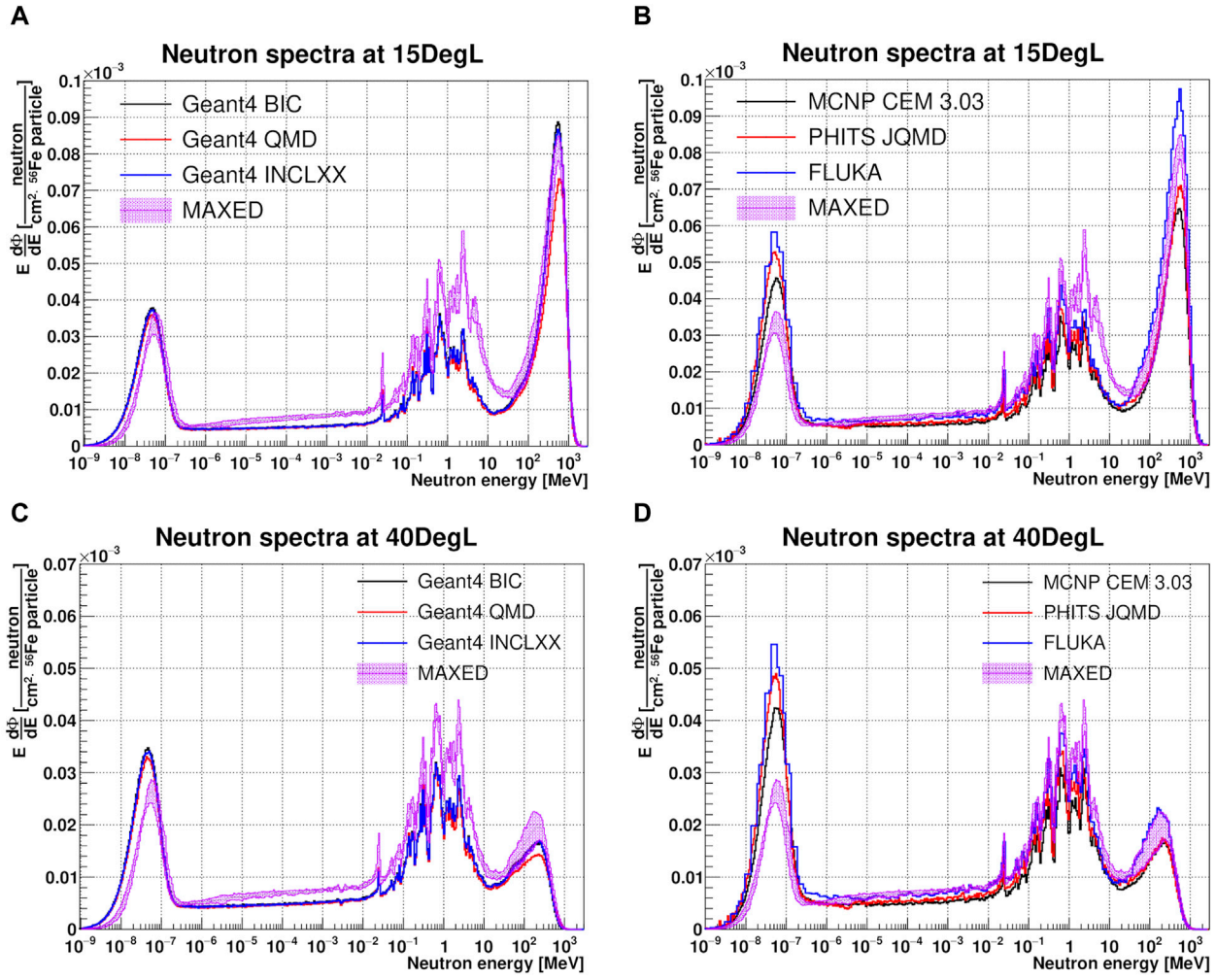

FIGURE 9
Comparison between simulated (lines) neutron spectra and MAXED solution set (purple shadow) of the unfolded neutron spectrum in lethargy units and normalized per ^{56}Fe particle for the 15DegL **(A, B)** and 40DegL **(C, D)** measurement positions.

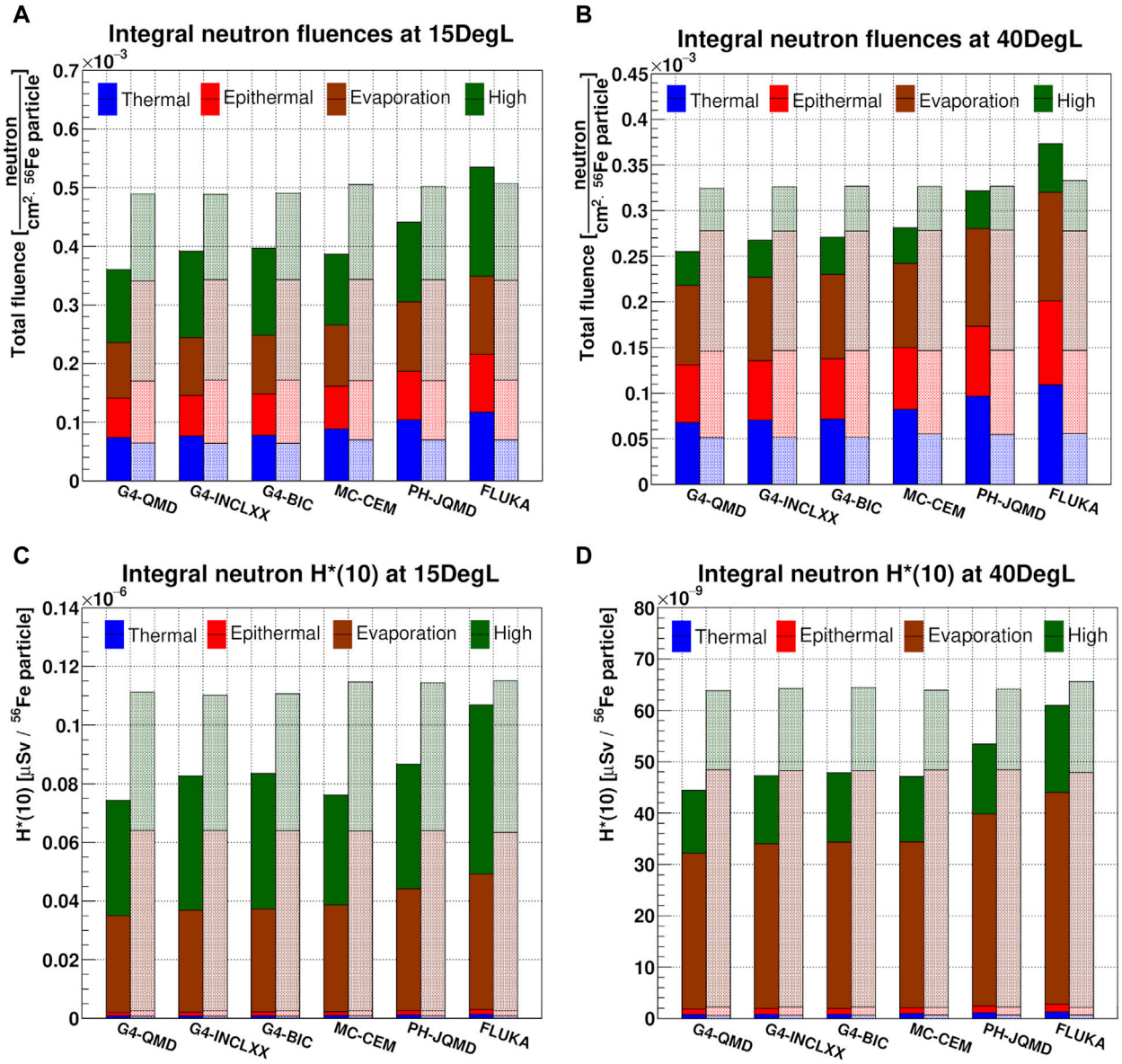

FIGURE 10
Integral neutron fluence and *H** (10) quantities between simulated (filled bar chart) and unfolded (semi-transparent bar chart) results according neutron energy ranges for the 15DegL **(A, C)** and 40DegL **(B, D)** measurement positions. Both pairs of data are normalized per ^{56}Fe particle.

such as the uncertainty of the NEMUS response functions, the uncertainty of the Monte Carlo simulations, and finally the uncertainty related to the correction of proton contributions (the latter was added only for the readings of the modified spheres). The main purpose of unfolding with MAXED is to have an estimate of the neutron spectrum that is consistent with the experimental data, which can be used to qualitatively evaluate the physical models implemented in the Monte Carlo simulations by comparing the unfolded spectra with those obtained by simulation.

Figure 8 shows the comparison between simulated (dashed line) spectra used as input default spectra and their corresponding unfolded (solid line) output neutron spectra, using G4-QMD (blue lines) and MCNP-CEM (red lines) for the 15DegL (A) and 40DegL (B) measurement position. The comparison shows that the two unfolded spectra are similar but not coincident over the entire energy range and this could be caused by the experimental and external statistical uncertainties introduced in MAXED. On the direct peak, the differences in the two unfolded spectra could also be caused by correction of the proton contributions (only on the direct peak), which are different for different Monte Carlo codes (see Section 3.1).

Figure 9 shows the comparison between simulated neutron spectra (lines) used as input default spectra and the range of MAXED solutions for the 15DegL (A,B) and 40DegL (C,D) measurement positions. The shaded area of MAXED was obtained by considering, bin by bin, the range between the minimum and maximum value among the different unfolding results. The results show that there are large deviations for all energy ranges. For the range between thermal and evaporation

TABLE 6 Estimated mean neutron fluences [neutron/cm^2 ^{56}Fe particle] with MAXED extracted from the 15DegL and 40DegL measurement positions and corresponding deviations [%] from the Monte Carlo results (Thermal: E < 0.4 eV, Epithermal: 0.4 eV < E < 100 keV, Evaporation: 100 keV < E < 20 MeV and Direct: E > 20 MeV).

Pos	Energy range	MAXED	G4 QMD	G4 INCLXX	G4 BIC	MCNP CEM	PHITS JQMD	FLUKA
15DEGL	Thermal	6.69 10^{-5} ± 4.46%	10.00	14.29	16.26	31.86	55.39	75.37
	Epithermal	1.04 10^{-4} ± 3.05%	−35.50	−33.83	−32.58	−29.81	−21.14	−5.21
	Evaporation	1.71 10^{-4} ± 0.35%	−44.69	−42.24	−41.34	−39.48	−30.35	−22.38
	Direct	1.55 10^{-4} ± 4.92%	−19.05	−4.94	−4.23	−21.95	−12.28	20.06
	Total	4.97 10^{-4} ± 1.54%	−27.42	−21.26	−20.20	−22.39	−11.25	7.59
40DEGL	Thermal	5.33 10^{-5} ± 3.39%	27.27	32.53	34.65	54.05	81.10	103.95
	Epithermal	9.33 10^{-4} ± 1.76%	−32.35	−30.52	−29.28	−27.31	−17.86	−1.47
	Evaporation	1.31 10^{-4} ± 0.39%	−33.65	−30.37	−29.70	−29.87	−18.27	−9.35
	Direct	4.92 10^{-5} ± 4.15%	−24.85	−17.61	−17.05	−20.55	−15.67	8.42
	Total	3.27 10^{-4} ± 0.60%	−22.04	−18.25	−17.20	−14.08	−1.58	14.01

TABLE 7 Estimated mean neutron H* (10) [μSv/^{56}Fe particle] with MAXED extracted from the 15DegL and 40DegL measurement points and corresponding deviations [%] from the Monte Carlo results (Thermal: E < 0.4 eV, Epithermal: 0.4 eV < E < 100 keV, Evaporation: 100 keV < E < 20 MeV and Direct: E > 20 MeV).

Pos	Energy range	MAXED	G4 QMD	G4 INCLXX	G4 BIC	MCNP CEM	PHITS JQMD	FLUKA
15DEGL	Thermal	7.85 10^{-10} ± 5.53%	6.29	10.46	12.39	31.59	53.34	74.06
	Epithermal	1.81 10^{-9} ± 3.31%	−35.11	−33.50	−32.31	−31.83	−22.04	−9.06
	Evaporation	6.13 10^{-8} ± 0.27%	−46.19	−43.29	−42.48	−40.60	−32.14	−24.58
	Direct	4.88 10^{-8} ± 4.35%	−19.41	−5.98	−5.38	−23.24	−12.92	18.08
	Total	1.13 10^{-7} ± 1.75%	−34.04	−26.60	−25.86	−32.43	−23.06	−5.17
40DEGL	Thermal	6.26 10^{-10} ± 4.57%	22.55	27.59	29.62	53.32	78.31	101.90
	Epithermal	1.60 10^{-9} ± 2.26%	−30.66	−29.18	−27.85	−28.77	−17.26	−4.52
	Evaporation	4.61 10^{-8} ± 0.32%	−34.11	−30.23	−29.69	−29.92	−18.81	−10.56
	Direct	1.61·10^{-8} ± 3.62%	−23.95	−17.25	−16.45	−21.40	−15.38	5.79
	Total	6.44·10^{-8} ± 0.68%	−30.93	−26.39	−25.76	−26.95	−16.97	−5.23

neutrons, the deviations are mainly due to the overly simplistic geometric model used for the simulations. In fact, the geometric model does not take into account the correct amount of water contained in the concrete walls and their heterogeneity, which explains the deviations between the evaporation and thermal energy ranges [96]. Further deviations in the evaporation energy range could be caused by the absence in the geometric model of materials that would induce the production of additional evaporation neutrons. Concerning the direct peaks, no major shift of the mean peak energy was found. For the 15DegL measurement position, the simulated spectra with smallest deviations for the direct peak (i.e., that are closest to the unfolded solution) are those given by Geant4-BIC and INCLXX, with deviations of 4% and 5%, respectively. Largest deviations have been found with Geant4-QMD, FLUKA and MCNP-CEM with deviations of the order of 20%. On the 40DegL position, FLUKA shows the lowest deviation of 8.4% followed by PHITS-JQMD with a deviation of 15.7%.

Figure 10 shows the integral neutron fluence quantities for simulated (filled bar chart) and unfolded (semi-transparent bar chart) results according to neutron energy ranges for the 15DegL (A) and 40DegL (B) measurement positions. The results show that all unfolded spectra have approximately the same total neutron fluence, with small standard deviations of the order of 2% and 1% for the 15DegL and 40DegL measurement positions, respectively. The mean fluence values of the unfolded spectra and the corresponding deviations from the Monte Carlo results are summarized in Table 6.

Neutron ambient dose equivalent H^* (10) distributions were obtained by multiplying neutron spectra with fluence-to-dose conversion coefficients [97, 98], and subsequently the integral values were calculated as a function of the energy range of the neutrons. This operation was done for both simulated and unfolded neutron spectra with MAXED. Figure 10 shows the integral neutron H^* (10) quantities for simulated (filled bar chart) and unfolded (semi-transparent bar chart)

results according to neutron energy ranges for the 15DegL (C) and 40DegL (D) measurement positions. Table 7 lists the mean integral neutron $H^*(10)$ values from the unfolded spectra and the corresponding deviations from the Monte Carlo results. The results show that for the 15DegL measurement position, evaporation neutrons and direct peak neutrons contribute to the $H^*(10)$ with weights of 54% and 43%, respectively. While for the 40DegL measurement position, evaporation neutrons and direct peak neutrons contribute to the $H^*(10)$ with weights of 72% and 25%, respectively. This is because the 252 MeV direct peak at the 40DegL position has both a lower fluence than the peak at 15DegL and the average energy of the peak is approximately at the minimum point (≈251.23.pSv cm^2) of the fluence-to-ambient dose equivalent conversion function for neutrons between 100 MeV and 1 GeV [98].

4 Conclusion

Manned space travel to the Moon and Mars will become more and more tangible in the near future. Spectroscopic knowledge of the secondary radiation field generated by GCRs interacting with spacecraft shielding materials are critical for both the design phase and the evaluation of possible biological risks to astronauts during the journey. In this study, we measured the secondary neutron field generated by a 1 GeV/u ^{56}Fe ion beam interacting with a cylindrical aluminum target in order to simulate a specific energy portion of the secondary radiation field that would be generated inside a spacecraft. The PTB's NEMUS system was used with three different thermal neutron sensors inside the GSI Cave A to perform neutron spectrometry measurements at three measurement angles with respect to the direction of the ion beam. Four Monte Carlo codes with different physical models were used both to estimate the neutron and proton energy spectra and to use these spectra as *a priori* information to initialize the unfolding process of neutron spectra using the MAXED code.

Before unfolding, the experimental data were corrected to exclude parasitic neutron contributions induced by the interaction of secondary protons with the metal shells of the modified Bonner spheres. The results showed that with the various unfolded spectra with MAXED, based on different simulations, a range of spectra was obtained. The unfolded spectra confirmed the average energies of the two direct peaks at 560 MeV and 230.MeV and showed that Geant4 with its BIC and INCLXX models, PHITS and FLUKA have the lowest deviations on direct peak intensities. The largest deviations were found with MCNP-CEM and Geant4-QMD.

The results showed that the total integral quantities of neutron fluence and equivalent ambient dose had standard deviations of less than 2%, regardless of the Monte Carlo code and physical model chosen. These results confirmed the validity of the NEMUS system with the MAXED unfolding code to perform characterization studies of wide energy range neutron spectra for energies above 500 MeV. Another important aspect of the capability of NEMUS other than that of satisfactory retrieving the full neutron spectrum is that of being able to calculate the total or energy-range-dependent neutron ambient dose equivalent quantities and so being used as neutron dosimeter.

Future data analysis will focus on the comparison of the experimental results obtained in this work and those obtained in previous experimental campaigns in which Thermoluminescent Dosimeters (TLDs) and Tissue Equivalent Proportional Counters (TEPCs) were used in the same secondary radiation field to carry out neutron dosimetry and microdosimentry studies. In addition, future studies will focus on experimental correction of neutron contributions induced by secondary protons by ΔE-E telescopes. Finally, the NEMUS system will be used in the future to characterize the secondary neutron field produced with other space shielding materials such as a Moon regolith simulant or polyethylene.

Data availability statement

The raw data supporting the conclusions of this article will be made available by the authors, without undue reservation.

Author contributions

AD: Writing–review and editing, Writing–original draft, Visualization, Software, Formal Analysis, Conceptualization. FH: Writing–review and editing, Software, Investigation, Conceptualization. DB: Writing–review and editing, Software, Investigation, Conceptualization. CS: Writing–review and editing, Investigation, Conceptualization. UW: Writing–review and editing, Supervision, Investigation, Conceptualization. MZ: Writing–review and editing, Supervision, Investigation, Funding acquisition, Data curation, Conceptualization.

Funding

The author(s) declare that financial support was received for the research, authorship, and/or publication of this article. The results presented here are based on the experiment AO-2017-IBER_010, which was performed in Cave A at the GSI Helmholtzzentrum fuer Schwerionenforschung, Darmstadt (Germany) in the frame of FAIR Phase-0. AO-2017-IBER_010 is supported by the European Space Agency (ESA) – IBER program and by the German Aerospace Center (DLR) under the funding number 50WB2125.

Acknowledgments

The authors would like to thank the whole GSI and PTB technical team, for their collaboration and valuable assistance during the experiments.

Conflict of interest

Authors FH, DB, CS, and UW were employed by company GSI Helmholtzzentrum für Schwerionenforschung GmbH.

The remaining authors declare that the research was conducted in the absence of any commercial or financial relationships that could be construed as a potential conflict of interest.

Publisher's note

References

1. Durante M, Cucinotta FA. Physical basis of radiation protection in space travel. *Rev Mod Phys* (2011) 83:1245–81. doi:10.1103/revmodphys.83.1245

2. George JS, Lave KA, Wiedenbeck ME, Binns WR, Cummings AC, Davis AJ, et al. Elemental composition and energy spectra of galactic cosmic rays during solar cycle 23. *Astrophys J* (2009) 698(2):1666–81. doi:10.1088/0004-637x/698/2/1666

3. Norbury JW, Slaba TC. Space radiation accelerator experiments – the role of neutrons and light ions. *Life Sci Space Res* (2014) 3:90–4. doi:10.1016/j.lssr.2014.09.006

4. Veinot KG, Hertel NE. Effective quality factors for neutrons based on the revised ICRP/ICRU recommendations. *Radiat Prot Dosimetry* (2005) 115(1–4):536–41. doi:10.1093/rpd/nci004

5. Baiocco G, Barbieri S, Babini G, Morini J, Alloni D, Friedland W, et al. The origin of neutron biological effectiveness as a function of energy. *Sci Rep* (2016) 6(1):34033. doi:10.1038/srep34033

6. Zeitlin C, Castro AJ, Beard KB, Abdelmelek M, Hayes BM, Johnson AS, et al. Results from the radiation assessment detector on the international space station, Part 2: the fast neutron detector. *Life Sci Space Res* (2023) 39:76–85. doi:10.1016/j.lssr.2023.03

7. Zeitlin C, Castro AJ, Beard KB, Hayes BM, Abdelmelek M, Laramore D, et al. Results from the radiation assessment detector on the international space station: Part 3, combined results from the CPD and FND. *Life Sci Space Res* (2023) 39:86–94. doi:10.1016/j.lssr.2023.06.002

8. Walker SA, Townsend LW, Norbury JW. Heavy ion contributions to organ dose equivalent for the 1977 galactic cosmic ray spectrum. *Adv Space Res* (2013) 51(9):1792–9. doi:10.1016/j.asr.2012.12.011

9. Slaba TC, Bahadori AA, Reddell BD, Singleterry RC, Clowdsley MS, Blattnig SR. Optimal shielding thickness for galactic cosmic ray environments. *Life Sci Space Res* (2017) 12:1–15. doi:10.1016/j.lssr.2016.12.003

10. Barthel J, Sarigul-Klijn N. Radiation production and absorption in human spacecraft shielding systems under high charge and energy Galactic Cosmic Rays: material medium, shielding depth, and byproduct aspects. *Acta Astronaut.* (2018) 144:254–62. doi:10.1016/j.actaastro.2017.12.040

11. Horst F, Boscolo D, Durante M, Luoni F, Schuy C, Weber U. Thick shielding against galactic cosmic radiation: a Monte Carlo study with focus on the role of secondary neutrons. *Life Sci Space Res* (2022) 33:58–68. doi:10.1016/j.lssr.2022.03.003

12. Nakamura T. Overview of experimental works on secondary particle production and transport by high-energy particle beams. *Radiat Prot Environ* (2012) 35(3):111. doi:10.4103/0972-0464.117665

13. Norbury JW, Battistoni G, Besuglow J, Bocchini L, Boscolo D, Botvina A, et al. Are further cross section measurements necessary for space radiation protection or ion therapy applications? *Helium Projectiles Front Phys* (2020) 8. doi:10.3389/fphy.2020.565954

14. Luoni F, Horst F, Reidel CA, Quarz A, Bagnale L, Sihver L, et al. Total nuclear reaction cross-section database for radiation protection in space and heavy-ion therapy applications. *New J Phys* (2021) 23(10):101201. doi:10.1088/1367-2630/ac27e1

15. McGirl N, Castellanos L, Srikrishna A, Heilbronn L. Secondary neutron yields produced by thick-target aluminum interactions (2016). Available from: https://ttu-ir.tdl.org/handle/2346/67707 (Accessed August 19, 2022).

16. Castellanos LA, McGirl NA, Srikrishna AP, Heilbronn L, La Tessa C, Rusek A, et al. Thick-target yields of secondary ions and neutrons for validation of radiation transport codes. In: 2017 IEEE Aerospace Conference; 4-11 March 2017; China (2017). p. 1–10.

17. Tsai PE, Lai BL, Heilbronn LH, Sheu RJ. Benchmark of neutron production cross sections with Monte Carlo codes. *Nucl Instrum Methods Phys Res Sect B Beam Interact Mater At* (2018) 416:16–29. doi:10.1016/j.nimb.2017.11.029

18. Chen J, Yun S, Dong T, Ren Z, Zhang X. Validation of Geant4 physics models for nuclear beams in extended media. *Nucl Instrum Methods Phys Res Sect B Beam Interact Mater At* (2018) 434:113–9. doi:10.1016/j.nimb.2018.08.022

19. Boscolo D, Scognamiglio D, Horst F, Weber U, Schuy C, Durante M, et al. Characterization of the secondary neutron field produced in a thick aluminum shield by 1 GeV/u 56Fe ions using TLD-based ambient dosimeters. *Front Phys* (2020) 8. doi:10.3389/fphy.2020.00365

20. Sokolov A, Kozlova E, Boscolo D, Durante M, Horst F, Radon T, et al. Neutron spectra at a high energy heavy ion accelerator measured with a TLD-based Bonner spectrometer. *J Instrum* (2021) 16(10):P10022. doi:10.1088/1748-0221/16/10/p10022

21. Horst F, Boscolo D, Cartechini G, Durante M, Hartel C, Kozlova E, et al. A multi-detector experimental setup for the study of space radiation shielding materials: measurement of secondary radiation behind thick shielding and assessment of its radiobiological effect. *EPJ Web Conf* (2022) 261:03002. doi:10.1051/epjconf/202226103002

22. Durante M, Cucinotta FA. Heavy ion carcinogenesis and human space exploration. *Nat Rev Cancer* (2008) 8(6):465–72. doi:10.1038/nrc2391

23. Zeitlin C, Guetersloh SB, Heilbronn LH, Miller J. Measurements of materials shielding properties with 1GeV/nuc 56Fe. *Nucl Instrum Methods Phys Res Sect B Beam Interact Mater At.* (2006) 252(2):308–18. doi:10.1016/j.nimb.2006.08.011

24. Durante M, Golubev A, Park WY, Trautmann C. Applied nuclear physics at the new high-energy particle accelerator facilities. *Phys Rep* (2019) 800:1–37. doi:10.1016/j.physrep.2019.01.004

25. Bramblett RL, Ewing RI, Bonner TW. A new type of neutron spectrometer. *Nucl Instrum Methods* (1960) 9(1):1–12. doi:10.1016/0029-554x(60)90043-4

26. Thomas DJ, Alevra AV. Bonner sphere spectrometers—a critical review. *Nucl Instrum Methods Phys Res Sect Accel Spectrometers Detect Assoc Equip* (2002) 476(1):12–20. doi:10.1016/s0168-9002(01)01379-1

27. Alevra AV, Thomas DJ. Neutron spectrometry in mixed fields: multisphere spectrometers. *Radiat Prot Dosimetry* (2003) 107(1–3):37–72. doi:10.1093/oxfordjournals.rpd.a006388

28. Mares V, Schraube H. *High energy neutron spectrometry with Bonner spheres*. China: Czech Republic (1998). p. 671.

29. Wiegel B, Alevra AV. NEMUS—the PTB neutron multisphere spectrometer: bonner spheres and more. *Nucl Instrum Methods Phys Res Sect Accel Spectrometers Detect Assoc Equip* (2002) 476(1):36–41. doi:10.1016/s0168-9002(01)01385-7

30. fachabteilungen. Dep. 6 W. Neutron spektrometer NEMUS (neutron multisphere spectrometer) (2016). Available from: https://www.ptb.de/cms/en/ptb/fachabteilungen/abt6/fb-64/643-neutron-spectrometry/nemus/neutron-spektrometer-nemus-neutron-multisphere-spectrometer.html.

31. Dommert M, Reginatto M, Zbořil M, Lutz B. Dead time corrections for Bonner sphere measurements of secondary neutrons at a proton therapy facility. *J Instrum* (2021) 16(03):P03038. doi:10.1088/1748-0221/16/03/p03038

32. Goldhagen P, Reginatto M, Kniss T, Wilson JW, Singleterry RC, Jones IW, et al. Measurement of the energy spectrum of cosmic-ray induced neutrons aboard an ER-2 high-altitude airplane. *Nucl Instrum Methods Phys Res Sect Accel Spectrometers Detect Assoc Equip* (2002) 476(1):42–51. doi:10.1016/s0168-9002(01)01386-9

33. Rollet S, Agosteo S, Fehrenbacher G, Hranitzky C, Radon T, Wind M. Intercomparison of radiation protection devices in a high-energy stray neutron field, Part I: Monte Carlo simulations. *Radiat Meas* (2009) 44(7):649–59. doi:10.1016/j.radmeas.2009.03.029

34. Luoni F, Weber U, Boscolo D, Durante M, Reidel CA, Schuy C, et al. Beam monitor calibration for radiobiological experiments with scanned high energy heavy ion beams at FAIR. *Front Phys* (2020) 8. doi:10.3389/fphy.2020.568145

35. Battistoni G, Boehlen T, Cerutti F, Chin PW, Esposito LS, Fassò A, et al. Overview of the FLUKA code. *Ann Nucl Energy* (2015) 82:10–8. doi:10.1016/j.anucene.2014.11.007

36. Ahdida C, Bozzato D, Calzolari D, Cerutti F, Charitonidis N, Cimmino A, et al. New capabilities of the FLUKA multi-purpose code. *Front Phys* (2022) 9. doi:10.3389/fphy.2021.788253

37. Vlachoudis V. *Flair: a powerful but user friendly graphical interface for FLUKA*. 2009.

38. Sorge H, Stöcker H, Greiner W. Poincaré invariant Hamiltonian dynamics: modelling multi-hadronic interactions in a phase space approach. *Ann Phys* (1989) 192(2):266–306. doi:10.1016/0003-4916(89)90136-x

39. Oh J, Lee HS, Park S, Kim M, Hong S, Ko S, et al. Comparison of the FLUKA, MCNPX, and PHITS codes in yield calculation of secondary particles produced by intermediate energy proton beam. *Prog Nucl Sci Technol* (2011) 25:85–8. doi:10.15669/pnst.1.85

40. Agosteo S, Mereghetti A, Sagia E, Silari M. Shielding data for hadron-therapy ion accelerators: attenuation of secondary radiation in concrete. *Nucl Instrum Methods Phys Res Sect B Beam Interact Mater At.* (2014) 319:154–67. doi:10.1016/j.nimb.2013.10.015

41. Nakao N, Kajimoto T, Sanami T, Froeschl R, Iliopoulou E, Infantino A, et al. Measurements and Monte Carlo simulations of high-energy neutron streaming through

the access maze using activation detectors at 24 GeV/c proton beam facility of CERN/CHARM. *J Nucl Sci Technol* (2021) 58(8):899–907. doi:10.1080/00223131.2021.1887003

42. De Saint-Hubert M, Farah J, Klodowska M, Romero-Exposito MT, Tyminska K, Mares V, et al. The influence of nuclear models and Monte Carlo radiation transport codes on stray neutron dose estimations in proton therapy. *Radiat Meas* (2022) 150: 106693. doi:10.1016/j.radmeas.2021.106693

43. Beskrovnaia L, Florko B, Paraipan M, Sobolevsky N, Timoshenko G. Verification of Monte Carlo transport codes FLUKA, GEANT4 and SHIELD for radiation protection purposes at relativistic heavy ion accelerators. *Nucl Instrum Methods Phys Res Sect B Beam Interact Mater At.* (2008) 266(18):4058–60. doi:10.1016/j.nimb.2008.07.003

44. Robert C, Dedes G, Battistoni G, Böhlen TT, Buvat I, Cerutti F, et al. Distributions of secondary particles in proton and carbon-ion therapy: a comparison between GATE/Geant4 and FLUKA Monte Carlo codes. *Phys Med Biol* (2013) 58(9):2879–99. doi:10.1088/0031-9155/58/9/2879

45. Kim DH, Oh JH, Jung NS, Lee HS, Shin YS, Kwon DY, et al. A benchmarking study of high energy carbon ion induced neutron using several Monte Carlo codes. 2014 Available from: https://www.osti.gov/etdeweb/biblio/22355632.

46. Chen WL, Jiang SH, Sheu RJ. Cosmic-ray neutron simulations and measurements in Taiwan. *Radiat Prot Dosimetry* (2014) 161(1–4):303–6. doi:10.1093/rpd/ncu030

47. Lee KW, Sheu RJ. Comparing two measurements of the same cosmic-ray neutron spectrum using standard bonner spheres and high-sensitivity bonner cylinders. *Radiat Prot Dosimetry* (2017) 177(4):450–7. doi:10.1093/rpd/ncx063

48. Norbury JW, Slaba TC, Sobolevsky N, Reddell B. Comparing HZETRN, SHIELD, FLUKA and GEANT transport codes. *Life Sci Space Res* (2017) 14:64–73. doi:10.1016/j.lssr.2017.04.001

49. Wiegel B, Agosteo S, Bedogni R, Caresana M, Esposito A, Fehrenbacher G, et al. Intercomparison of radiation protection devices in a high-energy stray neutron field, Part II: bonner sphere spectrometry. *Radiat Meas* (2009) 44(7):660–72. doi:10.1016/j.radmeas.2009.03.026

50. Goorley JT, James MR, Booth TE, Brown FB, Bull JS, Cox LJ, et al. *Initial MCNP6 release overview - MCNP6 version 1.0*. Los Alamos, NM (United States): Los Alamos National Lab. LANL (2013). Available from: https://www.osti.gov/biblio/1086758.

51. Amgarou K, Bedogni R, Domingo C, Esposito A, Gentile A, Carinci G, et al. Measurement of the neutron fields produced by a 62MeV proton beam on a PMMA phantom using extended range Bonner sphere spectrometers. *Nucl Instrum Methods Phys Res Sect Accel Spectrometers Detect Assoc Equip* (2011) 654(1):399–405. doi:10.1016/j.nima.2011.07.027

52. Chadwick MB, Herman M, Obložinský P, Dunn ME, Danon Y, Kahler AC, et al. ENDF/B-VII.1 nuclear data for science and technology: cross sections, covariances, fission product yields and decay data. *Nucl Data Sheets* (2011) 112(12):2887–996. doi:10.1016/j.nds.2011.11.002

53. Chadwick MB, Obložinský P, Herman M, Greene NM, McKnight RD, Smith DL, et al. ENDF/B-VII.0: next generation evaluated nuclear data library for nuclear science and technology. *Nucl Data Sheets* (2006) 107(12):2931–3060. doi:10.1016/j.nds.2006.11.001

54. Krylov A, Paraipan M, Sobolevsky N, Timoshenko G, Tret'yakov V. GEANT4, MCNPX, and SHIELD code comparison concerning relativistic heavy ion interaction with matter. *Phys Part Nucl Lett* (2014) 11(4):549–51. doi:10.1134/s1547477114040232

55. Lee A, Kim D, Jung NS, Oh JH, Oranj LM, Lee HS. Comparison of physics model for 600 MeV protons and 290 MeV·n^{-1} oxygen ions on carbon in MCNPX. *J Radiat Prot Res* (2016) 41(2):123–31. doi:10.14407/jrpr.2016.41.2.123

56. Lapins J, Guilliard N, Bernnat W, Buck A. Simulation of irradiation exposure of electronic devices due to heavy ion therapy with Monte Carlo Code MCNP6. *EPJ Web Conf* (2017) 153:04015. doi:10.1051/epjconf/201715304015

57. Wilson WH, Johnson CM, Lowrey JD, Biegalski SR, Haas DA. Cosmic-ray induced production of radioactive noble gases in the atmosphere, ground, and seawater. *J Radioanal Nucl Chem* (2015) 305(1):183–92. doi:10.1007/s10967-015-4181-7

58. Mesick KE, Feldman WC, Coupland DDS, Stonehill LC. Benchmarking Geant4 for simulating galactic cosmic ray interactions within planetary bodies. *Earth Space Sci* (2018) 5(7):324–38. doi:10.1029/2018ea000400

59. Lee JH, Kim HN, Jeong HY, Cho SO. Optimization of shielding to reduce cosmic radiation damage to packaged semiconductors during air transport using Monte Carlo simulation. *Nucl Eng Technol* (2020) 52(8):1817–25. doi:10.1016/j.net.2020.01.016

60. Agostinelli S, Allison J, Amako K, Apostolakis J, Araujo H, Arce P, et al. Geant4—a simulation toolkit. *Nucl Instrum Methods Phys Res Sect Accel Spectrometers Detect Assoc Equip* (2003) 506(3):250–303. doi:10.1016/s0168-9002(03)01368-8

61. Walker SD, Abramov A, Nevay LJ, Shields W, Boogert ST. Pyg4ometry: a Python library for the creation of Monte Carlo radiation transport physical geometries. *Comput Phys Commun* (2022) 272:108228. doi:10.1016/j.cpc.2021.108228

62. Plompen AJM, Cabellos O, De Saint Jean C, Fleming M, Algora A, Angelone M, et al. The joint evaluated fission and fusion nuclear data library, JEFF-3.3. *Eur Phys J A* (2020) 56(7):181. doi:10.1140/epja/s10050-020-00141-9

63. Dudouet J, Cussol D, Durand D, Labalme M. Benchmarking GEANT4 nuclear models for hadron therapy with 95 MeV/nucleon carbon ions. *Phys Rev C* (2014) 89(5): 054616. doi:10.1103/physrevc.89.054616

64. Bolst D, Cirrone GAP, Cuttone G, Folger G, Incerti S, Ivanchenko V, et al. Validation of Geant4 fragmentation for heavy ion therapy. *Nucl Instrum Methods Phys Res Sect Accel Spectrometers Detect Assoc Equip* (2017) 869:68–75. doi:10.1016/j.nima.2017.06.046

65. Ivanchenko V, Dondero P, Fioretti V, Ivantchenko A, Lei F, Lotti S, et al. Validation of Geant4 10.3 simulation of proton interaction for space radiation effects. *Exp Astron* (2017) 44(3):437–50. doi:10.1007/s10686-017-9556-z

66. Lamrabet A, Maghnouj A, Tajmouati J, Bencheikh M. GEANT4 characterization of the neutronic behavior of the active zone of the MEGAPIE spallation target. *Nucl Eng Technol* (2021) 53(10):3164–70. doi:10.1016/j.net.2021.05.002

67. Domingo C, Lagares JI, Romero-Expósito M, Sánchez-Nieto B, Nieto-Camero JJ, Terrón JA, et al. Peripheral organ equivalent dose estimation procedure in proton therapy. *Front Oncol* (2022) 12:882476. doi:10.3389/fonc.2022.882476

68. Brall T, Mares V, Bütikofer R, Rühm W. Assessment of neutrons from secondary cosmic rays at mountain altitudes – Geant4 simulations of environmental parameters including soil moisture and snow cover. *The Cryosphere* (2021) 15(10):4769–80. doi:10.5194/tc-15-4769-2021

69. Brall T, Mares V, Bütikofer R, Rühm W. Assessment of secondary neutrons from galactic cosmic rays at mountain altitudes – Geant4 simulations and ground-based measurements of neutron energy spectra. *Radiat Meas* (2021) 144:106592. doi:10.1016/j.radmeas.2021.106592

70. Sato T, Niita K, Matsuda N, Hashimoto S, Iwamoto Y, Noda S, et al. Particle and heavy ion transport code system, PHITS, version 2.52. *J Nucl Sci Technol* (2013) 50(9): 913–23. doi:10.1080/00223131.2013.814553

71. Sato T, Iwamoto Y, Hashimoto S, Ogawa T, Furuta T, ichiro AS, et al. Features of particle and heavy ion transport code system (PHITS) version 3.02. *J Nucl Sci Technol* (2018) 55(6):684–90. doi:10.1080/00223131.2017.1419890

72. Shibata K, Iwamoto O, Nakagawa T, Iwamoto N, Ichihara A, Kunieda S, et al. JENDL-4.0: a new library for nuclear science and engineering. *J Nucl Sci Technol* (2011) 48(1):1–30. doi:10.3327/jnst.48.1

73. Matsuda N, Kunieda S, Okamoto T, Tada K, Konno C. ACE library of JENDL-4.0/HE. *Prog Nucl Sci Technol* (2019) 6(0):225–9. doi:10.15669/pnst.6.225

74. Heilbronn L, Nakamura T, Iwata Y, Kurosawa T, Iwase H, Townsend LW. Overview of secondary neutron production relevant to shielding in space. *Radiat Prot Dosimetry* (2005) 116(1–4):140–3. doi:10.1093/rpd/nci033

75. Yonai S, Matsumoto S. Monte Carlo study toward the development of a radiation field to simulate secondary neutrons produced in carbon-ion radiotherapy. *Radiat Phys Chem* (2020) 172:108787. doi:10.1016/j.radphyschem.2020.108787

76. Matthiä D, Ehresmann B, Lohf H, Köhler J, Zeitlin C, Appel J, et al. The Martian surface radiation environment – a comparison of models and MSL/RAD measurements. *J Space Weather Space Clim* (2016) 6:A13. doi:10.1051/swsc/2016008

77. Naito M, Hasebe N, Shikishima M, Amano Y, Haruyama J, Matias-Lopes JA, et al. Radiation dose and its protection in the Moon from galactic cosmic rays and solar energetic particles: at the lunar surface and in a lava tube. *J Radiol Prot* (2020) 40(4): 947–61. doi:10.1088/1361-6498/abb120

78. Zaman FA, Townsend LW, de Wet WC, Burahmah NT. The lunar radiation environment: comparisons between PHITS, HETC-HEDS, and the CRaTER instrument. *Aerospace* (2021) 8(7):182. doi:10.3390/aerospace8070182

79. Zaman FA, Townsend LW, de Wet WC, Looper MD, Brittingham JM, Burahmah NT, et al. Modeling the lunar radiation environment: a comparison among FLUKA, Geant4, HETC-HEDS, MCNP6, and PHITS. *Space Weather* (2022) 20(8): e2021SW002895. doi:10.1029/2021sw002895

80. Brun R, Rademakers F. ROOT — an object oriented data analysis framework. *Nucl Instrum Methods Phys Res Sect Accel Spectrometers Detect Assoc Equip* (1997) 389(1): 81–6. doi:10.1016/s0168-9002(97)00048-x

81. Nandy M. Secondary radiation in ion therapy and theranostics: a review. *Front Phys* (2021) 8. doi:10.3389/fphy.2020.598257

82. Gunzert-Marx K, Iwase H, Schardt D, Simon RS. Secondary beam fragments produced by 200 MeV u−1 12C ions in water and their dose contributions in carbon ion radiotherapy. *New J Phys* (2008) 10(7):075003. doi:10.1088/1367-2630/10/7/075003

83. Haettner E, Iwase H, Krämer M, Kraft G, Schardt D. Experimental study of nuclear fragmentation of 200 and 400 MeV/u12C ions in water for applications in particle therapy. *Phys Med Biol* (2013) 58(23):8265–79. doi:10.1088/0031-9155/58/23/8265

84. Rovituso M, Schuy C, Weber U, Brons S, Cortés-Giraldo MA, Tessa CL, et al. Fragmentation of 120 and 200 MeV u−1 4He ions in water and PMMA targets. *Phys Med Biol* (2017) 62(4):1310–26. doi:10.1088/1361-6560/aa5302

85. Nakamura T, Heilbronn L. Overview of secondary particle production and transport by high-energy heavy ions. *Nucl Instrum Methods Phys Res Sect Accel Spectrometers Detect Assoc Equip* (2006) 562(2):706–9. doi:10.1016/j.nima.2006.02.027

86. Shrestha S, Newhauser WD, Donahue WP, Pérez-Andújar A. Stray neutron radiation exposures from proton therapy: physics-based analytical models of neutron spectral fluence, kerma and absorbed dose. *Phys Med Biol* (2022) 67(12):125019. doi:10.1088/1361-6560/ac7377

87. Piotrowski T, Mazgaj M, Żak A, Skubalski J. Importance of atomic composition and moisture content of cement based composites in neutron radiation shielding. *Proced Eng* (2015) 108:616–23. doi:10.1016/j.proeng.2015.06.188

88. Reginatto M, Goldhagen P, Neumann S. Spectrum unfolding, sensitivity analysis and propagation of uncertainties with the maximum entropy deconvolution code MAXED. *Nucl Instrum Methods Phys Res Sect Accel Spectrometers Detect Assoc Equip* (2002) 476(1):242–6. doi:10.1016/s0168-9002(01)01439-5

89. Reginatto M. What can we learn about the spectrum of high-energy stray neutron fields from Bonner sphere measurements? *Radiat Meas* (2009) 44(7):692–9. doi:10.1016/j.radmeas.2009.04.005

90. Wiegel B, Alevra AV, Matzke M, Schrewe UJ, Wittstock J. Spectrometry using the PTB neutron multisphere spectrometer (NEMUS) at flight altitudes and at ground level. *Nucl Instrum Methods Phys Res Sect Accel Spectrometers Detect Assoc Equip* (2002) 476(1):52–7. doi:10.1016/s0168-9002(01)01387-0

91. Goldhagen P, Clem JM, Wilson JW. The energy spectrum of cosmic-ray induced neutrons measured on an airplane over a wide range of altitude and latitude. *Radiat Prot Dosimetry* (2004) 110(1–4):387–92. doi:10.1093/rpd/nch216

92. Howell RM, Burgett EA. Secondary neutron spectrum from 250-MeV passively scattered proton therapy: measurement with an extended-range Bonner sphere system. *Med Phys* (2014) 41(9):092104. doi:10.1118/1.4892929

93. Dommert M, Reginatto M, Zboril M, Fiedler F, Helmbrecht S, Enghardt W, et al. Measurement of the energy spectrum of secondary neutrons in a proton therapy environment. *Curr Dir Biomed Eng* (2017) 3(2):83–6. doi:10.1515/cdbme-2017-0018

94. Dommert M, Reginatto M, Zbořil M, Fiedler F, Helmbrecht S, Enghardt W, et al. A bayesian approach for measurements of stray neutrons at proton therapy facilities: quantifying neutron dose uncertainty. *Radiat Prot Dosimetry* (2018) 180(1–4):319–23. doi:10.1093/rpd/ncx264

95. Gómez-Ros JM, Bedogni R, Domingo C, Eakins JS, Roberts N, Tanner RJ. Results of the EURADOS international comparison exercise on neutron spectra unfolding in Bonner spheres spectrometry. *Radiat Meas* (2022) 153:106755. doi:10.1016/j.radmeas.2022.106755

96. Petit M. Concrete modeling for neutron transport and associated sensitivity studies performed at the AMANDE-MIRCOM facility. *Nucl Sci Eng* (2021) 195(8):864–76. doi:10.1080/00295639.2020.1867436

97. ICRP. Conversion coefficients for use in radiological protection against external radiation. 1996. Report No.: 74.

98. Pelliccioni M. Overview of fluence-to-effective dose and fluence-to-ambient dose equivalent conversion coefficients for high energy radiation calculated using the FLUKA code. *Radiat Prot Dosimetry* (2000) 88(4):279–97. doi:10.1093/oxfordjournals.rpd.a033046

frontiers | Frontiers in Physiology

TYPE Original Research
PUBLISHED 13 November 2024
DOI 10.3389/fphys.2024.1486767

OPEN ACCESS

EDITED BY
Alessandro Bartoloni,
National Institute of Nuclear Physics of Rome, Italy

REVIEWED BY
Alexandra Charalampopoulou,
National Center of Oncological Hadrontherapy, Italy
Giulia Tomagra,
University of Turin, Italy

*CORRESPONDENCE
Jacob Raber,
raberj@ohsu.edu

RECEIVED 26 August 2024
ACCEPTED 07 October 2024
PUBLISHED 13 November 2024

CITATION
Raber J, Chaudhari M, De la Torre A, Holden S, Kessler K, Glaeser B, Lenarczyk M, Leonard SW, Borg A, Kwok A, Patel C, Kronenberg A, Olsen CM, Willey JS, Morré J, Choi J, Stevens JF, Bobe G, Minnier J and Baker J (2024) Effects of 5-ion 6-beam sequential irradiation in the presence and absence of hindlimb or control hindlimb unloading on behavioral performances and plasma metabolic pathways of Fischer 344 rats.
Front. Physiol. 15:1486767.
doi: 10.3389/fphys.2024.1486767

Effects of 5-ion 6-beam sequential irradiation in the presence and absence of hindlimb or control hindlimb unloading on behavioral performances and plasma metabolic pathways of Fischer 344 rats

Jacob Raber[1,2,3]*, Mitali Chaudhari[1], Alexis De la Torre[1], Sarah Holden[1], Kat Kessler[1], Breanna Glaeser[4], Marek Lenarczyk[5], Scott Willem Leonard[6], Alexander Borg[6], Andy Kwok[6], Chirayu Patel[6], Amy Kronenberg[7], Christopher M. Olsen[4], Jeffrey S. Willey[6], Jeffrey Morré[8], Jaewoo Choi[8,9], Jan Frederik Stevens[3,8,9], Gerd Bobe[9,10], Jessica Minnier[1] and John Baker[5]

[1]Department of Behavioral Neuroscience, Oregon Health & Science University, Portland, OR, United States, [2]Departments of Neurology, Psychiatry, and Radiation Medicine, Division of Neuroscience ONPRC, Oregon Health and Science University, Portland, OR, United States, [3]College of Pharmacy, Oregon State University, Corvallis, OR, United States, [4]Neuroscience Center and Department of Pharmacology and Toxicology, Medical College of Wisconsin, Milwaukee, WI, United States, [5]Radiation Biosciences laboratory, Medical College of Wisconsin, Milwaukee, WI, United States, [6]Department of Radiation Oncology, Wake Forest School of Medicine, Winston-Salem, NC, United States, [7]Biological Systems and Engineering Division, Lawrence Berkeley National Laboratory, Berkeley, CA, United States, [8]Mass Spectrometry Center, Oregon State University, Corvallis, OR, United States, [9]Linus Pauling Institute, Oregon State University, Corvallis, OR, United States, [10]Department of Animal & Rangeland Sciences, Oregon State University, Corvallis, OR, United States

Introduction: Effects and interactions between different spaceflight stressors are expected to be experienced by crew on missions when exposed to microgravity and galactic cosmic rays (GCRs). One of the limitations of previous studies on simulated weightlessness using hindlimb unloading (HU) is that a control HU condition was not included.

Methods: We characterized the behavioral performance of male Fischer rats 2 months after sham or total body irradiation with a simplified 5-ion 6-mixed-beam exposure representative of GCRs in the absence or presence of HU. Six months later, the plasma, hippocampus, and cortex were processed to determine whether the behavioral effects were associated with long-term alterations in the metabolic pathways.

Results: In the open field without and with objects, interactions were observed for radiation × HU. In the plasma of animals that were not under the HU or control HU condition, the riboflavin metabolic pathway was affected most

for sham irradiation vs. 0.75 Gy exposure. Analysis of the effects of control HU on plasma in the sham-irradiated animals showed that the alanine, aspartate, glutamate, riboflavin, and glutamine metabolisms as well as arginine biosynthesis were affected. The effects of control HU on the hippocampus in the sham-irradiated animals showed that the phenylalanine, tyrosine, and tryptophan pathway was affected the most. Analysis of effects of 0.75 Gy irradiation on the cortex of control HU animals showed that the glutamine and glutamate metabolic pathway was affected similar to the hippocampus, while the riboflavin pathway was affected in animals that were not under the control HU condition. The effects of control HU on the cortex in sham-irradiated animals showed that the riboflavin metabolic pathway was affected. Animals receiving 0.75 Gy of irradiation showed impaired glutamine and glutamate metabolic pathway, whereas animals receiving 1.5 Gy of irradiation showed impaired riboflavin metabolic pathways. A total of 21 plasma metabolites were correlated with the behavioral measures, indicating that plasma and brain biomarkers associated with behavioral performance are dependent on the environmental conditions experienced.

Discussion: Phenylalanine, tyrosine, and tryptophan metabolism as well as phenylalanine and tryptophan as plasma metabolites are biomarkers that can be considered for spaceflight as they were revealed in both Fischer and WAG/Rij rats exposed to simGCRsim and/or HU.

KEYWORDS

Fischer rats, 5-ion beam irradiation, hindlimb unloading, open-field, object recognition, metabolomics

1 Introduction

Astronauts are frequently exposed to different types of ionizing radiations in space that could impact their brain functions (Braby et al., 2019). Microgravity is another environmental stressor experienced by astronauts during space missions that could cause brain dysfunction. Hindlimb unloading (HU) has been used to simulate microgravity on Earth (Ray et al., 2001) and shown to reduce the hippocampal levels of pyruvate dehydrogenase, which is a part of glucose metabolism and is associated with oxidative stress and brain ischemia, as well as the structural protein tubulin (Sarkar et al., 2006). In addition, microgravity achieved using parabolic flights has been shown to impair visuospatial tuning and orientation in mice during the flights (Oman, 2007). Irradiation and microgravity may also interact in the manner in which they cause DNA damage (Moreno-Villanueva et al., 2017) and other injury-related cellular pathways, including oxidative stress, mitochondrial functions (Yatagai et al., 2019), cardiovascular health (Patel, 2020), and bone functions (Krause et al., 2017), as well as the brain (Raber et al., 2021). Recently, we reported the complex interactions of simulated microgravity achieved by HU and a simplified field of simulated space radiation (SimGCRsim) on the behavioral and cognitive performances as well as metabolic pathways in the plasma and brain of WAG/Rij rats (Raber et al., 2021). Sham-irradiated WAG/Rij rats exposed to simulated microgravity with HU were impaired in terms of hippocampus-dependent spatial habituation learning, unlike irradiated WAG/Rij rats (1.5 Gy). In addition, rats exposed to 1.5 Gy of SimGCRsim showed increased depressive-like behaviors in the absence but not in the presence of simulated microgravity. Specific behavioral measures, such as activity and anxiety measures as well as spatial habituation in the open field and depressive-like behaviors in the forced swim test, were associated with the plasma levels of distinct metabolites 10 months after the behavioral testing. The phenylalanine, tyrosine, and tryptophan metabolic pathway was the one most profoundly affected by radiation in the absence and presence of microgravity in terms of the plasma and by microgravity itself.

One of the limitations of simulated spatialradiation studies in the absence or presence of simulated weightlessness using hindlimb unloading (HU) is the absence of a control HU condition. Therefore, to determine whether these effects of irradiation and simulated microgravity are specific to WAG/Rij rats and whether these effects are specific to simulated space radiation, we characterized the behavioral and cognitive performance of male Fischer rats 2 months after exposure to sham irradiation or total body irradiation with simGCRsim (0.75 or 1.5 Gy) in the absence or presence of simulated microgravity along with HU or control HU condition. In addition, we collected plasma samples 9 months after sham irradiation or total body irradiation and analyzed them for distinct alterations in the metabolic pathways to determine whether changes to the metabolic measures were associated with specific behavioral and cognitive measures. Finally, we compared the metabolic measures associated with specific behavioral and cognitive performances following simGCRsim exposure in the present study with the findings following photon irradiation in our previous study (Raber et al., 2024).

TABLE 1 Experimental radiation and HU groups.

Radiation dose (Gy)	HU	Number of rats for behavioral testing	Number of rats for metabolomics analysis
0	Sham	22	12
0.75	Sham	22	12
1.5	Sham	22	12
0	Control HU	12	12
0.75	Control HU	12	12
1.5	Control HU	12	12
0	HU	10	
0.75	HU	10	
1.5	HU	10	

2 Materials and methods

2.1 Animals and radiation exposure

Male 7–8 months old Fischer 344 rats (RRID:RGD_734478) (n = 132, see Table 1 for details of the experimental groups) were shipped to the Brookhaven National Laboratory (BNL), Upton, NY, United States. Male rats were used in this study as they are an established model of radiation injury to the cardiovascular system (Baker et al., 2009), and the current study was based on extant studies. After 2 weeks of acclimatization and at 9 months of age, they were sham-irradiated or irradiated with a standardized simplified 5-ion 6-beam prescribed by NASA referred to as simGCRsim, which consists of sequential and rapidly switched exposures to protons (1000 MeV/n), ^{28}Si ions (250 MeV/n), ^{4}He ions (350 MeV/n), ^{16}O ions (600 MeV/n), ^{56}Fe ions (250 MeV/n), and protons (250 MeV/n) (0, 0.75, or 1.5 Gy) in the absence or presence of simulated weightlessness achieved by HU or a control HU condition. The control HU condition was identical to the HU condition with the exception that the animals could use all four paws for movement.

The HU procedure was performed 5 days prior to sham-irradiation or irradiation, as described below. The rats remained in the HU condition for 25 days following sham-irradiation or irradiation. At the end of one week following the HU period, the animals were shipped to the Medical College of Wisconsin (MCW). The animals were then maintained on a Teklad 8904 diet (Indianapolis, IN, United States) and fed *ad libitum* during the study. The animals were housed in a reverse light cycle room with lights off from 07.30–19.30. All behavioral and cognitive tests were performed during the dark period starting 2 months after irradiation or sham-irradiation. All animal procedures were consistent with ARRIVE guidelines and were reviewed and approved by the Institutional Animal Care and Use Committees at BNL and MCW. All analyses were performed blinded to the treatment, and the code was revealed only after the data were analyzed.

2.2 HU

On day 1, the rats were randomly grouped into full weightbearing (non-HU), HU via tail suspension, or no HU (sham). The HU procedure was a modified version of that published previously (Raber et al., 2021; Wiley et al., 2016) (Figure 1). In brief, the rats were anesthetized with isoflurane (2.5%–3.0% at 5% oxygen flow rate). Then, a tincture of benzoin was applied to the lateral surface of the tail before placing one of the free ends of an adhesive medical traction tape (3M, St. Paul, MN, United States) starting approximately 1 cm from the base of the tail and adhering up to 3/4th of the tail length. The free end was then looped through a catch on a plastic ball-bearing swivel and adhered to the opposite lateral side of the tail. Strips of micropore tape (3M) were adhered perpendicularly over the traction tape. A 1.56-inch carabiner clip (Nite Ize, Boulder, CO, United States) was connected to the swivel and a zipper hook to permit vertical adjustment along an attached Perlon cord (STAS group, BA, Eindhoven, the Netherlands). The cord was then connected to a pulley (Blue Hawk, Gilbert, AZ, United States) that permitted the setup to slide securely over a 5/16-inch-diameter steel rod (Hillman, Cincinnati, OH, United States). Adjustment of the zipper lock lifted the hind limbs off the substrate, with the abdomen and thorax suspended at 30° from the horizontal plane. The sham HU rats received isoflurane but were not tail suspended. For placement along the beamline (Figure 1) for both the irradiation and sham procedures, the swivel was disconnected from the carabiner clip, and a plastic bead chain cord (Luanxu, Guangzhou City, China) was looped through the swivel at the point of the carabiner attachment. The rats were then transferred to specialized rat boxes in 60 cm × 60 cm aluminum frames, and the bead chain lengths were adjusted to ensure that the hind limbs remained suspended at the same angle as in the HU cages. The bead chain was then placed in a slot at the top of the frame to ensure suspension of the rodent hind limbs, and the swivel permitted rotation in the boxes.

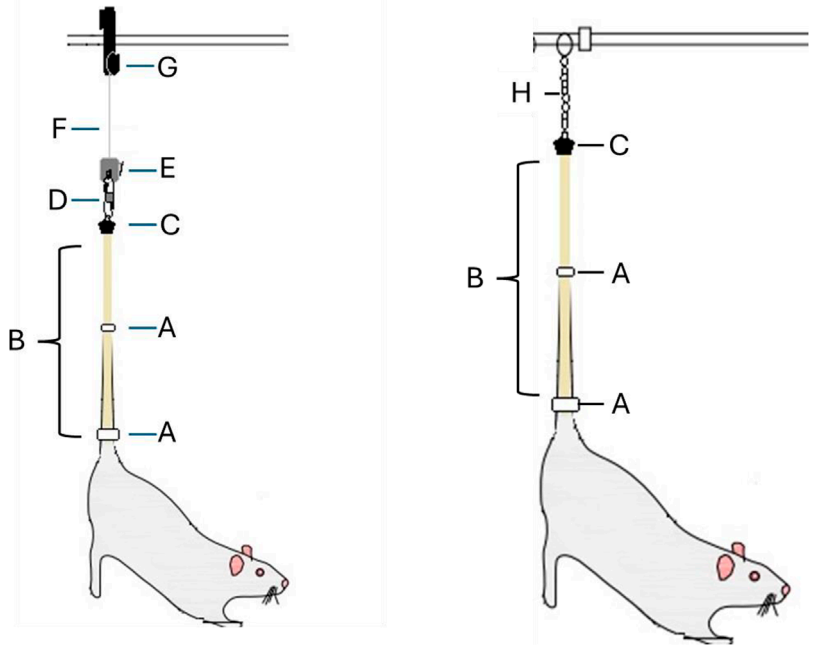

FIGURE 1
Schematic detailing the components associated with the tail suspension procedure for placement in the specialized hindlimb unloading (HU) housing cages (Left) or transfer to the NASA Space Radiation Laboratory (NSRL) for placement in the beamline (Right). Common components for both methods: [A] strips of wrap-around micropore tape; [B] medical traction tape applied along the lateral portion of the tail that is then wrapped through a hole in the bottom portion of [C], which is a specialized and custom-made swivel for HU housing cage-specific components (Left). [D] is a carabiner connected to the underlying swivel, and [E] is a zipper hook above, which is attached to and permits adjustment of the height of the rat through vertical movements along a [F] Perlon cord attached to a [G] pulley to permit sliding of the setup over a steel bar. Beamline housing-specific components (Right). [H] is a bead chain connected to the underlying swivel that is then connected to the grooves in the aluminum frame placed in the beamline.

2.3 Performances in the open field in the absence and presence of objects (week 1)

Exploratory behaviors, measures of anxiety, and hippocampus-dependent spatial habituation learning were assessed in a black open field (90.49 cm × 90.49 cm × 45.72 cm) during two consecutive days, similar to that in the previous study with middle-aged male WAG/Rij rats (Raber et al., 2021). The animal cages were brought into the testing room; then, the rats were picked up gently by placing the thumb and forefinger behind the forelegs and wrapping the palm around the stomach. The researchers supported the animals by their stomachs during transportation to and from the enclosure. The animals were placed in the middle of the open field for 5 min each day. The researchers vacated the testing room during behavioral testing. Following the testing of each rat, the enclosure was cleaned with a solution of 70% isopropyl alcohol. The outcome measures analyzed using video tracking (AnyMaze software, Stoelting Co., Wood Dale, IL, United States) were the total distance moved, time spent freezing, and percentage of time spent in the more anxiety-provoking center zone (45.25 cm × 45.25 cm).

On day 3, the rats were tested in the open field containing 3D-printed objects based on the protocol, as reported previously (Aguilar et al., 2018), with the following modifications. The objects were placed 45.72 cm from the top as well as 30.48 cm from the left and right sides of the enclosure, with the distance between the two objects also being 30.48 cm. The rats were then placed in the enclosure containing two identical blue objects (squares) or two identical red objects (cylinders) for an acquisition trial of 5 min. The objects were counterbalanced for this task, where half the rats started with the blue squares and the other half started with the red cylinders. Sixty minutes following the acquisition trial (A), the rats were again placed in the enclosure with one of the familiar objects replaced with a novel red or blue object for the test trial (T). The outcome measures analyzed using video tracking were the total distance moved and percentage of time spent in the center zone (45.25 cm × 45.25 cm) containing the objects. In addition, the percentage of time that each animal explored the novel and familiar objects in the test trial was analyzed by manually scoring the digital videos. The light intensity during the open field and object recognition tests was 50 lux. A white noise generator (setting II) and overhead lights were used during testing.

2.4 Plasma metabolomics analysis

Nine months following sham-irradiation or irradiation and 7 months after the behavioral and cognitive tests, blood samples of 72 rats (Table 1) were collected in EDTA-containing tubes, the samples were centrifuged at 2,000*g* for 10 min, and the plasma supernatant was collected and stored at −80°C for plasma metabolomics. To compare the results of the current study with those of our earlier HU rat studies and due to COVID-19-related travel restrictions, the time points for the plasma analyses were not the same as those of the behavioral tests. The rats were euthanized

by guillotine without anesthesia; the brain was then cut along the midline on ice in phosphate-buffered saline (PBS), and the entire hippocampus and complete cortex were dissected as described by Raber et al. (2002) before being stored at −80°C. The tissues were homogenized in 300 µL (per 30 µg of tissue) of cold methanol and water (8:2, v/v), and the metabolites were extracted from 100 µL of plasma. Untargeted metabolomic analysis was then performed as described by Kirkwood et al. (2013). Liquid chromatography (LC) was performed using a Shimadzu Nexera system with an insertil phenyl-3 column (4.6 × 150 mm, 100 Å, 5 µm; GL Sciences, Rolling Hills Estates, CA, United States) coupled to a quadrupole time-of-flight mass spectrometer (Q-TOF MS; AB SCIEX, Triple TOF 5600) operated in the information-dependent MS/MS acquisition mode. The samples were ordered randomly and included multiple quality control (QC) samples. To ensure stability and repeatability of the LC-MS system, we included QC samples comprising equal mixtures of 10 µL aliquots of the representative biological samples from the same study; after every 10 samples, a total of seven QC assessments were performed so that the analytical variations would be much smaller than the biological variability. The coefficient of variation was generally within 15% when the signal-to-noise ratio was >10. All samples were tested in both positive and negative ion modes. In the case that metabolites were present in both ion modes, the mode with the higher peak value was selected for further analysis. The column temperature was maintained at 50°C, and the samples were preserved at 10°C. To detect the metabolic features and normalize the data, the metabolomics data were processed using Markerview (version 1.3.1, SCIEX, Framingham, MA, United States) software. After removing the isotopologs and adducts of the same molecular species, the metabolite identities were assigned using Peakview software (SCIEX) by matching for accurate mass (error <10 ppm), retention time (error <10%), MS/MS fragmentation (library score >70), and isotope distribution (error <20%) using an in-house library consisting of IROA standards (IROA Technologies, Bolton, MA, United States) and other commercially available standards (650 total) for integrated pathway and statistical analyses. In addition to the IROA database, the fragmentation spectra of all peaks were verified with data from Metlin (Scripps, La Jolla, CA, United States) and HMDB (University of Alberta, Edmonton, Canada). This confirmation of the metabolites using retention time, mass-to-charge (m/z) ratio, and comparisons with authentic standards (±1 min) through the in-house library (IROA Technologies) allowed streamlined identification of the metabolites. LipidMaps (Welcome Trust, United Kingdom), Metlin, and HMDB were used for the MS and MS/MS matching. MetaboAnalyst pathway analysis (Montreal, Quebec, Canada) was performed as described earlier (Kirkwood et al., 2013; Xia and Wishart, 2010). The raw metabolomite peak values from the plasma, hippocampus, and cortex were analyzed by Pareto scaling through six distinct comparisons: 1) effects of radiation (0.75 Gy) compared to sham irradiation in rats without HU; 2) effects of radiation (1.5 Gy) compared to sham irradiation in rats without HU; 3) effects of radiation compared to sham irradiation, in rats with control HU; 4) effects of control HU in sham-irradiated rats: sham vs. control HU; 5) effects of control HU in 0.75-Gy-irradiated rats: sham vs. control HU; 6) effects of control HU in 1.5-Gy-irradiated rats: sham vs. control HU. The pathways were visualized using scatter plots (testing for significant features) in MetaboAnalyst with "global test" and "relative-betweenness centrality" as the parameters for the enrichment method and topological analysis, respectively.

2.5 Statistical analyses

All data were presented as means ± standard errors of the means (SEMs). The behavioral and cognitive data were analyzed with SPSS v.25 software (IBM, Armonk, NY, United States). To analyze the behavioral and cognitive performances after sham irradiation or simGCRsim irradiation (0, 0.75, or 1.5 Gy), we performed analyses of variance (ANOVAs) with *post hoc* tests comparing the sham-irradiated animals where appropriate. To assess the role of microgravity, we performed ANOVAs including the radiation (0, 0.75, or 1.5 Gy) and HU conditions (sham, control HU, or HU) as between-group factors with repeated measures where appropriate. For some analyses, as indicated and appropriate, two-sided *t*-tests were used. We set the statistical significance to $p < 0.05$. Greenhouse–Geisser corrections were used if the sphericity was found to be violated (Mauchly's test).

The plasma metabolomics were analyzed for the comparisons described above. To identify the potential plasma biomarkers of radiation exposure or HU condition on behavioral or cognitive performance, we used regression analyses. Based on Pareto scaling, we selected the metabolites that were consistently included in the models. MetaboAnalyst software was used to generate the impact plots, and the graphs were generated using GraphPad software v.8.2.0 (La Jolla, CA, United States). As MetaboAnalyst is not ideal for analyzing amino-acid-related pathways, we analyzed them separately as described under the metabolomics analysis above.

3 Results

3.1 Effects of HU and radiation on performance in the open field

When the activity levels were analyzed for two consecutive days in the open field, there was a condition × day interaction (F (day, condition) (2, 123) = 6.367, $p = 0.002$). In the control HU group, there was a trend toward radiation effects (F (2, 33) = 3.102, $p = 0.058$), with higher activity levels in animals irradiated with 1.5 Gy than the sham-irradiated animals ($p = 0.0183$, Dunnett's test). There was also a main effect of HU on the activity level in the open field (F (2, 123) = 4.606, $p = 0.012$), with HU animals moving less than animals under control HU ($p = 0.015$, Tukey's test) or no HU ($p = 0.029$, Tukey's test). There was also a day effect (F (1, 123) = 150.240, $p < 0.001$), with lower activity levels on day 2 than day 1, indicating that all groups showed spatial habitation learning (Figure 2A). There was also a trend toward an overall effect of radiation that was not significant (F (2, 123) = 2.698, $p = 0.071$).

Similar results were obtained for the analysis of the time spent mobile (Figure 2B). In the control HU group, there was a radiation effect (F (2, 33) = 3.775, $p = 0.033$), with higher activity levels in animals irradiated with 1.5 Gy than the sham-irradiated animals ($p = 0.0161$, Dunnett's test); these effects were not observed in animals under the HU or no HU condition.

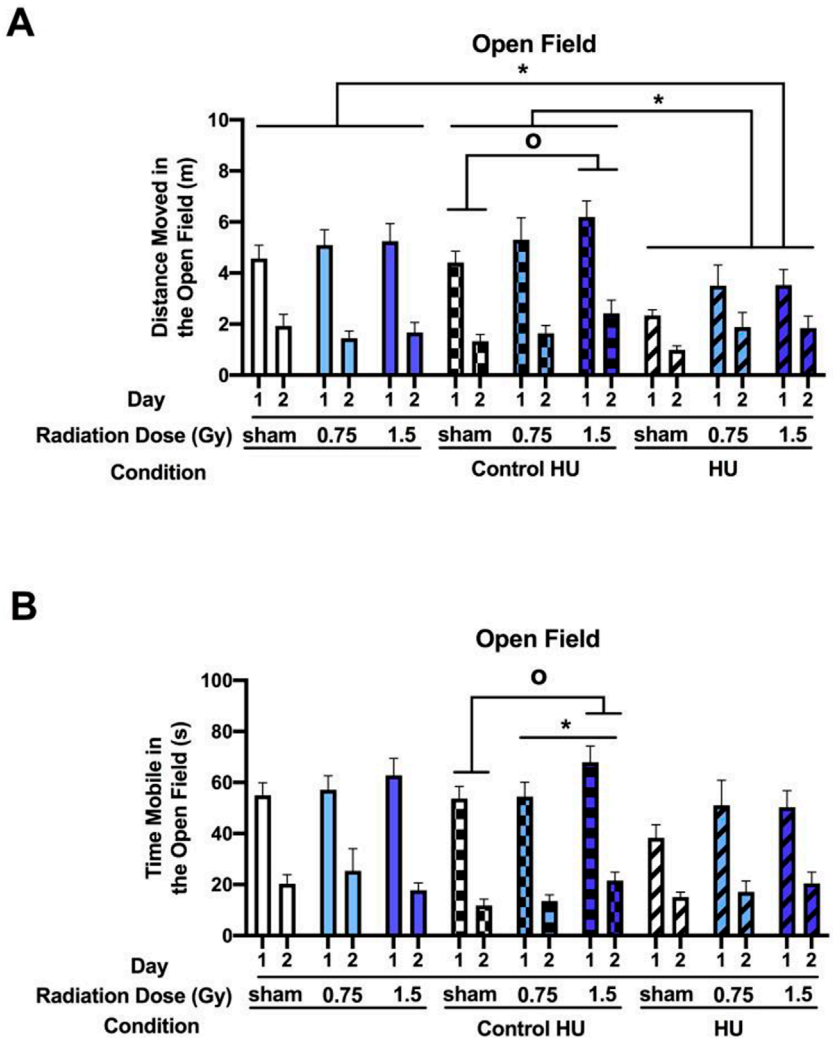

FIGURE 2
Performance in the open field in the absence of objects. The rats were tested for exploratory behaviors in the open field on two consecutive days, with the trials lasting 5 min each and spaced 24 h apart. **(A)** Analysis of the activity levels on two consecutive days in the open field showed a condition × day interaction (F (2, 123) = 6.367, p = 0.002). In the control HU group, activity levels were higher in animals exposed to 1.5 Gy than the sham-irradiated animals ($^{o}p < 0.05$, Dunnett). There was also a main effect of HU (F (2, 123) = 4.606, p = 0.012), with the animals under HU moving less than those under control HU or without HU ($^{*}p < 0.05$, Tukey). **(B)** Analysis of the time spent mobile showed a similar pattern. In the control HU group, there was a radiation effect, with higher activity levels in animals exposed to 1.5 Gy than the sham-irradiated animals ($^{*}p < 0.05$, Tukey; $^{o}p < 0.05$, Dunnett). These effects were not observed in animals under HU or without HU.

3.2 Effects of HU and radiation on performance in the open field with objects

The activity levels were analyzed for two consecutive days in the open field containing objects. There was an effect of the HU condition (F (2, 123) = 3.164, p = 0.046) and a radiation × HU condition interaction (F (4, 123) = 3.118, p = 0.018) (Figure 3A). Animals under HU moved less than those under control HU (p = 0.035, Tukey's test). In the HU group, there was a radiation effect (F (2, 27) = 4.704, p = 0.018); HU animals that were irradiated with 0.75 Gy (p = 0.0087, Dunnett's test) or 1.5 Gy (p = 0.0283, Dunnett's test) moved less than the sham-irradiated HU animals. In contrast, there were no significant effects of radiation in the control HU group (F (2, 33) = 2.950, p = 0.066). There was a trend toward lower activity in the control HU animals irradiated with 1.5 Gy than those irradiated with 0.75 Gy that did not reach significance (p = 0.0959, Dunnett's test). There was also a day effect (F (1, 123) = 136.269, $p < 0.001$), with higher activity levels on day 4 for one familiar and one novel object than day 3 for two identical objects, indicating that the animals responded to the novelty.

The animals spent relatively little time exploring the objects on day 4 (Figure 3B). There was no effect of radiation or HU condition. When rats that did not explore the objects on a day were excluded from the analysis, there was no significant effect of the condition (F (2, 54) = 2.813, p = 0.0689) but animals under HU spent more time exploring the objects than animals without HU (p = 0.0464, Dunnett's test, Figure 3C). When the percentage of animals that explored the objects on day 4 was examined, the animals under

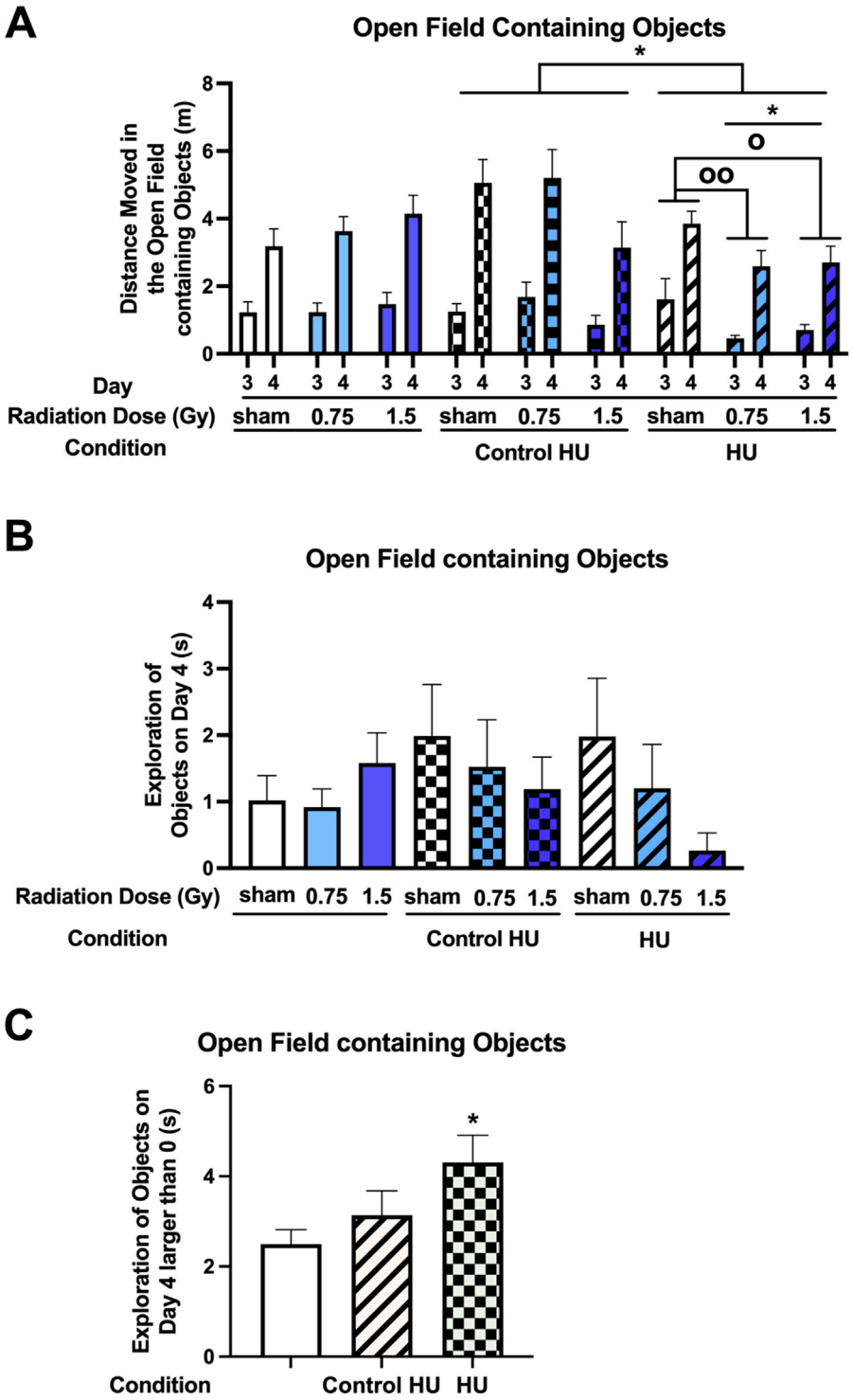

FIGURE 3
(A) Performance assessment in the open field containing objects showed that there was an effect of HU condition (F (2, 123) = 3.164, p = 0.046) and a radiation × HU condition interaction (F (4, 123) = 3.118, p = 0.018). Animals under HU moved less than animals under control HU (*p < 0.05, Tukey). In the HU group, there was a radiation effect (F (2, 27) = 4.704, p = 0.018); HU animals irradiated with 0.75 or 1.5 Gy moved less than the sham-irradiated HU animals (°p < 0.05, °°p < 0.01, Dunnett). There was also a day effect (F (1, 123) = 136.269, p < 0.001), with higher activity levels on day 4 involving one familiar and one novel object than on day 3 involving two identical objects. **(B)** There was no effect of radiation or HU condition on the time spent exploring the objects on day 4. **(C)** When the rats that did not explore the objects on a particular day were excluded from the analysis, the animals under HU were noted to have spent more time exploring the objects than those without HU (*p < 0.05, Dunnett).

HU showed a trend toward a lower percentage (27%) than animals without HU (48%) (z (1, 3.805) = 1.951, p = 0.051, two-sided chi-squared test) or animals under the control HU condition (50%) (z (1, 3.732) = 1.932, p = 0.053, two-sided chi-squared test).

3.3 Plasma metabolomics analysis

When the effects of radiation were analyzed in the plasma of animals without HU or control HU, the riboflavin metabolic pathway was affected most along with glycerophospholipid, sphingolipid, and glutathione metabolic pathways being less affected in the comparison of sham irradiation vs. 0.75 Gy (Figure 4A). Comparison of sham irradiation vs. 1.5 Gy irradiation in animals without HU or control HU showed that the riboflavin metabolic pathway was also affected (Figure 4B). The arginine biosynthesis; glutamine and glutamate metabolism; and alanine, aspartate, and glutamate metabolic pathways were also affected (Figure 3B). Riboflavin, glutamine, and arginine concentrations were higher in the plasma of animals that received 1.5 Gy irradiation than the sham-irradiated animals (Figure 4C).

When the effects of radiation were analyzed in the plasma of animals under the control HU condition, the riboflavin metabolic pathway was maximally affected, while the glutathione metabolic pathway was affected to a lesser extent (Figure 4D). In contrast, none of the pathways were significantly affected when comparing the 1.5 Gy vs. sham-irradiation animals.

When comparing the effects of the control HU condition on plasma in the sham-irradiated animals with those not under the condition, the alanine, aspartate, and glutamate metabolism, as well as riboflavin metabolism, arginine biosynthesis, and glutamine and glutamate metabolism were found to be affected (Figure 4E). Next, in the 0.75-Gy-irradiated animals, the effects of the control HU condition on plasma were analyzed by comparison with those not under the condition. The phenylalanine, tyrosine, and tryptophan pathway was the most affected one but the alanine, aspartate, and glutamate metabolic pathway was also strongly affected (Figure 4F). In contrast, none of the pathways were found to be significantly affected when assessing the effects of the control HU condition on 1.5-Gy-irradiated animals.

3.4 Metabolomics analysis of the hippocampus

When the effects of radiation were analyzed in the hippocampi of animals without HU or control HU, none of the pathways were found to be affected in animals receiving 0.75 Gy of radiation and none of the pathways had impacts of 0.5 or higher in animals receiving 1.5 Gy. The purine metabolism and pyrimidine pathway was affected and had impacts of 0.28 and 0.23, respectively (Supplementary Figure S1).

When the effects of exposure to 0.75 Gy of irradiation were analyzed in the hippocampi of animals under the control HU condition, the glutamine and glutamate metabolic pathway was found to be affected (Figure 5A). In contrast, when the effects of exposure to 1.5 Gy of irradiation were analyzed in the hippocampi of animals under the control HU condition, only fatty acid biosynthesis was identified, with an impact of 0.015 (Supplementary Figure S2).

In the sham-irradiated animals, the effects on the hippocampus were compared in animals under and not under the control HU condition, and it was found that the phenylalanine, tyrosine, and tryptophan pathway was affected most followed by the riboflavin metabolic pathway (Figure 5B). In the 0.75-Gy-irradiated animals, the phenylalanine, tyrosine, and tryptophan pathway was also affected the most, followed by the riboflavin metabolic as well as D-glutamine and D-glutamate pathways (Figure 5C). In the 1.5-Gy-irradiated animals, the phenylalanine, tyrosine, and tryptophan pathway was also the most affected, followed by the riboflavin metabolic pathway (Figure 5D).

3.5 Metabolomics analysis of the cortex

When the effects of radiation were analyzed in the cortexes of animals not under the HU or control HU condition, there were no pathways that had impacts of 0.5 or greater in animals irradiated with 0.75 Gy (Supplementary Figure S3A) or 1.5 Gy (Supplementary Figure S3B).

When the effects of exposure to 0.75 Gy of irradiation were analyzed in the cortexes of animals under the control HU condition, the glutamine and glutamate metabolism pathway was found to be affected, similar to that of the hippocampus (Figure 6A). Next, exposure to 1.5 Gy of irradiation on the cortexes of animals under the control HU condition showed that the riboflavin pathway was affected (Figure 6B).

In the sham-irradiated animals, the cortical effects were analyzed by comparing animals under and not under the control HU condition, which showed that the riboflavin metabolic pathway was affected (Figure 6C). In the 0.75-Gy-irradiated animals, the glutamine and glutamate metabolic pathway was affected (Figure 6D), while the riboflavin metabolic pathway was affected in the 1.5-Gy-irradiated animals (Figure 6E).

3.6 Individual metabolites in the affected pathways in the plasma, hippocampus, and cortex

The individual metabolites in the glutamine and glutamate pathway are shown in Figure 7. In the plasma of animals without HU, the glutamine levels were higher in animals exposed to 1.5 Gy irradiation than the sham-irradiated animals (Figure 7A); these levels were also higher in sham-irradiated animals in the control HU condition than those without HU (Figure 7A). In the hippocampi (Figure 7B) and cortexes (Figure 7C) of animals under the control HU condition, the glutamine levels were lower for exposure to 0.75 Gy than in the sham-irradiated animals. In the 0.75-Gy-irradiated animals, the glutamine levels were lower in the hippocampi (Figure 7B) and cortexes (Figure 7C) under the control HU condition than without HU. In addition, in the hippocampi of animals exposed to 0.75 Gy of radiation, the levels of 4/5-oxo-proline were higher in animals under HU than those without HU. In the hippocampi of animals exposed

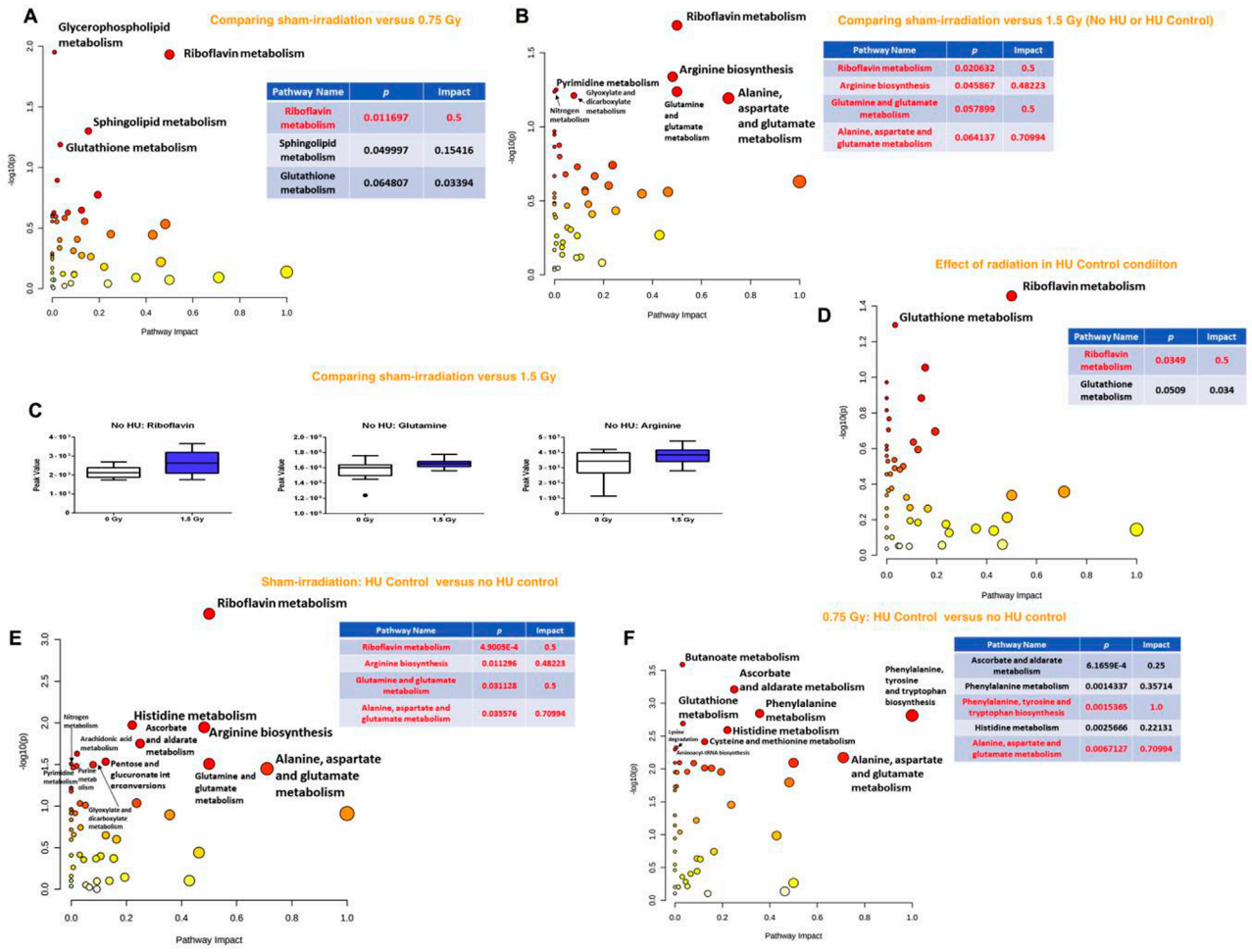

FIGURE 4
(A) Analysis of the effects of radiation in the plasma of animals without HU or control HU showed that the riboflavin metabolic pathway was most affected with the glycerophospholipid, sphingolipid, and glutathione metabolic pathways being less affected for sham irradiation vs. 0.75 Gy exposure. **(B)** Sham irradiation vs. 1.5 Gy exposure in animals without HU or control HU showed that the riboflavin metabolic pathway was affected most along with the arginine biosynthesis, glutamine and glutamate metabolic, and alanine, aspartate, and glutamate metabolic pathways. **(C)** Riboflavin, glutamine, and arginine levels were higher in the plasma of animals irradiated with 1.5 Gy than the sham-irradiated animals. **(D)** In the plasma of animals without control HU, the riboflavin metabolic pathway was the most affected, while the glutathione metabolic pathway was less affected. **(E)** In the assessment of the effects of the control HU condition on plasma in sham-irradiated animals, the alanine, aspartate, and glutamate metabolic, riboflavin metabolic, arginine biosynthesis, and glutamine and glutamate metabolic pathways were found to be affected. **(F)** In the animals exposed to 0.75 Gy, assessment of the effects of the control HU condition on plasma showed that the phenylalanine, tyrosine, and tryptophan pathway was most affected, followed by strong effects on the alanine, aspartate, and glutamate metabolic pathways. The metabolome view figures contain all the matched pathways (metabolomes) arranged by *p*-values (generated as part of the pathway enrichment analysis) along the *Y* axis and pathway impact values (generated as part of the pathway topology analysis) along the *X* axis. The node colors are based on the *p* values, and the node radii are determined on the basis of the pathway impact values. The red nodes indicate strong impact and significance, while the yellow nodes indicate weak impact and non-significant *p*-value. The pathway impact and *p*-values are indicated in the tables.

to 1.5 Gy of radiation, the riboflavin levels were higher in animals under the control HU condition than those without HU (Figure 7B).

The individual metabolites in the riboflavin metabolic pathway are indicated in Figure 8. In the plasma of animals without HU, the riboflavin levels were higher when exposed to 0.75 Gy or 1.5 Gy of radiation than the sham-irradiated animals (Figure 8A). The riboflavin levels were also higher in the plasma of sham-irradiated animals under the control HU condition than those without HU. In the plasma of animals under the HU condition, the riboflavin levels were lower when exposed to 0.75 Gy of radiation than in the sham-irradiated animals. In the hippocampi of sham-irradiated and 0.75-Gy-irradiated animals, the riboflavin levels were higher under the control HU condition than those without HU (Figure 8B). In the 0.75-Gy-irradiated animals, the flavin adenine dinucleotide (FAD) levels were higher in the hippocampi (Figure 8B) and cortixes (Figure 8C) of animals under HU than without HU. In the cortixes of animals under the control HU condition, the riboflavin levels were higher and FAD levels lower when exposed to 1.5 Gy of radiation than sham irradiation.

The individual metabolites in the phenylalanine, tyrosine, and tryptophan biosynthesis pathway are shown in Figure 9.

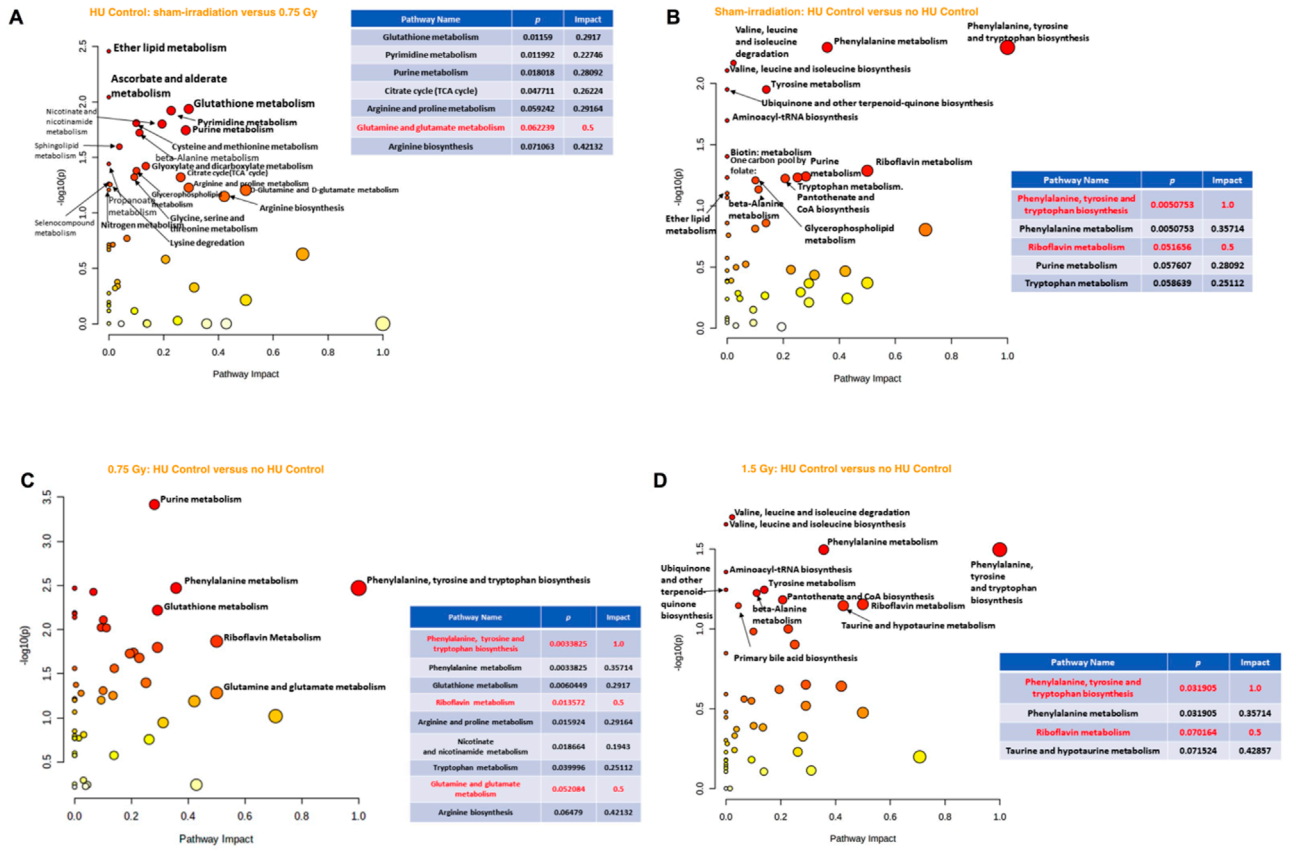

FIGURE 5
(A) Analysis of the effects of 0.75 Gy irradiation in the hippocampus of animals under the control HU condition showed that the glutamine and glutamate metabolic pathway was affected. **(B)** In sham-irradiated animals, assessment of the effects of the control HU condition on the hippocampus showed that the phenylalanine, tyrosine, and tryptophan pathway was most affected, followed by the riboflavin metabolic pathway. **(C)** In animals exposed to 0.75 Gy, the phenylalanine, tyrosine, and tryptophan pathway was the most affected, followed by the riboflavin metabolic as well as D-glutamine and D-glutamate pathways. **(D)** In animals exposed to 1.5 Gy, the phenylalanine, tyrosine, and tryptophan pathway was the most affected, followed by the riboflavin metabolic pathway. The red nodes indicate strong impact and significance, while the yellow nodes indicate weak impact and a non-significant *p*-value. The pathway impact and *p*-values are indicated in the tables.

In the plasma of animals exposed to 0.75 Gy of radiation, phenylalanine levels were higher under the HU condition than without HU (Figure 9A); tyrosine and phenylalanine were higher in the hippocampi of the sham-, 0.75-Gy-, and 1.5-Gy-irradiated animals (Figure 9B).

The individual metabolites in the arginine biosynthesis pathway are indicated in Figure 10. In animals without HU or control HU, glutamine and arginine levels were higher when exposed to 1.5 Gy radiation than sham irradiation (Figure 10A). In addition, glutamine and arginine levels were higher in the plasma of sham-irradiated animals under the control HU condition than those without HU (Figure 10A).

The individual metabolites in the alanine, aspartate, and glutamate metabolic pathway are indicated in Figure 10B. In the plasma of animals without HU or control HU, glutamine levels were higher upon exposure to 1.5 Gy than sham irradiation (Figure 10B). In addition, in the sham- and 0.75-Gy-irradiated animals, glutamine levels were higher under the control HU condition than without HU (Figure 10B). In the plasma of 0.75-Gy-irradiated animals, acetyl aspartate, succinate, and glutamate were also higher under the control HU condition than without HU. Finally, in the primary bile acid synthesis pathway, taurine levels in the hippocampi of animals exposed to 1.5 Gy irradiation under the HU condition were lower than those without HU or control HU (Figure 10C).

3.7 Regression analysis of individual metabolites and specific behavioral or cognitive measures

We used univariate linear regression analyses stratified by radiation exposure and HU condition along with Z-scores for the behavioral measures (dependent variables) and metabolite values (independent variables) to identify potential plasma biomarkers of radiation exposure or HU condition on the behavioral or cognitive performance. We selected only those metabolites that were consistently included in the models. Table 2 lists all the behavioral measures used in the regression analysis in this study.

Table 3 illustrates the 21 plasma metabolites that were consistently included in the models (at least four times each) and the

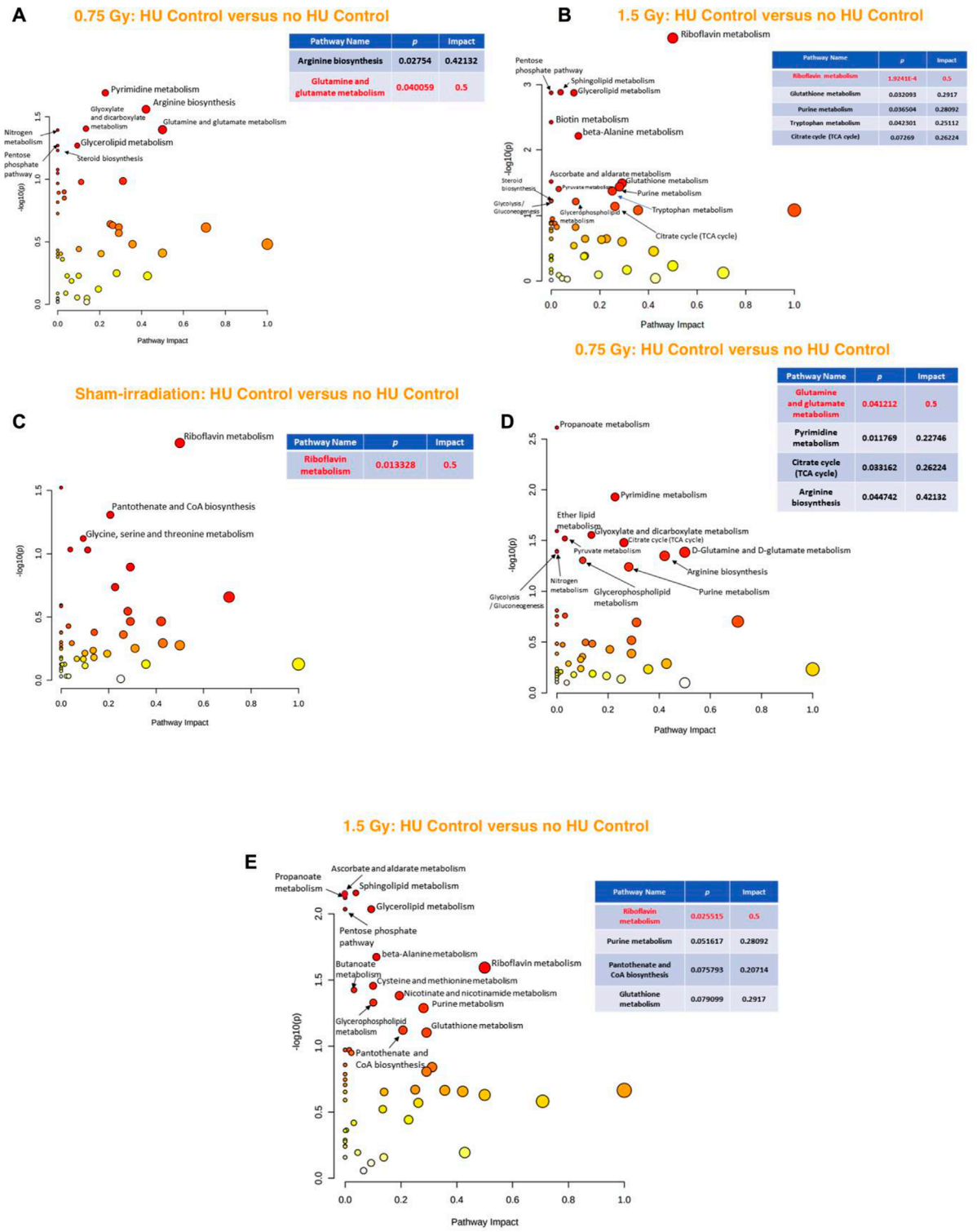

FIGURE 6
(A) Analysis of the effects of 0.75 Gy irradiation in the cortixes of animals under the control HU condition showed that the glutamine and glutamate metabolic pathway was affected. **(B)** Assessment of the effects of 1.5 Gy irradiation in the cortixes of animals under the control HU condition showed that the riboflavin pathway was affected. **(C)** In sham-irradiated animals, assessment of the effects of the control HU condition on the cortex showed that the riboflavin metabolic pathway was affected. **(D)** In animals exposed to 0.75 Gy, the glutamine and glutamate metabolic pathway was affected. **(E)** In animals exposed to 1.5 Gy, the riboflavin metabolic pathway was affected. The red nodes indicate strong impact and significance, while the yellow nodes indicate weak impact and non-significant *p*-value. The pathway impact and *p*-values are indicated in the tables.

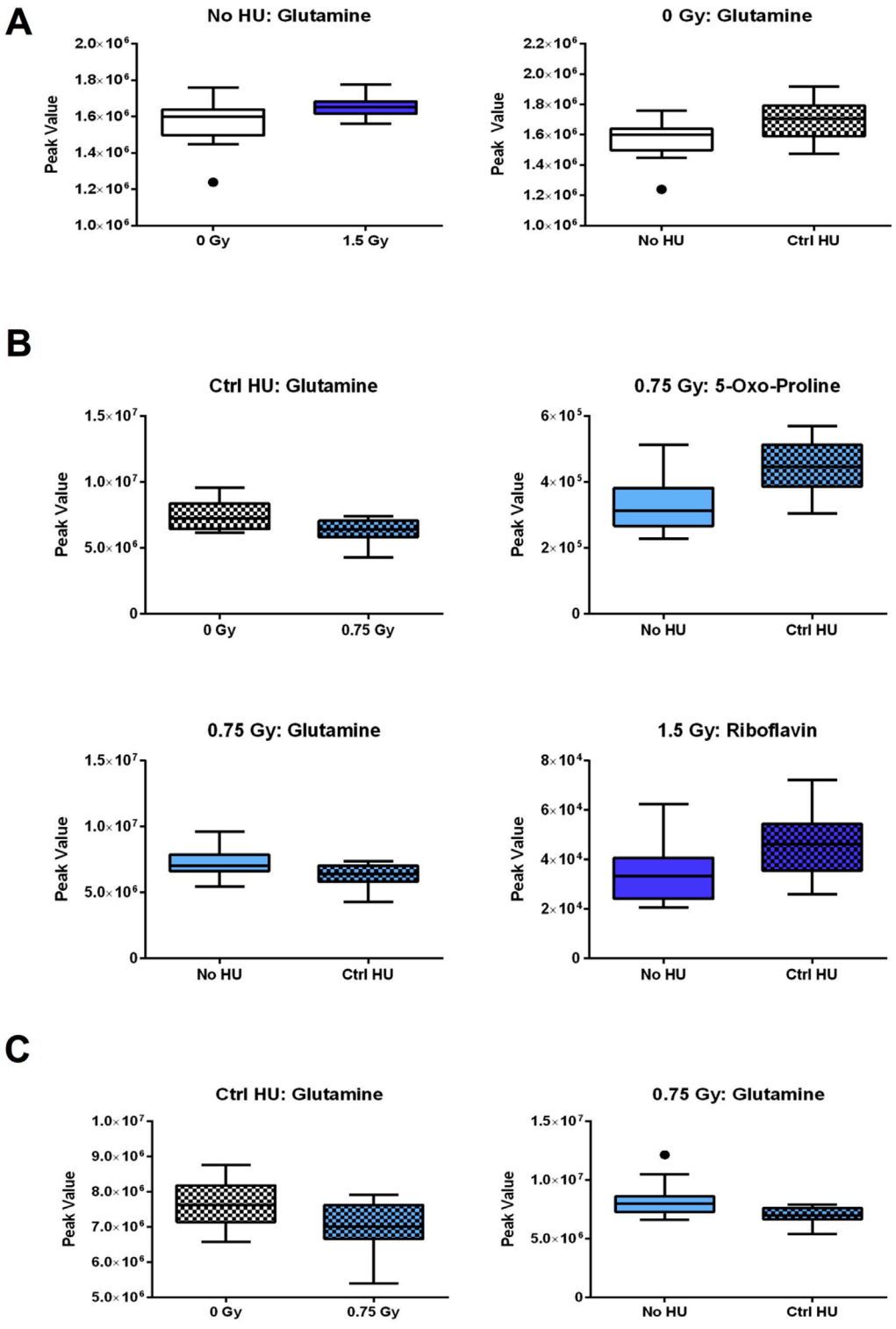

FIGURE 7
Individual metabolites in the glutamine and glutamate pathway. **(A)** In the plasma of animals without HU, the glutamine levels were higher for 1.5 Gy exposure than sham irradiation; the glutamine levels were also higher in the sham-irradiated animals in the control HU condition than those without HU. In the **(B)** hippocampi and **(C)** cortixes of animals in the control HU condition, the glutamine levels were lower for exposure to 0.75 Gy than sham irradiation; furthermore, the glutamine levels were lower in animals in the control HU condition than those without HU. **(B)** In the hippocampi of animals exposed to 0.75 Gy, the 5-oxo-proline levels were higher under HU than without HU. In the hippocampi of animals exposed to 1.5 Gy, the riboflavin levels were higher under the control HU condition than without HU. The red nodes indicate strong impact and significance, while the yellow nodes indicate weak impact and non-significant *p*-value. The pathway impact and *p*-values are indicated in the tables.

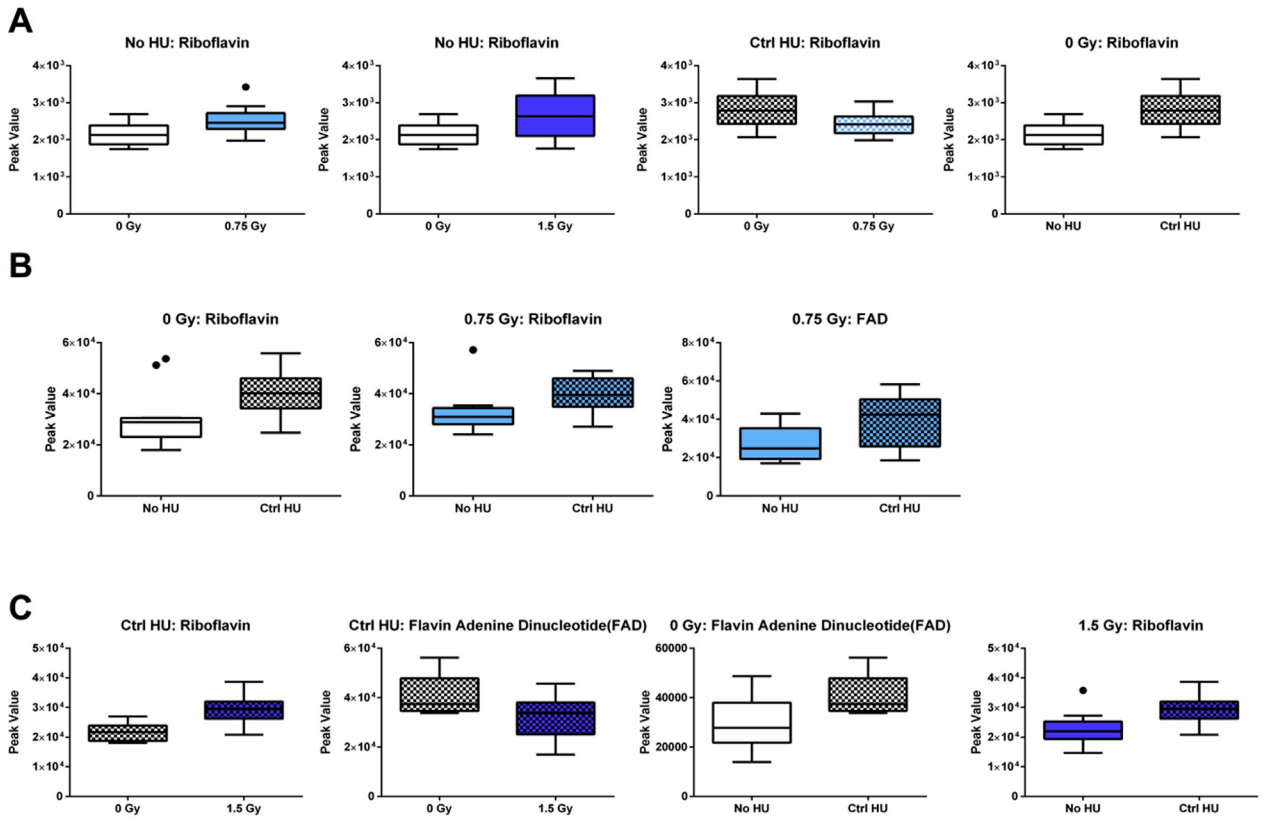

FIGURE 8
Individual metabolites in the riboflavin metabolic pathway. **(A)** In the plasma of animals without HU, the riboflavin levels were higher for exposure to 0.75 or 1.5 Gy than sham irradiation; the riboflavin levels were also higher in the plasma of sham-irradiated animals under the control HU condition than those without HU. In the plasma of animals under the HU condition, the riboflavin levels were lower for 0.75 Gy exposure than sham irradiation. **(B)** In the hippocampi of animals receiving sham or 0.75 Gy irradiation, the riboflavin levels were higher under the control HU condition than without HU. In the 0.75-Gy-irradiated animals, FAD levels were higher in the **(B)** hippocampus and **(C)** cortex under HU than without HU. In the cortixes of animals under the control HU condition, the riboflavin levels were higher and FAD levels were lower for 1.5 Gy exposure than sham irradiation. In the 1.5-Gy-irradiated animals, the riboflavin levels were higher under the control HU condition than without HU. The red nodes indicate strong impact and significance, while the yellow nodes indicate weak impact and a non-significant *p*-value. The pathway impact and *p*-values are indicated in the tables. The box plots help with identifying outliers based on data points with values beyond the whiskers (indicated as black circles).

10 behavioral measures related to them. Twelve of the associations between the metabolites and behavioral measures were purely positive, as indicated in green font in Table 3. One of the metabolites was purely negatively associated with the behavioral measures (aspartate), as indicated in red font in Table 3. The remaining eight metabolites showed both positive and negative associations with the behavioral measures, as indicated in blue font in Table 3.

In the cortixes of the sham-irradiated animals without HU, two metabolites were purely positively correlated and one metabolite was both positively and negatively correlated with the behavioral measures.

In animals under the control HU condition exposed to 0.75 Gy of radiation, seven metabolites were purely positively correlated with the behavioral measures (one in the hippocampus and six in the plasma).

In contrast, in animals without HU that were exposed to 0.75 Gy of radiation, seven metabolites that were both positively and negatively correlated with the behavioral measures (six in the cortex and one in the hippocampus).

In the control HU animals exposed to 1.5 Gy of radiation, one metabolite in the hippocampus was purely negatively correlated with the behavioral measures. In contrast, in animals without HU exposed to 1.5 Gy of radiation, three metabolites were purely positively correlated with the behavioral measures (one in the hippocampus and two in the plasma).

We next assessed whether any of the 21 metabolites identified in the present study were also among the 27 metabolites in the plasma of photon-irradiated Fischer rats in our previous study 9 months after exposure (Raber et al., 2024). Succinate and 5-methylcytosine were the two metabolites identified in both studies that showed positive associations with the behavioral measures of both studies (Table 4). In the current study, succinate in the hippocampus and 5-methylcytosine in the plasma of the control HU rats exposed to 0.75 Gy of radiation were associated with the behavioral measures. In our previous study in photon-irradiated rats, only the plasma metabolites were analyzed. Succinate in the sham-irradiated rats without HU and 5-methylcytosine in rats exposed to 8 Gy without HU were associated with the behavioral measures. Regarding the behavioral measures, the percentage of

10.3389/fphys.2024.1486767

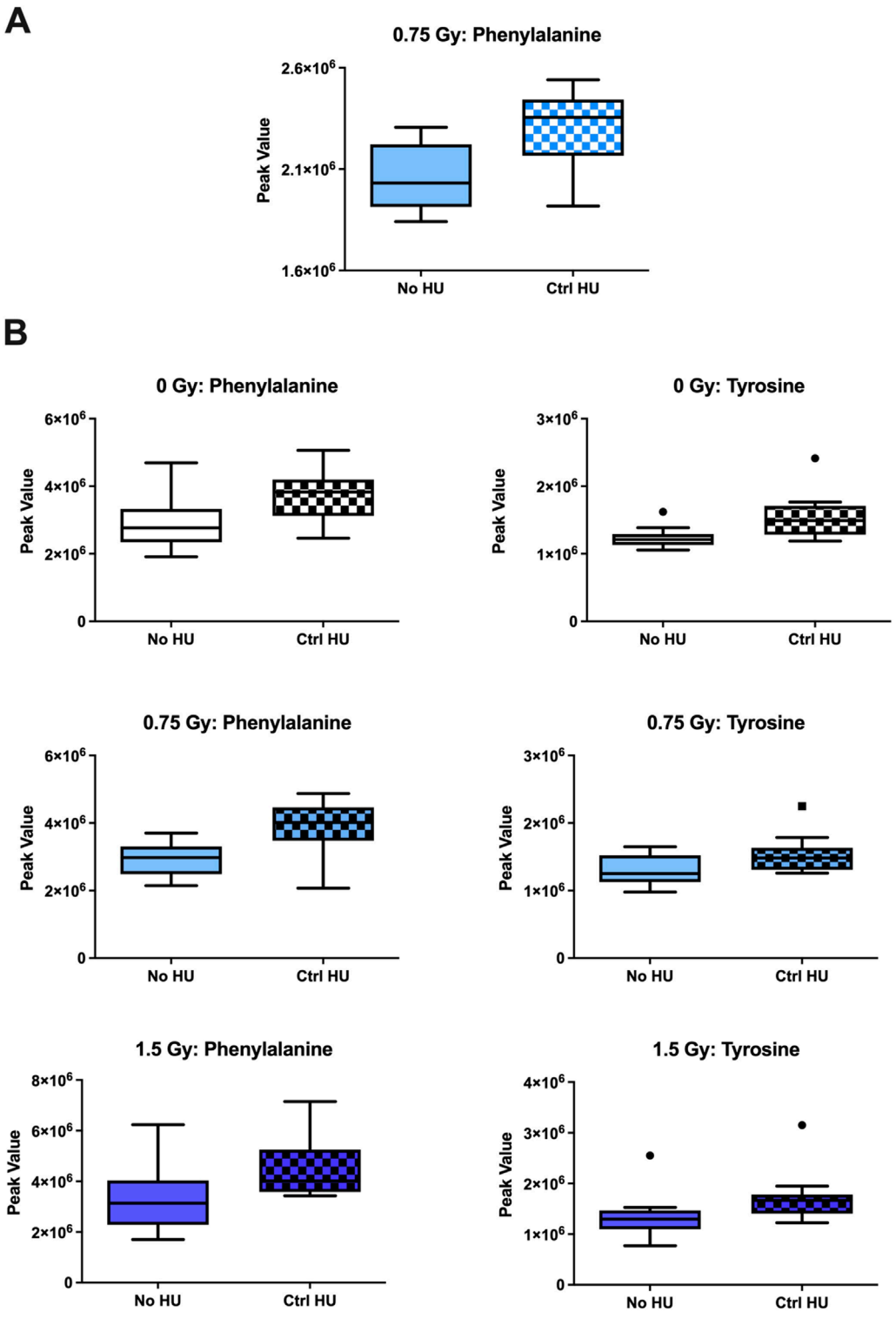

FIGURE 9
Individual metabolites in the phenylalanine, tyrosine, and tryptophan biosynthesis pathway. **(A)** In the plasma of animals exposed to 0.75 Gy, the phenylalanine levels were higher under HU than without HU. **(B)** Tyrosine and phenylalanine levels were higher in the hippocampi of the animals receiving sham, 0.75 Gy, and 1.5 Gy irradiation. The box plots help with identifying outliers based on data points with values beyond the whiskers (indicated as black circles).

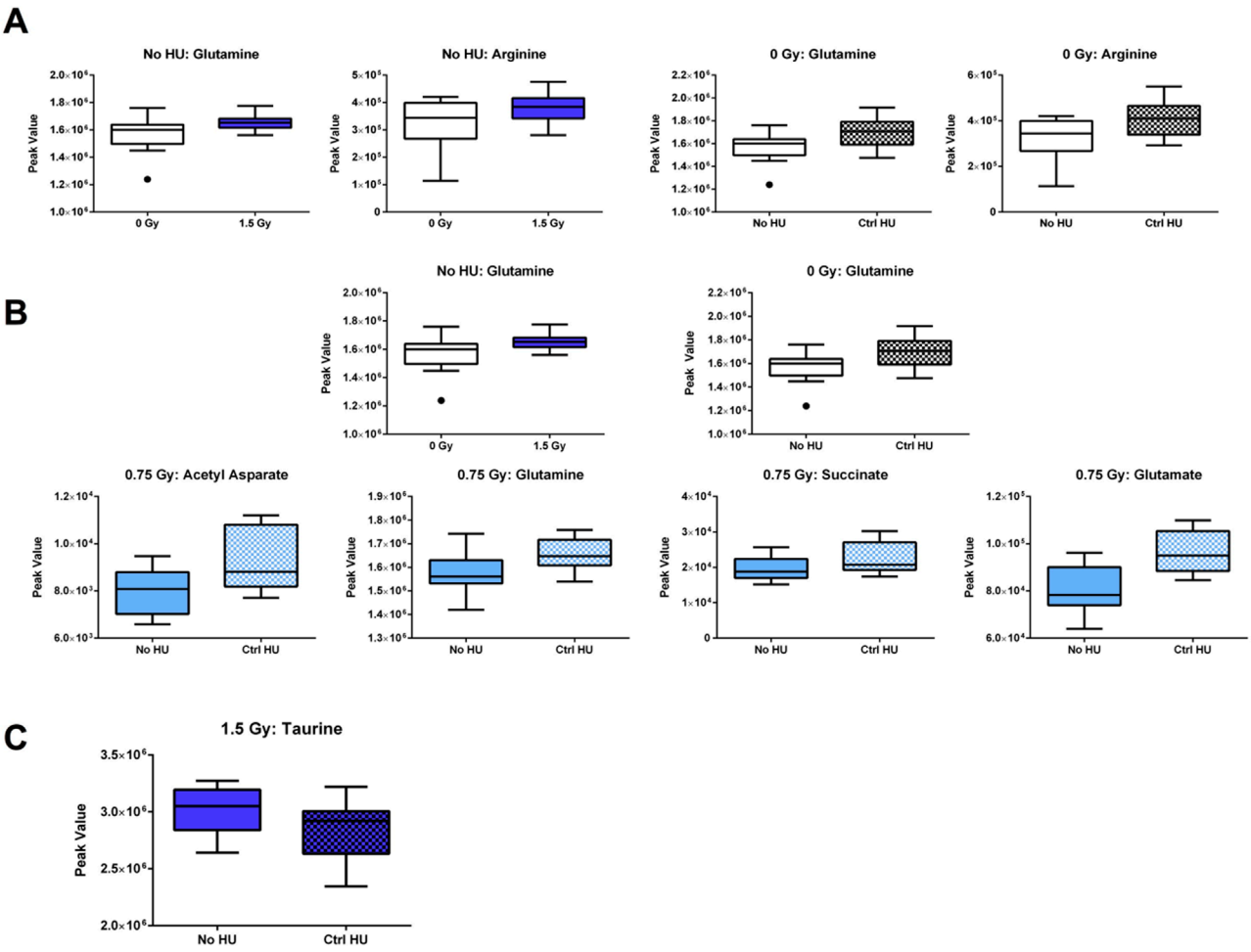

FIGURE 10
(A) Individual metabolites in the arginine biosynthesis pathway. In animals without HU or under the control HU condition, glutamine and arginine levels were higher for exposure to 1.5 Gy than sham irradiation; glutamine and arginine levels were also higher in the plasma of sham-irradiated animals under the control HU condition than those without HU. **(B)** Individual metabolites in the alanine, aspartate, and glutamate metabolic pathway. In the plasma of animals without HU or under the control HU condition, the glutamine levels were higher for 1.5 Gy exposure than sham irradiation. In animals exposed to sham irradiation and 0.75 Gy, the glutamine levels were higher under the control HU condition than without HU. In the plasma of 0.75-Gy-irradiated animals, acetyl aspartate, succinate, and glutamate were higher under the control HU condition than without HU. **(C)** In the primary bile acid synthesis pathway, taurine levels in the hippocampi of 1.5-Gy-irradiated animals under the HU condition were lower than those in animals without HU or control HU. The box plots help with identifying outliers based on data points with values beyond the whiskers (indicated as black circles).

time spent in the field was correlated with succinate levels in both studies. For 5-methylcytosine, there was no overlap in the behavioral measures identified to be correlated in both studies. However, the common behavioral measures used in both studies were for object recognition. In the present study, correlations were observed with the behavioral measures on the second day of the object recognition test; however, in the photon irradiation study, correlations with the behavioral measures were observed on the first day of the object recognition test.

Next, we used the same univariate linear regression analyses stratified by radiation exposure and HU condition with the Z-scores for behavioral measures (dependent variables) and metabolite values (independent variables) to identify potential plasma biomarkers of radiation exposure or HU condition on the behavioral or cognitive performances in our earlier study with WAG/Rij rats (Raber et al., 2021). Male WAG/Rij rats were behaviorally and cognitively tested 3 months after exposure to sham irradiation or simGCRsim in the absence or presence of HU alone. Six months following the behavioral and cognitive tests or 9 months following sham or total body irradiation, the plasma and brain tissues (hippocampus and cortex) were processed to determine whether the behavioral and cognitive effects were associated with long-term alterations in the metabolic pathways in the plasma and brain. We selected only those metabolites that were consistently included in the models. Table 5 illustrates 40 metabolites that were consistently included in the models (at least four times each) and the behavioral measures related to them. Of these 40 metabolites, 15 were present in the cortex, 4 were identified in the hippocampus, and 21 were observed in the plasma.

Eighteen associations between the metabolites and behavioral measures were purely positive, as indicated in green font in Table 5; seven metabolites were purely negatively associated with the

TABLE 2 Behavioral measures included for regression analyses with individual metabolites[a].

Measure	Definition
Activity	Distance moved in the open field on the first day of testing
Activity	Distance moved in the open field on the second day of testing
Activity	Distance moved in the object recognition training trial
Activity	Distance moved in the object recognition test trial
Anxiety	Percentage of time spent in the center of the open field on the first day of testing
Anxiety	Percentage of time spent in the center of the open field on the second day of testing
Cognition	Total time spent exploring the objects in the object recognition test
Cognition	Percentage of time spent in the center of the open field during the object recognition training trial
Cognition	Percentage of time spent in the center of the open field during the object recognition test trial
Cognition	Discrimination index for the object recognition test

[a]The same measures were used in the current study and our earlier study on Fischer rats with the following three exceptions: 1) in the previous study, a measure of anhedonia was included; 2) in the previous study, a measure of anxiety in the elevated plus maze was included; 3) in the previous study, the total time spent exploring during the object recognition training trial was included.

behavioral measures, as indicated in red font in Table 5; and fifteen metabolites showed both positive and negative associations with the behavioral measures, as indicated in blue font in Table 5.

In the sham-irradiated animals without HU, three metabolites in the hippocampus were correlated with the behavioral measures (one purely negatively and two both positively and negatively).

In addition, two metabolites were correlated purely positively with the behavioral measures.

In the animals without HU exposed to 1.5 Gy of radiation, 11 metabolites in the cortex, one metabolite in the hippocampus, and 4 metabolites in the plasma were purely positively correlated with the behavioral measures, while 7 metabolites showed both positive and negative associations.

In the sham-irradiated animals under HU, one metabolite in the cortex was purely positively associated with the behavioral measures, whereas one metabolite in the hippocampus and 3 metabolites in the plasma were both positively and negatively associated with the behavioral measures.

In the animals under HU exposed to 1.5 Gy of radiation, two metabolites in the cortex and four metabolites in the plasma were purely negatively associated with the behavioral measures, while one metabolite in the plasma showed both positive and negative associations.

We next assessed whether any of the 21 metabolites identified in the present study were also among the 40 metabolites in the plasma, hippocampus, or cortex of the simGCRsim-irradiated WAG/Rij rats in our previous study. Phenylalanine and tryptophan were the two metabolites that showed both positive and negative associations with the behavioral measures of both studies (Table 6). Although these metabolites were found in the hippocampus in the previous study on WAG/Rij rats, they were found in the cortex in the present study on Fischer rats. Carnitine in the plasma in the current study showed both positive and negative associations with the behavioral measures in the WAG/Rij rats, while lauroylcarnitine in the cortex and deoxycarnitine in the plasma showed purely positive associations with the behavioral measures in the Fischer rats.

4 Discussion

In this study, we characterized the behavioral and cognitive performances of male Fischer rats after sham or total body irradiation with simGCRsim in the absence and presence of HU or control HU. The HU condition is a surrogate measure for weightlessness that is used in simulation studies on Earth (Ray et al., 2001; Morey-Holton and Globus, 2002; Ferreira et al., 2011; Trinel et al., 2013; Kok et al., 2019). The 5-ion, 6-beam simGCRsim radiation source was designed by NASA to provide a simplified radiation field that represents the type of exposure that astronauts are expected to receive from galactic cosmic rays on a Mars mission (Simonsen et al., 2020). In this study, specific behavioral outcomes were measured in response to these two types of spaceflight stressors. In the open field with both absence and presence of objects, there was a radiation × HU interaction in which the effects of radiation were modulated by the HU condition. We evaluated these effects in different body compartments, namely the plasma, hippocampus, and cerebral cortex.

The effects of radiation analyzed in the plasma of animals without HU or control HU showed that the riboflavin metabolic pathway was the most affected, while the glycerophospholipid, sphingolipid, and glutathione metabolic pathways were less affected when comparing sham irradiation vs. 0.75 Gy exposure. The dose of 0.75 Gy is directly relevant to the exposure conditions predicted for a 3-year Mars mission for a human (Hassler et al., 2014; Simonsen et al., 2020). Comparing sham irradiation vs. a higher anchor dose of 1.5 Gy of simGCRsim exposure in animals without HU or control HU, the riboflavin metabolic pathway was found to be affected, confirming the results at the lower, space-relevant dose. In addition, arginine biosynthesis, glutamine and glutamate metabolism, as well as alanine, aspartate, and glutamate metabolic pathways were affected. Riboflavin, glutamine, and arginine levels were higher in the plasma of animals irradiated with 1.5 Gy than the sham-irradiated animals. When the effects of radiation were analyzed in the plasma in animals under the control HU condition, the riboflavin metabolic pathway was found to be the most strongly affected, with the glutathione metabolic pathway being less affected. The effects of the control HU condition on the plasma of sham-irradiated animals were analyzed through comparisons with animals without HU, and the alanine, aspartate, and glutamate metabolism, riboflavin metabolism, arginine biosynthesis, as well as glutamine and glutamate metabolism were affected.

The metabolic outcomes in different regions of the brain were also considered directly to evaluate links to behavioral patterns. When the effects of 0.75 Gy irradiation exposure were analyzed

TABLE 3 Associations of specific metabolites with the behavioral measures[b].

Condition	Dose (Gy)	Compartment	Metabolite[b]	N[b]	Significant positive associations	Significant negative associations
No HU	0	Cortex	2-Hydroxy-C18-cerebroside	4	Percentage of time spent in the center of the open field during the object recognition training trial; distance moved in the object recognition training trial: distance moved in the object recognition test trial	Discrimination index for the object recognition test
No HU	0	Cortex	Lauroylcarnitine	4	Total time spent exploring the objects in the object recognition test; percentage of time spent in the center of the open field during the object recognition test trial; distance moved in the object recognition test trial; percentage of time spent in the center of the open field during the object recognition test trial	
No HU	0	Cortex	Sphingosine-1-phosphate	5	Total time spent exploring the objects in the object recognition test; percentage of time spent in the center of the open field during the object recognition test trial; distance moved in the object recognition test trial; percentage of time spent in the center of the open field in the object recognition test trial; distance moved in the object recognition test trial	
No HU	0.75	Cortex	2-Aminoethyl dihydrogen phosphate	4	Percentage of time spent in the center of the open field during the object recognition training trial; distance moved in the object recognition test trial	Total time spent exploring the objects in the object recognition test; percentage of time spent in the center of the open field in the object recognition test trial
No HU	0.75	Cortex	Hypoxanthine	4	Percentage of time spent in the center of the open field on the first day of testing	Total time spent exploring the objects in the object recognition test; percentage of time spent in the center of the open field in the object recognition test trial; distance moved in the object recognition test trial
No HU	0.75	Cortex	Phenylalanine	4	Percentage of time spent in the center of the open field on the first day of testing	Total time spent exploring the objects in the object recognition test; percentage of time spent in the center of the open field in the object recognition test trial; distance moved in the object recognition test trial
No HU	0.75	Cortex	Sphingomyelin	4	Percentage of time spent in the center of the open field during the object recognition training trial; distance moved in the open field on the second day of testing	Total time spent exploring the objects in the object recognition test; percentage of time spent in the center of the open field during the object recognition test trial

(Continued on the following page)

TABLE 3 (*Continued*) Associations of specific metabolites with the behavioral measures[b].

Condition	Dose (Gy)	Compartment	Metabolite[b]	*N*[b]	Significant positive associations	Significant negative associations
No HU	0.75	Cortex	Tryptophan	4	Percentage of time spent in the center of the open field on the first day of testing	Total time spent exploring the objects in the object recognition test; percentage of time spent in the center of the open field during the object recognition test trial; distance moved in the object recognition test trial
No HU	0.75	Cortex	Valine	4	Percentage of time spent in the center of the open field on the first day of testing	Total time spent exploring the objects in the object recognition test; percentage of time spent in the center of the open field in the object recognition test trial; distance moved in the object recognition test trial
Ndo HU	0.75	Hippocampus	Adenine	4	Discrimination index for the object recognition test	Percentage of time spent in the center of the open field in the object recognition training trial; distance moved in the object recognition training trial; distance moved in the open field on the second day of testing
No HU	1.5	Hippocampus	Sodium benzoate	5	Percentage of time spent in the open field in the object recognition training trial; distance moved in the object recognition training trial; percentage of time spent in the center of the open field on the first day of testing; distance moved in the open field on the first day of testing; distance moved in the open field on the second day of testing	
No HU	1.5	Plasma	Deoxycarnitine	4	Discrimination index for the object recognition test; percentage of time spent in the center of the open field in the object recognition test trial; distance moved in the open field on the first day of testing; distance moved in the open field on the second day of testing	
No HU	1.5	Plasma	Sphingomyelin	4	Discrimination index for the object recognition test; total time spent exploring the objects in the object recognition test; percentage of time spent in the center of the open field in the object recognition test trial; distance moved in the object recognition test trial	

(Continued on the following page)

TABLE 3 (*Continued*) Associations of specific metabolites with the behavioral measures[b].

Condition	Dose (Gy)	Compartment	Metabolite[b]	*N*[b]	Significant positive associations	Significant negative associations
Control HU	0.75	Hippocampus	Succinate/methylmalonate	4	Percentage of time spent in the center of the open field during the object recognition training trial; percentage of time spent in the open field during the object recognition test trial; distance moved in the open field on the first day of testing	
Control HU	0.75	Plasma	4-Guanidinobutanoic acid	4	Percentage of time spent in the center of the open field in the object recognition training trial; distance moved in the object recognition training trial; percentage of time spent in the center of the open field on the first day of testing; distance moved in the open field on the first day of testing	
Control HU	0.75	Plasma	5-Methylcytosine	4	Percentage of time spent in the center of the open field in the object recognition training trial; distance moved in the object recognition training trial; percentage of time spent in the center of the open field on the first day of testing; distance moved in the open field on the first day of testing	
Control HU	0.75	Plasma	Citrulline	4	Percentage of time spent in the center of the open field in the object recognition training trial; distance moved in the object recognition training trial; percentage of time spent in the center of the open field on the first day of testing; distance moved in the open field on the first day of testing	
Control HU	0.75	Plasma	Lauroylcarnitine	4	Percentage of time spent in the center of the open field in the object recognition training trial; distance moved in the object recognition training trial; percentage of time spent in the center of the open field on the first day of testing; distance moved in the open field on the first day of testing	
Control HU	0.75	Plasma	Pipecolic acid	4	Percentage of time spent in the center of the open field in the object recognition training trial; distance moved in the object recognition training trial; percentage of time spent in the center of the open field on the first day of testing; distance moved in the open field on the first day of testing	

(Continued on the following page)

TABLE 3 (*Continued*) Associations of specific metabolites with the behavioral measures[b].

Condition	Dose (Gy)	Compartment	Metabolite[b]	*N*[b]	Significant positive associations	Significant negative associations
Control HU	0.75	Plasma	Protoporphyrin	5	Percentage of time spent in the center of the open field in the object recognition training trial; percentage of time spent in the center of the open field in the object recognition test trial; distance moved in the object recognition test trial; percentage of time spent in the center of the open field on the first day of testing; distance moved in the open field on the first day of testing	
Control HU	1.5	Hippocampus	Aspartate	5		Total time spent exploring the objects in the object recognition test; percentage of time spent in the center of the open field during the object recognition training trial; percentage of time spent in the center of the open field in the object recognition test trial

[a]Metabolites that are purely positively associated with behavioral measures are indicated in green; metabolites that are purely negatively associated with behavioral measures are indicated in red; metabolites that are both positively and negatively associated with behavioral measures are indicated in blue.
[b]N indicates the number of significant associations.

TABLE 4 Metabolites shown to be correlated with behavioral measures in our previous photon-irradiated animals[a] that were also found to be associated with the behavioral measures in the present study.

Non-HU/HU	Dose (Gy)	Metabolite[a]	N[b]	Significant positive associations	Significant negative associations
No HU	0	Succinate	7	Ratio of time spent in the open arms in the elevated plus maze; percentage of time spent in the center of the open field in the object recognition test trial; distance moved in the object recognition test trial; total time spent exploring the objects in the object recognition test; percentage of time spent in the center of the open field on the first day of testing; percentage of time spent in the center of the open field on the second day of testing	
No HU	8	5-Methylcytosine	5	Percentage of M&M consumed on days 2 and 3 compared to day 1; percentage of time spent in the center of the open field in the object recognition test trial; discrimination index for the object recognition test; distance moved in the object recognition test trial; total time spent exploring the objects in the object recognition test	

[a]Plasma metabolites positively associated with behavioral measures are indicated in green.
[b]N indicates the number of significant associations.

in the hippocampus of animals under the control HU condition, the glutamine and glutamate metabolic pathway was found to be affected. In the sham-irradiated animals, the effects of the control HU condition on the hippocampus were analyzed through comparisons with those without HU, which showed that the phenylalanine, tyrosine, and tryptophan pathway was the most affected, followed by the riboflavin metabolic pathway. When the effects of 0.75 Gy irradiation exposure were analyzed in the cerebral cortex of animals under the control HU condition, the glutamine and glutamate metabolic pathway was affected similar to that in the hippocampus, while animals without the control HU condition showed changes in the riboflavin pathway. For the sham-irradiated

TABLE 5 Associations of specific metabolites with the behavioral measures[b].

Condition	Dose (Gy)	Compartment	Metabolite[b]	N[b]	Significant positive associations	Significant negative associations
No HU	0	Hippocampus	N(pai)-methyl-l-histidine	6		Total time spent exploring the objects in the training trial; total time spent exploring the objects in the test trial; distance moved in the object recognition training trial; distance moved in the object recognition test trial; distance moved in the open field on the first day of testing; distance moved in the open field on the second day of testing
No HU	0	Hippocampus	Phenylalanine	4	Total time spent exploring the objects in the test trial; distance moved in the object recognition test trial; distance moved in the open field on the second day of testing	Percentage immobility in the forced swim test
No HU	0	Hippocampus	Tryptophan	4	Total time spent exploring the objects in the test trial; distance moved in the object recognition test trial; distance moved in the open field on the second day of testing	Percentage immobility in the forced swim test
No HU	0	Plasma	4-Acetamidobutanoate	4	Total time spent exploring the objects in the test trial; distance moved in the object recognition training trial; distance moved in the open field on the second day of testing	Percentage immobility in the forced swim test
No HU	0	Plasma	N-Acetyl-L-phenylalanine	4	Total time spent exploring the objects in the test trial; distance moved in the object recognition test trial; distance moved in the open field on the first day of testing; distance moved in the open field on the second day of testing	
No HU	1.5	Cortex	3-Methylhistamine	4	Total time spent exploring the objects in the habituation trial; distance moved in the habituation trial; distance moved in the open field on the second day of testing; percentage of time spent in the center of the open field on the second day of testing	
No HU	1.5	Cortex	Cytidine	5	Total time spent exploring the objects in the acquisition trial; total time spent exploring the objects in the training trial; distance moved in the object recognition training trial; distance moved in the open field on the first day of testing; distance moved in the open field on the second day of testing	

(Continued on the following page)

TABLE 5 (*Continued*) Associations of specific metabolites with the behavioral measures[b].

Condition	Dose (Gy)	Compartment	Metabolite[b]	N[b]	Significant positive associations	Significant negative associations
No HU	1.5	Cortex	Elaidic acid	4	Percentage of time spent in the center of the open field during the object recognition acquisition trial; percentage of time spent in the center of the open field in the object recognition training trial; distance moved in the object recognition acquisition trial; distance moved in the object recognition training trial	
No HU	1.5	Cortex	Heptadecanoate	4	Total time spent exploring the objects in the acquisition trial; total time spent exploring the objects in the training trial; distance moved in the object recognition training trial; distance moved in the open field on the second day of testing	
No HU	1.5	Cortex	Histamine	5	Total time spent exploring the objects in the acquisition trial; total time spent exploring the objects in the training trial; distance moved in the object recognition acquisition trial; distance moved in the object recognition training trial; distance moved in the object recognition test trial; distance moved in the open field on the second day of testing	
No HU	1.5	Cortex	Inosine	5	Total time spent exploring the objects in the acquisition trial; total time spent exploring the objects in the training trial; distance moved in the object recognition acquisition trial; distance moved in the object recognition training trial; distance moved in the object recognition test trial; distance moved in the open field on the first day of testing; distance moved in the open field on the second day of testing	
No HU	1.5	Cortex	Kynurenine	4	Total time spent exploring the objects in the training trial; Percentage of time spent in the center of the open field in the object recognition training trial; total distance in the object recognition acquisition trial; distance moved in the open field on the first day of testing	
No HU	1.5	Cortex	Myristic acid	4	Total time spent exploring the objects in the object recognition training trial; distance moved in the object recognition acquisition trial; distance moved in the object recognition training trial; distance moved in the open field on the second day of testing	

(Continued on the following page)

TABLE 5 (*Continued*) Associations of specific metabolites with the behavioral measures[b].

Condition	Dose (Gy)	Compartment	Metabolite[b]	N[b]	Significant positive associations	Significant negative associations
No HU	1.5	Cortex	Palmitate	5	Total time spent exploring the objects in the training trial; time spent in the center of the open field in the object recognition training trial; distance moved in the object recognition acquisition trial; percentage of time spent in the center of the open field on the second day of testing; distance moved in the open field on the second day of testing	
No HU	1.5	Cortex	Palmitoleic acid	4	Total time spent exploring the objects in the object recognition acquisition trial; total time spent exploring the objects in the object recognition training trial; distance moved in the object recognition acquisition trial; distance moved in the object recognition training trial	
No HU	1.5	Cortex	Pantothenic acid	5	Total time spent exploring the objects in the object recognition acquisition trial; total time spent exploring the objects in the object recognition training trial; distance moved in the object recognition acquisition trial; distance moved in the open field on the first day of testing; distance moved in the open field on the second day of testing	
No HU	1.5	Hippocampus	Fructose-1,6-biphosphate	4	Total time spent exploring the objects in the object recognition acquisition trial; total time spent exploring the objects in the object recognition training trial; percentage of time spent exploring the novel object in the object recognition test trial; percentage of time spent in the center of the open field on the first day of testing	
Npo HU	1.5	Plasma	Carnitine	4	Total time spent exploring the objects in the test trial; percentage of time spent exploring the familiar object in the object recognition test trial	Total time spent exploring the objects in the object recognition acquisition trial; percentage of time spent in the center of the open field in the object recognition acquisition trial
No HU	1.5	Plasma	Carnosine	4	Time spent exploring objects in the object recognition test trial; percentage of time spent exploring the familiar object in the object recognition test trial; percentage immobility in the forced swim test	Distance moved in the object recognition acquisition trial
No HU	1.5	Plasma	Elaidic acid	4	Distance moved in the object recognition training trial; distance moved in the object recognition test trial; distance moved in the open field on the second day of testing	Percentage immobility in the forced swim test

(Continued on the following page)

TABLE 5 (*Continued*) Associations of specific metabolites with the behavioral measures[b].

Condition	Dose (Gy)	Compartment	Metabolite[b]	N[b]	Significant positive associations	Significant negative associations
No HU	1.5	Plasma	Glucosamine	4	Percentage of time spent in the open field on the second day of testing; percentage of time spent in the center of the open field in the object recognition test trial; distance moved in the object recognition acquisition trial; distance moved in the object recognition test trial	
No HU	1.5	Plasma	Glucose	4	Percentage of time spent in the center of the open field on the second day of testing; distance moved in the open field on the second day of testing; distance moved in the object recognition acquisition trial; distance moved in the object recognition test trial	
Ndo HU	1.5	Plasma	Methyl-indole-3-acetate	5	Percentage of time spent in the center of the open field on the second day of testing; distance moved in the open field on the second day of testing; total time spent exploring the objects in the object recognition training trial; distance moved in the object recognition acquisition trial; distance moved in the object recognition test trial	
No HU	1.5	Plasma	Myristic acid	4	Percentage of time spent in the center of the open field during the object recognition test trial; distance moved in the object recognition acquisition trial; distance moved in the object recognition test trial	Percentage immobility in the forced swim test
No HU	1.5	Plasma	Nonanoate	4	Distance moved in the object recognition acquisition trial; distance moved in the object recognition test trial; distance moved in the open field on the second day of testing	Percentage immobility in the forced swim test
No HU	1.5	Plasma	Palmitate	4	Percentage of time spent in the center of the open field in the object recognition test trial; distance moved in the open field in the object recognition acquisition trial; distance moved in the object recognition test trial	Percentage immobility in the forced swim test
No HU	1.5	Plasma	Palmitoleic acid	4	Percentage of time spent in the center of the open field in the object recognition test trial; distance moved in the open field in the object recognition acquisition trial; distance moved in the object recognition test trial	Percentage immobility in the forced swim test

(Continued on the following page)

TABLE 5 (*Continued*) Associations of specific metabolites with the behavioral measures[b].

Condition	Dose (Gy)	Compartment	Metabolite[b]	N[b]	Significant positive associations	Significant negative associations
No HU	1.5	Plasma	Sphinganine	5	Percentage of time spent in the center of the open field on the second day of testing; distance moved in the open field on the second day of testing; total time spent exploring the objects in the object recognition training trial; distance moved in the object recognition acquisition trial; distance moved in the object recognition test trial	
HU	0	Cortex	Phospho(enol)pyruvic acid	4	Discrimination index for the object recognition test trial; percentage of time spent in the center of the open field in the object recognition training trial; percentage of time spent in the center of the open field in the object recognition test trial; percentage of time spent in the center of the open field on the second day of testing	
HU	0	Cortex	Spermine	5	Percentage of time spent in the center of the open field on the second day of testing; distance moved in the open field on the second day of testing; percentage of time spent in the center of the open field in the object recognition training trial	Percentage of time spent in the center of the open field on the first day of testing; percentage of time spent exploring the familiar object in the object recognition test trial
HU	0	Plasma	Betaine	4	Percentage of time spent in the center of the open field on the first day of testing; percentage of time spent exploring the novel object in the object recognition test trial	Distance moved in the open field on the first day of testing; distance moved in the open field in object recognition training trial
HU	0	Plasma	Gluconic acid	4	Percentage of time spent exploring the familiar object in the object recognition test trial	Percentage of time spent in the center of the open field on the second day of testing; discrimination index for the object recognition test trial; percentage of time spent in the center of the open field in the object recognition test trial
HU	0	Plasma	N-Acetyl-L-methionine	4	Distance moved in the open field during the first day of testing; distance moved in the object recognition acquisition trial	Percentage of time spent in the center of the open field on the first day of testing; discrimination index for the object recognition test trial
HU	1.5	Cortex	Guanosine 5′-diphosphate	4		Percentage of time spent in the center of the open field on the second day of testing; percentage of time spent in the center of the open field in the object recognition acquisition trial; percentage of time spent in the center of the open field in the object recognition training trial; percentage of time spent in the center of the open field in the object recognition test trial

(Continued on the following page)

10.3389/fphys.2024.1486767

TABLE 5 (*Continued*) Associations of specific metabolites with the behavioral measures[b].

Condition	Dose (Gy)	Compartment	Metabolite[b]	N[b]	Significant positive associations	Significant negative associations
HU	1.5	Cortex	Maleic acid	4		Percentage of time spent in the center of the open field on the second day of testing; total time spent exploring the objects in the object recognition acquisition trial; percentage of time spent in the center of the open field in the object recognition test trial; percentage of time exploring the familiar object in the object recognition test trial
HU	1.5	Plasma	Alanine	4		Distance moved in the open field on the first day of testing; distance moved in the open field on the second day of testing; distance moved in the object recognition acquisition trial; distance moved in the object recognition test trial
HU	1.5	Plasma	Gluconic acid	5	Percentage immobility in the forced swim test	Distance moved in the open field on the first day of testing; distance moved in the open field on the second day of testing; distance moved in the object recognition acquisition trial; distance moved in the object recognition training trial
HU	1.5	Plasma	Hippurate	4		Distance moved in the open field on the first day of testing; distance moved in the object recognition acquisition trial; distance moved in the open field in the object recognition training trial; distance moved in the open field in the object recognition test trial
HU	1.5	Plasma	Proline	4		Distance moved in the open field on the second day of testing; distance moved in the object recognition acquisition trial; distance moved in the open field in the object recognition training trial; distance moved in the open field in the object recognition test trial
HU	1.5	Plasma	Trigonelline	4		Distance moved in the open field on the first day of testing; distance moved in the open field in the object recognition acquisition trial; distance moved in the open field in the object recognition training trial; percentage of time spent in the center of the open field in the object recognition test trial

[a]Metabolites that are purely positively associated with behavioral measures are indicated in green; metabolites that are purely negatively associated with behavioral measures are indicated in red; metabolites that are both positively and negatively associated with behavioral measures are indicated in blue.
[b]N indicates the number of significant associations.

animals, the effects of the control HU condition on the cortex were analyzed through comparisons with those without HU, which revealed that the riboflavin metabolic pathway was affected. In the 0.75-Gy-irradiated animals, the glutamine and glutamate metabolic pathway was affected, while the riboflavin metabolic pathway was affected in the 1.5-Gy-irradiated animals. The distinctly affected pathways between the control HU 0.75-Gy- vs. 1.5-Gy-irradiated animals may be related to their differential effects on the behavioral

TABLE 6 Metabolites shown to be correlated with behavioral measures in our previous simGCRsim-irradiated WAG/Rij animals[a] that were also found to be associated with the behavioral measures in the present study.

Condition	Dose (Gy)	Compartment	Metabolite[b]	N[c]	Significant positive associations	Significant negative associations
No HU	0	Hippocampus	Phenylalanine	4	Total time spent exploring the objects in the test trial; distance moved in the object recognition test trial; distance moved in the open field on the second day of testing	Percentage immobility in the forced swim test
No HU	0	Hippocampus	Tryptophan	4	Total time spent exploring the objects in the test trial; distance moved in the object recognition test trial; distance moved in the open field on the second day of testing	Percentage immobility in the forced swim test
No HU	1.5	Plasma	Carnitine	4	Total time spent exploring the objects in the test trial; percentage of time spent exploring the familiar object in the object recognition test trial	Total time spent exploring the objects in the object recognition acquisition trial; percentage of time spent in the center of the open field in the object recognition acquisition trial

[a]The experimental design of the WAG/Rij rat study was slightly different from that of the current study on Fischer rats. In the WAG/Rij study, only a single radiation dose (1.5 Gy) was used while the current study involved two radiation doses (0.75 and 1.5 Gy). In the WAG/Rij rat study, three trials were performed with objects in the object recognition test, namely, an acquisition trial, a training trial, and a test trial; however, the current study included only the training and test trials. In the WAG/Rij rat study, depressive-like behaviors were assessed through the forced swim test, which was not included in the current study.
[b]Metabolites that were both positively and negatively associated with behavioral measures are indicated in blue.
[c]N indicates the number of significant associations.

performances in the open field in the absence and presence of objects.

The levels of 4/5-oxo-proline were higher in animals with HU than those without HU; 4-hydroxyproline (which when oxidized becomes oxo-proline) is formed by prolylhydroxylase (with vitamin C as the cofactor) in procollagen tissues. If the mature, crosslinked collagen breaks down, then 4-hydroxyproline is released. The higher levels of 4/5-oxo-proline in HU animals may reflect the collagen breakdown in the hippocampus linked to neuronal injury (Wareham et al., 2024). Although we noted both 4- and 5-oxo-proline in our library, we cannot distinguish between them and have therefore denoted it as 4/5-oxo-proline.

A total of 21 plasma metabolites were correlated with the behavioral measures, of which twelve associations were purely positive and one association was purely negative; furthermore, eight metabolites were both positively and negatively associated with the behavioral measures. The integrated analysis indicates that the plasma and brain biomarkers associated with behavioral and cognitive performance are dependent on the environmental conditions experienced (i.e., HU, control HU or simulated space radiation).

We were especially interested in the interactions between simGCRsim exposure and each of the HU conditions. Our new data show that the groupings of both the phenylalanine, tyrosine, and tryptophan metabolism as well as phenylalanine metabolism and biosynthesis exhibit very strong pathway changes after simGCRsim irradiation and in the control HU condition. Remarkably, the phenylalanine, tyrosine, and tryptophan metabolic pathway was also the most affected by simulated space radiation and HU in the plasma, hippocampus, and cortex of WAG/Rij rats (Raber et al., 2021) and by photon irradiation in Fischer rats (Raber et al., 2024). In addition, the phenylalanine and tryptophan levels were associated with better behavioral measures in both WAG/Rij and Fischer rats. Higher phenylalanine and tryptophan levels in the cortexes of Fischer rats without HU exposed to 0.75 Gy of radiation were associated with reduced measures of anxiety in the open field. Higher phenylalanine and tryptophan levels in the hippocampi of sham-irradiated WAG/Rij rats without HU were associated with reduced depressive-like behaviors in the forced swim test. Tryptophan and tyrosine play executive functional roles (Aquili, 2020) and were earlier shown to be negatively affected by X-ray irradiation (Davis et al., 2014; Hienz et al., 2008; Tang et al., 2022). Tryptophan is the precursor of serotonin, and elevated dietary tryptophan levels were shown to suppress post-stress plasma glucocorticoid levels in another study (Hoglund et al., 2019).

HU had detrimental effects on activity and freezing levels in the open field as well as on the measures of anxiety in the elevated plus maze. These findings are consistent with the reported detrimental effects of simulated microgravity on three-dimensional visuospatial tuning and orientation in mice (Oman, 2007). Additionally, phenylalanine and tyrosine (found to be elevated by HU) are precursors of norepinephrine (Fernstrom and Fernstrom, 2007); elevated norepinephrine levels are indicators of stress (Koob, 1999) and may have contributed to the anxiety-like behaviors observed in HU rats. In the present study, sham-irradiated mature male Fischer rats under HU showed spatial habituation learning in the open field and moved less on day 2 than day 1. In contrast, sham-irradiated male WAG/Rij rats of a similar age under

HU showed impaired spatial habituation learning (Raber et al., 2021). These data suggest that Fischer rats may be less susceptible to HU than WAG/Rij rats.

Two metabolites were found to be associated with the behavioral measures between the current simGCRsim and earlier photon studies with mature male Fischer rats (Raber et al., 2024), namely succinate and 5-methylcytosine. Succinate levels in the hippocampus in the present study and in the plasma in the previous study (Table 4) were positively correlated with the activity levels and reduced anxiety-like behaviors (time spent in the center of the open field without and with objects). Owing to COVID-19-related travel restrictions when vaccines were not available, we were unable to travel to the Medical College of Wisconsin to euthanize and dissect the brains of the rats. We recognize that correlations with the behavioral measures involved the same metabolites in distinct compartments between the two studies; consistent with these results, succinate feeding enhanced the endurance exercise capacities of mice (Xu et al., 2022) while succinic acid administration had anxiolytic effects in the mice (Gang et al., 2009). The second metabolite was 5-methylcytosine, whose presence in the plasma suggests that there was modification and degradation of the DNA. Consistent with this notion, the positive correlation between plasma 5-methylcytosine and increased activity levels as well as reduced measures of anxiety were noted in the control HU mice exposed to 0.75 Gy of radiation in the present study, along with increased activity levels and cognitive performance in the object recognition test in rats exposed to 8 Gy of photons in the absence of HU in the previous study (Table 4). These results are consistent with the simulated space irradiation-induced alterations in hippocampal DNA methylation reported in mice (Impey et al., 2016a, 2016b, 2017, 2023; Torres et al., 2019). These results indicate that 5-methylcytosine may specifically be a good plasma biomarker of behavioral and cognitive performances following irradiation.

Lauroylcarnitine is important for energy metabolism to convert fat into energy, and increased lauroylcarnitine levels have been shown to slow disease progression in various cognitive and behavioral conditions like schizophrenia (Zhao et al., 2023), Alzheimer's disease (Kepka et al., 2020), autism spectrum disorders (Kepka et al., 2021), traumatic brain injury (Sharma et al., 2024), and liver cirrhosis (Li and Zhao, 2021). Consistent with these patterns, there were positive correlations between the cortical levels of lauroylcarnitine and behavioral performance in the sham-irradiated animals without HU for the object recognition test. Lauroylcarnitine is also known to improve exercise performance (Mielgo-Ayuso et al., 2021; Vecchio et al., 2021); accordingly, plasma lauroylcarnitine levels were positively correlated with enhanced activity and reduced anxiety levels in the control HU animals exposed to 0.75 Gy of radiation.

The level of sphingosine-1-phosphate generated by degradation of ceramides is higher in the brain than any other organ and lower in the cortex than the spinal cord, brainstem, or cerebellum (Jiang and Han, 2006). Sphingosine-1-phosphate has been reported to have both neuroprotective and neurotoxic effects that are hypothesized to depend on the amount and subcellular site of generation. For example, sphingosine-1-phosphate modulates calcium homeostasis, synaptic transmission, epigenetic regulation, and integrity of the blood–brain barrier such that reduced levels are noted in schizophrenia, while the release of sphingosine-1-phosphate from astrocytes has been reported to impair autophagy (Xiao et al., 2023), be proinflammatory [please see van Echten-Deckert (2023) for a review], and play a role in the development and progress of Parkinson's disease (Wang et al., 2023). Consistent with the role of sphingosine-1-phosphate in synaptic transmission, its cortical levels were positively correlated with the behavioral measures in the object recognition test in the sham-irradiated animals without HU.

In an earlier work, exogenous administration of sodium benzoate was shown to increase the measures of anxiety and impair the activity levels, exploratory behaviors, and memory in rats (Asejeje et al., 2022). In contradistinction to the findings in rats, sodium benzoate has been shown to improve cognition in women with dementia (Lin et al., 2021). In the current study, hippocampal levels of sodium benzoate in rats exposed to 1.5 Gy of radiation without HU were positively correlated with activity and reduced anxiety levels in the open field without and with objects. These results suggest that following an environmental challenge like simulated space irradiation or a severe neurological condition, increased levels of sodium benzoate may be beneficial for behavioral performance. However, it is also conceivable that the beneficial effects of sodium benzoate are evident only at lower doses than those typically used in pharmacological studies.

A combination of metabolic activators (nicotinamide riboside, N-acetyl-L-cysteine, and L-carnitine tartrate) has been shown to improve cognition in patients with Alzheimer's disease; this cognitive improvement was also associated with increased plasma levels of deoxycarnitine (Yulug et al., 2023). Consistent with this finding, the plasma deoxycarnitine levels in male Fischer rats exposed to 1.5 Gy of radiation without HU in this study were positively correlated with activity levels in the open field and cognitive performance in the object recognition test.

In earlier work by other researchers, the level of sphingomyelin 18:0 in the hippocampus was associated with better cognitive performance in the Y maze and object recognition test (Kalinichenko et al., 2022). Consistent with this finding, the plasma sphingomyelin levels in animals exposed to 1.5 Gy of radiation without HU in the present study were positively correlated with activity levels and cognitive performance in the object recognition test.

Supplementation with citrulline, a byproduct of NOS-mediated conversion of arginine to nitric oxide, has been shown to enhance athletic performance (Gentilin et al., 2022), prevent age-related decline in long-term potentiation (Ginguay et al., 2019), and improve cognitive performance in animal models of neurological conditions (Martinez-Gonzalez et al., 2021; Yabuki et al., 2013). Consistent with these results, the plasma citrulline levels were positively correlated with increased activity and reduced anxiety levels in the control HU animals exposed to 0.75 Gy of radiation. Citrulline appears to reflect NO synthesis, which increases during activity and may be related to greater blood flow in muscles.

Lauroylcarnitine has been shown to improve exercise performance (Mielgo-Ayuso et al., 2021; Vecchio et al., 2021). Consistent with this result, the plasma lauroylcarnitine levels that are potentially markers of beta oxidation of fatty acids were positively correlated with enhanced activity and reduced anxiety levels in the control HU animals exposed to 0.75 Gy of radiation.

In contrast to the positive associations of plasma deoxycarnitine and cortical lauroylcarnitine levels with the behavioral measures in

Fischer rats in the present study, higher levels of carnitine in the plasma of WAG/Rij rats exposed to 1.5 Gy of radiation without HU were positively associated with the total time spent exploring objects and percentage of time exploring the familiar object in the object recognition test trial but negatively associated with the total time spent exploring the objects in the object recognition acquisition trial. Deoxycarnitine is a direct precursor of carnitine and is involved with tissue exchange with carnitine (Sartorelli et al., 1989). These data suggest that the beneficial effects of the carnitine pathway may be dependent on the genetic background and/or dose-dependent.

Serum levels of pipecolic acid were found to be decreased and anxiety levels increased in patients with active ulcerative colitis (Yuan et al., 2021). Consistent with this result, the plasma pipecolic acid levels were positively correlated with enhanced activity and reduced anxiety levels in the control HU animals exposed to 0.75 Gy of radiation.

In the present study, the plasma and brain tissue samples were analyzed 9 months after sham irradiation or total body irradiation in the absence or presence of HU and 7 months after the behavioral and cognitive performance evaluations. Together with our earlier study on mature male WAG/Rij rats following simulated space radiation in the absence and presence of HU, the metabolic pathways affected by HU and to a lesser extent by photon irradiation as well as the relationships between the behavioral measures and individual metabolite levels in plasma support the feasibility of developing stable long-term biomarkers of the responses to HU as well as behavioral and cognitive performance.

In summary, the detrimental effects of HU on behavioral and cognitive performance as well as metabolic pathways in plasma illustrate the importance of developing mitigators to reduce the effects of microgravity and space radiation on the brain functions of astronauts during and after space missions. The integrated analysis in this study indicates that plasma and brain biomarkers associated with behavioral and cognitive performance are dependent on the environmental conditions experienced (i.e., HU, control HU, or simulated space radiation). The metabolomics data of the current study on Fischer rats and previous study on WAG/Rij rats suggest that it may be possible to develop stable plasma biomarkers of HU, simulated space radiation, as well as behavioral and cognitive performances that could be used to develop and test such mitigators. Phenylalanine, tyrosine, and tryptophan metabolism as well as the metabolites phenylalanine and tryptophan in plasma are especially good candidates for mitigation to consider for spaceflights as these were found in both the Fischer and WAG/Rij rats exposed to simGCRsim and/or HU.

Data availability statement

The original contributions presented in the study are included in the article/Supplementary Material; further inquiries can be directed to the corresponding author.

Ethics statement

The animal study was approved by the institutional animal care and use committees (IACUCs) of the Medical College of Wisconsin (MCW) as well as Brookhaven National Laboratory (BNL). The study was conducted in accordance with all local legislations and institutional requirements.

Author contributions

JR: conceptualization, formal analysis, funding acquisition, investigation, methodology, project administration, resources, supervision, visualization, writing–original draft, and writing–review and editing. MC: formal analysis, investigation, visualization, and writing–review and editing. AT: formal analysis and writing–review and editing. SH: formal analysis, investigation, visualization, and writing–review and editing. KK: formal analysis and writing–review and editing. BG: formal analysis, investigation, and writing–review and editing. ML: investigation and writing–review and editing. SL: investigation and writing–review and editing. AB: investigation and writing–review and editing. AK: investigation and writing–review and editing. CP: investigation and writing–original draft. AK: investigation and writing–review and editing. CO: formal analysis, investigation, and writing–review and editing. JW: investigation and writing–review and editing. JM: investigation and writing–review and editing. JC: formal analysis, investigation, and writing–review and editing. JS: formal analysis, investigation, supervision, and writing–review and editing. GB: formal analysis, methodology, and writing–review and editing. JM: formal analysis, methodology, and writing–review and editing. JB: conceptualization, funding acquisition, resources, supervision, and writing–review and editing.

Funding

The authors declare that financial support was received for the research, authorship, and/or publication of this article. This study was supported by NASA (80NSSC19K0498–P00001) and partially by the R21 grant (AG079158). LC-MS/MS instrumentation used in this study was funded by NIH grant S10RR027878.

Acknowledgments

The authors thank the members of the BNL physics team led by A. Rusek and biology support team led by P. Guida and M.A. Petry for support with the experiments conducted at BNL.

Conflict of interest

The authors declare that the research was conducted in the absence of any commercial or financial relationships that could be construed as a potential conflict of interest.

The author(s) declared that they were an editorial board member of Frontiers, at the time of submission. This

had no impact on the peer review process and the final decision.

Publisher's note

Supplementary material

The Supplementary Material for this article can be found online at: https://www.frontiersin.org/articles/10.3389/fphys.2024.1486767/full#supplementary-material

References

Aguilar, B., Malkova, L., N'Gouemo, P., and Forcelli, P. (2018). Genetically epilepsy-prone rats display anxiety-like behaviors and neuropsychiatric comorbidities of epilepsy. *Front. Neurol.* 9, 476. doi:10.3389/fneur.2018.00476

Aquili, L. (2020). The role of tryptophan and tyrosine in executive function and reward processing. *Int. J. Tryptophan Res.* 13, 1178646920964825–13. doi:10.1177/1178646920964825

Asejeje, F. O., Ajayi, B. O., Abiola, M. A., Samuel, O., Asejeje, G. I., Ajiboye, E. O., et al. (2022). Sodium benzoate induces neurobehavioral deficits and brain oxido-inflammatory stress in male Wistar rats: ameliorative role of ascorbic acid. *J. Biochem. Mol. Toxicol.* 36, e23010. doi:10.1002/jbt.23010

Baker, J. E., Fish, B. L., Su, J., Haworth, S. T., Strande, J. L., Komorowski, R. A., et al. (2009). 10 Gy total body irradiation increases risk of coronary sclerosis, degeneration of heart structure and function in a rat model. *Int. J. Radiat. Biol.* 85, 1089–1100. doi:10.3109/09553000903264473

Braby, L. A., et al. (2019) "Radiation exposures in space and the potential for central nervous system effects (phase II)," in *Ncrp SC 1-24P2 report*.

Davis, C., Roma, P. G., Armour, E., Gooden, V. L., Brady, J. V., Weed, M. R., et al. (2014). Effects of X-ray radiation on complex visual discrimination learning and social recognition memory in rats. *PLOSOne* 9, e104393. doi:10.1371/journal.pone.0104393

Fernstrom, J., and Fernstrom, M. (2007). Tyrosine, phenylalanine, and catecholamine synthesis and function in the brain. *J. Nutr.* 137, 1539S-1547S; discussion 1548S–1547S. doi:10.1093/jn/137.6.1539S

Ferreira, J., Crissey, J., and Brown, M. (2011). An alternant method to the traditional NASA hindlimb unloading model in mice. *JoVe* e2467, 2467. doi:10.3791/2467

Gang, L., Bien-Ly, N., Andrews-Zwilling, Y., Xu, Q., Bernardo, A., Ring, K., et al. (2009). GABAergic interneuron dysfunction impairs hippocampal neurogenesis in adult apolipoprotein E4 knockin mice. *Cell Stem Cell* 5, 634–645. doi:10.1016/j.stem.2009.10.015

Gentilin, A., Zanini, P., Cevese, A., Schena, F., and Tarperi, C. (2022). Ergogenic effects of citrulline supplementation on exercise performance and physiological indexes of exercise performance during cycling tests: a review. *Sci. Sports* 37, 665–674. doi:10.1016/j.scispo.2021.12.011

Ginguay, A., Regazzetti, A., Laprevote, O., Moinard, C., De Bandt, J. P., Cynober, L., et al. (2019). Citrulline prevents age-related LTP decline in old rats. *Sci. Rep.* 9, 20138. doi:10.1038/s41598-019-56598-2

Hassler, D., Zeitlin, C., Wimmer-Schweingruber, R. F., Ehresmann, B., Rafkin, S., Eigenbrode, J. L., et al. (2014). Mars' surface radiation environment measured with the Mars Science Laboratory's Curiosity rover. *Science* 343, 1244797. doi:10.1126/science.1244797

Hienz, R., Brady, J., Gooden, V., Vazquez, M., and Weed, M. (2008). Neurobehavioral effects of head-only gamma-radiation exposure in rats. *Radiat. Res.* 170, 292–298. doi:10.1667/RR1222.1

Hoglund, E., Overli, O., and Winberg, S. (2019). Tryptophan metabolic pathways and brain serotonergic activity: a comparative review. *Front. Endocrinol. (Lausanne)* 10, 158. doi:10.3389/fendo.2019.00158

Impey, S., Pelz, C., Riparip, L. K., Tafessu, A., Fareh, F., Zuloaga, D. G., et al. (2023). Postsynaptic density radiation signature following space irradiation. *Front. Physiol.* 14, 1215535. doi:10.3389/fphys.2023.1215535

Impey, S., Jopson, T., Pelz, C., Tafessu, A., Fareh, F., Zuloaga, D., et al. (2016a). Short- and long-term effects of 56Fe irradiation on cognition and hippocampal DNA methylation and gene expression. *BMC Genomics* 17, 825. doi:10.1186/s12864-016-3110-7

Impey, S., Jopson, T., Pelz, C., Tafessu, A., Fareh, F., Zuloaga, D., et al. (2017). Bi-directional and shared epigenomic signatures following proton and 56Fe irradiation. *Sci. Rep.* 7, 10227. doi:10.1038/s41598-017-09191-4

Impey, S., Pelz, C., Tafessu, A., Marzulla, T., Turker, M. S., and Raber, J. (2016b). Proton irradiation induces persistent and tissue-specific DNA methylation changes in the left ventricle and hippocampus. *BMC genomics* 17, 273. doi:10.1186/s12864-016-2581-x

Jiang, X., and Han, X. (2006). Characterization and direct quantitation of sphingoid base-1-phosphates from lipid extracts: a shotgun lipidomics approach. *J. Lipid Res.* 47, 1865–1873. doi:10.1194/jlr.D600012-JLR200

Kalinichenko, L., Gulbins, E., Kornhuber, J., and Muller, C. (2022). Sphingolipid control of cognitive functions in health and disease. *Prog. Lipid Res.* 86, 101162. doi:10.1016/j.plipres.2022.101162

Kepka, A., Ochocinska, A., Chojnowska, S., Borzym-Kluczyk, M., Skorupa, E., Knaś, M., et al. (2021). Potential role of L-carnitine in autism spectrum disorder. *J. Clin. Med.* 10, 1202. doi:10.3390/jcm10061202

Kepka, A., Ochocinska, A., Borzym-Kluczyk, M., Skorupa, E., Stasiewicz-Jarocka, B., Chojnowska, S., et al. (2020). Preventive role of L-carnitine and balanced diet in Alzheimer's disease. *Nutrients* 12, 1987. doi:10.3390/nu12071987

Kirkwood, J. S., Maier, C. S., and Stevens, J. F. (2013). Simultaneous, untargeted metabolic profiling of polar and non-polar metabolites by LC-Q-TOF mass spectrometry. *Curr. Prot. Toxicol.* 4 (4), Unit4.39. doi:10.1002/0471140856.tx0439s56

Kok, A., Moore, J. E., Rosas, S., Kerr, B. A., Andrews, R. N., Nguyen, C. M., et al. (2019). Knee and hip joint cartilage damage from combined spaceflight hazards of low-dose radiation less than 1 Gy and prolonged hindlimb unloading. *Radiat. Res.* 191, 497–506. doi:10.1667/RR15216.1

Koob, G. F. (1999). Corticotropin-releasing factor, norepinephrine, and stress. *Biol. Psychiatry* 46, 1167–1180. doi:10.1016/s0006-3223(99)00164-x

Krause, A., Speacht, T., Zhang, Y., Lang, C., and Donahue, H. (2017). Simulated space radiation sensitizes bone but not muscle to the catabolic effects of mechanical unloading. *PLOSOne* 12, e0182403. doi:10.1371/journal.pone.0182403

Li, N., and Zhao, H. (2021). Role of carnitine in non-alcoholic fatty liver disease and other related diseases: an update. *Front. Med.* 8, 3389. doi:10.3389/fmed.2021.689042

Lin, C.-H., Chen, P.-K., Wang, S.-H., and Lane, H. Y. (2021). Effect of sodium benzoate on cognitive function among patients with behavioral and psychological symptoms of dementia: secondary analysis of a randomized clinical trial. *JAMA Netw. open* 4, e216156. doi:10.1001/jamanetworkopen.2021.6156

Martinez-Gonzalez, K., Serrano-Cuevas, L., Almeida-Gutiérrez, E., Flores-Chavez, S., Mejía-Aranguré, J. M., and Garcia-delaTorre, P. (2021). Citrulline supplementation improves spatial memory in a murine model for Alzheimer's disease. *Nutr. Burbank, Los Angel. Cty. Calif.* 90, 111248. doi:10.1016/j.nut.2021.111248

Mielgo-Ayuso, J., Pietrantonio, L., Viribay, A., Calleja-González, J., González-Bernal, J., and Fernández-Lázaro, D. (2021). Effect of acute and chronic oral l-carnitine supplementation on exercise performance based on the exercise intensity: a systematic review. *Nutrients* 13, 4359. doi:10.3390/nu13124359

Moreno-Villanueva, M., Wong, M., Lu, T., Zhang, Y., and Wu, H. (2017). Interplay of space radiation and microgravity in DNA damage and DNA damage response. *npj Microgravity* 3, 14. doi:10.1038/s41526-017-0019-7

Morey-Holton, E., and Globus, R. (2002). Hindlimb unloading rodent model: technical aspects. *J. Appl. Physiol.* 92, 1367–1377. doi:10.1152/japplphysiol.00969.2001

Oman, C. (2007) "Spatial orientation and navigation in microgravity. Spatial processing in navigation," in *Imagery percept*, 209–247.

Patel, S. (2020). The effects of microgravity and space radiation on cardiovascular health: from low-Earth orbit and beyond. *Int. J. Cardiol. Heart Vasc.* 30, 100595. doi:10.1016/j.ijcha.2020.100595

Raber, J., Bongers, G., LeFevour, A., Buttini, M., and Mucke, L. (2002). Androgens protect against apolipoprotein E4-induced cognitive deficits. *J. Neurosci.* 22, 5204–5209. doi:10.1523/JNEUROSCI.22-12-05204.2002

Raber, J., Holden, S., Kessler, K., Glaeser, B., McQuesten, C., Chaudhari, M., et al. (2024). Effects of photon irradiation in the presence and absence of hindlimb unloading on the behavioral performance and metabolic pathways in the plasma of Fischer rats. *Front. Physiol.* 14, 1316186. doi:10.3389/fphys.2023.1316186

Raber, J., Holden, S., Sudhakar, R., Hall, R., Glaeser, B., Lenarczyk, M., et al. (2021). Effects of 5-ion beam irradiation and hindlimb unloading on metabolic pathways in plasma and brain of behaviorally tested WAG/rij rats. *Front. Physiol.* 12, 746509. doi:10.3389/fphys.2021.746509

Ray, C., Vasques, M., Miller, T., Wilkerson, M., and Delp, M. (2001). Effect of short-term microgravity and long-termhindlimb unloading on rat cardiac mass and function. *J. Appl. Physiol.* 91, 1207–1213. doi:10.1152/jappl.2001.91.3.1207

Sarkar, P., Sarkar, S., Ramesh, V., Hayes, B. E., Thomas, R. L., Wilson, B. L., et al. (2006). Proteomic analysis of mice hippocampus in simulated microgravity environment. *J. proteome Res.* 5, 548–553. doi:10.1021/pr050274r

Sartorelli, L., Mantovani, G., and Ciman, M. (1989). Carnitine and deoxycarnitine concentration in rat tissues and urine after their administration. *Biochimica biophysica acta* 1006, 15–18. doi:10.1016/0005-2760(89)90317-2

Sharma, B., Schmidt, L., Nguyen, C., Kiernan, S., Dexter-Meldrum, J., Kuschner, Z., et al. (2024). The effect of L-carnitine on critical illnesses such as traumatic brain injury (TBI), acute kidney injury (AKI), and hyperammonemia (HA). *Metabolites* 14, 363. doi:10.3390/metabo14070363

Simonsen, L., Slaba, T., Guida, P., and Rusek, A. (2020). NASA's first ground-based Galactic Cosmic Ray Simulator: enabling a new era in space radiobiology research. *PLoS Biol.* 18, e3000669. doi:10.1371/journal.pbio.3000669

Tang, T., Zawaski, J. A., Kesler, S., Beamish, C. A., Inoue, T., Perez, E. C., et al. (2022). Cognitive and imaging differences after proton and photon whole brain irradiation in a preclinical model. *Int. J. Radiat. Oncol. Biol. Phys.* 112, 554–564. doi:10.1016/j.ijrobp.2021.09.005

Torres, E. R. S., Hall, R., Bobe, G., Choi, J., Impey, S., Pelz, C., et al. (2019). Integrated metabolomics-DNA methylation analysis reveals significant long-term tissue-dependent directional alterations in aminoacyl-tRNA biosynthesis in the left ventricle of the heart and Hippocampus following proton irradiation. *Front. Mol. Biosci.* 6, 77. doi:10.3389/fmolb.2019.00077

Trinel, D., Pickuet, F., Batside, B., and Canu, M. (2013). Dendritic spine remodeling induced by hindlimb unloading in adult rat sensorimotor cortex. *Beh Brain Res.* 249, 1–7. doi:10.1016/j.bbr.2013.04.015

van Echten-Deckert, G. (2023). The role of sphingosine 1-phosphate metabolism in brain health and disease. *Pharmacol. Ther.* 244, 108381. doi:10.1016/j.pharmthera.2023.108381

Vecchio, M., Chiaramonte, R., Testa, G., and Pavone, V. (2021). Clinical effects of L-carnitine supplementation on physical performance in healthy subjects, the key to success in rehabilitation: a systematic review and meta-analysis from the rehabilitation point of view. *J. Funct. Morphol. Kinesiol* 6, 93. doi:10.3390/jfmk6040093

Wang, W., Zhao, Y., and Zhu, G. (2023). The role of sphingosine-1-phosphate in the development and progression of Parkinson's disease. *Front. Cell Neurosci.* 17, 1288437. doi:10.3389/fncel.2023.1288437

Wareham, L., Baratta, R., Del Buono, B., Schlumpf, E., and Calkins, D. (2024). Collagen in the central nervous system: contributions to neurodegeneration and promise as a therapeutic target. *Mol. Neurodegen* 19, 11. doi:10.1186/s13024-024-00704-0

Wiley, J., Kwok, A. T., Moore, J. E., Payne, V., Lindburg, C. A., Balk, S. A., et al. (2016). Spaceflight-relevant challenges of radiation and/or reduced weight bearing cause arthritic responses in knee articular cartilage. *Radiat. Res.* 186, 333–344. doi:10.1667/RR14400.1

Xia, J., and Wishart, D. (2010). MetPA: a web-based metabolomics tool for pathway analysis and visualization. *Bioinformatics* 26, 2342–2344. doi:10.1093/bioinformatics/btq418

Xiao, S., Peng, K. P., Li, C., Long, Y., and Yu, Q. (2023). The role of sphingosine-1-phosphate in autophagy and related disorders. *Cell Death Discov.* 9, 380. doi:10.1038/s41420-023-01681-x

Xu, G., Yuan, Y., Luo, P., Yang, J., Zhou, J., Zhu, C., et al. (2022). Acute succinate administration increases oxidative phosphorylation and skeletal muscle explosive strength via SUCNR1. *Front. Vet. Sci.* 8, 808863. doi:10.3389/fvets.2021.808863

Yabuki, Y., Shioda, N., Yamamoto, Y., Shigano, M., Kumagai, K., Morita, M., et al. (2013). Oral l-Citrulline administration improves memory deficits following transient brain ischemia through cerebrovascular protection. *Brain Res.* 1520, 157–167. doi:10.1016/j.brainres.2013.05.011

Yatagai, F., Honma, M., Dohmae, N., and Ishioka, N. (2019). Biological effects of space environmental factors: a possible interaction between space radiation and microgravity. *Life Sci. Space Res.* 20, 113–123. doi:10.1016/j.lssr.2018.10.004

Yuan, X., Chen, B., Duan, Z., Xia, Z., Ding, Y., Chen, T., et al. (2021). Depression and anxiety in patients with active ulcerative colitis: crosstalk of gut microbiota, metabolomics and proteomics. *Gut Microbes* 13, 1987779. doi:10.1080/19490976.2021.1987779

Yulug, B., Altay, O., Li, X., Hanoglu, L., Cankaya, S., Lam, S., et al. (2023). Combined metabolic activators improve cognitive functions in Alzheimer's disease patients: a randomised, double-blinded, placebo-controlled phase-II trial. *Transl. Neurodegener.* 12, 4. 10.1186/s40035-023-00336-2.

Zhao, L., Liu, H., Wang, W., Wang, Y., Xiu, M., and Li, S. (2023). Carnitine metabolites and cognitive improvement in patients with schizophrenia treated with olanzapine: a prospective longitudinal study. *Front. Pharmacol.* 14, 1255501. doi:10.3389/fphar.2023.1255501

frontiers | Frontiers in Physiology

TYPE Original Research
PUBLISHED 28 November 2024
DOI 10.3389/fphys.2024.1482860

OPEN ACCESS

EDITED BY
FR Tang,
National University of Singapore, Singapore

REVIEWED BY
Jörn Rittweger,
German Aerospace Center (DLR), Germany
Satoshi Iwase,
Aichi Medical University, Japan

*CORRESPONDENCE
P. Arbeille,
arbeille@med.univ-tours.fr

RECEIVED 18 August 2024
ACCEPTED 08 November 2024
PUBLISHED 28 November 2024

CITATION
Arbeille P, Zuj K and Guillon L (2024) Exercise combined with artificial gravity and exercise only countermeasures prevent organ and blood vessel morpholgical changes induced by 55 days HDT bedrest.
Front. Physiol. 15:1482860.
doi: 10.3389/fphys.2024.1482860

Exercise combined with artificial gravity and exercise only countermeasures prevent organ and blood vessel morpholgical changes induced by 55 days HDT bedrest

P. Arbeille*, K. Zuj and L. Guillon

UMPS-CERCOM (Unit Med Physiol Spatiale) Faculte de Medicine Universite de Tours, Tours, France

Background: Changes in blood vessel properties have been identified with confinement, spaceflight, bedrest, and dry immersion. Subsequently, it was suspected that other organs may also be affected in these extreme environments. The purposes of the current study were to determine the effects of head-down bedrest (HDT) on cardiovascular and organ measurements made using ultrasound imaging similar to that currently available on the International Space Station, and to evaluate the efficacy of two different countermeasure protocols in preventing any observed changes in the ultrasound measurements with HDT.

Methods: Ultrasound measures were conducted on 24 individuals (3 groups of 8) pre HDT and on day 55 of the HDT. The control group (C°) remained in passive HDT for the 55 days, the C1 group performed aerobic exercise daily (EX), and the C2 group practiced aerobic exercise under artificial gravity conditions (EX-AG). Fifteen parameters were measured on 10 different organs and blood vessels including the right common carotid artery, abdominal aorta, right tibial artery, left ventricle, right jugular vein, portal vein, right kidney, cervical and lumbar vertebra, and the vastus intermedius muscle.

Results: HDT resulted in changes for many of the parameters investigated. Observed changes in carotid IMT and distensibility, cardiac ejection fraction, portal vein diameter, and vastus intermedius muscle thickness were attenuated with EX and EX-AG, with EX-AG having a greater effect than exercise alone on measures of carotid distensibility.

Conclusion: Results from this study indicate changes in many structures assessed with ultrasound imaging after 55 days of HDT bedrest with some changes being attenuated with the two investigated countermeasure protocols.

KEYWORDS

bedrest, echography, organ and vessel imaging, countermeasure, exercise

Introduction

Cardiovascular adaptations to real and simulated microgravity have been well documented. Common carotid artery wall thickness has been found to increase with reductions in distensibility after 6 months spaceflight, prolonged confinement, and dry immersion in approximately 75% of the subjects (Arbeille et al., 2001; Arbeille et al., 2014; Arbeille et al., 2015; Hughson et al., 2016; Arbeille et al., 2017a; Yuan et al., 2019). These changes have been associated with alterations in common carotid artery wall properties evaluated through the processing of the ultrasound frequency signal (Arbeille et al., 2021b). Additionally, jugular vein and portal vein size have also been found to increase with similar exposure to real and simulated microgravity (Arbeille et al., 2001; Arbeille et al., 2014; Marshall-Goebel et al., 2018; Marshall-Goebel et al., 2019; Arbeille et al., 2021a; Patterson et al., 2023). While it is believed that the cardiovascular adaptations primarily result from the fluid shifts associated with microgravity exposure, other factors, such as induced confinement physical and mental stress, or absence of physical activity may also contribute to the observed adaptations.

Physiological changes have also been noted in other anatomical regions. Ultrasound assessments during spaceflight have revealed abnormal vertebral disc shape (herniation) and muscle atrophy with these changing being confirmed postflight using MRI (Belavy et al., 2016; Bailey et al., 2017; Garcia et al., 2017; Harrison et al., 2018). However, limited work has been done to investigate potential changes in organ structure with real and simulated microgravity exposure. As ultrasound is currently the only diagnostic imaging modality aboard the International Space Station (ISS), the current study used ultrasound to investigate vascular and organ structures suspected to be affected by bedrest in alignment with a similar series of ultrasound assessments currently used on the ISS (CIPHER).

The current study was designed to investigate both the effects of 55 days of 6° head-down tilt bedrest (HDT) on blood vessel and organ structures and to evaluate the efficacy of two countermeasure protocols, aerobic exercise alone (EX), and aerobic exercise combined with artificial gravity exposure (EX-AG), in reducing or preventing any inappropriate changes induced by HDT. It was hypothesized that 55 days of HDT would affect most of the blood vessels and organs investigated. It was also hypothesized that both countermeasures would attenuate the effects of bedrest and that exercise with artificial gravity exposure would show a greater protective effect than exercise alone.

Research design and methods

Subjects

Data were collected from 24 males who participated in the 6° HDT bedrest "BRACE" experiment. Participants had a mean age of 29.4 ± 5.6 years, height of 176 ± 6.4 cm, and body mass index of 23.88 ± 1.83 kg/cm^2. All study protocols and procedures were in accordance with the Declaration of Helsinki and were approved by the local research ethics committee, CPP Ile de France VI on 12/19/2022. Decision Favorable- Authorization ANSM on 11/01/2023 - N° ID-RCB: 2022-A02074-39. Each participant gave written informed consent before participating in the study.

Experimental protocol

Participants were assigned to one of three experimental conditions before completing 55 days of continuous, 6° HDT bedrest. The control group (C°; n = 8) completed the bedrest without any countermeasures. Participants in the exercise countermeasure group (EX; C1; n = 8) used a supine cycle ergometer to perform daily aerobic exercise during HDT. The program was similar to that used on the ISS where participants started at 40% of VO_2max for 5 minutes followed by 2-min intervals at 65%, 70%, 80%, 70%, and 65% VO_2max each separated by 2 minutes of cycling at 40% VO_2max and ended with 3 min of cycling at 40% VO_2max.

The third group (EX-AG; C2, n = 8) completed aerobic exercise with artificial gravity exposure. Artificial gravity (AG) was generated with a 2.8 m radius human centrifuge where participants remained supine with their head towards the centre of the centrifuge. The applied level of AG was determined for each participant based on their respective cardiovascular orthostatic threshold (OT) and the AG level for presyncope (PS). Threshold values were determined at the start of the study using an AG tolerance centrifuge run. This run started with 10 min of centrifugation at 0.6 Gz acceleration (at heart level) followed by 0.1 Gz increases every 3 minutes until participants experienced presyncopal symptoms or monitoring of blood pressure, heart rate, and cardiac output showed marked reductions indicating the onset of presyncope.

During the bed rests period, C2 participants (EX-AG) completed the same cycling protocol as the C1 group (EX), but with the application of AG. Participants started peddling with AG applied at 0.15 Gz less than the individual's OT threshold with AG increased by 0.15 Gz every 4 minutes, synchronized with the cycling intervals. AG was only increased up to 70% of the participants tolerance level (0.7(PS - OT) + OT) and was decreased by 0.15 Gz every 4 minutes until the cycling protocol was completed.

Measurements

Ultrasound assessments were performed during the 1-week ambulatory period before the start of HDT bedrest and on day 55 of the bedrest. The device used was the CNES Sonoscanner echograph (Paris, France) equipped with motorized probes (superficial 17 MHz, abdominal 3.5 MHz, cardiac/transcranial 1.5 MHz) for 2D echography, volume acquisition, 3D reconstruction, RF modality (radio frequency), and speckle tracking post processing (Arbeille et al., 2018). This device is the ground model of the echograph presently in use onboard the ISS.

The following 10 organs and blood vessels were investigated: right carotid artery, right jugular vein, tibial artery, left ventricle, portal vein, aorta, cervical and lumbar vertebrae, right kidney, and the right vastus intermedius thigh muscle. For these 10 structures, 15 parameters were determined: carotid intima media thickness [CC IMT (mm)], carotid distensibility index [CC DI = (systolic diameter–diastolic diameter)/diastolic diameter], carotid blood flow (Qcc = vessel cross sectional area*mean blood velocity; ml/min), carotid vascular resistance index [CC RI = (systolic velocity–diastolic velocity)/systolic velocity], tibial artery vascular resistance index (RI tib = Negative end systolic velocity/peak systolic velocity), jugular vein volume [JV vol (cm^3)], portal vein diameter

[PV (mm)], aorta diam [Ao (mm)], left ventricle stoke volume [SV (cm^3)], ejection fraction [EF = (systolic volume–diastolic volume)/diastolic volume], left ventricle myocardium posterior wall thickness [PW (mm)], anterior cervical intervertebral distance [C Vert (mm)], anterior lumbar intervertebral distance [L Vert (mm)], right kidney area [Kid A = long axis distance × short axis distance (mm^2)], and vastus Intermedius thigh muscle thickness [VI thick (mm)]. These measurements were chosen as they have previously been investigated during the Deep Time experiment (Arbeille et al., 2023), dry immersion (Greaves et al., 2021), and the current NASA CIPHER routine ultrasound program. In addition to these measurements, all organs and vessels assessed were examined qualitatively for detection of possible structural abnormalities.

Ultrasound assessments were performed during the 1-week ambulatory period before participants started 60 days of HDT bedrest and at day 55 of the HDT. All ultrasound assessments were performed by two trained sonographers with the participant in a relaxed, supine position. The sonographer performed 2-dimensional imaging, arterial Doppler, and cardiac time motion as well as volume captures with 3D reconstructions and RF processing of each organ. The 3D modality allowed for post analysis of the ultrasound assessments and the optimization of the 2D images for accurate parameter measurements.

Statistical analysis

To examine the effects of both exposure to HDT and differences in potential responses with the two countermeasure conditions, a two-way repeated measures analysis of variance was used with the main effects of HDT and experimental group (SigmaPlot 12.5, Systat Software Inc., San Jose, CA). The statistical software performed tests for both normality (Shaprio-Wilk test) and equal variance (Levene Median test) with all assessed variables passing both tests before further assessment. In the case of significant main effects or a significant interaction between HDT and experimental condition, Tukey *post hoc* testing was performed to determine significance of pairwise comparisons. Differences in responses to HDT between the control condition and the two countermeasure conditions were further assessed using a one-way analysis of variance to test for differences in the percent change with HDT. In the case of significant main effects, Tukey *post hoc* testing was again used to test all pairwise comparisons. For all tests, significance was set at $p < 0.05$ without correction for multiple comparisons. All data is reported as mean ± standard deviation.

Results

Ultrasound images for assessment were successfully obtained from each participant. Examples of 2D images used for assessment are presented in Figure 1. Qualitative evaluation of each of the structures investigated found no changes indicative of pathology development with 55 days of HDT bedrest. Quantitative measurements of the structures investigated with individual and mean responses are presented in Figures 2–4. Percent changes with HDT for each experimental condition and each variable assessed are presented in Table 1.

Assessments of the common carotid artery found significant HDT by group interactions for intima media thickness (Figure 2A; $p < 0.001$), and the distensibility index (DI) (Figure 2B; $p < 0.001$). In the control condition, CC IMT was increased with HDT ($p = 0.002$), and CC DI was decreased ($p < 0.001$). In contrast, CC IMT was decreased with both EX ($p = 0.002$) and EX-AG ($p < 0.001$) where CC DI was not changed with EX ($p = 0.893$) and increased with EX-AG ($p < 0.001$). Assessment of the percent changes (Table 1) confirmed that there was no difference between the EX and EX-AG groups for the CC IMT response to HDT ($p = 0.98$), but there was a statistically significant difference in the DI response between the EX and EX-AG groups ($p = 0.004$). CC RI (Figure 2C) was decreased with HDT in all groups ($p = 0.007$) and common carotid artery blood flow (Figure 2D) was not changed with HDT.

A significant group by HDT interaction was found for ejection fraction (Figure 3A; $p < 0.001$) where EF was decreased in the control group ($p < 0.001$) but not changed with EX ($p = 0.235$) or EX-AG ($p = 0.208$). Assessment of the percent changes in EF (Table 1) found that responses in both countermeasure groups were different from the control condition ($p = 0.014$ and $p = 0.003$ for EX and EX-AG respectively) but not different between each other ($p = 0.715$). Left ventricle Posterior wall thickness was decreased with HDT (Figure 3B; $p = 0.045$) with no effect of experimental group. Cardiac stroke volume (Table 1) and abdominal aorta diameter (Figure 3C) were not changed with HDT.

Tibial vascular resistance (Figure 3D) decreased ($p < 0.001$) and jugular vein volume (Figure 3E) increased ($p = 0.005$) in all three groups with HDT. A significant group by HDT interaction was found for portal vein diameter (Figure 3F; $p = 0.019$) were PV diameter increased in the control group ($p = 0.006$) but was not changed with EX ($p = 0.235$) or EX-AG ($p = 0.208$). Assessment of the precent changes in PV diameter (Table 1) found a difference between the control condition and EX-AG ($p = 0.013$), but not between EX and the control condition ($p = 0.291$) or EX and EX-AG ($p = 0.266$).

Quantitative assessments of non-cardiovascular structures found an increase in kidney long axis area (Figure 4C; $p = 0.008$) with HDT. Cervical intervertebral distance was also increased with HDT (Figure 4A; $p = 0.005$) but not affected by C1 (EX) or C2 (Ex-AG) countermeasures. Conversely lumbar intervertebral distance (Figure 4B) was not changed in any of the three groups. Vastus intermedius thickness measured on a transverse view of the thigh (Figure 4D) showed a significant group by HDT interaction effect ($p > 0.001$) with thickness decreasing in the control group ($p < 0.001$), not changing in C1 (EX $p = 0.119$), and increasing in C2 (EX-AG $p = 0.002$) after HDT. Assessment of percent change with HDT (Table 1) found that the VI response was different between EX and the control group ($p = 0.002$) and EX-AG and the control group ($p < 0.001$) but not between EX and EX-AG ($p = 0.177$).

Discussion

The primary objective of this experiment was to quantify the effects of 55 days of HDT bedrest on vascular and organ structures assessed using ultrasound imaging and evaluate the efficacy of two countermeasures; aerobic exercise (EX), like that already used by astronauts in space, and exercise with artificial gravity exposure

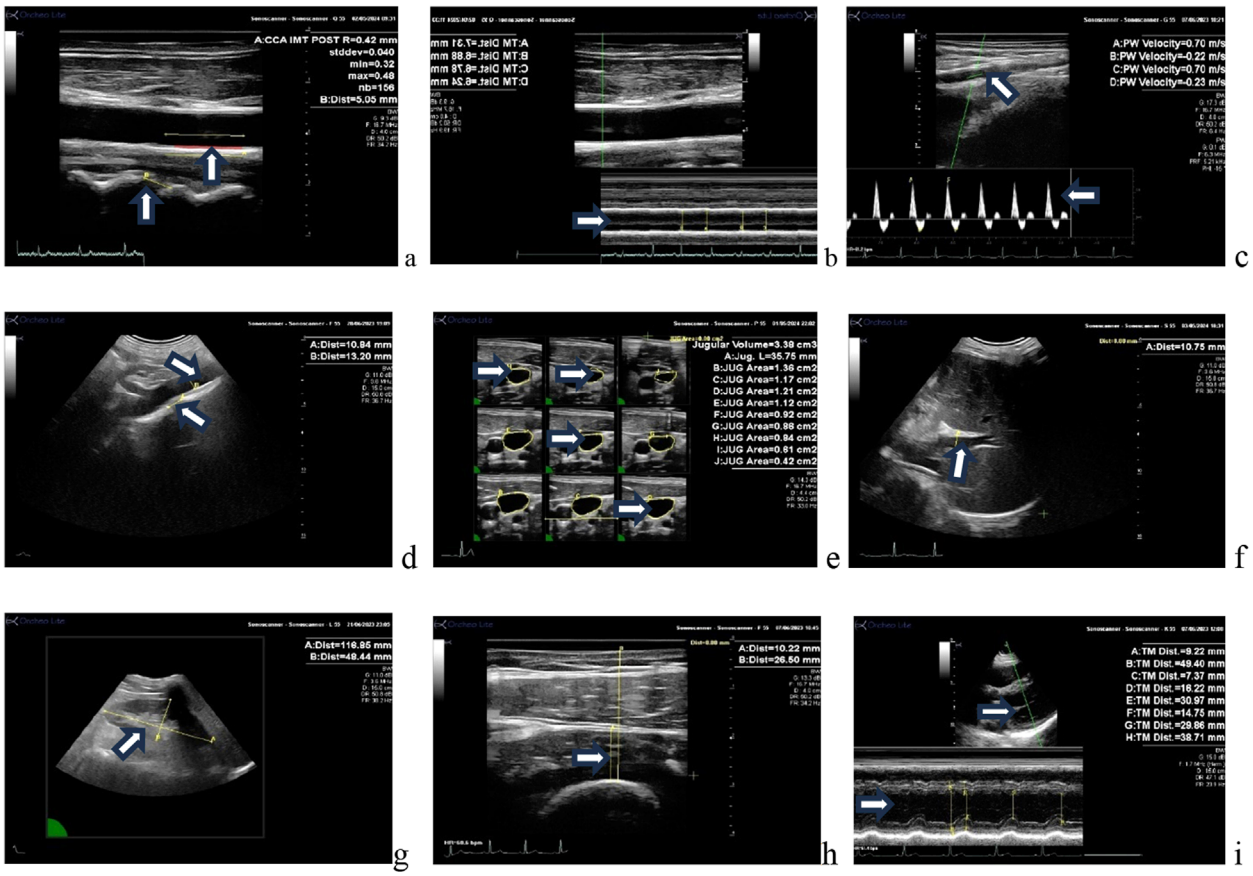

FIGURE 1
Ultrasound images of various vessels/organs assessed in this study. **(A)** Longitudinal view of the common carotid artery intima media thickness and cervical intervertebral distance, **(B)** carotid anterior and posterior wall time motion trace (systolic and diastolic diameter), **(C)** tibial artery image and Doppler velocity (lower limb vascular resistance). **(D)** Abdominal aorta diameter and lumbar intervertebral distance; **(E)** jugular vein volume (3D display); **(F)** portal vein diameter, **(G)** right kidney long axis area; **(H)** vastus intermedius thigh muscle thickness; **(I)** left ventricle parasternal long axis (volume, stroke volume posterior wall thickness).

(EX-AG) which has not been tested yet during spaceflight. Past ground-based and spaceflight experiments using ultrasound assessments have identified several unexpected changes in vascular parameters including altered carotid artery wall and jugular vein properties. As these alterations were identified incidentally, it is possible that other organs and blood vessels might also be affected by spaceflight or conditions associated with spaceflight analogue studies. Therefore, the current bedrest study investigated a large number of organs and blood vessels accessible to ultrasound imaging to provide greater understanding of the effects of HDT on the entire body. Additionally, this study looked at the effects of two different countermeasure protocols on potential vascular and organ structure changes with HDT.

Only ultrasound imaging was used in the present study as it is currently the only imaging modality available during spaceflight. This allows for direct comparisons to be made between response to HDT and spaceflight to both understand similarities and differences between adaptations to both conditions and the potential benefit of various countermeasure protocols. Other imaging methods (CT Scan MRI, PQct) were used during the current bedrest study by other experimental groups and will be available in the future for comparison with ultrasound data according to a data sharing agreement.

In the present HDT study, a set of 10 organs and blood vessels were successfully investigated by ultrasound following a similar protocol to that used during a 40-day isolation experiment (Arbeille et al., 2023), dry immersion experiment (Arbeille et al., 2017b), and the program presently running onboard the International Space Station (Routine ultrasound CIPHER program). The effect of HDT was clearly identified as well as the effect of each of the two countermeasures. The main new findings of the study were that HDT resulted in adaptations that altered ultrasound measurements in more vascular and non-vascular structures than have previously been reported, and that the exercise and exercise artificial gravity had a protective effect on some of the parameters assessed. For some measures of carotid artery distensibility and portal vein diameter, exercise with artificial gravity exposure completely negated the HDT effect possibly due to artificial gravity counteracting the microgravity induced fluid shift contributing to the maintenance of vascular structure.

The common carotid artery intima media thickness (IMT) was slightly but significantly increased in the control participants

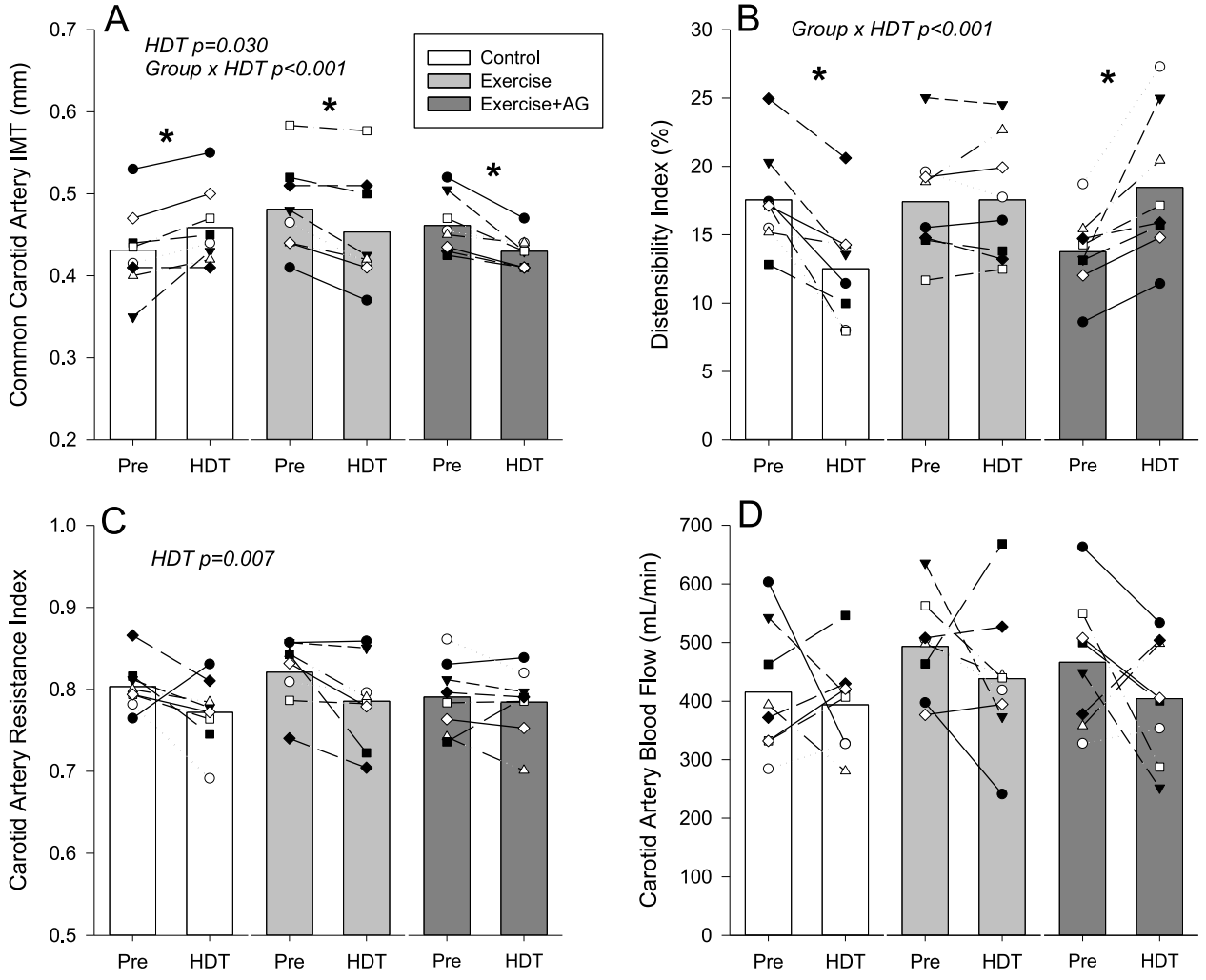

FIGURE 2
Mean (bars) and individual cardiovascular ultrasound measurements of common carotid artery IMT thickness **(A)**, distensibility index **(B)**, resistance index **(C)**, and quantitative blood flow **(D)** before (Pre) and after 55 days of HDT bedrest (HDT) for the control group (white bars), exercise countermeasure group (grey bars), and exercise with artificial gravity countermeasure group (dark grey bars). Significant main effects of HDT and group by HDT interactions are indicated. In the case of significant group by HDT interactions, groups that showed differences Pre to HDT are denoted by*$p < 0.05$.

consistent with the findings of increased IMT during a spaceflight (Arbeille et al., 2017a), during the simulated space exploration (Mars 500 confinement study) (Arbeille et al., 2014), and the 180 days CELSS confinement (Yuan et al., 2019). The morphological transformation of the carotid wall intima was found to be associated with alteration of the liver metabolism after a 6-month spaceflight (Hughson et al., 2016) and similar to the IMT increase observed with 20 years of aging on Earth (Hughson et al., 2016; Arbeille et al., 2017a), but the mechanisms for this change remain unclear.

In the present bedrest the increase in IMT in the control group was smaller (~6%) than in spaceflight or long-term confinement (~15%). This was potentially due to the duration of the study only being 55 days compared to 180 days of spaceflight (Arbeille et al., 2017a) or 520 days of confinement (Arbeille et al., 2014; Yuan et al., 2019). Additionally, the level of environmental stress could also contribute to the differences. Participants in the current study interacted daily with approximately 15 different people (nurses, doctors, scientists, manager and administrator…). In contrast, during spaceflight and confinement, study participants are limited to interacting only with the same five other crewmembers and were confined in a smaller space which could produce a more stressful environment resulting in greater vascular changes. The reduction in IMT thickness in both the C1, EX group and the C2, EX-AG group suggest that the exercise counteracts the adverse effect of HDT at the carotid level with the additional benefit making the carotid IMT thinner (younger) compared to pre HDT.

Along with the increase in carotid artery intima media thickness, the carotid distensibility (DI) was significantly decreased in the control group. This is consistent with previous observations during spaceflight and dry immersion (Hughson et al., 2016; Arbeille et al., 2017a; Greaves et al., 2021). That DI was reduced less in the C1, (EX) group and slightly increased in the C2, (EX-AG) subjects which suggests the protective effects of the exercise and an additional benefit of artificial gravity exposure. While decreased

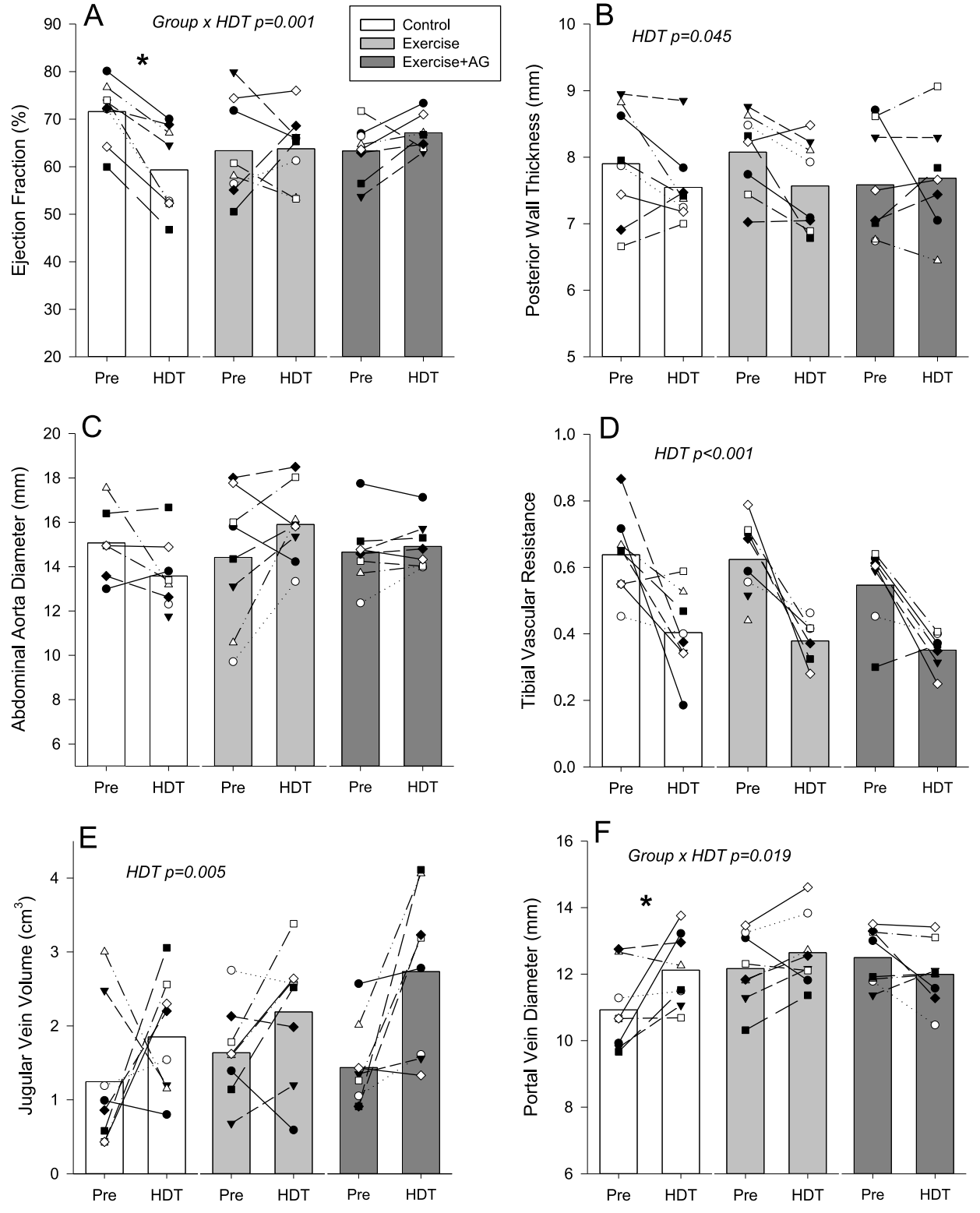

FIGURE 3
Mean (bars) and individual non-cardiovascular ultrasound measurements for cardiac ejection fraction **(A)**, posterior cardiac wall thickness **(B)**, abdominal aorta diameter **(C)**, tibial vascular resistance **(D)**, jugular vein volume **(E)**, and portal vein diameter **(F)** before (Pre) and after 55 days of HDT bedrest (HDT) for the control group (white bars), exercise countermeasure group (grey bars), and exercise with artificial gravity countermeasure group (dark grey bars). Significant main effects of HDT and group by HDT interactions are indicated. In the case of significant group by HDT interactions, groups that showed differences Pre to HDT are denoted by*$p < 0.05$.

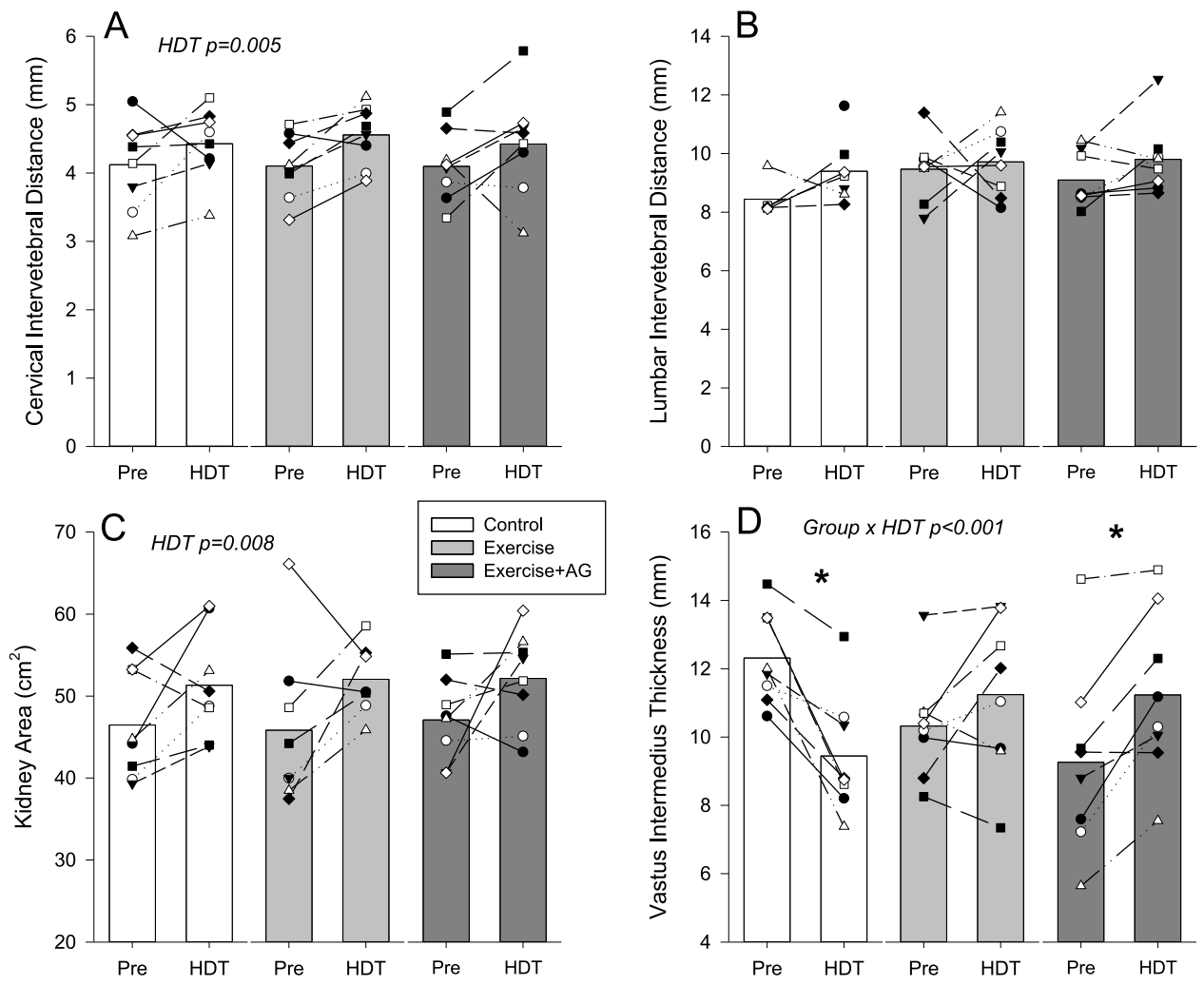

FIGURE 4
Mean (bars) and individual non-cardiovascular ultrasound measurements of cervical intervertebral distance **(A)**, lumbar intervertebral distance **(B)**, kidney area **(C)** and vastus intermedius thickness **(D)** before (Pre) and after 55 days of HDT bedrest (HDT) for the control group (white bars), exercise countermeasure group (grey bars), and exercise with artificial gravity countermeasure group (dark grey bars). Significant main effects of HDT and group by HDT interactions are indicated. In the case of significant group by HDT interactions, groups that showed differences Pre to HDT are denoted by*p < 0.05. End doc.

DI indicates a stiffer arterial wall, similar to aging, exercise alone and exercise with artificial gravity exposure contributed to maintain vessel wall properties or make the vessel more compliant (younger).

The carotid vascular resistance index (CC RI) and carotid artery blood flow (Qcc) were not altered with HDT in the current study. This is consistent with previous observations during spaceflight and spaceflight analog experiments (Arbeille et al., 2017b). The CC RI provides an indication of total downstream vascular resistance. Cerebral vascular resistance (measured on the middle cerebral artery) likely increased in relation to brain and fluid compressive effect on intracranial vessels (Roberts et al., 2017; Arbeille et al., 2017b; Arbeille et al., 2021b) as jugular vein volume was found to increase in all groups with HDT indicating a fluid shift towards the head similar to what has been previously observed with spaceflight and dry immersion (Arbeille et al., 2001; Arbeille et al., 2017b; Marshall-Goebel et al., 2018; Arbeille et al., 2021b; Greaves et al., 2022). However, vascular resistance outside the skull (measured on the external carotid) may have decreased with the presence of facial skin edema resulting in no change in the vascular resistance index measured at the level of the common carotid artery. Additionally, CC RI, Qcc, and JV vol were not affected by the countermeasures indicating that the exercise and artificial gravity countermeasures were either ineffective as alleviating fluid congestion in the neck and head or that the effects were transient.

With HDT, while cardiac stroke volume was maintained, the posterior wall thickness of the left ventricle tended to decrease in all three groups. In a previous study (Greaves et al., 2019) intensive physical activity maintained posterior wall thickness after 21 days of HDT. In contrast, it appears that the daily exercise performed in the current study was not sufficient to prevent changes in cardiac morphology with the longer duration HDT. However, ejection fraction was maintained in the countermeasures

10.3389/fphys.2024.1482860

TABLE 1 Percent change in ultrasound measurements with HDT (mean ± SD) for carotid intima media thickness (CC IMT) and distensibility index (DI), cerebrovascular resistance (CC RI), carotid flow volume (Qcc), tibial vascular resistance (Tib RI), abdominal aorta diameter (Aorta), cardiac ejection fraction (EF), left ventricle myocardium posterior wall thickness (PW), jugular vein volume (JV vol), portal vein diameter (PV). Cervical (C Vert) and lumbar (L Vert) intervertebral distance, kidney area (Kidney), and vastus intermedius muscle thickness (VI). Exercise and Exercise + AG values that are statistically different from the control condition are denoted by* ($p < 0.05$), Exercise + AG values that are statistically different from the Exercise group are denoted by # ($p < 0.05$).

Parameter	Control group	Exercise group	Exercise + AG group
CC IMT	6.79 ± 6.96	−6.04 ± 4.37*	−6.55 ± 4.22*
DI	−29.0 ± 16.4	0.81 ± 10.0*	33.9 ± 25.1*#
CC RI	−3.82 ± 5.97	−4.29 ± 4.79	−0.70 ± 3.96
Qcc	−0.11 ± 28.0	−9.71 ± 27.7	−8.83 ± 32.7
Tib RI	−33.7 ± 25.9	−42.0 ± 17.1	−30.7 ± 27.4
Aorta	−5.81 ± 11.1	14.0 ± 22.0	2.10 ± 5.57
SV	−1.52 ± 33.3	9.34 ± 32.7	20.3 ± 11.4
EF	−17.3 ± 8.34	2.38 ± 17.1*	7.50 ± 10.1*
PW	−3.94 ± 7.94	−6.18 ± 6.38	0.14 ± 9.89
JV vol	176 ± 239	42.9 ± 60.1	116 ± 129
PV	11.9 ± 14.0	4.16 ± 6.66	−3.85 ± 7.59*
C Vert	8.87 ± 15.1	11.6 ± 8.67	8.63 ± 17.8
L Vert	8.30 ± 12.7	4.40 ± 20.5	8.15 ± 12.4
Kidney	11.6 ± 15.7	14.8 ± 20.4	12.2 ± 20.3
VI	−23.1 ± 12.2	9.13 ± 18.5*	24.3 ± 17.6*

groups and decreased in the control group suggesting that the countermeasure did have a protective effect on cardiac function. These results are consistent with previous studies which have shown reductions in ejection fraction with HDT and spaceflight (Arbeille et al., 2001; Greaves et al., 2019) and protective effects of physical activity on the left ventricle function (Greaves et al., 2019; Arbeille et al., 2023).

Consistent with previous studies of spaceflight, bedrest, and dry immersion (Arbeille et al., 2015; Arbeille et al., 2017b) portal vein diameter was increased with HDT in the control group due to headward fluid shifts and blood pooling into the liver. In contrast, portal vein diameter was not increased in either of the countermeasure groups suggesting a protective effect. However, the countermeasures were not completely effective against the fluid shift effect as the right kidney area increased with HDT in all three groups.

The cervical intervertebral distance (C Vert) increased in all three groups with HDT. This is likely related to the −6° head down position that participants maintained throughout the study. During −6° HDT, gravity acts to pull the weight of the head away from the body, lengthening the cervical column. Other studies have measured cervical disc height before, during, and post spaceflight using ultrasound, but the correlation with MRI data was poor (Harrison et al., 2018). Regardless, ultrasounds assessment can still determine changes in this parameter even if the absolute values are not completely accurate (Greaves et al., 2024).

In contrast to the cervical vertebra, lumber intervertebral distance (L Vert) did not change in any of the three groups. This is also contrary to lumbar spinal changes expected to occur with spaceflight as many astronauts report back pain and have a greater risk of intervertebral disc herniation after spaceflight (Bailey et al., 2017; Bellavy et al., 2016). Additionally, ultrasound assessments have also identified spinal structural changes (herniation, desiccation, osteophytes) with spaceflight on the ISS (Garcia et al., 2017). In the current study, no abnormal structural changes in the spine were noted and the lack of changes in lumbar intervertebral distance could be due to gravity still being present throughout HDT preventing lengthening of the lumbar spine to the same extent as exposure to microgravity during spaceflight.

At the leg level, tibial vascular resistance (Tib RI) was significantly decreased in all three groups likely due to the emptying of fluid from the legs and the absence of muscular activity. The measures of vastus intermedius thigh muscle thickness (VI) confirmed the atrophy of this muscle with HDT in the control group. As the vastus intermedius contributes to maintaining upright posture in normal gravity, similar atrophy may also be present in other postural leg muscles. In contrast to the control condition, while

the countermeasures did not affect tibial vascular resistance, they did maintain VI muscle thickness in the C1, EX group and increased thickness in the C2, EX-AG group.

The systematic investigation, of 10 organs and blood vessels accessible to ultrasound in the present study showed that many systems are affected with prolonged HDT bedrest. Many of these adaptations appear to be related to inactivity and fluid shifts as the exercise and artificial gravity countermeasures were able to provide some protective effects. Additionally, a similar investigation performed during 40-day of isolation in a cavern (Arbeille et al., 2023) where participants remained active in a large habitat and did not experience fluid shifts, showed no changes at all in organs and blood vessels investigated.

Currently, the same ultrasound protocol used in this study is running onboard ISS (CIPHER Routine ultrasound program) using remote ultrasound imaging, teleoperated from the ground, to assist astronauts with minimal ultrasound experience, in obtaining images that can be used for diagnostics to determine the effects of long duration spaceflight and investigate the recovery of these parameters as astronauts return to Earth (Arbeille et al., 2023). To date, none of the changes observed, with the exception of one reported case of jugular vein thrombosis during flight (Marshall-Goebel et al., 2019), have related to pathological conditions, and the corresponding parameters recover 6 months after returning to Earth. Preliminary results from another study (VASC AGING), have indicated that vascular parameters, affected by 6 months of spaceflight, may generally recover 6 month after returning to Earth suggesting the transient nature of the observed adaptations (personal data). However, with longer duration spaceflight or HDT, it is still unknown if these parameters will recover in a similar timeline or if the observed changes will become the starting point of pathological situations such as vessel atheromatous process, vein thrombosis, organ cellular/structural change, and subsequent metabolic disorders.

Conclusion

After 55 days of continuous −6° head down bedrest, changes in ultrasound measures of cardiovascular targets were similar to those previously observed during long duration spaceflight. Additionally, the ultrasound evaluation identified HDT induced changes on non cardiovascular targets like the leg muscle atrophy, increased cervical intervertebral distance and kidney area. The exercise (EX) and artificial gravity (EX-AG) countermeasures prevented changes in some of the measured variables, but not all. Results from this study help to provide a framework for interpreting ultrasound diagnostic assessments during long duration spaceflight.

New and noteworthy

Results from this study indicate significant physiological effects of 55-day bedrest in the control subjects while the exercise alone and the exercise with artificial gravity countermeasures and maintained the parameters relatively stable.

Data availability statement

The raw data supporting the conclusions of this article will be made available by the authors, without undue reservation.

Ethics statement

The studies involving humans were approved by all study protocols and procedures were in accordance with the Declaration of Helsinki and were approved by the local research ethics committee, CPP Ile de France VI on 12/19/2022. Decision Favorable- Authorization ANSM on 11/01/2023 - N° ID-RCB: 2022-A02074-39. Each participant gave written informed consent before participating in the study. The studies were conducted in accordance with the local legislation and institutional requirements. The participants provided their written informed consent to participate in this study.

Author contributions

PA: Conceptualization, Funding acquisition, Investigation, Methodology, Supervision, Writing–original draft, Writing–review and editing, Resources, Validation. KZ: Data curation, Formal Analysis, Writing–review and editing, Funding acquisition. LG: Formal Analysis, Investigation, Writing–review and editing.

Funding

The author(s) declare that financial support was received for the research, authorship, and/or publication of this article. CNES (French space agency) Grant 2023 No. DAR: 4800001115 (to PA).

Acknowledgments

The authors would like to acknowledge the organizers and participants of the BRACE experiment, Mrs. Maryannick Gaveau-Porcher MGP (Nurse, sonographer) Mrs Roselyne Claveau RC for their contribution to the ultrasound data collection, the MEDES institute for space medicine team and the French Space Agency (CNES) for financial support.

Conflict of interest

The authors declare that the research was conducted in the absence of any commercial or financial relationships that could be construed as a potential conflict of interest.

The author(s) declared that they were an editorial board member of Frontiers, at the time of submission. This had no impact on the peer review process and the final decision.

Publisher's note

References

Arbeille, P., Avan, P., Treffel, L., Zuj, K., Normand, H., and Denise, P. (2017b). Denise Jugular and Portal Vein Volume, Middle Cerebral Vein Velocity, and Intracranial Pressure in Dry Immersion. *Aerosp. Med. Hum. Perform.* 88, 457, 462. doi:10.3357/AMHP.4762.2017

Arbeille, P., Chaput, D., Zuj, K., Depriester, A., Maillet, A., Belbis, O., et al. (2018). Remote echography between a ground control center and the international space station using a tele-operated echograph with motorized probe. *Ultrasound Med. Biol.* 44, 2406–2412. doi:10.1016/j.ultrasmedbio.2018.06.012

Arbeille, P., Fomina, G., Roumy, J., Alferova, I., Tobal, N., and Herault, S. (2001). Adaptation of the left heart, cerebral and femoral arteries, and jugular and femoral veins during short- and long-term head-down tilt and spaceflights. *Eur. J. Physiol.* 86, 157–168. doi:10.1007/s004210100473

Arbeille, P., Greaves, D., Chaput, D., Maillet, A., and Hughson, R. L. (2021a). Index of reflectivity of ultrasound radio frequency signal from the carotid artery wall increases in astronauts after a 6 mo spaceflight. *Ultrasound Med. Biol.* 47, 2213–2219. doi:10.1016/j.ultrasmedbio.2021.03.028

Arbeille, P., Provost, R., Vincent, N., and Aubert, A. (2014). Adaptation of the main peripheral artery and vein to long term confinement (MARS 500). *PLoS One* 9, e83063. doi:10.1371/journal.pone.0083063

Arbeille, P., Provost, R., and Zuj, K. (2017a). Carotid and femoral arterial wall distensibility during long-duration spaceflight. *Aerosp. Med. Hum. Perform.* 88, 924–930. doi:10.3357/AMHP.4884.2017

Arbeille, P., Provost, R., Zuj, K., and Vincent, N. (2015). Measurements of jugular, portal, femoral, and calf vein cross-sectional area for the assessment of venous blood redistribution with long duration spaceflight (Vessel Imaging Experiment). *Eur. J. Appl. Physiol.* 115, 2099–2106. doi:10.1007/s00421-015-3189-6

Arbeille, P., Zuj, K., Besnard, S., Mauvieux, B., Hingrand, C., Delaunay, P.-L., et al. (2023). Ultrasound assessments of organs and blood vessels before and after 40 days isolation in a cavern (Deep Time experiment 2021). *Front. Physiol.* 14, 1174565. doi:10.3389/fphys.2023.1174565

Arbeille, P., Zuj, K. A., Macias, B. R., Ebert, D. J., Laurie, S. S., Sargsyan, A. E., et al. (2021b). Lower body negative pressure reduces jugular and portal vein volumes and counteracts the elevation of middle cerebral vein velocity during long-duration spaceflight. *J. Appl. Physiol.* 131, 1080–1087. doi:10.1152/japplphysiol.00231.2021

Bailey, J. F., Miller, S. L., Khieu, K., O'Neill, C. W., Healey, R. M., Coughlin, D. G., et al. (2017). From the international space station to the clinic: how prolonged unloading may disrupt lumbar spine stability. *Spine J.* 18 (17). 7–14. doi:10.1016/j.spinee.2017.08.261[Epub ahead of print] PubMed PMID: 28962911 .

Belavy, D. L., Adams, M., Brisby, H., Cagnie, B., Danneels, L., Fairbank, J., et al. (2016). Disc herniations in astronauts: what causes them, and what does it tell us about herniation on earth? *Eur. Spine J.* 25, 144–154. doi:10.1007/s00586-015-3917-y

Garcia, K. M, Harrison, M. F., Sargsyan, A. E., Douglas, P. D., Scott, A., et al. (2017). Real-timeUltrasound assessment of astronaut spinal anatomy and disorders on the international space statio. *J. UltrasoundMed* 37, 987–999. doi:10.1002/jum.14438

Greaves, D., Arbeille, P., Guillon, L., Zuj, K., and Caiani, E. G. (2019). Effects of exercise countermeasure on myocardial contractility measured by 4D speckle tracking during a 21-day head-down bed rest. *Eur. J. Appl. Physiol.* 119, 2477–2486. [Epub Ahead Of Print]. doi:10.1007/S00421-019-04228-0

Greaves, D., Guillon, L., Besnard, S., Navasiolava, N., and Arbeille, P. (2021). 4 day in dry immersion reproduces partially the aging effect on the arteries as observed during 6 month spaceflight or confinement. *Npj microgravity*, Springer 7, 43. doi:10.1038/s41526-021-00172-6

Greaves, D., Petersen, L., and Arbeille, P. (2024) "Cervical intervertebral distance measured using 3D ultrasound after dry immersion and 6 Month spaceflight," in *Proceeding HRP meeting galveston*.

Harrison, M. F., Garcia, K. M., Sargsyan, A. E., Ebert, D., Riascos-Castaneda, R. F., and Dulchavsky, S. A. (2018). Preflight, in-flight, and postflight imaging of the cervical and lumbar spine in astronauts. *Aerosp. Med. Hum. Perform.* 89 (1), 32–40. doi:10.3357/AMHP.4878.2018

Hughson, R. L., Robertson, A. D., Arbeille, P., Shoemaker, J. K., Rush, J. W. E., Fraser, K. S., et al. (2016). Increased postflight carotid artery stiffness and inflight insulin resistance resulting from 6-mo spaceflight in male and female astronauts. *Am. J. Physiol. - Hear Circ. Physiol.* 310, H628–H638. doi:10.1152/ajpheart.00802.2015

Marshall-Goebel, K., Laurie, S. S., Alferova, I. V., Arbeille, P., Auñón-Chancellor, S. M., Ebert, D. J., et al. (2019). Assessment of jugular venous blood flow stasis and thrombosis during spaceflight. *JAMA Netw. open* 2, e1915011. doi:10.1001/jamanetworkopen.2019.15011

Marshall-Goebel, K., Stevens, B., Rao, C. V., Suarez, J. I., Calvillo, E., Arbeille, P., et al. (2018). Internal jugular vein volume during head-down tilt and carbon dioxide exposure in the SPACECOT study. *Aerosp. Med. Hum. Perform.* 89 (4), 351–356. doi:10.3357/AMHP.4934.2018

Patterson, C. A., Greaves, D. K., Robertson, A., Hughson, R., and Arbeille, P. (2023). Motorized 3D ultrasound and jugular vein dimension measurement on the international space station. *Aerosp. Med. Hum. Perform.* 94, 466–469. doi:10.3357/amhp.6219.2023

Roberts, D. R., Albrecht, M. H., Collins, H. R., Asemani, D., Chatterjee, A. R., Spampinato, M. V., et al. (2017). Effects of spaceflight on astronaut brain structure as indicated on MRI. *N. Engl. J. Med.* 377, 1746–1753. doi:10.1056/nejmoa1705129

Yuan, M., Custaud, M. C., Xu, Z., Wang, J., Yuan, M., Tafforin, C., et al. (2019). Multi-system adaptation to confinement during the 180-day controlled ecological life support system (CELSS) experiment. *Front. Physiology* 10, 575. doi:10.3389/fphys.2019.00575

frontiers | Frontiers in Immunology

TYPE Original Research
PUBLISHED 06 February 2025
DOI 10.3389/fimmu.2025.1538421

OPEN ACCESS

EDITED BY
Alessandro Bartoloni,
National Institute of Nuclear Physics of Rome, Italy

REVIEWED BY
Giacomo Fais,
University of Cagliari, Italy
Silvana Miranda,
Belgian Nuclear Research Centre (SCK CEN), Belgium

*CORRESPONDENCE
Brian E. Crucian
brian.crucian-1@nasa.gov

RECEIVED 02 December 2024
ACCEPTED 14 January 2025
PUBLISHED 06 February 2025

CITATION
Crucian BE, Quiriarte H, Lam C-w, Nelman M, Colorado AA, Diak DM and James JT (2025) Pulmonary and systemic immune alterations in rats exposed to airborne lunar dust. *Front. Immunol.* 16:1538421. doi: 10.3389/fimmu.2025.1538421

Pulmonary and systemic immune alterations in rats exposed to airborne lunar dust

Brian E. Crucian[1]*, Heather Quiriarte[2], Chiu-wing Lam[3], Mayra Nelman[4], Audrie A. Colorado[3], Douglass M. Diak[5] and John T. James[1]

[1]Environmental Sciences Branch, NASA Johnson Space Center, Houston, TX, United States, [2]School of Kinesiology, Louisiana State University, Baton Rouge, LA, United States, [3]Toxicology Laboratory, KBR, Inc., Houston, TX, United States, [4]Immunology/Virology Laboratory, KBR, Inc., Houston, TX, United States, [5]Immunology/Virology Laboratory, Aegis Aerospace, Inc., Houston, TX, United States

Background: Due to cosmic radiation bombardment and over 4 billion meteorite and micrometeoroid impacts on the airless Moon, the lunar surface is covered by a layer of fine, reactive dust. Very little is known regarding the toxicity of lunar dust on human physiology. This study assessed airborne lunar dust exposure in rats on localized pulmonary and systemic immune parameters.

Methods: Rats were exposed to 0 (air only), 20.8 (low), and 60.6 (high) mg/m^3 of respirable-size lunar dust for 4 weeks (6 h/day, 5 days/week). Rats were then euthanized either 1 day, 7 days, 4 weeks, or 13 weeks after the last exposure. Peripheral blood and lung lavage fluid samples were collected for analysis. Assays included leukocyte distribution by multicolor flow cytometry and electron/fluorescent microscopy to visualize cell–particulate interactions and lavage/plasma cytokine concentration. Mitogen-stimulated cytokine production profiles, as a measure of cellular function, were performed on whole blood samples only.

Results: Untreated lavage fluid was comprised primarily of pulmonary macrophages. High-dose lunar dust inhalation (60.6 mg/m^3) resulted in an influx of both neutrophils and lymphocytes. Although the percentage of lymphocytes increased, the T-cell CD4:CD8 ratio was unchanged. Cytokine analysis of the lavage fluid showed increased levels of IL-1β and TNFα. These alterations generally persisted through the 13-week sampling. Blood analysis showed few systemic immune alterations from the lunar dust inhalation. By week 4, the peripheral granulocyte percentage was elevated in the treated rats. Plasma cytokine levels were unchanged in all treated rats compared to controls; however, altered mitogen-stimulated cytokine production profiles were observed consisting of increased IL-1β and IL-6 and decreased IL-2. There were minimal adverse immune effects, in both lung or peripheral blood, following low-dose exposure to 20.8 mg/m^3 lunar dust.

Conclusion: Exposures to high concentrations of lunar dust resulted in persistent lung inflammation and some systemic immune dysregulation that did not

subside even 13 weeks after the dust exposure. This information is beneficial in deriving an exposure limit to airborne lunar dust and for spacecraft engineers considering dust mitigation systems in lunar landers or habitats.

KEYWORDS

lunar dust, spaceflight, immunology, gravity, inflammation

1 Introduction

Immune system dysregulation, consisting of altered leukocyte distribution, reduced T- and NK-cell function, and low-level inflammation, persists in astronauts for the duration of a 6-month orbital spaceflight (1–3). B-cell function and general hematologic indices appear unaltered in astronauts during spaceflight (4, 5). Suggested causal mission factors include stress, isolation, radiation, microgravity, and circadian misalignment (6). In the same astronaut crew members, elevated levels of latent herpesvirus DNA were detected in saliva, suggesting diminished immunity was associated with virus reactivation (7, 8). Astronauts do experience clinical symptoms during flight, and several case studies of ISS astronauts have been published associating stress and immune compromise with atopic dermatitis and laboratory-confirmed zoster (9–11). It has been suggested that persistent immune dysregulation may increase specific clinical risks for astronaut crew members participating in exploration-class deep space missions (12). As conditions onboard the ISS have continued to improve, and several biomedical countermeasures have been deployed to the ISS, data suggest immunological improvement in more recent crew members (13). Most of these countermeasures do not translate, as currently constituted, to deep space missions, so a specific deep space countermeasure is required (14).

Deep space exploration was recently initiated via the "Artemis" program, planning a return to the Moon to establish an extended human presence. Deployments will include long operations in lunar orbit at the "Gateway" station and landings to extensively explore and inhabit the lunar surface. During Apollo missions, lunar dust was found to pervasively adhere to crew members and lunar landing vehicles, and multiple reports stated this exposure caused notable upper respiratory symptoms in select crew members. It is reasonable to expect that crew immune system dysregulation will worsen during long-duration deep space missions as all the mission stressors will increase in magnitude, habitable volume and power will decrease, and there will be no rapid return option.

Unique surface hazards will include lunar dust as a particulate irritant or allergen. Lunar dust is a unique substance that poses a potential health hazard for lunar surface operations. Due to eons of meteorite bombardment with a complete lack of wind or water erosion, the constant high-speed micrometeoroid bombardments have fractured lunar surface material producing fine dust particles of which approximately 1% to 2% are respirable sizes (≤3 μm). This fraction of fine particles could pose an inhalation hazard to lunar explorers. Trace amounts of virtually all elements ranging from the ppb level to the ppm level can be found in lunar dust (15, 16). However, the bulk chemical composition of lunar dust varies across the lunar surface and is approximately 50% SiO_2, 15% Al_2O_3, 10% CaO, 10% MgO, 5% TiO_2, and 5%–15% iron, with lesser amounts of sodium, potassium, chromium, and zirconium. The Earth mineral quartz is a standard simulant used by the National Institutes of Health to study respiratory system toxicity as it is known to cause silicosis, and this was used as a positive control in this inhalation exposure study (17).

During exploration missions, human exposure to lunar dust, with the composition as described above, is inevitable regardless of engineering controls (16). Understanding the immune reactivity to lunar dust will provide key knowledge for researchers as we prepare to support prolonged deep space missions. Here, we report our findings in animal exposure studies using lunar dust collected from the Apollo 14 mission relating to immune cell and cytokine responses in both the pulmonary and systemic compartments. Other relevant findings from this extensive animal model study were reported separately (18).

2 Methods

2.1 Subjects

Subjects for this study were healthy Fischer 344 adult male rats, 8–10 weeks old. Animals were housed in pairs at the AAALAC-approved animal facility at the Johnson Space Center. Subjects were under a controlled environment consisting of HEPA-filtered air and a 12-h day/night cycle. There were 20 rats for each of the four inhalation exposure groups: air control, low-dose lunar dust, and high-dose lunar dust. For each group, a single day of intratracheal quartz treatment was used as a positive control for neutrophilic inflammation. The NASA Institutional Animal Care and Use Committee guidelines were followed.

2.2 Lunar dust/quartz exposure

The lunar dust samples consisted of Apollo 14 regolith that had been stored under nitrogen from collection to study initiation. Dust composition and details for this study have been previously disclosed

(19). An aerosolized fine fraction was separated using a cyclone and respirable dust was captured on a paper membrane for the inhalation study. Subjects were given a lunar dust inhalation treatment of either low (20.8 ± 2.5 mg/m^3) or high (60.8 ± 8.1 mg/m^3) exposure. Quartz used as a control particulate for this study was fine-sized crystalline silica obtained from U.S. Silica (Berkeley Springs, WV). The average size of the quartz particles used for the inhalation study was 0.4 µm. Rats were exposed to sample inhalation for 6 h per day, 5 days per week. Five rats per group were sacrificed and biosamples were collected at each of the following timepoints: +1 day (sampling the next day after exposure), +7 days, +4 weeks, or +13 weeks.

2.3 Samples

Biosamples consisted of 1.0 mL of heparin anticoagulated whole blood for immunophenotype, plasma cytokine concentrations and whole blood mitogenic stimulation, and 1.0 mL of peritoneal lavage fluid for immunophenotype and cytokine analysis. Lavage and biosample collection details are previously described (19).

2.4 Immunophenotype analysis

To determine cellular composition, flow cytometric analysis was performed on both blood and lavage samples. A multicolor flow cytometry antibody matrix was created that assessed the relevant leukocyte and lymphocyte subsets as follows: granulocytes, lymphocytes, monocytes (CD32 FITC, CD45 PE), B cells, NK cells (CD45RA FITC, CD161a PE), T-cell subsets (CD8 FITC, CD3 PE, CD4 PC5), pulmonary macrophages, dendritic cells, and activated leukocytes (CD11c FITC, CD71 PE). For blood staining, 100 µL of whole blood was then combined with 10 µL of appropriately labeled monoclonal antibodies. Staining was performed by incubating the mixture at room temperature for a minimum of 20 min. Red blood cells were then lysed using the Beckman-Coulter Optilyse reagent as described by the manufacturer, and the cells were washed in phosphate buffered saline (PBS). Lavage staining was performed in a similar fashion, by adding 100 µL of lavage fluid to 10 µL each of the antibodies. After 20 min of incubation at room temperature, the cells were washed in PBS. The stained leukocytes were then fixed in 1.0% paraformaldehyde in PBS for 10 min and analyzed on a Beckman-Coulter Gallios flow cytometer. The cytometer was configured to set the threshold for positive based on isotype control antibody staining or internal negative staining cellular populations. Pure samples of both lunar dust and quartz (the same product administered to the animal subjects) were run to ensure that particulate debris did not interfere with cellular analysis. Electronic compensation was set to eliminate interference due to spectral overlap.

2.5 Whole blood cultures

For functional analysis of mitogen-stimulated cytokine profiles, three whole blood cultures were set up by combining 150 µL of heparinized blood and 1.0 mL of RPMI media. Mitogenic stimulation consisted of 0.125 µg/mL of anti-CD3 and 0.25 µg/mL of anti-CD28 soluble antibodies (both from Beckton Dickinson, Franklin Lakes, NJ) to activate T cells only via the T-cell receptor/costimulatory complex, 10 ng/mL of phorbol-12-myristate-13-acetate (PMA) and 2 µg/mL of ionomycin (both from Sigma-Aldrich, St. Louis, MO) as a broader pharmacologic stimulus, or 20 µL of lipopolysaccharide (LPS) to activate the monocytes/macrophages. Cultures were incubated at 37°C for 48 h. Following the culture, the supernatants were removed and frozen until batch analysis.

2.6 Soluble cytokine concentration

Concentrations of cytokines were determined in the mitogen-stimulated culture supernatants, plasma, and lavage fluid. The rat Fluorokine MAP MultiAnalyte Profiling immunoassay was performed according to the manufacturer's instructions (R&D Systems, Minneapolis, MN, USA). This array simultaneously analyzes secreted IFNγ, TNFα, IL-10, IL-6, IL-4, IL-2, and IL-1β using distinct bead populations that fluoresce at different intensities along a single emission wavelength. This assay was performed in a 96-well plate and was analyzed using a Luminex 100 instrument.

2.7 Electron microscopy

Electron microscopy analysis was conducted on an XL30 FEI/Philips Environmental Scanning Electron (ESEM) microscope. The environmental mode was used for all imaging. Lung tissue samples were fixed in 2% glutaraldehyde/3% formaldehyde prepared in sterile PBS, pH 7.4, for a minimum of 1 h at room temperature and then stored at 4°C until processing. Lung lavage samples were diluted 1:1 with 4% glutaraldehyde/6% formaldehyde prepared in sterile PBS, pH 7.4, then fixed for a minimum of 1 h at room temperature, and stored at 4°C until processing. Prior to analysis, lung tissue samples were placed into 35 mm dishes (Thermo Fisher Scientific, Waltham, MA, USA), gently rinsed three times with filter sterilized Milli-Q, and then slowly dehydrated (2 changes with each %, 1 h each) with graded alcohol series to 100% ethanol. Samples were placed on double-sided carbon tape mounted on T-stubs and then dried overnight in a dry chamber prior to imaging.

Prior to analysis, lavage samples were placed into filtration units containing 0.05 µm of VmTP Isopore membrane filter (Millipore), gently rinsed three times with filter-sterilized Milli-Q, and then dehydrated with graded alcohol series to 100% ethanol. The VmTP membranes containing the cells were placed on double-sided carbon tape mounted on T-stubs and then dried overnight in a dry chamber. Samples were sputter-coated with gold-palladium prior to imaging. Samples were imaged on a Phillips/FEI Quanta 250 environmental scanning electron microscope (ESEM) with (EDX) under the environmental mode with dual imaging for both secondary (general image morphology) and backscatter modes (highlights elemental variations). Low-magnification imaging was used to acquire large area image mosaics. From these mosaics, regions of interest (ROIs) were identified for subsequent high-

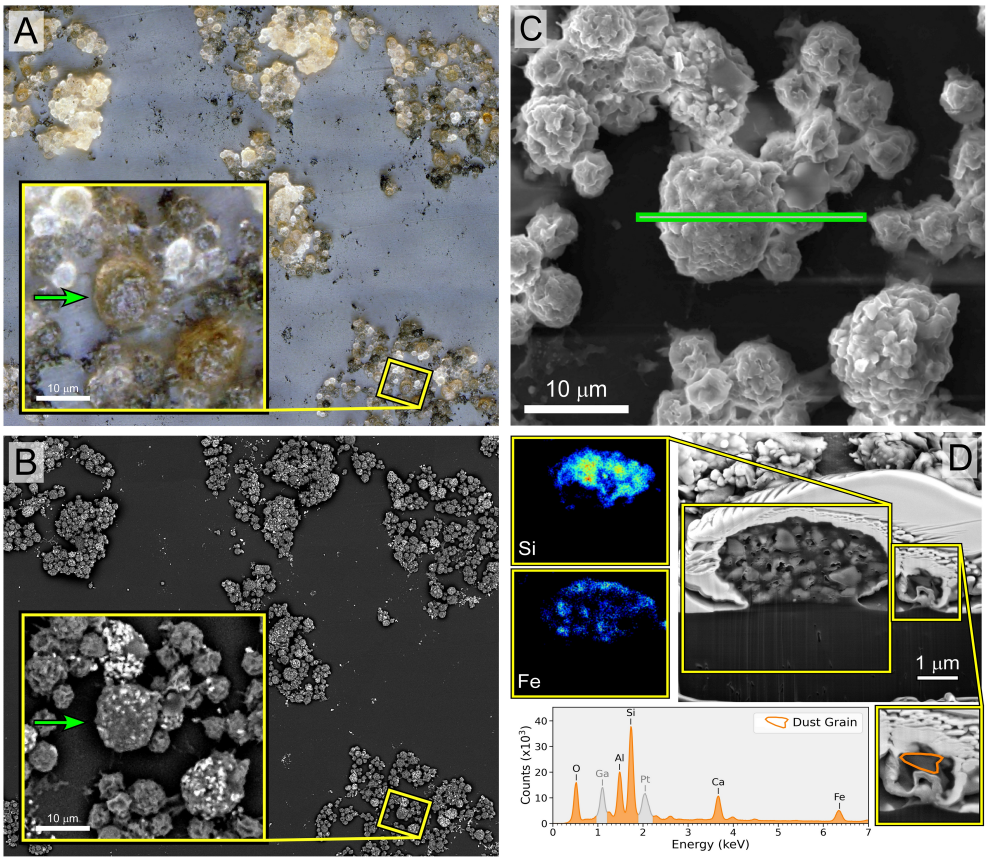

FIGURE 1
Image panel of macrophage/neutrophil cells isolated from the rat lunar dust inhalation study lung lavage samples from a rat exposed to high lunar dust loads for 13 weeks. The application of different methods of imaging to the same region enabled the identification of cells that have ingested lunar particles for confirmation by EDX. **(A)** Extended depth-of-field image of a lung lavage sample with visible lunar dust (black debris) and macrophage and neutrophil cells that ingested lunar dust particles (brown and black cells). **(B)** Backscatter electron microscopy imaging of the same region, highlighting elemental variations of the lunar dust on the outside of the cells (bright particles). **(C)** The cross-section of the region of interest for focused ion beam (FIB) sectioning of both macrophage and neutrophils that were identified in **(A)** to have ingested particles. **(D)** The cross-section of the two cell types along with EDX analysis of the macrophage interior showing the presence of Si and Fe confirming the presence of lunar dust.

resolution imaging and chemical mapping using EDX. Assessment of cellular internalization of particles was carried out by milling selected ROIs with a gallium (Ga)-focused ion beam (FIB) on a Phillips/FEI Quanta 3D field emission gun (FEG) FIB ESEM. Once the cells were selected, a platinum (Pt) protective "bandaid" was layered over the cells followed by milling through the cell regions with the FIB until the cell internal layers were reached, followed by EDX analysis of the internal particles ingested by the cells. Contaminating Pt and Ga peaks are expected due to the layering of the protective Pt coating and milling with the Ga FIB. Remainder peaks are representative of the particle composition inside the cell.

2.8 Light microscopy

Conducting light microscopy analysis, lung lavage cells were imaged with an Olympus ×100, 0.95 UMPanF for depth of field illumination. The lavage samples used were similar to the ones fixed for electron microscopy (please see electron microscopy materials and methods). The samples were placed onto a T-stub mount holder and imaged so that the same regions could be imaged using different microscopy techniques and mapped for the identification of cells ingesting particles. Manual 1-µm step images were collected in addition to images in a serpentine pattern with 30% overlap to create an in-focus depth of field mosaic. Final 3D projection images were produced using the Fiji (ImageJ) software package and seamless stitching of the acquired overlapping 3D projections generated with the Hugin software package. Light microscopy analysis of the lung tissues was performed on a Keyence VHX-600 microscope. The lung tissues used were similar to the ones fixed for electron microscopy (please see electron microscopy materials and methods). The samples were placed onto a T-stub mount holder and imaged with a full illumination cap on a ×20–×200 objective; images were collected at ×75 magnification. Manual 1-µm step images (4,800 × 3,600) were collected from the base of the tissue to the top, with the final 3D projection produced using the Fiji (ImageJ) software package. Large tissue sections requiring stitching several 3D projections were generated using the Hugin software package.

2.9 Statistical analysis

Statistical significance was evaluated for air control and low- and high-dose lunar dust using a two-way ANOVA (treatment and time) for each analyte tested. Multiple comparisons (Dunnett) were analyzed for the air control at each timepoint (dose) and for each group's day 1 value (time). Quartz was not included in the analysis as it was used as a positive control to ensure assay quality (data not shown but provided upon request). The mean differences between time course and treatment type were considered significant if $p < 0.05$.

3 Results

3.1 Microscopy analysis

Light microscopy analysis of the lavage samples confirmed the presence of both leukocytes and lunar dust (Figures 1A, B). Focused ion beam sectioning indicated that phagocytic cells did ingest lunar dust particles, confirmed by elemental analysis (Figures 1C, D).

3.2 Control cytometry

Flow cytometric analysis of both lunar dust and quartz alone confirmed that these particles did not possess either forward- or side-light scatter properties which would interfere with the cellular analysis of the lavage fluid (Figure 2). Both particles possessed forward-scatter properties below that expected for normal lymphocyte size (~10 µm), which would likely be the smallest expected cell population of interest within either the lavage or blood samples. Lunar dust appeared to possess higher side-scatter properties, whereas the quartz particles possessed lower side-scatter properties.

3.3 Lavage cytometry

After identifying and gating all leukocytes via CD45 expression, based on CD32 expression and scatter characteristics, it was possible to resolve normal pulmonary macrophage and lymphocyte populations by flow cytometric analysis of lavage samples from air-treated subjects (Figure 3). A similar analysis of rat peripheral blood revealed a primary composition consisting of neutrophils and lymphocyte subsets (Figure 3). Analysis of lavage samples from lunar dust-treated animals demonstrated the influx of neutrophils and lymphocytes into the lungs (Figure 3). Lavage fluid was further analyzed based on the expression of both CD71 and CD11c (ungated to resolve all populations) to confirm the phenotype of the pulmonary macrophage population ($CD71^{+}CD11c^{+}$) and quantify the relative percentage of macrophages, lymphocytes, neutrophils, and dendritic cells in all samples. The analysis strategy with the identification of the leukocyte populations for the representative air, lunar dust, and quartz lavage samples is shown in Figure 4.

3.4 Lavage leukocyte distribution

Flow cytometric analysis of the air-treated lavage samples confirmed that the normal lavage (air-treated, day 1) consisted of mostly pulmonary macrophages (>90%), with a small percentage of lymphocytes and granulocytes also present (Figure 5). Among the lymphocytes present, the majority were $CD4^{+}$ T cells and not $CD8^{+}$ T cells (Figure 5). Following treatment with either lunar dust (low or high concentration) or quartz, the lavage cellular composition changed over time primarily due to a significant influx of granulocytes and lymphocytes (Figure 5). Although inconsistent across the timepoints, it appears that the lymphocytic infiltrate consisted of $CD4^{+}$ T cells, significant at the 4- and 13-week timepoints, as compared to the air-treated control samples. This shift in $CD4^{+}$ T cells also coincided with a lower relative percentage of $CD8^{+}$ T cells in the low- and high-dose lunar dust groups at week 13 (Figure 5). Dendritic cell percentages in lavage fluid were variable between the low-dose and high-dose groups, with higher lunar dust concentrations yielding a significant increase at week 4 in dendritic cell percentage, whereas both the low and high doses were actually significantly reduced at week 13 compared to air controls (Figure 5).

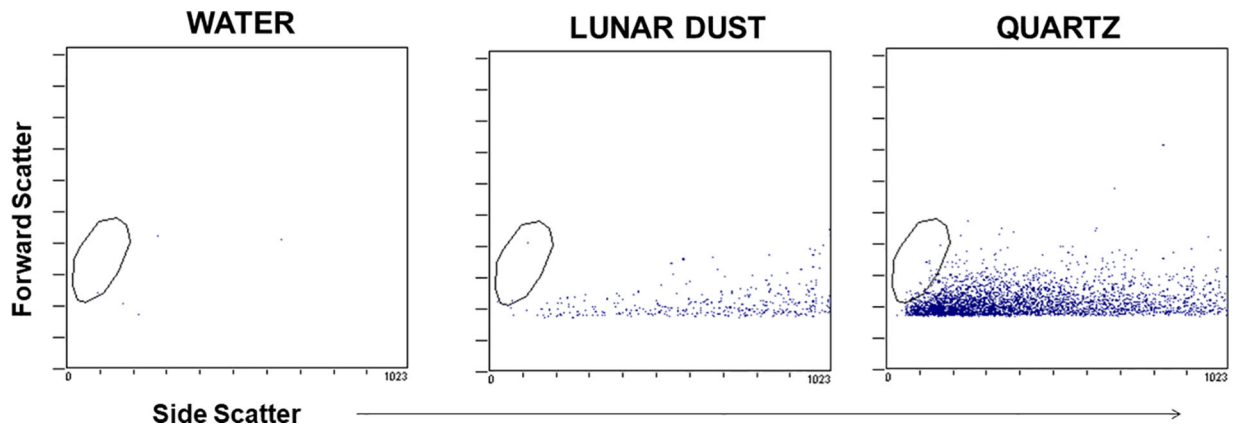

FIGURE 2
Representative flow cytometry dot plots demonstrate that the optical scatter properties for the lunar dust and quartz inhalation mixtures did not overlap with the cellular analysis areas (typical lymphocyte size indicated by the visible gate region).

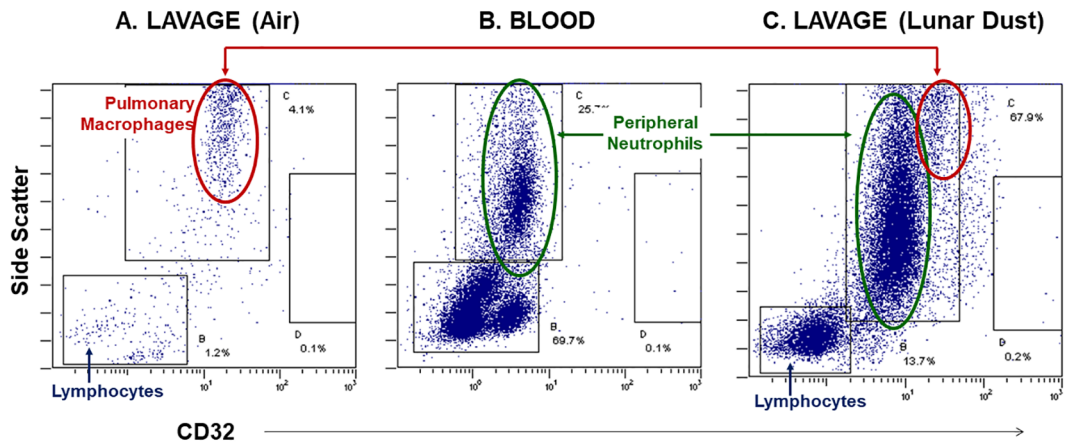

FIGURE 3
Representative flow cytometry dot plots, side-scatter vs. CD32 expression, illustrate the neutrophil influx into the peritoneal space following lunar dust inhalation. **(A)** Control lavage consists primarily of pulmonary macrophages; **(B)** rat blood staining illustrates the location of peripheral granulocytes; **(C)** the treated lavage fluid consists of both macrophages and neutrophils, with an increased population of lymphocytes.

3.5 Lavage cytokine levels

Although an array of seven cytokines was assessed in the subjects' lavage fluid, statistically significant differences were only observed following inhalation in the concentration of IL-1β and TNFα. Compared to the air-treated control subjects, the concentration of IL-1β was significantly elevated by day +7 for high-dose lunar dust. By 4 weeks, both low- and high-dose lunar dust were significantly high, and the concentration continued to increase through 13 weeks of treatment (Figure 6). Additionally, IL-1β was significantly increased in the low lunar dust-treated subjects at week 4 and week 13 compared to their retrospective day 1

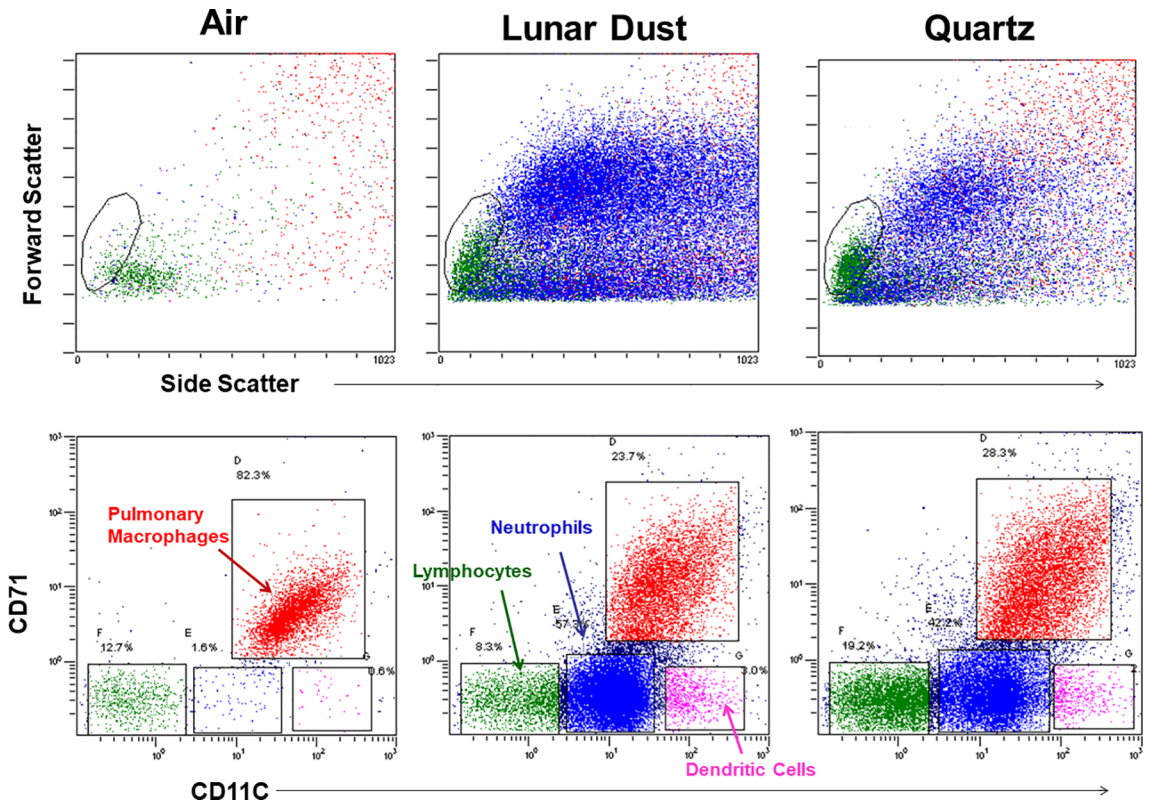

FIGURE 4
Flow cytometry cellular characterization of pulmonary lavage from air-, lunar dust-, and quartz-treated representative subjects based on scatter properties and expression of CD71 and CD11c. The air-treated normal lavage fluid consists primarily of $CD11c^{+}/CD71^{+}$ pulmonary macrophages. After lunar dust and quartz inhalation treatment, a pulmonary influx of neutrophils, dendritic cells, and lymphocytes is evident.

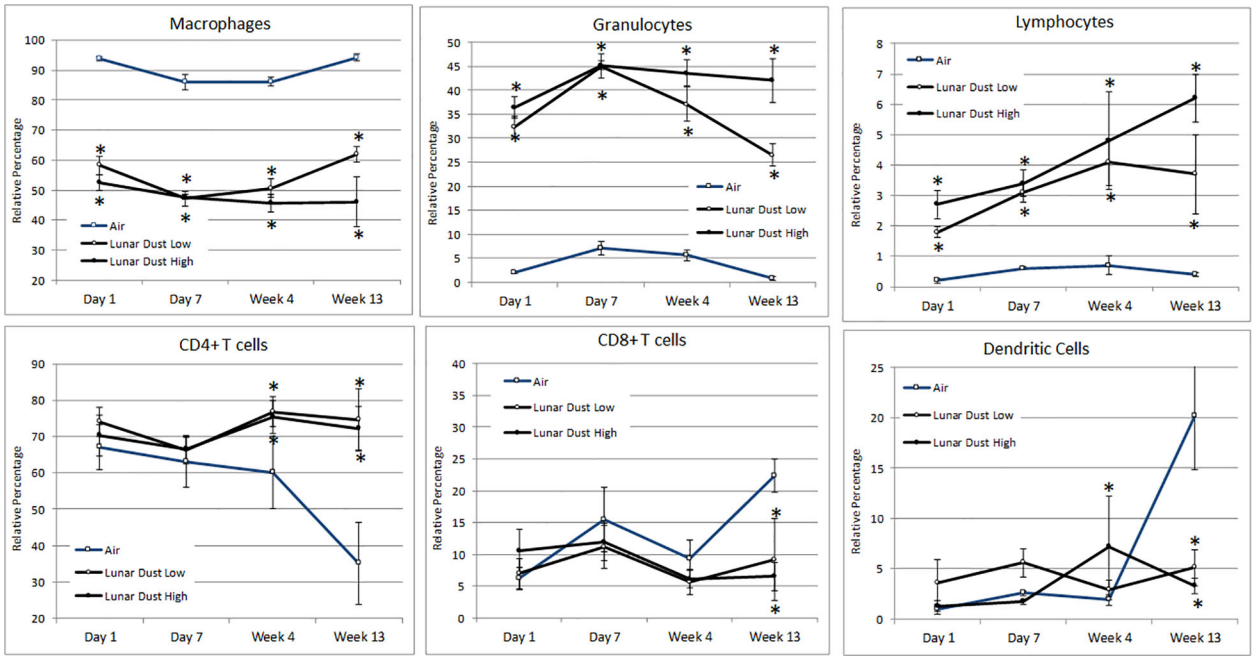

FIGURE 5
Mean alterations in lavage leukocyte distribution by inhalation treatment and time course. Data are expressed as relative percentage mean ± SEM for the indicated parameters. Lunar dust data, high and low concentrations, were evaluated for significance at each timepoint against the corresponding "air control" data point ("*," $p \leq 0.05$).

subjects. Within the high-dose lunar dust groups, all three timepoints (day 7, week 4, and week 13) were significantly increased in IL-1β compared to day 1.

The lavage concentration of TNFα was significantly elevated in all treatment groups at day 1 as compared to the air-treated control subjects and continued to be significant at each timepoint thereafter (Figure 6). Similar to IL-1β, the concentration of TNFα continued to rise for all treatment groups through week 13; however, this was only significantly increased in the high-dose lunar dust group at weeks 4 and 13. The low-dose lunar dust group did not reach statistical significance (day 1 vs. week 13; −1.74 pg/mL, $p = 0.07$).

3.6 Blood immune alterations

The same leukocyte subset analysis as used for the lavage samples was also performed for the peripheral blood samples from each subject. Compared to the air-treated control subjects, a

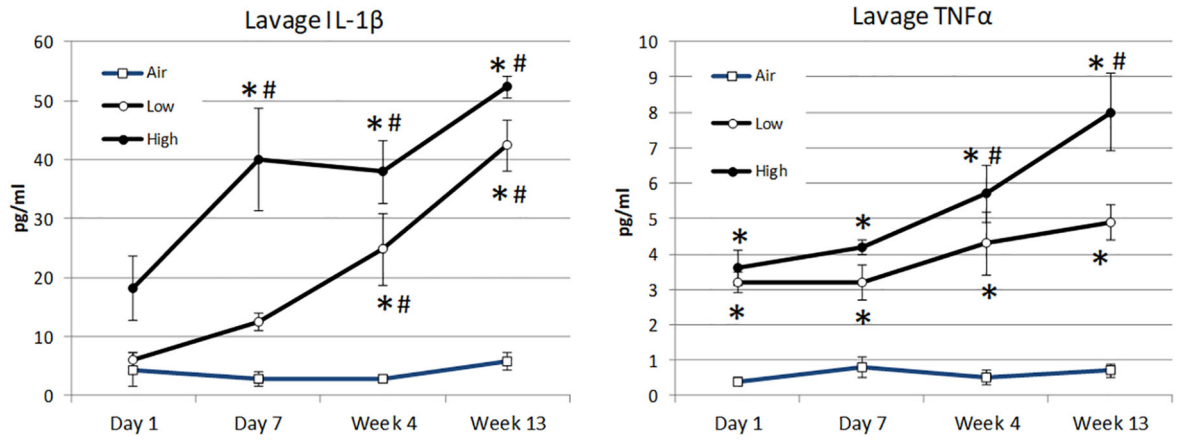

FIGURE 6
Mean alterations in lavage cytokine concentration of IL-1β **(A)** and TNFα **(B)** by inhalation treatment and time course. Data are expressed as mean pg/mL cytokine concentration ± SEM for the indicated analytes. Lunar dust data, high and low concentrations, were evaluated for significance at each timepoint against the corresponding "air control" data point ("*," $p \leq 0.05$). Significance was also evaluated over time, comparing day 7, week 4, and week 13 to the day 1 timepoint ("#").

significant increase in the peripheral blood granulocyte percentage was observed in the lunar dust-treated subjects at day 7 and week 4, for the high-dose subjects, and at weeks 4 and 13, for the low-dose subjects (Figure 7). A concurrent significant decrease in the peripheral lymphocyte percentage was observed for the lunar dust-treated subjects (both doses) only at the week 4 timepoint (data not shown). Within the lymphocyte subsets, $CD4^+$ T cells in the high-dose lunar dust group did rise significantly at day 7 compared to their corresponding day 1 values, but this leveled off by week 4. Activated leukocytes in the bloodstream were lower in the lunar dust groups compared to the air-treated control. However, this was only significantly lower at day 7 for the high-dose lunar dust group (data not shown). Additionally, this drop in activated leukocytes at day 7 for the high-dose lunar dust group was also significantly lower than the high-dose lunar dust group at day 1. There were no other consistent significant differences observed in the peripheral blood leukocyte subsets for any subjects.

Plasma cytokine levels were assessed for all subjects, using the same seven-cytokine array as was used for the lavage analysis. Opposite to the lavage fluid data, IL-1β was significantly lower in the high-dose lunar dust group compared to the air-treated controls at day 1 (data not shown). Additionally, IL-1β was significantly higher in the low-dose lunar dust group compared to the air-treated controls at day 7. IL-1β leveled out to the same as the controls at week 4 and beyond. The concentrations for all cytokines measured were unchanged within all treated groups, at all timepoints, compared to the air-treated control subjects (data not shown).

As a measure of leukocyte functional capability, the supernatant cytokine levels were also assessed from mitogen-stimulated whole blood cultures. Following lunar dust treatment, no significant differences were observed in cytokine production following T-cell stimulation (antibodies to CD3 and CD28) or following LPS stimulation (data not shown). Following stimulation in the presence of PMA + ionomycin, as a more powerful pharmacologic stimulus, there were significant differences observed in both the lunar dust doses as compared to the air-treated control with a decreased production of IL-2 (week 13) (Figure 7). While not statistically significant, there was a notable increase of IL-1β following PMA+I stimulation in both the low- (+2.44 pg/mL; $p = 0.05$) and high-dose lunar dust (+2.24 pg/mL; $p = 0.08$) groups compared to the air-treated control at day 1. There were no other consistent significant differences observed in the functional capacity of peripheral blood leukocytes in response to PMA + ionomycin.

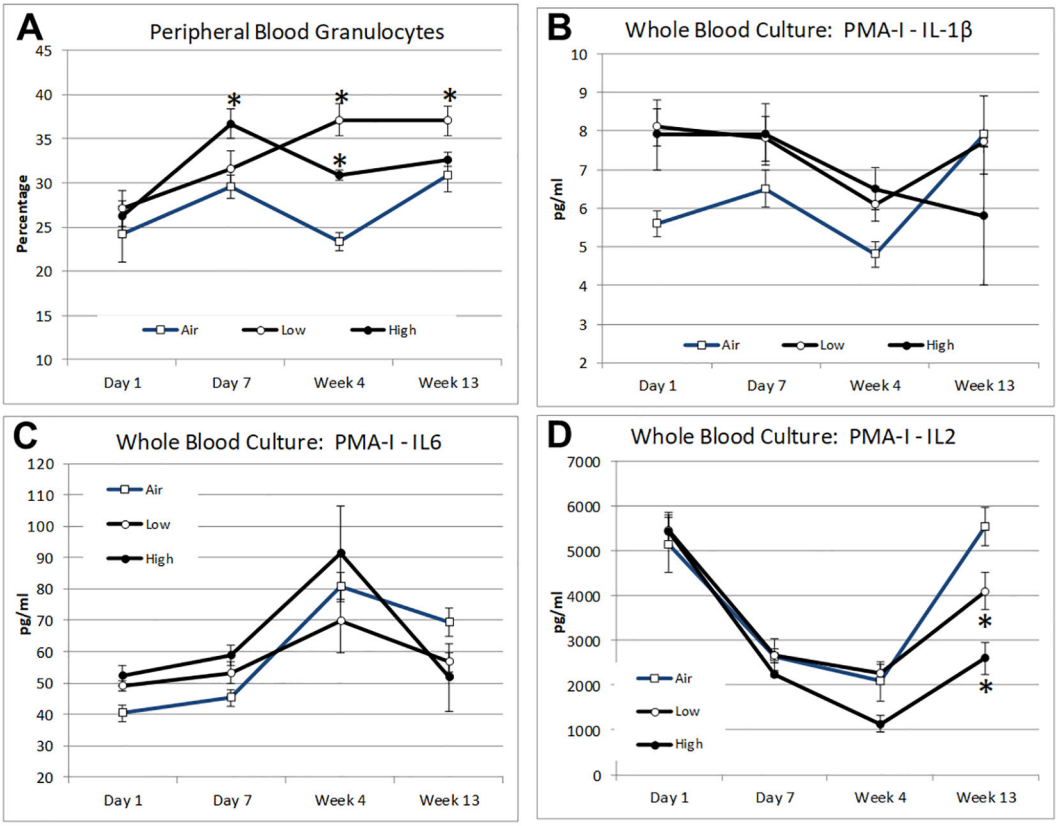

FIGURE 7
Mean alterations in peripheral blood leukocyte distribution and mitogen-stimulated cytokine response by inhalation treatment and time course for peripheral blood granulocytes **(A)**, whole blood treated with PMA + ionomycin IL-1β **(B)**, whole blood treated with PMA + ionomycin IL-6 **(C)**, and whole blood treated with PMA + ionomycin IL-2 **(D)**. Data are expressed as mean (relative percentage or pg/mL concentration as indicated) ± SEM for the indicated parameters. Lunar dust data, high and low concentrations, were evaluated for significance at each timepoint against the corresponding "air control" data point ("*," $p \leq 0.05$).

4 Discussion

Immune system dysregulation involved with spaceflight has been well documented by researchers, and we can only expect this to worsen with future deep space, longer-duration missions (12). Recent data have confirmed that this phenomenon occurs during short- and long-duration spaceflight, indicating an in-flight occurrence, not merely a post-flight landing effect (2, 20). T cell, natural killer (NK) cell, monocyte, and neutrophil function are all found to be diminished following spaceflight (1–3). The reactivation of latent herpesviruses, likely as a result of diminished immune control, has also been documented to occur during spaceflight (7, 8). There have been Apollo program reports of lunar dust exposure leading to notable upper respiratory symptoms in select crew members (21, 22). As human exploration of the Moon may soon resume, the immunoreactivity of lunar dust must be considered as frequent lunar surface operations will be conducted to begin building for mankind's long-term presence in deep space (15).

Lunar dust is a unique substance that poses a potential health hazard to crew members that may already be experiencing a decrease in immune function. Most studies performed in other animal and *in-vitro* models use simulant, as true lunar regolith is federally controlled, and to obtain samples, laboratories must go through a lengthy approval process. The current study is novel and uniquely designed to assess actual lunar dust immune-reactivity. As such, our laboratory applied and was approved to obtain lunar dust from the Apollo 14 mission. This was a large and interdisciplinary rodent model investigation. The parent investigation thoroughly investigated the toxicity of lunar dust in the same rat inhalation model, and the overall relevant findings, including the bulk characterization of neutrophils and lymphocytes in blood and lung tissue, were previously reported (18). This current immune-centric substudy examined immunotoxicity and reactivity, specifically in lung lavage fluid and peripheral blood leukocyte distribution and cytokine responses.

Lunar dust is comprised of micron-sized sharp particles, and the bulk chemical composition of lunar dust varies across the lunar surface (15). For this study, we used the Earth mineral quartz as a standard simulant commonly used by the National Institutes of Health to study respiratory system toxicity as it is known to cause silicosis (17). We confirmed that the optical scatter properties for the lunar dust inhalation or quartz treatment mixtures did not interfere with the flow cytometric cellular analysis (Figure 2) and that it was possible to resolve normal pulmonary macrophage and lymphocyte populations by flow cytometric analysis of lavage samples from air-treated subjects (Figures 3, 4). Our study showed an influx of neutrophils, dendritic cells, and lymphocytes, primarily $CD4^+$ T cells, into the lungs of animals treated with lunar dust and quartz inhalation (Figure 5). A reduction in dendritic cells was observed after 13 weeks of lunar dust treatment (both doses); however, this finding appeared to be artifactual and resulted from an increase in the air control-treated subjects (Figure 5). Within the lavage fluid, cytokine analysis showed only that IL-1β and TNFα were significantly increased after treatment with lunar dust and quartz by day 7 through week 13 (Figure 6).

The same analysis was conducted in the peripheral blood samples and showed an increase in the blood granulocyte population in the lunar dust-treated animals. The only significant differences observed in plasma cytokine levels were after PMA + ionomycin stimulation in the high-dose lunar dust concentration treatments including increased IL-1β and IL-6 and decreased IL-12 (Figure 7).

The findings from the current investigation are in relative alignment with the observations terrestrially of lung inflammation resulting from particulate inhalation (23) and from the parent studies' high-level assessment of bulk lymphocyte subsets in conjunction with other biomarkers (18). Lam reported concentration-dependent increases, as detected by the simple Wright stain and manual differential analysis, in the levels of lung neutrophils and lymphocytes but no increase in the total cellular concentration. This likely reflects the influx of the neutrophils and lymphocytes in response to the particulate and only a relative decrease in pulmonary macrophages, as this method does not quantify absolute concentrations of cells (only relative percentages). The current study adds to this dataset via positively identifying populations by surface marker expression and by adding a higher resolution snapshot of leukocyte distribution assessing additional populations (T-cell subsets, etc.). The influx of lymphocytes is revealed to be primarily $CD4^+$ T cells, also in accordance with the expectations for a particulate pulmonary insult.

This work has implications for ensuring crew safety during the upcoming "Artemis" missions to the lunar surface. Lunar dust as a human health hazard has been known since the Apollo missions, which found the dust to be extremely adherent to surfaces and clothing and became somewhat pervasive within the crew cabin. A lack of gravity (or 1/6 reduced gravity) only serves to worsen the exposure as small particles do not settle out readily over time. These challenges must be addressed through appropriate operational (e.g., cleaning) and engineering controls (e.g., high-efficiency particulate air filtration), and these mitigations must be informed by health-based guidelines to adequately protect crew health. Compounding the immune crew health risk are the other stressors associated with lunar exploration, including elevated radiation exposure, the stress associated with confinement and isolation, and circadian misalignment. In synergy, these combined effects may increase the hazard over the effects that might be observed during a terrestrial exposure. For example, onboard the ISS, several case studies have documented that the persistent immune system dysregulation in astronauts has, in selected crew members, been associated with adverse clinical outcomes. These included atopic dermatitis, atypical allergy, and in a recent case, laboratory-confirmed zoster. These data are relevant therefore to understanding the true clinical risk associated with lunar dust inhalation, as they establish "baseline consequences".

We acknowledge several limitations of this study, including a focus on animal models. Care must be taken in extrapolating rodent data to human clinical risk, but these data represent a first step in understanding that risk. We suggest that future studies assess the effect of lunar dust exposure in similarly immune-compromised subjects. These could include cell culture-modeled microgravity

studies, additional rat studies using hindlimb unloading, or even human documentation of occupational exposures in extreme environments such as undersea or military deployment or during Antarctica winterover. Indeed, in a submitted companion article to this work, we disclose the results from a recent human primary immune cell culture experiment also using actual lunar dust samples, to assess both immediate and inducible "allergic" responses (data not shown). The goal regarding all mission-associated stressors is mitigation. Recent progress has been made toward a biomedical countermeasure to rectify immune competence for deep space missions. This includes the identification of countermeasure options (14) and validation of perhaps the most appropriate human mission analog platform for countermeasure validation (24). Recently, NASA has initiated a study to assess the effectiveness of a specific targeted multisystem biomedical countermeasure during Antarctica winterover deployment. We further suggest that the "challenge" of immune cells from such individuals may be informative regarding how sensitivity to lunar dust evolves during an immune compromise situation, or the even post-flight challenge of the first Artemis crew members, the first humans since Apollo to have a true "occupational exposure" to actual lunar dust, will also be informative. Taken all together, the rodent and human study data could be expanded and greatly facilitate our understanding and mitigation of lunar dust risk for the upcoming Artemis missions.

Data availability statement

The raw data supporting the conclusions of this article will be made available upon request to the NASA Life Sciences Data Archive.

Ethics statement

The animal study was approved by NASA Johnson Space Center - Institutional Animal Care and Use Committee. The study was conducted in accordance with the local legislation and institutional requirements.

Author contributions

BC: Conceptualization, Data curation, Formal analysis, Funding acquisition, Investigation, Methodology, Project administration, Resources, Supervision, Validation, Writing – original draft, Writing – review & editing. HQ: Conceptualization, Data curation, Funding acquisition, Investigation, Methodology, Writing – original draft. C-wL: Conceptualization, Data curation, Formal analysis, Funding acquisition, Investigation, Methodology, Resources, Validation, Writing – review & editing. MN: Data curation, Formal analysis, Funding acquisition, Project administration, Writing – review & editing. AC: Data curation, Formal analysis, Writing – review & editing. DD: Data curation, Formal analysis, Writing – review & editing. JJ: Conceptualization, Data curation, Funding acquisition, Methodology, Project administration, Resources, Supervision, Writing – review & editing.

Funding

The author(s) declare financial support was received for the research, authorship, and/or publication of this article. This work was supported by the National Aeronautics and Space Administration.

Acknowledgments

The authors express their gratitude to Mr. Zia Rahman and Dr. Simon Clemett of JETS/Amentum, Houston, Texas, for their expertise in setting up the EDX analysis. The authors are also grateful to Torin McCoy, NASA Johnson Space Center, Lunar Dust Risk Custodian, for critical reading of this manuscript and specific suggestions for improvement.

Conflict of interest

C-wL, AC, and MN are employees of KBR Inc., Houston, Texas. DD is an employee of Aegis Inc., Houston, Texas.

The remaining authors declare that the research was conducted in the absence of any commercial or financial relationships that could be construed as a potential conflict of interest.

Generative AI statement

The author(s) declare that no Generative AI was used in the creation of this manuscript.

Publisher's note

Supplementary material

The Supplementary Material for this article can be found online at: https://www.frontiersin.org/articles/10.3389/fimmu.2025.1538421/full#supplementary-material

References

1. Crucian B, Mehta S, Simpson R, Stowe R, Chouker A, Hwang S-A, et al. Review: terrestrial stress analogs for spaceflight associated immune system dysregulation. *Brain Behav Immun*. (2014) 39:23–32. doi: 10.1016/j.bbi.2014.01.011

2. Crucian B, Stowe RP, Mehta S, Quiriarte H, Pierson D, Sams C. Alterations in adaptive immunity persist during long-duration spaceflight. *NPJ Microgravity*. (2015) 1:15013. doi: 10.1038/npjmgrav.2015.13

3. Simpson RJ, Bigley AB, Spielmann G, Kunz HE, Agha N, Baker F, et al. Long duration spaceflight impairs NK-cell function in astronauts. *Med Sci Sports Exerc*. (2016) 48:87. doi: 10.1249/01.mss.0000485269.23662.1f

4. Kunz H, Quiriarte H, Simpson RJ, Ploutz-Snyder R, McMonigal K, Sams C, et al. Alterations in hematologic indices during long-duration spaceflight. *BMC Hematol*. (2017) 17:12. doi: 10.1186/s12878-017-0083-y

5. Spielmann G, Agha N, Kunz H, Simpson R, Crucian B, Mehta S, et al. B-cell homeostasis is maintained during long duration spaceflight. *J Appl Physiol*. (2019) 126 (2):469–76. doi: 10.1152/japplphysiol.00789.2018

6. Makedonas G, Chouker A, Mehta S, Simpson R, Stowe R, Sams C, et al. Mechanistic clues to overcome spaceflight-induced immune dysregulation. *Curr Pathobiology Rep*. (2018) 6:185–92. doi: 10.1007/s40139-018-0178-6

7. Mehta SK, Laudenslager ML, Stowe RP, Crucian BE, Feiveson AH, Sams CF, et al. Latent virus reactivation in astronauts on the international space station. *NPJ Microgravity*. (2017) 3:11. doi: 10.1038/s41526-017-0015-y

8. Rooney BV, Crucian BE, Pierson DL, Laudenslager ML, Mehta SK. Herpes virus reactivation in astronauts during spaceflight and its application on Earth. Frontiers in Microbiology. *Front Microbiol*. (2019) 07:16. doi: 10.3389/fmicb.2019.00016

9. Crucian B, Babiak-Vazquez A, Mehta S, Pierson D, Ott M, Sams C. Incidence of clinical symptoms during long-duration spaceflight. *Int J Gen Med*. (2016) 9:383–91. doi: 10.2147/IJGM.S114188

10. Mehta SK, Szpara ML, Rooney BV, Diak DM, Shipley MM, Renner DW, et al. Dermatitis during spaceflight associated with HSV-1 reactivation. *Viruses;*. (2022) 14:789. doi: 10.3390/v14040789

11. Mehta SK, Suresh R, Brandt K, Diak D, Smith SM, Zwart SR, et al. Immune system dysregulation preceding a case of laboratory-confirmed zoster/dermatitis onboard the international space station. *JACI Global*. (2024) 3:100244. doi: 10.1016/j.jacig.2024.100244

12. Crucian B, Sams C. Immune system dysregulation during spaceflight: clinical risk for exploration-class missions. *J Leukoc Biol*. (2009) 86:1017–8. doi: 10.1189/jlb.0709500

13. Crucian BE, Makedonas G, Sams CF, Pierson DL, Simpson R, Stowe RP, et al. Countermeasures-based improvements in stress, immune system dysregulation and latent herpesvirus reactivation onboard the international space station – relevance for deep space missions and terrestrial medicine. *Neurosci Biobehav Rev*. (2020) 115:68–76. doi: 10.1016/j.neubiorev.2020.05.007

14. Crucian BE, Choukér A, Simpson RJ, Mehta S, Marshall G, Smith SM, et al. Immune system dysregulation during spaceflight: potential countermeasures for deep space exploration missions. *Front Immunol*. (2018) 9:1437. doi: 10.3389/fimmu.2018.01437

15. Loftus DJ, Tranfield EM, Rask JC, McCrossin C. *The Chemical Reactivity of Lunar Dust Relevant to Human Exploration of the Moon*. NASA Ames Research Center (2009). Available at: https://www.lpi.usra.edu/decadal/leag/DavidJLoftus.pdf.

16. Heiken GH, Vaniman DT, French BM. *Lunar Sourcebook, A User's Guide to the Moon*. (1991) Lunar and Planetary Institute, Houston, Texas, USA: Cambridge University Press.

17. IARC Working Group on the Evaluation of Carcinogenic Risks to Humans. Arsenic, M., Fibres and Dusts, SILICA DUST, CRYSTALLINE, IN THE FORM OF QUARTZ OR CRISTOBALITE. In: *Arsenic, Metals, Fibres and Dusts*. WHO, IARC Publications, Lyon, France: IARC Monographs on the Evaluation of Carcinogenic Risks to Humans (2012).

18. Lam CW, Scully RR, Zhang Y, Renne RA, Hunter RL, McCluskey RA, et al. Toxicity of lunar dust assessed in inhalation-exposed rats. *Inhal Toxicol*. (2013) 25:661–78. doi: 10.3109/08958378.2013.833660

19. Lam C-w, Castranova V, Driscoll K, Warheit D, Ryder V, Zhang Y, et al. A review of pulmonary neutrophilia and insights into the key role of neutrophils in particle-induced pathogenesis in the lung from animal studies of lunar dusts and other poorly soluble dust particles. *Crit Rev Toxicol*. (2023) 53(8):441–79. doi: 10.1080/10408444.2023.2258925

20. Crucian B, Stowe R, Mehta S, Uchakin P, Quiriarte H, Pierson D, et al. Immune system dysregulation occurs during short duration spaceflight on board the space shuttle. *J Clin Immunol*. (2013) 33:456–65. doi: 10.1007/s10875-012-9824-7

21. Gaier J. The effects of lunar dust on EVA systems: lessons learned from apollo. *NASA*. (2005), 213610.

22. Scheuring RA, Jones JA, Novak JD, Polk JD, Gillis DB, Schmid J, et al. The Apollo Medical Operations Project: Recommendations to improve crew health and performance for future exploration missions and lunar surface operations. *Acta Astronautica*. (2008) 63:980–7. doi: 10.1016/j.actaastro.2007.12.065

23. Tamagawa E, Bai N, Morimoto K, Gray C, Mui T, Yatera K, et al. Particulate matter exposure induces persistent lung inflammation and endothelial dysfunction. *Am J Physiol Lung Cell Mol Physiol*. (2008) 295:L79–85. doi: 10.1152/ajplung.00048.2007

24. Diak DM, Krieger S, Gutierrez C, Mehta S, Nelman-Gonzalez M, Babiak-Vazquez A, et al. Palmer station, Antarctica: A ground-based spaceflight analog suitable for validation of biomedical countermeasures for deep space missions. *Life Sci Space Res (Amst)*. (2024) 40:151–7. doi: 10.1016/j.lssr.2023.08.001

frontiers | Frontiers in Physiology

TYPE Hypothesis and Theory
PUBLISHED 24 April 2025
DOI 10.3389/fphys.2025.1558625

OPEN ACCESS

EDITED BY
Lidia Strigari,
IRCCS Azienda Ospedaliero-Universitaria di Bologna, Italy

REVIEWED BY
Adel B Elmoselhi,
University of Sharjah, United Arab Emirates
Melvin S. Marsh,
Alabama State University, United States

*CORRESPONDENCE
Arthur Saniotis,
arthur.saniotis@cihanuniversity.edu.iq

RECEIVED 19 January 2025
ACCEPTED 08 April 2025
PUBLISHED 24 April 2025

CITATION
Saniotis A, Henneberg M and Mohammadi K (2025) Evolutionary medicine and bioastronautics: an innovative approach in addressing adverse mental health effects to astronauts during long term space missions. *Front. Physiol.* 16:1558625.
doi: 10.3389/fphys.2025.1558625

Evolutionary medicine and bioastronautics: an innovative approach in addressing adverse mental health effects to astronauts during long term space missions

Arthur Saniotis[1,2]*, Maciej Henneberg[2,3] and Kazhaleh Mohammadi[4]

[1]Department of Medical Microbiology, Cihan University-Erbil, Erbil, Iraq, [2]School of Biomedicine, Faculty of Health and Medical Sciences, The University of Adelaide, Adelaide, SA, Australia, [3]Institute of Evolutionary Medicine, University of Zurich, Zurich, Switzerland, [4]Department of Medical Microbiology, College of Science, Knowledge University, Erbil, Iraq

Although evolutionary medicine has produced several novel insights for explaining prevalent health issues, it has yet to sufficiently address possible adverse mental health effects of humans during long-term space missions While evolutionary applications to medicine have increased over the past 20 years, there is scope for the integration of evolutionary applications in the new branch of space medicine called bioastronautics, which analyses the effects on human bodies when in outer space. Evolutionary principles may explain what kinds of space environments increase mental health risks to astronauts, both in the short and long term; secondly, evolutionary principles may provide a more informed understanding of the evolutionary mismatch between terrestrial and space environments in which astronauts exist. This information may assist in developing frameworks for improving mental health of astronauts and future space colonists. Consequently, this paper will focus on some of the major evolutionary mismatches currently confronting astronauts' mental health, with an aim to improve medical knowledge. It will also provide possible therapeutic countermeasures based on evolutionary principles for reducing adverse mental effects on astronauts.

KEYWORDS

evolutionary mismatch, hormonal dysregulation, spaceflight-associated neuro-ocular syndrome, spaceflight-associated dysbiosis, circadian disruption, Earth-out-of-view-phenomenon, relaxed natural selection, evolutionary based countermeasures

1 Introduction

Evolutionary medicine is a growing discipline integrating the principles of evolutionary biology, medicine, genetics and psychology, providing a range of concepts and insights for explaining human vulnerability to disease. (Beeson and Kosal, 2023; Nesse and Williams, 2012; Stearns et al., 2010; Stearns, 2012; Dolgova, 2021). Evolutionary medicine speculates that the human body has evolved under various conflicts of evolutionary forces, trade-offs, mismatches and constraints intrinsic to biological organisms under the influence of

natural selection and non-directional forces of evolution such as the genetic drift, gene flow and inbreeding (Nesse and Williams, 2012; Dolgova, 2021). An understanding of these evolutionary phenomena provides a feasible framework for classifying and understanding the complex interaction between genes, environment and history in relation to disease (Dolgova, 2021). Next, the human genome has undergone various adaptations over evolutionary history in response to ancestral environments, disease load and cultural behaviours, which inform current susceptibility to disease (Perry, 2021). Notwithstanding its growth in the English speaking world and in Europe, evolutionary medicine has yet to be established within global medical curricula (Natterson-Horowitz et al., 2023).

Even though evolution has been traditionally considered integral to biology, medical practitioners and public health experts have generally overlooked evolution's role in human susceptibility to disease. Recent medical science developments such as the Human Genome Project, recombinant DNA, and the Haplotype Map have reaffirmed the significance of genes for human health and disease. Concomitantly, evolutionary psychology examines the gene/environmental interplay and its enduring effect on traits of extant humans.

Thus far, evolutionary medicine has produced several novel insights for explaining prevalent health issues such as cancer, antimicrobial resistance, autoimmune disorders, diabetes, heart disease, depression/anxiety disorders, dementia and the advent of new anatomical variations. Evolutionary medicine also addresses the role of medical and public health interventions in reducing natural selection, which has been proposed to have led to an increase in fitness-reducing alleles with subsequential genetic load (Saniotis et al., 2021; Saniotis et al., 2024). For example, recent studies of 190 countries have suggested a correlation between type-1 diabetes and cancer incidence and the proliferation of harmful genes due to relaxed natural selection (You and Henneberg, 2016; 2017). Alterations in gene patterns due to relaxed selection could be important in mapping out possible future trajectories in human population health.

However, evolutionary medicine has yet to sufficiently address possible adverse mental health effects of humans during long-term space missions (LTSM). "Long term" can be referred to as being in outer space for a couple of months to years (Criscuolo et al., 2020). It will also apply eventually to life in human colonies on celestial bodies (Moon, Mars, *etc.*). While evolutionary applications to medicine have increased over the past 20 years, there is scope for the integration of evolutionary applications in the new branch of space medicine called bioastronautics, which analyses the effects on human bodies when in outer space (Arone et al., 2021). For example, evolutionary principles may explain what kinds of space environments increase mental health risks to astronauts, both in the short and long term; secondly, evolutionary principles may provide a more informed understanding of the evolutionary mismatch between terrestrial and space environments in which astronauts transit. This information may assist in developing frameworks for improving human mental health for future space colonists (Saniotis et al., 2016).

Consequently, this paper will focus on some of the major evolutionary mismatches currently confronting astronauts' mental health, with an aim to improve bioastronautical knowledge. It will also provide possible therapeutic countermeasures based on evolutionary principles for reducing adverse mental effects to astronauts.

2 Evolutionary mismatch, adaptation and outer space

A central concept in evolutionary medicine is "evolutionary mismatch," which refers to the discordance between the ancestral environments in which hominins lived and the novel societies' extant human habitat (Trevathan, 2007), resulting from cultural evolution outpacing biological evolution. This is consistent with the rapid rate of allele substitution during the Holocene Epoch, which is thought to be 100 times higher than for most of the evolution of *Homo* (Hawks et al., 2007; Keller, 2008).

It has been speculated that accelerated cultural evolution has left extant humans susceptible to a plethora of diseases and disorders. Like other organisms, the human genetic profile has been shaped by the complex interplay of various evolutionary forces (i.e., natural selection, mutation, gene flow, genetic drift) and sexual selection.

Notwithstanding the evolutionary discordance between ancestral and modern environments, human evolution is on-going, even though, natural selection has been relaxed in our species (Saniotis and Henneberg, 2011b; 2023). Some studies have highlighted rapid human micro-evolution during the Holocene (10,000 ka-present) (Rühli and Henneberg, 2013). Recent microevolution has occurred *via* lactase persistence (Itan et al., 2009), amylase gene copy variation [Zuk, 2013; Perry et al., 2007) malarial resistance, high altitude adaptation, brain volume reduction (Henneberg, 1988; Henneberg and Steyn, 1993)) decreasing musculoskeletal robusticity (Ruff, 2002), and ongoing Abnormal Spindle-like, Microcephaly-associated (ASPM) gene adaptation [Mekel-Bobrov et al., 2005).

Humans have not evolved to live in the outer space environment. This is evident by the numerous studies on the Soviet Mir space station (1986–2001), and American Shuttle and ISS missions, which have shown that even short-term space flight may cause deleterious changes to muscles and skeletal function (Fitts et al., 2001; Adams et al., 2003), vestibular system (Ross and Tomko, 1998), cardiopulmonary system, immunological system, motor system (Kozlovskaya et al., 1981), neuro-behavioural and cognitive function (Kanas and Manzey, 2008; De La Torre et al., 2012).

While understanding of the effect of space flight on the human body and mind has improved in the last two decades, there is still a great deal of medical research needed on mid (1–5 years) to long duration (>5 years) consequences of space flight. The proposed permanent Moon base will provide a basis for monitoring the human body in conditions beyond low Earth orbit. Furthermore, NASA's intention to send a manned space mission to Mars in the next-generation (the return trip will take approximately 21 months) will further identify health risks due to high exposure to radiation (astronauts could be exposed to ~1 Sievert (Sv) radiation during the trip) (Cucinotta and Durante, 2006; Wilson et al., 1995), as well as potential neuro-behavioural issues due to the extended duration of the mission.

Evolutionary history indicates that humans exhibit significant plasticity and adaptability across various environments. In the context of evolution, outer space represents a distinct environment

that necessitates a range of new adaptations. A key focus is how humans adjust to ensure neuro-behavioural allostasis, which involves sustaining neurohormonal balance for prolonged survival in space. This paper will further explore mental health challenges in bioastronautics, considering the implications of evolutionary mismatch.

3 Stress and glucocorticoid dysregulation in outer space

A major area of space medicine is the role of stress during long-duration space missions. Stress has been shown to affect astronaut behaviours and their ability to perform multiple tasks (Kanas, 1985; 1987). Space flight stressors include microgravity, living in small and enclosed confines, isolation, arduous workload, boredom, disconnection from the natural world, circadian disruption, unpredictable events, *etc.* These issues have received various levels of attention from space researchers.

Human stress response (HSR) is mediated by the Hypothalamus-Pituitary-Adrenal axis (HPA). The HPA axis evolved in our pre-hominin ancestors as an adaptive mechanism for triggering the sympathetic nervous system (SNS) in response to threats (de Kloet et al., 2005). Second, the HSR evolved to deal mainly with acute stressors (a few hours) and not with sub-acute (several days) or chronic stress (de Kloet, 2004). Prolonged exposure to chronic stress (several weeks/months to years) has been shown to play a role in depressive disorder and psychotic illness (de Kloet, 2004). In the hippocampus, long term glucocorticoid hormonal insults lead to impaired declarative and spatial memory [Ortiz and Conrad 2018), with diminished fear learning. Although dendritic recovery is possible in the hippocampal and pre-frontal cortex, this is only possible with the discontinuation of chronic stress (Conrad et al., 1999; Vyas et al., 2004). However, continuing dendritic retraction has a potential for damaging the hippocampus if persisting for months to years–referred to as the Glucocorticoid Vulnerability Hypothesis (Conrad, 2008).

Due to the various major stressors encountered by astronauts during LTSM, outer space presents an evolutionary mismatch with consequential risk for increasing neurotoxic challenges to emotional, learning and memory functions of the CNS. This is problematic since astronauts will be space-bound and isolated for a long duration when travelling to Mars.

4 Spaceflight-associated neuro-ocular syndrome (SANS)

From an ocular perspective the space environment presents critical challenges to human eyes and the visual system. In the absence of gravity, which has been a major evolutionary force in informing the structure, function and health of the human eyes, these organs are especially prone to visual pathologies such as spaceflight-associated neuro-ocular syndrome (SANS) (Mehare et al., 2024). This syndrome has been well documented in space medical literature given its relevance to neurological and mental health issues in astronauts. SANS presents as a collection of neuro-ocular symptoms due to a combination of factors such as exposure to micro-gravity, radiation, as well as, genetic factors (Ong et al., 2023; Mehare et al., 2024; Huang et al., 2019; Yang et al., 2022). Environmental increase in CO_2, onboard lighting, high sodium intake and poor diet may also contribute to SANS (Mehare et al., 2024). However, microgravity plays a major role in the development of SANS, since micro-gravity may alter the distribution of CSF leading to increased cranial pressure (ICF), compression to the optic nerve and optic disc edema (Mehare et al., 2024; Mader et al., 2011). SANS may also induce intra/extraocular muscle atrophy with subsequent ocular impairments (i.e., blurred vision, hyperopic shift) (Paez et al., 2020). Importantly, there is a strong correlation between duration of flight and the development of SANS. Medical reports reveal that even short-term spaceflight (<2–3 weeks) may trigger visual disturbances (Paez et al., 2020), with increasing SANS related symptoms during LTSM (Mehare et al., 2024). Although, various potential treatments have been proposed (i.e., diuretics, nutritional supplements, anti-inflammatory drugs, neuroprotective agents, low vision aids) (Hartmann et al., 1977; Ghlichloo and Gerriets, 2023; Nucci et al., 2018) to mitigate SANS induced damage, astronauts will further need extensive monitoring and behavioural counselling due to the psychological impact of possible long-term visual alterations in space (Mehare et al., 2024). Moreover, more studies need to examine psychological stressors due to microgravity (Marsh, 2007).

5 Enteric gut microbiome and outer space: dysbiosis increases the risk of psychiatric diseases

The human intestinal tract, primarily the colon, is the site of the enteric gut microbiome (EGM) which consists of large communities of bacteria (numbering ~ 10^{14}) (Ley et al., 2006), comprising 150–400 species (Lloyd-Price et al., 2016), that differ significantly between individuals (The Human Microbiome Project Consortium, 2012), and which can alter over lifetime (Davenport et al., 2017; Odamaki et al., 2016; Aleman and Valenzano, 2019). The EGM is an important source of gene encoding as it contains a vast number of genes (>100 times greater than in the human genome) (O'Hara and Shanahan, 2006).

The EGM is involved in several key functions such as digestion, immune response (Shahab and Shahab, 2022), skeletal integrity, as well as neuro-behavioural and psychological functions (i.e., neuro-hormonal regulation, cognition (Davidson et al., 2018; Saniotis et al., 2020) and mood regulation (Desbonnet et al., 2008). Consequently, dysbiosis of the EGM can have a deleterious health outcome for individuals in several of these mentioned areas.

For millions of years hominins have co-evolved with microbial communities in the EGM. The EGM would have undergone continual evolutionary changes along with hominin adaptations to their environments and diets. For example, probably during the Pliocene/Pleistocene transition (~3.2–2.6 Ma), the GIT of hominins underwent size reduction due to the introduction of meat and, later on, cooked food (Aiello and Wheeler, 1995; Henneberg et al., 1998; Mann, 2007). These two elements would have also contributed to alterations in the microbiome, which selected bacteria that favoured omnivorous diets (Shahab and Shahab, 2022).

Although, the human EGM is less diverse than that of the great apes, (Moeller et al., 2014; Davenport et al., 2017), intestinal biodiversity has further been altered by several bio-cultural changes from the Neolithic revolution (*circa* 10,000 ka) onwards. This trend was accelerated in the 20th century with global socio-cultural changes such as the introduction of anti-biotics, industrialised food products, increasing sedentism and chronic stress, and shifts to "western" style diets with significantly high omega-6 and inflammatory profiles (Bednarik et al., 2022), which have contributed to the "disappearing microbiome" (Blaser and Falkow, 2009).

Outer space represents a radical evolutionary mismatch for the EGM. It is well known that the EGM of astronauts is affected during outer space missions. Many stressors contribute to EGM dysbiosis during manned space missions which include microgravity, radiation, circadian desynchronisation cloistered living conditions and monotonous diets (Garrett-Bakelman et al., 2019; Voorhies et al., 2019; Marazziti et al., 2022; Arone et al., 2021; Siddiqui et al., 2021a; Siddiqui et al., 2021b; Mortazavi et al., 2024). The spacecraft/station environment does not contain many organisms that on Earth are sources of bacteria that may enrich the EGM. The EGM dysbiosis is significant since there are complex bidirectional interactions between the EGM and central nervous system (Kim et al., 2018; Saniotis et al., 2020), which also include microbiotic modulation of the vagus nerve *via* the microbiota-gut-vagus-brain-axis which may modify human behaviour (Montiel-Castro et al., 2013; Alcock et al., 2014). Interesting is that the probiotic influence of the EGM is annulled with either partial excision of the vagus nerve or vagotomy (Cryan and Dinan, 2012; Saniotis et al., 2020). Besides vagus transmitting sensations resulting from EGM's activity (Liao et al., 2016) this may suggest that EGM produced neurometabolites are reliant on vagus nerve stimulation (Cryan and Dinan, 2012). Alterations to the microbiota-gut-brain-axis are associated with the pathogenesis of neurologic and psychiatric disorders (Cryan and Dinan, 2012; Kim et al., 2015; Mohajeri et al., 2018; Peterson, 2020).

Several types of microorganisms inhibit space-ship environments (Siddiqui et al., 2021a). Earlier microbiome studies found that astronauts were passing *Staphylococcus aureus* to each other (Pierson et al., 1996). A more recent International Space Ship (ISS) found that alteration to the EGM of astronauts increased inflammatory markers (*Fusicatenibacter* was negatively associated with "pro-inflammatory cytokines IL-8, IL-1b, IL4, and TNFa," while genus *Dorea* was negatively correlated with cytokine IL-1b (Voorhies et al., 2019). It should be noted that studies have identified pro-inflammatory cytokines IL-8 and IL-1b as being implicated in higher risk of psychiatric pathologies (Tsai, 2021; Liu et al., 2022). In conclusion, the space environment increases the likelihood of EGM dysbiosis with subsequent risk of psychiatric disorders.

6 Circadian disruption during outer space missions and evolutionary mismatch

Like in other animals, human neurohormonal regulation is modulated by circadian rhythms. In humans, circadian rhythms regulate sleep/wake cycles, temperature, endocrine mechanisms, mental health, and wellbeing. Circadian synchronisation is an ancient adaptation to evolutionary environments in which the visceral neuroendocrine system (NS) was attuned to natural light fluctuations. In humans, the NS is regulated by a master biological clock (orchestrated by retinal, hypothalamic and reticular pathways), based on a 24 h cycle with light as the key zeitgeber (Anderson and Bradley, 2013). Any alteration of this circadian cycle (i.e., jetlag or shift workers) often leads to sleep disturbances or interruptions with subsequent reduced cognitive performance, tiredness, as well as higher risk for the onset of mental health problems (Anderson and Bradley, 2013).

Outer space represents a major mismatch for astronauts since they are removed from their evolutionary circadian environment. Astronautic sleep studies have identified that astronauts undergo sleep alteration due to circadian desychronisation, bright lighting, noisy internal spaceship environment, interior temperature, and sleeping bag discomfort (Arone et al., 2021; Marazziti et al., 2022). Even microgravity may diminish sleep duration (Gonfalone, 2016).

Analysis of sleep patterns of Shuttle crew members reported a 15% sleep reduction (Kelly et al., 2005), and 20 min less sleep during a 2-week mission relative to ground-based sleep (Barger et al., 2014). Consequently, due to insufficient additional light exposure in space, the 90-min light/dark cycle is disrupted eliciting homeostatic imbalance (Guo et al., 2014; Flynn-Evans et al., 2016; Wu et al., 2018). Despite NASA scheduling 8.5 h of sleep per night for crew members in space flight the average duration of sleep during space flight is just over 6 hours on Shuttle and ISS missions (Barger et al., 2014). Despite being allowed to sleep more hours astronauts still may have unproductive sleep quality (Flynn-Evans et al., 2016). Sleep alterations in astronauts are associated with increasing glucocorticoid secretion and inflammatory markers, memory and cognitive impairments, mood changes, altered relationship quality with crew members and reduced work performance (Chaumet et al., 2009).

Thus far, astronauts' major recourse for improved sleep has been taking sleeping drugs and melatonin. However, long term use of benzodiazepine derivative sleeping medications (e.g., zolpidem midazolam, flurazepam, temazepam) that are regularly prescribed to astronauts are associated with various adverse side effects such as reduced cognitive and motor performance, drowsiness, *etc.* (Maust et al., 2019). Despite this, one study found that 71% of spaceship crew members were using sleep medications to promote or preserve sleep (Wotring, 2015).

7 "Earth-out-of-view-phenomenon": neuro-behavioural risks of loss of connection with the natural world

Homo evolved in the natural world under intricate and on-going evolution. For tens of thousands of generations *Homo* evolved and adapted to various evolutionary environments which shaped its genome. The human body is an artefact of nature and exemplifies the complex gene/environment interplay. The entire emotional complex in *Homo*, both its neuro-hormonal substrates and psychosocial phenotypes were shaped and contoured by interaction with nature. In addition, the sensory perceptions which have been shaped by the natural world mediate our embodied awareness, which is

intrinsically intertwined with multiple life forms "whether we are conscious of this connection or not" (Abram, 1996). The idea that natural environments promote human wellbeing has received considerable scientific attention over the last 3 decades. Many of these studies suggest that immersion in the natural world has neuro-behavioural and psychosocial benefits, such as reduced blood pressure and stress, shorter post-operative hospital period, lower mental fatigue and fewer sick days taken off work (Bowler et al., 2010; Velarde et al., 2007). Other cited psychological benefits from natural environments are promotion of calmness (Heerwagen, 2009), mental health improvement (Gullone, 2000), reduction in anger and aggression (Groenewegen et al., 2006) and enhanced natural killer (NK) immune response (Li et al., 2008). The theoretical frameworks of many of the afore-mentioned studies are informed mainly by E.O. Wilson's "Biophilia Hypothesis" (2010), which argues that *Homo* has an innate preference for natural environments as a consequence of evolutionary history (Grinde and Patil, 2009).

The question remains that if psycho-somatic homeostasis is in some ways contingent on human/nature connection, what may be the mid to long term health consequences of astronauts stay in space? Will the evolutionary mismatch between the Gaian habitat and space lead to unknown health risks for future astronauts? Regarding physical health, some of these concerns have been addressed, and thus now regular exercise on board, recommendations for a balanced diet are common among astronauts, as well as sporadic leisure activities. However, much work still needs to be done on the psychological domain with long duration missions in perspective. On this note, some authors indicate that astronauts' psychological status could be disrupted as the vision of planet Earth becomes increasingly difficult (Kanas and Manzey, 2008; Ihle et al., 2006). Moreover, astronauts from previous space missions stated that observing the Earth was meaningful and a positive factor of space travel (Kanas, 2011). Many interviewed astronauts and cosmonauts stated that being in space endowed them with a feeling of unity with nature, awe and a sense of transcendence–synonymous with "the overview effect" (Opsina et al., 2007). Since the so called "Earth-out-of-view-phenomenon" is new to the human psyche (Kanas and Manzey, 2008), it could well exacerbate feelings of homesickness, isolation and monotony (Kanas, 2011), with possible adverse mental health risks during LTSM.

8 Reduced natural selection in outer space and potential psychiatric disorders

Evolutionary medicine makes special reference to mechanisms operating within natural selection in ancestral hominins, and how alterations in selection processes are having health consequences in extant humans. *Homo* evolved on Earth and has adapted to the terrestrial environment. During most of hominin history, our ancestors were subjected to predation, parasitic and infectious diseases, trauma and environmental changes which shaped our genotypes (Saniotis and Henneberg, 2011b). Natural selection controlled the ratio between fitness enhancing/fitness compromising genes *via* differential reproductive success, which favoured traits that gave adaptive and reproductive advantages (Saniotis and Henneberg, 2011b). It is only with the advent of the Industrial Revolution of the 19th century that natural selection became relaxed due to improvements in public sanitation, nutrition and medicine (Saniotis and Henneberg, 2011b). Although this meant that most individuals in developed countries could reach reproductive adulthood, greater dependence on human interventions meant that natural selection had less ability to eradicate harmful alleles from the human gene pool. (Saniotis et al., 2020; Henneberg, 2025). It has been speculated that natural selection in the developed world is currently operating at only <1% compared with ~50% prior to the Industrial Revolution (Saniotis and Henneberg, 2011b; Saniotis et al., 2020). Consequently, the proliferation of deleterious mutations may be leading to constrained fitness at a macro scale (Agrawal and Whitlock, 2012).

In outer space, humans are not only removed from the natural environment where natural selection operates–an evolutionary mismatch, but are entirely dependent on human technology and medical interventions to sustain them (Saniotis et al., 2016). (Figure 1).

Given that there is a strong correlation between relaxed selection and mutation load, we can anticipate that this process may continue in humans during LTSM and in permanent space colonies on the moon and Mars. Additionally, long term radiation exposure could increase the incidence of deleterious mutations (Horneck et al., 2010).

On this theme, we must consider the possibility of potential alterations in gene expression regarding neuro-hormonal regulation in outer space. Popova et al. (2020) state that we have just begun to examine the association between risk neurogenes and behavioural disorders during LTSM. Limited animal studies during spaceflight identify that serotonergic and dopaminergic metabolic pathways, as well as neurotrophic factors (GDNF, CDNF) - key regulators of neuroplasticity are all altered (Popova et al., 2020; Rappaport and Corbally, 2023). Serotonin and dopamine are involved in emotion, motivation, memory, learning, sleep and motor skills. Neuroanatomical changes to the substantia nigra, hypothalamus and striatum have also been identified–brain areas involved in endocrine regulation, mood, cognition and movement are also vulnerable during spaceflight (Popova et al., 2020). These preliminary results indicate characteristics that correspond with Spaceflight Neuroplastic Syndrome (Rappaport and Corbally, 2023). It should be noted that the reported changes in rodent brain neuroanatomy and neurohormonal regulation occurred after only 1 month in space (Popova et al., 2020). Rappaport and Corbally (2023) argue that, although hundreds of astronauts seem to have been shielded from similar deleterious neurological deficits (possibly due to a higher level of neuroplasticity), this does not discount the effect of relaxed natural selection conferring greater probability for risk neurogenes, especially to future permanent space colonies.

9 Evolutionary based countermeasures for reducing psychopathologies during LTSM

For several decades, a plethora of space research has been accumulated regarding the physiological/psychological responses of

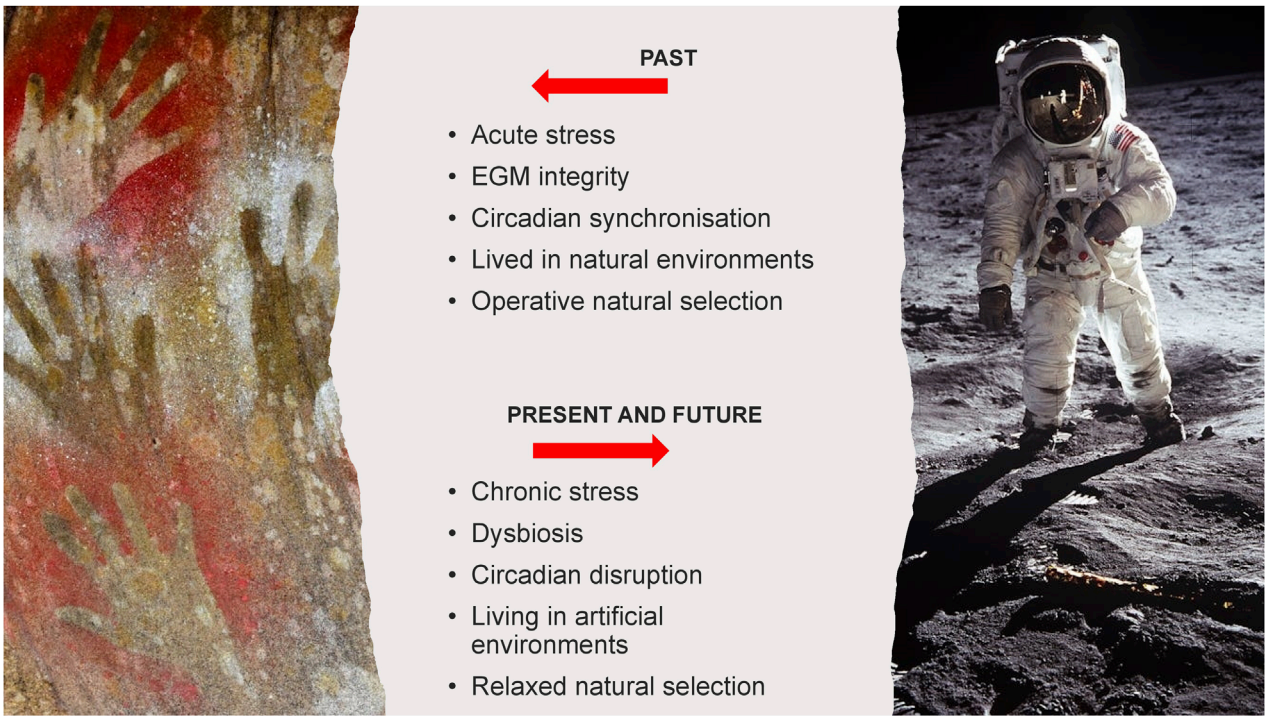

FIGURE 1
Types of evolutionary mismatch between past and extant/future humans.

astronauts during outer space missions. Thus far, scientists have been able to assess the health impact of astronauts, as well as the types of pre-mission acclimatising training necessary for alleviating exposure to the outer space environment (Criscuolo et al., 2020). Although humans have not adapted to living in outer space, it does not exclude that in the future, humans could be genetically engineered to better adapt to living in outer space for the long term. Human medical interventions have not only led to an unprecedented reduction in premature mortality since the 19th century, but are now preoccupied in developing techniques for artificially modifying the body at genetic and phenotypic levels (Saniotis and Henneberg, 2011b). We concur with Criscuolo et al. (2020) who point out that gene expression in outer space will have a major significance in the future evolution of permanent space colonists as we have suggested earlier regarding relaxation of natural selection. Due to psychiatric health issues that astronauts face, evolutionary medicine can provide various countermeasures for reducing the onset of psychopathologies and assisting astronauts' mental health during LTSM. We anticipate that the following countermeasures may benefit astronauts since they are based on evolutionary antecedents (Figure 2).

9.1 Use of mindfulness based intervention for astronauts

Various authors have proposed the use of yoga and mindfulness based intervention (MBI) as a therapeutic countermeasure reducing psychological side effects of astronauts during space missions (Vernikos, 2012; Saniotis et al., 2023; Le Roy et al., 2023). These techniques have been used for millennia in various cultures and function in stimulating parasympathetic response while reducing sympathetic induced stress reaction. It has been argued that meditational techniques are based on evolutionary antecedents such as neuro-hormonally regulated auto-hypnotic response to threat, which had been positively selected due to its fitness value (McClenon, 1997; Krippner, 2000; Winkelman, 2000; 2004; Saniotis and Henneberg, 2011b). It has also been noted that Upper Palaeolithic shamans may have used altered states of consciousness in order to reduce individual ailments, improve fertility and increase group cohesion (Winkelman, 2000; 2004). Since relaxation inducing techniques may reduce an individual's overall stress, this is important since astronauts have reported to have increasing stressors during LTSM (Marsh, 2007).

Mindfulness based intervention has been used in analog environments (Isolated and Confined Environments (ICE), Extreme and Unusual Environments (EUE)) with promising results in (i.e., better eating and sleeping habits, higher positive emotions states and lower negative emotions, reduced stress reactions) (Trousselard et al., 2010). Currently, more research needs to be conducted on whether MBI increases group cohesion among LTSM crew members or whether improving individual mindfulness has corresponding benefits at a group level (Le Roy et al., 2023). According to Saniotis et al. (2023), MBI is an inexpensive therapeutic technique that could be employed during pre-flight preparation and post-flight readaptation in order to assist astronauts' mental health.

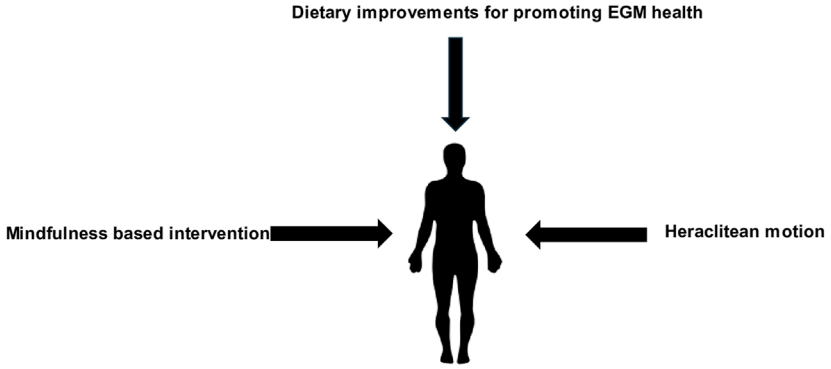

FIGURE 2
Evolutionary based countermeasures for reducing adverse mental health effects during LTSM.

9.2 New strategies for addressing EGM in LTSM

Given that the EGM is altered during space conditions (i.e., radiation, microgravity, reduced biodiversity) it is difficult to develop new strategies in order to maintain its "normal" function. We encourage the further use of *Lactobacillus* and *Bifidobacterium* strains in probiotic form due to their anti-depressant mechanisms (Yong et al., 2020; Johnson et al., 2021; Dicks, 2022). Consequently, reduction of these species in the EGM have been linked to psychiatric disorders (Johnson et al., 2023). These bacteria can be freeze-dried and used, as has been the case of the *Lactobacillus casei* strain, which was used for 1 month by astronauts on the International Space Station (ISS) with positive results in improving intestinal microbial balance and innate immunity (Bharindwal et al., 2023). Future research needs to be conducted on developing probiotics that enhance mental health in astronauts, including bacterial strains not mentioned in this paper.

Second, we suggest the administration of faecal microbiota transplantation (FMT) to astronauts in order to recolonise beneficial gut bacteria where ordinary probiotic use is not efficacious due to the effects of antibiotic induced gut dysbiosis, microgravity, stress and radiation. Faecal microbiota transplantation provides a potential therapy in treating gut dysbiosis and restoring beneficial microbiota with subsequent mental wellbeing in astronauts during LTSM (Gupta et al., 2016). However, long term clinical trials need to be conducted on astronauts during space flight in order to verify the feasibility of FMT.

Third, we endorse the prioritising of omega-3 polyunsaturated fatty acids (PUFAs) in astronauts' diets since they are critical to proper brain development and regulation. Human brain weight consists of approximately 50%–60% lipids, of which PUFAs account for 35% (Dighriri et al., 2022; Bos et al., 2016). Docosahexaenoic acid (DHA) is especially found in grey matter. It is well known that PUFAs are involved in numerous neuro-hormonal and cognitive processes (i.e., neurogenesis, neurotransmitter modulation, neuronal plasticity regulation, synthesis of neurotrophic factor BDNF) (Bednarik et al., 2022). Hominin intake of PUFAs increased during the Paleolithic period where the estimated ratio between omega-3 (α-linoleic acid) and omega-6 (linoleic acid) intake was ~1:1 (Roccisano et al., 2016). In contrast, the ratio between omega-6/omega-3 in the western diet is ~20:1. This difference is sufficient to increase the risk of psychiatric and neurological pathologies over time. For this reason, it is vital that astronauts maintain a healthy intake of PUFAs during LTSM.

9.3 Human space omics and personalised medicine

It is becoming clear that outer space has the potential to change gene expression which could affect metabolite synthesis and function across several neuro-physiological domains. As diverse human populations enter space natural selection will be further relaxed due to medical interventions and artificial conditions that will be necessary for humans to survive. We can only speculate to what extent gene-environment interaction may have in future gene expression of space travellers and colonists. For example, the enzyme Cytochrome P450 (CYP450), which is involved in~ 75% of drug metabolism and is considerably polymorphic, has shown alterations in some astronaut gene profiles (Rutter et al., 2024). Additionally, a contemporary pharmacogenetics study found that 24 out of 78 standard drugs available to astronauts on the ISS were not effectively metabolised in polymorphic enzymes due to gene variants (Stingl et al., 2015; Rutter et al., 2024). These findings point to possible "omic derived molecular changes" in astronauts during prolonged space flight (Cope et al., 2022; Willis et al., 2021), Other studies have examined proteomic alterations in astronauts post LTSM (Brzhozovskiy et al., 2019; Pastushkova et al., 2021). Consequently, omic profiling has been proposed as a medical countermeasure in storing and using genetic data of astronauts (Cope et al., 2022). Such genetic data sets could lead to the development of personalised medicine which would facilitate metagenomic based health monitoring of astronauts in future LTSM (Danko et al., 2020).

9.4 Incorporating Heraclitean motion and attention restoration for promoting mental wellbeing in astronauts

In an earlier section, it was noted that humans have an inherent connection with nature as a result of their evolutionary

history. It is an indisputable fact that human corporeality is rooted in sensuous engagement with the natural world, the latter operating as the inherent template for human biological and social processes (Saniotis et al., 2016). The loss of interaction with the natural world in outer space which has been referred to as "Earth-out-of-view-phenomenon" may have possible consequences in increasing psychopathologies especially during LTSM. We propose that developing relevant therapies to counter this problem should be based on the "Attention Restoration Hypothesis" which postulates that natural environments may provide temporary psychological relief from demanding cognitive routines that require high attention levels, such as various tasks performed by astronauts. Thus, short-term involvement in natural environments may reduce "depleted attentional resources" (Atchley et al., 2012). It has been identified that restoration occurs in the pre-frontal cortex, which regulates executive functions while also modulating hypothalamic-pituitary-adrenal axis (HPA) stress response (Winkelman, 2000; Saniotis et al., 2016).

Linked to attention restoration is the idea of "Heraclitean motion" which refers to environmental phenomena that are both static yet changing (i.e., fire, clouds, ocean, fish in an aquarium, fountains) (Katcher and Wilkins, 1993). According to some authors, the act of viewing phenomena that manifest Heraclitean motion produces a self-hypnotic state in the viewer after a few minutes (Saniotis et al., 2016). The relatively easy ability for humans to enter into self-hypnotic states was probably positively selected by natural selection since such states conferred ancestral hominins with reduced stress response to threat and induced relaxation which increased fertility and emotional wellbeing (McClenon, 1997; Saniotis and Henneberg, 2011a). Moreover, ancestral hominins may have gazed into fires which may have contributed to the evolution of cognitive abilities such as increased attention span, which is a hallmark of *Homo*. On this note, fire gazing was probably one of several behavioural and morphological characteristics which ancestral hominins were undergoing that were a result of self-amplifying feedback mechanisms probably starting already in the Miocene (Henneberg and Eckhardt, 2022; Henneberg, 2025). For example, the extant practice of fire gazing (*tatraka*) that has been practiced for centuries in India has been suggested to increase focus and attention, cognitive performance and mental relaxation (Kumar, 2010; Raghavendra and Singh, 2016; Chundawat and Panda, 2023).

We posit that effects of Heraclitean motion *via* prolonged exposure to the natural world may induce attention restoration. As Saniotis et al. (2016) note:

While more empirical studies are needed in testing the viability of Heraclitean motion in relation to astronauts, it seems likely that Heraclitean motion may improve individual resilience, especially in sensorially monotonous and enclosed environments such as spaceships.

1. We speculate that Heraclitean motion can be employed *via* the use of virtual reality (VR) technology that would provide images of natural environments to astronauts. Virtual reality technology could be employed at specified times during astronauts'work cycles as a way of restoring attentional resources, as well as countering the "Earth-out-of-view-phenomenon" in "home sick' individuals. The use of VR as a countermeasure for the "Earth-out-of-view-phenomenon" has been identified by Gushin et al. (2021).
2. In the near future, holographic technology (HT) may also incorporate 3D natural environments in different parts of the space craft in order to restore attention resources and foster connection with the Earth. Thus far, holographic teleportation has been successfully employed in teleporting members that have been projected virtually on the International Space Station (Llaca and Davidson, 2023). It is anticipated that as HT improves, specific natural environments could be projected in various areas of spacecraft accompanied by sounds and smells of the respective nature-based holographs. The combination of visual, auditory and olfactory-based holographic natural environments would provide a more realistic experience of natural scenes, as well as necessary sensorial stimulation for countering the claustrophobic and tedious spaceship ambience. It is also feasible to suggest that holographs combining the sights, sounds and smells of nature could act as:
    1) an important sleeping aid for astronauts
    2) increase psychological wellbeing by reducing stress induced glucocorticoids and maintaining healthy neuro-hormonal regulation in astronauts.
3. Due to the significant musculoskeletal deterioration effects of microgravity, astronauts are required to exercise for approximately 2 hours per day using stationary bicycles or treadmills (Braddock, 2018). Although exercise fills a mandatory part in astronauts' waking hours, this regime can be monotonous and boring. In the future, VR or HT can be employed during exercise programs where astronauts move through nature simulations (including sounds and smells of natural landscapes as well as flora and fauna). Such simulations would be designed to integrate executive, motor, sensory and limbic regions, thus providing cognitive, sensorial and emotional experiences for astronauts with subsequential neuroprotective and mental health benefits.

9.5 The problem of consciousness

Astronauts are highly educated and very intelligent people. Therefore, they may realise that their exposure to technologically created Earth environments is artificial. This realisation may interfere with them relaxing and restoring their attention. They may become stressed by what they will perceive as "fake" natural environments, especially that those may present them with repeated, like a broken record, experiences. During a space flight, there are real opportunities for observing Heraclitean motions–the slowly rotating view of the surrounding universe and of pondering details of the actual living environment that, although being a technological construct, is comprised of natural chemical compounds–plastics, metals, textiles, *etc.* Introducing astronauts to the acceptance of their immediate environment as a part of the nature may help in their personal adaptation to their unusual lifestyle. A spaceship consists of atoms linked in various ways to produce its structure. The ship moves through the space that contains the Earth and other objects. These objects move in regular ways that inform a rhythm of observing them. The schedule of human activities aboard

a spaceship also has its rhythm, that, though artificial, is also informed by the biological requirements of human bodies–sleep, meals, exercise, relaxation, work. A spaceflight is a natural portion of the universal world where feedbacks between human needs and activities and their surroundings occur in ways somewhat different from the past evolutionary experience, but essentially the same systemic interactions among humans and their surroundings.

9.6 Peri anthropon: natural selection and humans in outer space

It is more than likely that human beings born in space stations over several generations will undergo changes in their genome resulting from altered mutation/selection balance. Some space environments may be mutagenic due to different from the Earth levels of radiation. Spontaneous mutations occur on Earth at high rates. The human germline mutation rate is approximately 1.2×10^{-8} per nucleotide per generation (Wood and Goriely, 2022).

Operation of natural selection in space stations/colonies will be strongly relaxed due to the availability of medical technologies and artificial living conditions. Thus, the accumulation of even mildly deleterious mutations over generations may lead to genetic load, which is evident in extant human populations (Saniotis et al., 2020; You and Henneberg, 2016; 2017; You et al., 2022). Allelic changes may occur faster in more mutagenic environments.

Although the operation of natural selection will be largely relaxed, some extreme effects of changed environments may affect the reproductive fitness of some colonists, thus leading to microevolutionary adaptations to particular space environments. Possible effects of inbreeding resulting from small effective population size, pressures of gravity, radiation and magnetic fields may trigger mutational variants causing neuro-neurobehavioural changes in ways that we do not yet fully understand.

Notwithstanding medical and dietary interventions in ensuring healthy gut microbiomes in astronauts and future space station colonists, relaxed natural selection will probably reduce microbiota variability with subsequent alterations in neuro-hormonal/neuro-trophic regulation and the growth of gut derived neurotransmitters. On this theme, Silva et al. (2023) note that changes to the gut microbiome will likely occur in response to the lack of exposure to widely varied microbiota colonies found in terrestrial environments (Silva et al., 2023).

As noted in numerous space studies, changes in gravity during space missions exert fundamental changes to astronauts' bodies. The influence of gravity is significantly marked in growing offspring. Growth plates of human bones respond to mechanical forces acting on them (Alonso et al., 2022). Thus, children growing in an environment of lower force of gravity may have their growth disturbed in one way, e.g., growing very tall, while those growing under greater than Earth's force of gravity will have growth disturbed in a different way, e.g., being very short and stocky. Concomitantly, gravity also affects muscle growth that is dependent on mechanical loads during their use. This, in turn contributes to proprioceptive sensory nerve signals from the musculoskeletal apparatus and motor signals to muscles which probably influence cognition. On this point, it has been speculated that motor neural circuits are implicated in thinking and cognition (Pilacinski et al., 2025; Baladron and Hamker, 2024). Therefore, voluntary muscular control, involuntary reflexes and cognitive abilities in inter-generational space station colonists could evolve differently from humans on Earth.

10 Conclusion

This paper has aimed to improve our understanding of the neuro-behavioural challenges which current astronauts face, as well as future astronauts and space colonists, from an evolutionary perspective. Evolutionary medicine has yet to be used as an explanatory model for addressing possible adverse mental health effects of humans during LTSM. This oversight needs to be corrected due to the increasing investment by space agencies and national governments in outer space exploration. Due to the evolutionary mismatches currently confronting astronauts' mental health, this paper has discussed novel therapeutic countermeasures based on evolutionary principles for reducing adverse mental effects on astronauts and future space colonists. As we are still at a pioneering stage in space exploration the development of mental health strategies which privilege evolutionary principles will improve our current knowledge of bioastronautics.

Data availability statement

The original contributions presented in the study are included in the article/supplementary material, further inquiries can be directed to the corresponding author.

Author contributions

AS: Conceptualization, Validation, Writing – original draft, Writing – review and editing. MH: Validation, Writing – original draft, Writing – review and editing. KM: Writing – original draft, Writing – review and editing.

Funding

The author(s) declare that no financial support was received for the research and/or publication of this article.

Conflict of interest

The authors declare that the research was conducted in the absence of any commercial or financial relationships that could be construed as a potential conflict of interest.

Generative AI statement

The author(s) declare that no Generative AI was used in the creation of this manuscript.

Publisher's note

References

Abram, D. (1996). *The spell of the sensuous: perception and language in a more-than-human world*. 1st ed. New York: Pantheon Books.

Adams, G. R., Caiozzo, V. J., and Baldwin, K. M. (2003). Skeletal muscle unweighting: spaceflight and ground-based models. *J. Appl. Physiol.* 95 (6), 2185–2201. doi:10.1152/japplphysiol.00346.2003

Agrawal, A. F., and Whitlock, M. C. (2012). Mutation load: the fitness of individuals in populations where deleterious alleles are abundant. *Annu. Rev. Ecol. Evol. Syst.* 43 (1), 115–135. doi:10.1146/annurev-ecolsys-110411-160257

Aiello, L. C., and Wheeler, P. (1995). The expensive-tissue hypothesis: the brain and the digestive system in human and primate evolution. *Curr. Anthropol.* 36 (2), 199–221. doi:10.1086/204350

Alcock, J., Maley, C. C., and Aktipis, C. A. Is eating behavior manipulated by the gastrointestinal microbiota? Evolutionary pressures and potential mechanisms. *BioEssays* (2014) 36, 940–949. doi:10.1002/bies.201400071

Aleman, F. D. D., and Valenzano, D. R. (2019). Microbiome evolution during host aging. *PLoS Pathog.* 15 (7), e1007727. doi:10.1371/journal.ppat.1007727

Alonso, G., Yawny, A., and Bertolino, G. (2022). How do bones grow? A mathematical description of the mechanobiological behavior of the epiphyseal plate. *Biomechanics Model. Mechanobiol.* 21 (5), 1585–1601. doi:10.1007/s10237-022-01608-y

Anderson, K., and Bradley, A. J. (2013). Sleep disturbance in mental health problems and neurodegenerative disease. *Nat. Sci. Sleep* 5, 61–75. doi:10.2147/NSS.S34842

Arone, A., Ivaldi, T., Loganovsky, K., Palermo, S., Parra, E., Flamini, W., et al. (2021). The burden of space exploration on the mental health of astronauts: a narrative review. *Clin. Neuropsychi* 18 (5), 237–246. doi:10.36131/cnfioritieditore20210502

Atchley, R. A., Strayer, D. L., and Atchley, P. (2012). Creativity in the wild: improving creative reasoning through immersion in natural settings. *PLoS One* 7 (12), e51474. doi:10.1371/journal.pone.0051474

Baladron, J., and Hamker, F. H. (2024). Re-thinking the organization of cortico-basal ganglia-thalamo-cortical loops. *Cogn. Comput.* 16 (5), 2405–2410. doi:10.1007/s12559-023-10140-9

Barger, L. K., Flynn-Evans, E. E., Kubey, A., Walsh, L., Ronda, J. M., Wang, W., et al. (2014). Prevalence of sleep deficiency and use of hypnotic drugs in astronauts before, during, and after spaceflight: an observational study. *Lancet Neurol.* 13 (9), 904–912. doi:10.1016/S1474-4422(14)70122-X

Bednarik, R. G., Saniotis, A., and Henneberg, M. (2022). Auto-domestication hypothesis and the rise in mental disorders in modern humans. *Med. Hypothe.* 164, 110874. doi:10.1016/j.mehy.2022.110874

Beeson, C., and Kosal, E. (2023). Evolutionary medicine. *Am. Biol. Teach.* 85 (2), 80–84. doi:10.1525/abt.2023.85.2.80

Bharindwal, S., Goswami, N., Jha, P., Pandey, S., and Jobby, R. (2023). Prospective use of probiotics to maintain astronaut health during spaceflight. *Life* 13 (3), 727. doi:10.3390/life13030727

Blaser, M. J., and Falkow, S. (2009). What are the consequences of the disappearing human microbiota? *Nat. Rev. Microbiol.* 7 (12), 887–894. doi:10.1038/nrmicro2245

Bos, D. J., van Montfort, S. J., Oranje, B., Durston, S., and Smeets, P. A. (2016). Effects of omega-3 polyunsaturated fatty acids on human brain morphology and function: what is the evidence? *Eur. Neuropsychopharmacol.* 26 (3), 546–561. doi:10.1016/j.euroneuro.2015.12.031

Bowler, D. E., Buyung-Ali, L. M., Knight, T. M., and Pullin, A. S. (2010). A systematic review of evidence for the added benefits to health of exposure to natural environments. *BMC Public Health* 10 (1), 456. doi:10.1186/1471-2458-10-456

Braddock, M. (2018). Exercise and ergonomics on the international apace station and orion spacecraft. *J Ergon Res* 1, 2. doi:10.4172/JEOR.1001104

Brzhozovskiy, A. G., Kononikhin, A. S., Pastushkova, L. C., Kashirina, D. N., Indeykina, M. I., Popov, I. A., et al. (2019). The effects of spaceflight factors on the human plasma proteome, including both real space missions and ground-based experiments. *Int. J. Mol. Sci.* 20, 3194. doi:10.3390/ijms20133194

Chaumet, G., Taillard, J., Sagaspe, P., Pagani, M., Dinges, D. F., Pavy-Le-Traon, A., et al. (2009). Confinement and sleep deprivation effects on propensity to take risks. *Aviat. Space, Environ. Med.* 80 (2), 73–80. doi:10.3357/ASEM.2366.2009

Chundawat, A., and Panda, S. K. (2023). Tratak and its benefits: a review. *J. Ayurveda Integr. Med. Sci.* 8 (5), 61–65. doi:10.21760/jaims.8.5.10

Conrad, C. D. (2008). Chronic stress-induced hippocampal vulnerability: the glucocorticoid vulnerability hypothesis. *Rev. Neurosci.* 19 (6), 395–411. doi:10.1515/REVNEURO.2008.19.6.395

Conrad, C. D., LeDoux, J. E., Magariños, A. M., and McEwen, B. S. (1999). Repeated restraint stress facilitates fear conditioning independently of causing hippocampal CA3 dendritic atrophy. *Behav. Neurosci.* 113 (5), 902–913. doi:10.1037/0735-7044.113.5.902

Cope, H., Willis, C. R. G., MacKay, M. J., Rutter, L. A., Toh, L. S., Williams, P. M., et al. (2022). Routine omics collection is a golden opportunity for European human research in space and analog environments. *Patterns (N Y)* 3 (10), 100550. doi:10.1016/j.patter.2022.100550

Criscuolo, F., Sueur, C., and Bergouignan, A. (2020). Human adaptation to deep space environment: an evolutionary perspective of the foreseen interplanetary exploration. *Front. Public Health* 8, 119. doi:10.3389/fpubh.2020.00119

Cryan, J. F., and Dinan, T. G. (2012). Mind-altering microorganisms: the impact of the gut microbiota on brain and behaviour. *Nat. Rev. Neurosci.* 13 (10), 701–712. doi:10.1038/nrn3346

Cucinotta, F. A., and Durante, M. (2006). Cancer risk from exposure to galactic cosmic rays: implications for space exploration by human beings. *Lancet Oncol.* 7 (5), 431–435. doi:10.1016/S1470-2045(06)70695-7

Danko, D. C., Singh, N., Butler, D. J., Mozsary, C., Jiang, P., Keshavarzian, A., et al. (2020). Genetic and immunological evidence for microbial transfer between the international space station and an astronaut. *bioRxiv*, 1–24. doi:10.1101/2020.11.10.376954

Davenport, E. R., Sanders, J. G., Song, S. J., Amato, K. R., Clark, A. G., and Knight, R. (2017). The human microbiome in evolution. *BMC Biol.* 15 (1), 127. doi:10.1186/s12915-017-0454-7

Davidson, G. L., Cooke, A. C., Johnson, C. N., and Quinn, J. L. (2018). The gut microbiome as a driver of individual variation in cognition and functional behaviour. *Philosoph. Trans. R. Soc. B Biol. Sci.* 373 (1756), 20170286. doi:10.1098/rstb.2017.0286

De Kloet, E. R. (2004). Hormones and the stressed brain. *Ann. N. Y. Acad. Sci.* 1018 (1), 1–15. doi:10.1196/annals.1296.001

De Kloet, E. R., Joëls, M., and Holsboer, F. (2005). Stress and the brain: from adaptation to disease. *Nat. Rev. Neurosci.* 6 (6), 463–475. doi:10.1038/nrn1683

De La Torre, G. G., van Baarsen, B., Ferlazzo, F., Kanas, N., Weiss, K., Schneider, S., et al. (2012). Future perspectives on space psychology: recommendations on psychosocial and neurobehavioural aspects of human spaceflight. *Acta Astronaut.* 81 (2), 587–599. doi:10.1016/j.actaastro.2012.08.013

Desbonnet, L., Garrett, L., Clarke, G., Bienenstock, J., and Dinan, T. G. (2008). The probiotic Bifidobacteria infantis: an assessment of potential antidepressant properties in the rat properties in the rat. *J. Psychiatr. Res.* 43, 164–174. doi:10.1016/j.jpsychires

Dicks, L. M. T. (2022). Gut bacteria and neurotransmitters. *Microorganisms* 10 (9), 1838. doi:10.3390/microorganisms10091838

Dighriri, I. M., Alsubaie, A. M., Hakami, F. M., Hamithi, D. M., Alshekh, M. M., Khobrani, F. A., et al. (2022). Effects of omega-3 polyunsaturated fatty acids on brain functions: a systematic review. *Cureus* 14, e30091. [Preprint]. doi:10.7759/cureus.30091

Dolgova, O. (2021). Evolutionary medicine. *eLS* 2 (10), 1–8. doi:10.1002/9780470015902.a0028794

Fitts, R. H., Riley, D. R., and Widrick, J. J. (2001). Functional and structural adaptations of skeletal muscle to microgravity. *J. Exp. Biol.* 204 (18), 3201–3208. doi:10.1242/jeb.204.18.3201

Flynn-Evans, E. E., Barger, L. K., Kubey, A. A., Sullivan, J. P., and Czeisler, C. A. (2016). Circadian misalignment affects sleep and medication use before and during spaceflight. *NPJ Microgr.* 2 (1), 15019. doi:10.1038/npjmgrav.2015.19

Garrett-Bakelman, F. E., Darshi, M., Green, S. J., Gur, R. C., Lin, L., Macias, B. R., et al. (2019). The NASA Twins Study: a multidimensional analysis of a year-long human spaceflight. *Science* 364 (6436), eaau8650. doi:10.1126/science.aau8650

Ghlichloo, I., and Gerriets, V. (2023). "Nonsteroidal anti-inflammatory drugs (NSAIDs)," in *StatPearls [Internet]*. Treasure Island, FL: StatPearls Publishing.

Gonfalone, A. (2016). Sleep on manned space flights: zero gravity reduces sleep duration. *Pathophysiology* 23 (4), 259–263. doi:10.1016/j.pathophys.2016.08.003

Grinde, B., and Patil, G. G. (2009). Biophilia: does visual contact with nature impact on health and well-being? *Int. J. Environ. Res. Public Health* 6 (9), 2332–2343. doi:10.3390/ijerph6092332

Groenewegen, P. P., van, den, Berg, A. E., de Vries, S., and Verheij, R. A. (2006). Vitamin G: effects of green space on health, well-being, and social safety. *BMC Public Health* 6 (1), 149. doi:10.1186/1471-2458-6-149

Gullone, E. (2000). The biophilia hypothesis and life in the 21st century: increasing mental health or increasing pathology? *J. Happiness Stud.* 1 (3), 293–322. doi:10.1023/A:1010043827986

Guo, J.-H., Qu, W. M., Chen, S. G., Chen, X. P., Lv, K., Huang, Z. L., et al. (2014). Keeping the right time in space: importance of circadian clock and sleep for physiology and performance of astronauts. *Mil. Med. Res.* 1 (1), 23. doi:10.1186/2054-9369-1-23

Gupta, S., Allen-Vercoe, E., and Petrof, E. O. (2016). Fecal microbiota transplantation: in perspective. *Ther. Adv. Gastroenterol.* 9 (2), 229–239. doi:10.1177/1756283X15607414

Gushin, V., Ryumin, O., Karpova, O., Rozanov, I., Shved, D., and Yusupova, A. (2021). Prospects for psychological supportin interplanetary expeditions. *Front. Physiol.* 12, 750414. doi:10.3389/fphys.2021.750414

Hartmann, A., Schütz, H. J., Alberti, E., Schreckenberger, F., Loew, D., and Dýcka, J. (1977). Effects of a new diuretic on cerebrospinal fluid pressure in patients with supratentorial tumors. *Arch. Psychiatr. Nervenkr* 224, 351–360. doi:10.1007/BF00341617

Hawks, J., Wang, E. T., Cochran, G. M., Harpending, H. C., and Moyzis, R. K. (2007). Recent acceleration of human adaptive evolution. *Proc. Natl. Acad. Sci. U. S. A.* 104 (52), 20753–20758. doi:10.1073/pnas.0707650104

Heerwagen, J.(2009). Biophilia, health and well-being. In: restorative commons: Creating health and well-being through urban landscapes, 39–57.

Henneberg, M. (1988). Decrease of human skull size in the Holocene. *Hum. Biol.* 60, 395–405.

Henneberg, M. (1998). Evolution of the human brain: is bigger better. *Exp. Clin. Pharmacol.* 25, 745–749. doi:10.1111/j.1440-1681.1998.tb02289.x

Henneberg, M. (2025). *Our one human family. A story of continuing evolution*. New York: NOVA Publishers.

Henneberg, M., and Eckhardt, R. B. (2022). Evolution of modern humans is a result of self-amplifying feedbacks beginning in the Miocene and continuing without interruption until now. *Anthropol. Rev.* 85 (1), 77–83. doi:10.18778/1898-6773.85.1.05

Henneberg, M., Sarafis, V., and Mathers, K. (1998). Human adaptations to meat eating. *Hum. Evol.* 13 (3), 229–234. Available online at: https://www.jstor.org/stable/41464021. doi:10.1007/BF02436507

Henneberg, M., and Steyn, M. (1993). Trends in cranial capacity and cranial index in Subsaharan Africa during the Holocene. *Am. J. Hum. Biol.* 5 (4), 473–479. doi:10.1002/ajhb.1310050411

Horneck, G., Klaus, D. M., and Mancinelli, R. L. (2010). Space microbiology. *Microbiol. Mol. Biol. Rev.* 74 (1), 121–156. doi:10.1128/MMBR.00016-09

Huang, A. S., Stenger, M. B., and Macias, B. R. (2019). Gravitational influence on intraocular pressure: implications for spaceflight and disease. *J. Glaucoma* 28, 756–764. doi:10.1097/IJG.0000000000001293

Ihle, E. C., Ritsher, J. B., and Kanas, N. (2006). Positive psychological outcomes of spaceflight: an empirical study. *Aviat. Space, Environ. Med.* 77, 93–101.

Itan, Y., Powell, A., Beaumont, M. A., Burger, J., and Thomas, M. G. (2009). The origins of lactase persistence in Europe. *PLoS Comput. Biol.* 5 (8), e1000491. doi:10.1371/journal.pcbi.1000491

Johnson, D., Letchumanan, V., Thum, C. C., Thurairajasingam, S., and Lee, L. H. (2023). A microbial-based approach to mental health: the potential of probiotics in the treatment of depression. *Nutrients* 15 (6), 1382. doi:10.3390/nu15061382

Johnson, D., Thurairajasingam, S., Letchumanan, V., Chan, K. G., and Lee, L. H. (2021). Exploring the role and potential of probiotics in the field of mental health: major depressive disorder. *Nutrients* 13 (5), 1728. doi:10.3390/nu13051728

Kanas, N. (1985). Psychosocial factors affecting simulated and actual space missions. *Aviat. Space, Environ. Med.* 56, 806–811.

Kanas, N. (1987). Psychological and interpersonal issues in space. *Am. J. Psychiatry* 144 (6), 703–709. doi:10.1176/ajp.144.6.703

Kanas, N. (2011). From Earth's orbit to the outer planets and beyond: psychological issues in space. *Acta Astronaut.* 68 (5–6), 576–581. doi:10.1016/j.actaastro.2010.04.012

Kanas, N., and Manzey, D. (2008). *Space psychology and psychiatry*. 2nd ed. El Segundo, California, and Springer Dordrecht, Netherlands: Microcosm Press.

Katcher, A., and Wilkins, G. (1993). "Dialogue with animals: its nature and culture," in *The biophilia hypothesis*. Editors S. R. Kellert, and E. O. Wilson (Covelo, California: Island Press), 173–197.

Keller, M. C. (2008). The evolutionary persistence of genes that increase mental disorders risk. *Curr. Dir. Psychol. Sci.* 17 (6), 395–399. doi:10.1111/j.1467-8721.2008.00613.x

Kelly, T. H., Hienz, R. D., Zarcone, T. J., Wurster, R. M., and Brady, J. V. (2005). Crewmember performance before, during, and after spaceflight. *J. Exp. Analysis Behav.* 84 (2), 227–241. doi:10.1901/jeab.2005.77-04

Kim, E. J., Pellman, B., and Kim, J. J. (2015). Stress effects on the hippocampus: a critical review. *Learn. Mem.* 22 (9), 411–416. doi:10.1101/lm.037291.114

Kim, N., Yun, M., Oh, Y. J., and Choi, H. J. (2018). Mind-altering with the gut: modulation of the gut-brain axis with probiotics. *J. Microbiol.* 56 (3), 172–182. doi:10.1007/s12275-018-8032-4

Kozlovskaya, I. B., Kreidich, Y. V., Oganov, V. S., and Koserenko, O. P. (1981). Pathophysiology of motor functions in prolonged manned space flights. *Acta Astronaut.* 8 (9–10), 1059–1072. doi:10.1016/0094-5765(81)90079-5

Krippner, S. (2000). The epistemology and technologies of shamanic states of consciousness. *J. Conscious. Stud.* 7 (11–12), 93–118.

Kumar, V. (2010). The effect of tratakaon mental relaxation through - E. E.G. *Yoga* XLII (2), 97–102.

Le Roy, B., Martin-Krumm, C., and Trousselard, M. (2023). Mindfulness for adaptation to analog and new technologies emergence for long-term space missions. *Front. Space Technol.* 4, 1109556. doi:10.3389/frspt.2023.1109556

Ley, R. E., Peterson, D. A., and Gordon, J. I. (2006). Ecological and evolutionary forces shaping microbial diversity in the human intestine. *Cell* 124 (4), 837–848. doi:10.1016/j.cell.2006.02.017

Li, J., Mookerjee, B., Singh, P., and Wagner, J. L. (2008). Generation of bkv-specific t cells for adoptive therapy against bkv nephropathy. *Virology Res. Treat.* 1. VRT.S942. doi:10.4137/VRT.S942

Liao, W. H., Henneberg, M., and Langhans, W. (2016)Immunity-based evolutionary interpretation of diet-induced thermogenesis, *Cell Metab.* 23: 971–979. doi:10.1016/j.cmet.2016.05.002

Liu, X., Huang, J., Jiang, Y., Cao, Z., Wu, M., Sun, R., et al. (2022). IL-6 and IL-8 are likely associated with psychological status in treatment naïve general population. *J. Affect. Disord.* 298, 337–344. doi:10.1016/j.jad.2021.10.042

Llaca, F. D. L. P., and Davidson, P. L. (2023). Holographic teleportation in space and astronauts' stress: a Delphi study. *Sci. Talks* 6 (2), 100228. doi:10.1016/j.sctalk.2023.100228

Lloyd-Price, J., Abu-Ali, G., and Huttenhower, C. (2016). The healthy human microbiome. *Genome Med.* 8, 51. doi:10.1186/s13073-016-0307-y

Mader, T. H., Gibson, C. R., Pass, A. F., Kramer, L. A., Lee, A. G., Fogarty, J., et al. (2011). Optic disc edema, globe flattening, choroidal folds, and hyperopic shifts observed in astronauts after long-duration space flight. *Ophthalmology* 118 (10), 2058–2069. doi:10.1016/j.ophtha.2011.06.021

Mann, N. (2007). Meat in the human diet: an anthropological perspective. *Nutr. Dietet.* 64 (s4). doi:10.1111/j.1747-0080.2007.00194.x

Marazziti, D., Arone, A., Ivaldi, T., Kut, s K., and Loganovsky, K. (2022). Space missions: psychological and psychopathological issues. *CNS Spectrums* 27 (5), 536–540. doi:10.1017/S1092852921000535

Marsh, M. S. (2007). Identification of psychological stressors for long duration space missions: psychological stressors among five astronauts and cosmonauts. *Theses Diss.* 754. Available online at: https://commons.und.edu/theses/754.

Maust, D. T., Lin, L. A., and Blow, F. C. (2019). Benzodiazepine use and misuse among adults in the United States. *Psychiatr. Serv.* 70 (2), 97–106. doi:10.1176/appi.ps.201800321

McClenon, J. (1997). Shamanic healing, human evolution, and the origin of religion. *J. Sci. Study Relig.* 36 (3), 345. doi:10.2307/1387852

Mehare, A., Chakole, S., and Wandile, B. (2024). Navigating the unknown: a comprehensive review of spaceflight-associated neuro-ocular syndrome. *Cureus* 16 (2), e53380. doi:10.7759/cureus.53380

Mekel-Bobrov, N., Gilbert, S. L., Evans, P. D., Vallender, E. J., Anderson, J. R., Hudson, R. R., et al. (2005). Ongoing adaptive evolution of *aspm*, a brain size determinant in *homo sapiens*. *Science* 309 (5741), 1720–1722. doi:10.1126/science.1116815

Moeller, A. H., Li, Y., Mpoudi Ngole, E., Ahuka-Mundeke, S., Lonsdorf, E. V., Pusey, A. E., et al. (2014). Rapid changes in the gut microbiome during human evolution. *Proc. Natl. Acad. Sci. U. S. A.* 111 (46), 16431–16435. doi:10.1073/pnas.1419136111

Mohajeri, M. H., La Fata, G., Steinert, R. E., and Weber, P. (2018). Relationship between the gut microbiome and brain function. *Nutr. Rev.* 76, 481–496. doi:10.1093/nutrit/nuy009

Montiel-Castro, A. J., González-Cervantes, R. M., Bravo-Ruiseco, G., and Pacheco-López, G. (2013). The microbiota-gut-brain axis: neurobehavioral correlates, health and sociality. *Front. Integr. Neurosci.* 7, 70. doi:10.3389/fnint.2013.00070

Mortazavi, S. M. J., Said-Salman, I., Mortazavi, A. R., El Khatib, S., and Sihver, L. (2024). How the adaptation of the human microbiome to harsh space environment can determine the chances of success for a space mission to Mars and beyond. *Front. Microbiol.* 14, 1237564. doi:10.3389/fmicb.2023.1237564

Natterson-Horowitz, B., Aktipis, A., Fox, M., Gluckman, P. D., Low, F. M., Mace, R., et al. (2023). The future of evolutionary medicine: sparking innovation in biomedicine and public health. *Front. Sci.* 1, 997136. doi:10.3389/fsci.2023.997136

Nesse, R. M., and Williams, G. C. (2012). *Why we get sick: the new science of Darwinian medicine*. New York: Vintage Books.

Nucci, C., Martucci, A., Giannini, C., Morrone, L. A., Bagetta, G., and Mancino, R. (2018). Neuroprotective agents in the management of glaucoma. *Eye* 32, 938–945. doi:10.1038/s41433-018-0050-2

Odamaki, T., Kato, K., Sugahara, H., Hashikura, N., Takahash, S., Xiao, J. Z., et al. (2016). Age-related changes in gut microbiota composition from newborn to centenarian: a cross-sectional study. *BMC Microbiol.* 16 (1), 90. doi:10.1186/s12866-016-0708-5

O'Hara, A. M., and Shanahan, F. (2006). The gut flora as a forgotten organ. *EMBO Rep.* 7 (7), 688–693. doi:10.1038/sj.embor.7400731

Ong, J., Tarver, W., Brunstetter, T., Mader, T. H., Gibson, C. R., Mason, S. S., et al. (2023). Spaceflight associated neuro-ocular syndrome: proposed pathogenesis, terrestrial analogues, and emerging countermeasures. *Br. J. Ophthalmol.* 107 (7), 895–900. doi:10.1136/bjo-2022-322892

Opsina, M. B., Bond, K., Karkhaneh, M., Tjosvold, L., Vandermeer, B., Yuanyuan Liang, Y., et al. (2007). Meditation practices for health: state of the research. *Evid. Rep. Technol. Assess. (Full Rep.)* 155, 1–263.

Ortiz, J. B., and Conrad, C. D. (2018). The impact from the aftermath of chronic stress on hippocampal structure and function: is there a recovery? *Front. Neuroendocrinol.* 49, 114–123. doi:10.1016/j.yfrne.2018.02.005

Paez, M. Y., Mudie, L. I., and Subramanian, P. S. (2020). Spaceflight associated neuro-ocular syndrome (SANS): a systematic review and future directions. *Eye Brain* 19 (12), 105–117. doi:10.2147/EB.S234076

Pastushkova, L. K., Rusanov, V. B., Goncharova, A. G., Nosovskiy, A. M., Luchitskaya, E. S., Kashirina, D. N., et al. (2021). Blood plasma proteins associated with heart rate variability in cosmonauts who have completed long-duration space missions. *Front. Physiol.* 12, 760875. doi:10.3389/fphys.2021.760875

Perry, G. H. (2021). Evolutionary medicine. *eLife* 10, e69398. doi:10.7554/eLife.69398

Perry, G. H., Dominy, N. J., Claw, K. G., Lee, A. S., Fiegler, H., Redon, R., et al. (2007). Diet and the evolution of human amylase gene copy number variation. *Nat. Genet.* 39 (10), 1256–1260. doi:10.1038/ng2123

Peterson, C. T. (2020). Dysfunction of the microbiota-gut-brain axis in neurodegenerative disease: the promise of therapeutic modulation with prebiotics, medicinal herbs, probiotics, and synbiotics. *J. Evidence-Based Integr. Med.* 25, 2515690X20957225. doi:10.1177/2515690X20957225

Pierson, D. L., Chidambaram, M., Heath, J. D., Mallary, L., Mishra, S. K., Sharma, B., et al. (1996). Epidemiology of *Staphylococcus aureus* during space flight. *FEMS Immunol. Med. Microbiol.* 16 (3–4), 273–281. doi:10.1111/j.1574-695X.1996.tb00146.x

Pilacinski, A., Wagner, L., Besson, G., Matos, M. J., Araujo, E., and Klaes, C. (2025). Spontaneous eye movements reveal that premotor cortex is involved in human thinking. *bioRxiv*, 1–25. doi:10.1101/2025.03.11.642662

Popova, N. K., Kulikov, A. V., and Naumenko, V. S. (2020). Spaceflight and brain plasticity: spaceflight effects on regional expression of neurotransmitter systems and neurotrophic factors encoding genes. *Neurosci. Biobehav. Rev.* 119, 396–405. doi:10.1016/j.neubiorev.2020.10.010

Raghavendra, B. R., and Singh, P. (2016). Immediate effect of yogic visual concentration on cognitive performance. *J. Tradit. Complem. Med.* 6 (1), 34–36. doi:10.1016/j.jtcme.2014.11.030

Rappaport, M. B., and Corbally, C. J. (2023). Toward an etiology of spaceflight neuroplastic syndrome: evolutionary science leads to new hypotheses and program priorities. *NeuroSci* 4 (4), 247–262. doi:10.3390/neurosci4040021

Roccisano, D., Kumaratilake, J., Saniotis, A., and Henneberg, M. (2016). Dietary fats and oils: some evolutionary and historical perspectives concerning edible lipids for human consumption. *Food Nutr. Sci.* 07 (08), 689–702. doi:10.4236/fns.2016.78070

Ross, M. D., and Tomko, D. L. (1998). Effect of gravity on vestibular neural development. *Brain Res. Rev.* 28 (1–2), 44–51. doi:10.1016/S0165-0173(98)00025-3

Ruff, C. (2002). Variation in human body size and shape. *Annu. Rev. Anthropol.* 31 (1), 211–232. doi:10.1146/annurev.anthro.31.040402.085407

Rühli, F. J., and Henneberg, M. (2013). New perspectives on evolutionary medicine: the relevance of microevolution for human health and disease. *BMC Med.* 11 (1), 115. doi:10.1186/1741-7015-11-115

Rutter, L. A., Cope, H., MacKay, M. J., Herranz, R., Das, S., Ponomarev, S. A., et al. (2024). Astronaut omics and the impact of space on the human body at scale. *Nat. Commun.* 15 (1), 4952. doi:10.1038/s41467-024-47237-0

Saniotis, A., De la Torre, G. G., Galassi, F. M., Henneberg, M., and Mohammadi, K. (2023). Mindfulness meditation and spaceflight: a potential adjunct therapy for astronauts. *MIND Bull. Mind-Body Med. Res.* 3, 4–5. doi:10.61936/themind/202312222

Saniotis, A., Galassi, F. M., and Henneberg, M. (2024). Possible future evolutionary consequences to Homo as a result of the implementation of biotechnology. *Anthropol. Rev.* 87 (1), 69–80. doi:10.18778/1898-6773.87.1.05

Saniotis, A., Grantham, J. P., Kumaratilake, J., and Henneberg, M. (2020). Neuro-hormonal regulation is a better indicator of human cognitive abilities than brain anatomy: the need for a new paradigm. *Front. Neuroanat.* 13, 101. doi:10.3389/fnana.2019.00101

Saniotis, A., and Henneberg, M. (2011a). An evolutionary approach toward exploring altered states of consciousness, mind–body techniques, and non-local mind. *World Futur.* 67 (3), 182–200. doi:10.1080/02604027.2011.555250

Saniotis, A., and Henneberg, M. (2011b). Medicine could be constructing human bodies in the future. *Med. Hypothe.* 77 (4), 560–564. doi:10.1016/j.mehy.2011.06.031

Saniotis, A., Henneberg, M., and Ebrahimi, G. (2016). Human microevolution in outer space. *J. Futur. Stud.* 20 (4), 61–78. doi:10.6531/JFS.2016.20(4).A61

Saniotis, A., Henneberg, M., and Mohammadi, K. (2021). Genetic load and biological changes to extant humans. *J. Biosoc. Sci.* 53 (4), 639–642. doi:10.1017/S0021932020000413

Shahab, M., and Shahab, N.(2022). Coevolution of the human host and gut microbiome: Metagenomics of microbiota. *Cureus* 14(6), e26310. doi:10.7759/cureus.26310

Siddiqui, R., Akbar, N., and Khan, N. A. (2021b). Gut microbiome and human health under the space environment. *J. Appl. Microbiol.* 130 (1), 14–24. doi:10.1111/jam.14789

Siddiqui, R., Qaisar, R., Goswami, N., Khan, N. A., and Elmoselhi, A. (2021a). Effect of microgravity environment on gut microbiome and angiogenesis. *Life* 11 (10), 1008. doi:10.3390/life11101008

Silva, I. D. C. E., Russomano, T., Ferreira, R. A., Cupertino, M. D. C., Alcântara, F. A., Geller, M., et al. (2023). Physiological adaptations to life in space: an update. *J. Aerosp. Technol. Manag.* 15, 1–14. doi:10.1590/jatm.v15.1319

Stearns, S. C. (2012). Evolutionary medicine: its scope, interest and potential. *Proc. R. Soc. B Biol. Sci.* 279 (1746), 4305–4321. doi:10.1098/rspb.2012.1326

Stearns, S. C., Nesse, R. M., Govindaraju, D. R., and Ellison, P. T. (2010). Evolutionary perspectives on health and medicine. *Proc. Natl. Acad. Sci.* 107 (Suppl. l_1), 1691–1695. doi:10.1073/pnas.0914475107

Stingl, J. C., Welker, S., Hartmann, G., Damann, V., and Gerzer, R. (2015). Where failure is not an option—personalized medicine in astronauts. *PLoS One* 10, e0140764. doi:10.1371/journal.pone.0140764

The Human Microbiome Project Consortium (2012). Structure, function and diversity of the healthy human microbiome. *Nature* 486 (7402), 207–214. doi:10.1038/nature11234

Trevathan, W. (2007). Evolutionary medicine. *Annu. Rev. Anthropol.* 36, 139–154. doi:10.1146/annurev.anthro.36.081406.094321

Trousselard, M., Steiler, D., Raphel, C., Cian, C., Duymedjian, R., Claverie, D., et al. (2010). Validation of a French version of the Freiburg Mindfulness Inventory - short version: relationships between mindfulness and stress in an adult population. *Biopsychosoc. Med.* 4 (1), 8. doi:10.1186/1751-0759-4-8

Tsai, S.-J. (2021). Role of interleukin 8 in depression and other psychiatric disorders. *Prog. Neuro-Psychopharmacol. Biol. Psychi.* 106, 110173. doi:10.1016/j.pnpbp.2020.110173

Velarde, Ma.D., Fry, G., and Tveit, M. (2007). Health effects of viewing landscapes – landscape types in environmental psychology. *Urban For. Urban Green.* 6 (4), 199–212. doi:10.1016/j.ufug.2007.07.001

Vernikos, J., Deepak, A., Sarkar, D. K., Rickards, C. A., and Convertina, V. A. (2012). Yoga therapy as a complement to astronaut health and emotional fitness – stress reduction and countermeasure effectiveness before, during, and in post-flight rehabilitation: a hypothesis. *Gravitational Space Biol.* 26 (1), 65–76.

Voorhies, A. A., Mark Ott, C., Mehta, S., Pierson, D. L., Crucian, B. E., Feiveson, A., et al. (2019). Study of the impact of long-duration space missions at the International Space Station on the astronaut microbiome. *Sci. Rep.* 9 (1), 9911. doi:10.1038/s41598-019-46303-8

Vyas, A., Pillai, A. G., and Chattarji, S. (2004). Recovery after chronic stress fails to reverse amygdaloid neuronal hypertrophy and enhanced anxiety-like behavior. *Neuroscience* 128 (4), 667–673. doi:10.1016/j.neuroscience.2004.07.013

Willis, C. R. G., Gallagher, I. J., Wilkinson, D. J., Brook, M. S., Bass, J. J., Phillips, B. E., et al. (2021). Transcriptomic links to muscle mass loss and declines in cumulative muscle protein synthesis during short-term disuse in healthy younger humans. *FASEB J.* 35, e21830. doi:10.1096/fj.202100276RR

Wilson, E. O. (2010). *Biophilia* (Cambridge, Mass: Harvard University Press).

Wilson, J. W., Thibeault, S. A., Cucinotta, F. A., Shinn, J. L., Kim, M., Kiefer, R., et al. (1995). Issues in protection from galactic cosmic rays. *Radiat. Environ. Biophys.* 34 (4), 217–222. doi:10.1007/BF01209745

Winkelman, M. (2004). Shamanism as the original neurotheology. *Zygon* 39 (1), 193–217. doi:10.1111/j.1467-9744.2004.00566.x

Winkelman, M. J. (2000). *Shamanism: the neural ecology of consciousness and healing.* 1st ed. Westport, CT: Praeger. doi:10.5040/9798216986232

Wood, K. A., and Goriely, A. (2022). The impact of paternal age on new mutations and disease in the next generation. *Fertil. Steril.* 118 (6), 1001–1012. doi:10.1016/j.fertnstert.2022.10.017

Wotring, V. E. (2015). Medication use by u. S. Crewmembers on the international space station. *FASEB J.* 29 (11), 4417–4423. doi:10.1096/fj.14-264838

Wu, B., Wang, Y., Wu, X., Liu, D., Xu, D., and Wang, F. (2018). On-orbit sleep problems of astronauts and countermeasures. *Mil. Med. Res.* 5 (1), 17. doi:10.1186/s40779-018-0165-6

Yang, J. W., Song, Q. Y., Zhang, M. X., Ai, J. L., Wang, F., Kan, G. H., et al. (2022). Spaceflight-associated neuro-ocular syndrome: a review of potential pathogenesis and intervention. *Int. J. Ophthalmol.* 15, 336–341. doi:10.18240/ijo.2022.02.21

Yong, S. J., Tong, T., Chew, J., and Lim, W. L. (2020). Antidepressive mechanisms of probiotics and their therapeutic potential. *Front. Neurosci.* 13, 1361. doi:10.3389/fnins.2019.01361

You, W., and Henneberg, M. (2017). Cancer incidence increasing globally: the role of relaxed natural selection. *Evol. Appl.* 11 (2), 140–152. doi:10.1111/eva.12523

You, W., Henneberg, R., and Henneberg, M. (2022). Healthcare services relaxing natural selection may contribute to increase of dementia incidence. *Sci. Rep.* 12, 8873. doi:10.1038/s41598-022-12678-4

You, W.-P., and Henneberg, M. (2016). Type 1 diabetes prevalence increasing globally and regionally: the role of natural selection and life expectancy at birth. *BMJ Open Diabetes Res. Care* 4 (1), e000161. doi:10.1136/bmjdrc-2015-000161

Zuk, M. (2013). "Paleofantasy: what evolution really tells us about sex, diet," in *And how we live*. New York London: Norton.

frontiers | Frontiers in Immunology

TYPE Original Research
PUBLISHED 08 May 2025
DOI 10.3389/fimmu.2025.1539163

OPEN ACCESS

EDITED BY
Christopher D. Porada,
Wake Forest University, United States

REVIEWED BY
Andreas L. Lopata,
James Cook University, Australia
Stanislava Stanojevic,
University of Belgrade, Serbia
Giacomo Fais,
University of Cagliari, Italy

*CORRESPONDENCE
Brian E. Crucian
brian.crucian-1@nasa.gov

RECEIVED 03 December 2024
ACCEPTED 16 April 2025
PUBLISHED 08 May 2025

CITATION
Colorado AA, Gutierrez CL, Nelman-Gonzalez M, Marshall GD, Mccoy JT and Crucian BE (2025) Hazards of lunar surface exploration: determining the immunogenicity/allergenicity of lunar dust. *Front. Immunol.* 16:1539163. doi: 10.3389/fimmu.2025.1539163

Hazards of lunar surface exploration: determining the immunogenicity/ allergenicity of lunar dust

Audrie A. Colorado[1], Cody L. Gutierrez[2], Mayra Nelman-Gonzalez[1], Gailen D. Marshall[3], J. Torin Mccoy[4] and Brian E. Crucian[4]*

[1]KBR, Johnson Space Center Immunology Laboratory, Houston, TX, United States, [2]JES Tech, Johnson Space Center Immunology Laboratory, Houston, TX, United States, [3]Department of Medicine, The University of Mississippi Medical Center, Jackson, MS, United States, [4]National Aeronautics and Space Administration (NASA) Johnson Space Center, Houston, TX, United States

Although infrequent, there have been Apollo program reports of lunar dust exposure leading to notable upper respiratory symptoms in select crewmembers. Possible mechanisms include particulate irritation, inflammation from toxic insult, or legitimate adaptive immune-mediated response. Although sterile non-protein matter would not be expected to be immunogenic, one Apollo flight surgeon reported increasing symptoms upon repeated perceived exposure with associated eosinophilia, suggestive of possible allergic reactions. Many International Space Station (ISS) crews display a pattern of persistent immune system dysregulation and latent virus reactivation. Some ISS crews manifest atypical respiratory and/or dermatitis symptoms which could have an allergic component. It is logical to anticipate crew immune dysregulation could worsen during prolonged deep space missions and planetary surface hazards will only complicate crew health risks. Allergic (i.e. mast cell-mediated) reactivity could adversely increase negative clinical and operational impacts for long-duration lunar astronauts and affect countermeasure requirements for surface vehicles. This study investigated whether lunar dust exposure could possibly elicit an IgE mediated allergic response during spaceflight by utilizing in vitro cell culture models. Our laboratory was officially approved for receipt of actual lunar dust samples from the Apollo 16 mission from NASA. These samples were used to complete the proposed set of in vitro cell culture experiments, using human peripheral blood mononuclear cells (PBMC) from healthy individuals, and basophils and eosinophil cell lines. Cells were co-cultured with cellular mitogens, common recall antigens (Der p1), fine ground silica quartz (control), or lunar dust, to study whether lunar dust exposure could alter the generation of selective immune responses associated with clinical allergic reactions. Measured outputs included supernatant-derived total IgE, tryptase, histamine, and selected cytokine levels. Cellular activation was monitored by assessing activation markers via flow cytometry. EM/x-ray analysis was used to determine cellular interactions with dust particles. The assessments in primary

human blood immune cells indicated no evidence for cellular responsiveness nor 'allergy-like' reactivity to lunar dust. Assessments using purified 'allergic' cell lines, did yield some unique but mild responsiveness to lunar dust, however such cells lines can have response profiles somewhat different from their in vivo counterparts. This study determining the allergy specific immune responses, will help guide NASA to develop mitigation techniques and potential countermeasures necessary in the event of excessive exposure to lunar dust during lunar surface EVAs.

KEYWORDS

lunar dust, spaceflight, allergy, immunology, NASA

1 Introduction

Lunar dust is a unique material that consists of very sharp micron-scale particles that stick to skin, clothing, and equipment, and are easily inhaled (1). Crew members and landing vehicles will inevitably be exposed to lunar dust in future lunar missions. While much is known of the toxic hazard potential, some gaps are present in the evidence base. During the Apollo moon missions, there were consistent reports of lunar dust exposure, with this exposure sometimes leading to upper respiratory symptoms in both astronauts and ground support personnel (2). There could be several mechanisms by which lunar dust causes symptoms, including simple particulate irritation of mucus membranes, the dust acting as a toxin, or by activating the immune system to demonstrate one or more inflammatory reactions, some of which could be allergic in nature. International Space Station (ISS) crews have displayed a pattern of immune system dysregulation that predispose them to both inflammation and allergy-like respiratory and cutaneous symptoms (3–5). The potential for lunar dust to generate immediate sensitivity reactions that could impact mission operations remains uninvestigated.

This study directly addresses whether actual lunar dust elicits an immunogenic response. Our laboratory received lunar dust acquired from the Apollo 16 mission from soil and rake sample collections from surface regolith of the ejector blanket of South Ray Crater at Station 8 (6). A previous JSC animal lunar dust inhalation study examined direct lung toxicology and inflammatory responses but did not assess any allergy-related sensitizations or reactions (7). The area of focus for this study is the unique aspect of dust exposure related to development of an immune milieu indicative of increased allergic sensitization of reactivity. As previously detailed, there are credible anecdotal reports from the Apollo program of both crewmembers and flight surgeons experiencing what were described as 'allergic' (upper respiratory) symptoms. One surgeon documented increasing symptoms with repeat perceived exposure, and documented eosinophilia which can be observed during more severe allergic reactions. However, there is currently only anecdotal data regarding allergy risk and lunar dust exposure. The data from this study will help inform how NASA responds if an astronaut experiences upper respiratory symptoms on the lunar surface. The data will also potentially influence operations and/or vehicle engineering design for dust containment. The goal of this study is to address, in a simple cell culture experiment, whether lunar dust can act as an allergen, an adjuvant, or a cellular toxin.

2 Methods

2.1 Human subjects

The conducted work met all federal and local requirements for human subjects' protection and complies with the NASA Policy Directive (NPD) 7100.8E "Protection of Human Research Subjects". The Immunology laboratory at Johnson Space Center (JSC) has performed numerous ground and flight studies using human test subjects, with the review and approval of the local Institutional Review Board (IRB). All study participants were provided informed written consent prior to participation.

Subjects were active, healthy test subjects enrolled and screened by the NASA JSC Test Subject Facility (TSF). A total of 6 subjects were recruited (5 M, 1 F). Subject solicitation was mediated by the TSF and informed consent was obtained by the PI. Institutional review board approval was obtained from the Committee for the Protection of Human Subjects at the JSC; Houston, TX. Subject confidentiality is maintained, and data will only be publicly disclosed in a summarized, nonidentifiable fashion.

2.2 Cell lines

Basophil cell line, KU812 (ATCC, USA), was maintained as recommended in RPMI media + 2mM glutamine (Gibco, Rockville, MD, USA) supplemented with 10% fetal bovine serum (ATCC, USA). Cultures used 1e6 cells/mL cocultured with mitogens and recall antigens for 48 hours. All cells were cultured at 37°C, 95% humidity and 5% CO_2.

Eosinophil cell line, Eol-1 (Millipore Sigma, Burlington, MA, USA), was maintained as recommended in RPMI media + 2mM

glutamine supplemented with 10% fetal bovine serum. In preparation of experimental setup, cells were treated with 5μM butyrate (Sigma, St. Louis, MA, USA) for 7 days to induce differentiation of mature eosinophils (Supplementary Figure S1). Cultures used 1e6 cells/mL cocultured with mitogens and recall antigens for 48 hours. All cells were cultured at 37°C, 95% humidity and 5% CO_2.

2.3 Human donor primary cell cultures

For this study, peripheral blood samples were collected in lithium heparin blood tubes (Greiner BioOne, Monroe, NC, USA) by venipuncture. All live cell culture assays were performed using whole blood or isolated peripheral blood mononuclear cells (PBMCs), which were purified by Ficoll (Cytiva, Marlborough, MA, USA) density-gradient centrifugation as previously described (3). The PBMC cultures were performed using 1e6 PBMCs/mL and whole blood cultures used 100μL/mL culture media.

2.4 Culture stimulations

Lunar dust from Apollo 16 missions was procured from NASA Johnson Space Center through the official "Request for Lunar Dust Samples for Biomedical Research" process. Through preliminary work, and per the supplying NASA archivist statements, the variability in size of the dust (sample ID 68501) made it difficult to precisely refine and weigh less than 1mg of dust of the appropriately sized particles for testing. Essentially, the particles received were of great varying size, below their ability to refine. To ensure adequate cell interaction with the dust for downstream assays, a decision was made to use approximately 2mg total weight of lunar dust mixed with 1mL of culture media per culture test. There was no apparent bacterial or yeast growth in the culture media following incubation up to 14 days during protocol development.

Pure, fine ground (5μM) silica was cultured with cells at 100μg/mL culture (U.S. Silica, Katy, TX, USA). Silica is a standard simulant used by the National Institutes of Health to study respiratory system toxicity as it is known to cause silicosis and was used as a terrestrial control to lunar dust in this study similar to the previous NASA animal lunar dust inhalation toxicity study (7, 8).

The common house dust mite allergen, *Dermatophagoides pteronyssinus* allergen 1 (nDerp1) (9), was used to stimulate cultures for the recall antigenic control (InBio, Charlottesville, VA, USA). Natural Derp1 was activated before each test using 1mM Dithiothreitol to regenerate its thiol group, which becomes oxidized during purification. Activated nDerp1 was cultured with cells at 1μg/mL.

Mitogen stimulation cultures, as a stimulatory positive control to induce activation, used 0.125 μg/mL anti-CD3 and 0.05 μg/mL anti-CD28 soluble antibodies (both Cytek Biosciences, Freemont, CA, USA), or 10 μg/mL of Staphylococcus enterotoxin B (SEB) (Sigma-Aldrich, St Louis, MO, USA).

2.5 Flow cytometry

Flow cytometry was performed on the Northern Lights (Cytek Biosciences, Freemont, CA, USA) using a panel of antibodies listed in Supplementary Table S1.

2.6 Proliferation assay

Isolated human PBMCs were stained with CFSE cell division tracking dye according to manufacture instructions (Biolegend, San Diego, CA, USA). Briefly, cells were stained with 1μM CFSE dye in the dark and quenched with 100% FBS followed by multiple PBS washes before culture set up. Stained PBMCs were cultured with mitogens or stimulations and incubated at 37°C, 95% humidity and 5% CO_2 for 6 days. After culture, the cells were stained with a cell viability stain, CD4 and CD19 antibodies to distinguish cell proliferation in live T and B cells, respectively. Cell division was determined by flow cytometry.

2.7 Enzyme linked immunosorbent assays

Supernatants from whole blood cultures were collected after the 48 hour culture times and leukotriene, histamine and IgE were quantified using ELISA kits (Abcam, Cambridge, UK). Supernatants were undiluted to quantify leukotriene B4, diluted 1:50 to quantify histamine, and diluted 1:50 to quantify IgE production. Optical density was measured using the Tecan microplate reader (Tecan, Switzerland). Protein concentration was interpolated using a four parameter logistic algorithm standard curve. Data was analyzed using Prism v10.0 (Graphpad, Boston, MA, USA).

2.8 Cytokine detection

Supernatants from whole blood cultures were collected after the 48 hour culture times and cytokine production was determined using the MILLIPLEX 13-plex cytokine array (Millipore Sigma, Chicago, IL, USA). Mean fluorescent intensity of the cytokine bead array was measured and data was generated using the Luminex® 200™, HTS, FLEXMAP 3D®, MAGPIX® instrument with xMAP® INTELLIFLEX software (Luminex, Austin, TX, USA). Data was analyzed using Prism v10.0 (Graphpad, Boston, MA, USA).

2.9 Microscopy

Samples processed for environmental scanning electron microscopy (ESEM) were fixed following culture using a solution containing 2% glutaraldehyde (Sigma-Aldrich, St. Louis, MO, USA) and 3% formaldehyde (Sigma-Aldrich) in sterile phosphate buffer solution (PBS, pH 7.4, ThermoFisher Scientific, Waltham, MA, USA) for 1 hour at room temperature in the dark, then stored at 4°C.

Thefixed solutions were covered in aluminum foil and kept at ambient temperature for 30 minutes. The samples were then stored at 4°C until processing.

Approximately 100mL of fixed sample was loaded onto an Isopore TSTP membrane filter (3.0 µm pore size, 13 mm diameter, Millipore Sigma) and gravity filtered to reduce disturbance to any structure present in the sample. The samples were washed twice with 200µL PBS (ThermoFisher Scientific) then rinsed with 1000µL of filtered, sterile milli-Q water. Samples were then sequentially dehydrated using freshly prepared ethanol (200 proof, Sigma-Aldrich) in filtered, sterile milli-Q water. Initial dehydration involved two sequential 30 minute rinses with 500µL of 25% ethanol then 500µL of 50% ethanol. This process was continued by applying increasing concentrations of ethanol at 60%, 70%, 80%, 90% and 100% for 10–15 minutes each. Following dehydration, the filter was mounted on an aluminum mount flat pin with carbon conductive tab (Electron Microscopy Sciences, EMS, Hatfield, PA, USA). The samples were dried for 24 hour inside a biosafety cabinet, then placed into the ESEM chamber overnight for additional drying under vacuum. Following drying, the samples were sputter coated with 2 nm iridium on a Cressington Sputter Coater 298 HR that uses a Cressington Thickness Controller MTM 20.

Imaging was performed with a ThermoFisher Scientific FEI Quanta 250 using the ESEM mode along with a GAD detector. All images were acquired at 10 kV in back scatter electron mode at a pressure of ~1.4 Torr. EDS analysis was conducted using an Ametek EDS system with an Apollo X/Octane Pro detector and TEAM EDS software.

2.10 Statistical analysis

This study incorporated *in vitro* cell culture analysis from primary human subject blood samples for both whole blood and PBMCs as well as cell lines. A total of 6 human subjects were enrolled for this study to analyze T, B, monocyte, eosinophil, and basophil cell activation, and IgE, leukotriene, histamine, and cytokine production. Cell lines used were of eosinophil and basophil lineage and experiments were conducted in replicates of 3. Statistical analysis was performed on each separate output of data. Cellular activation of all cell populations in whole blood or PBMC cultures were analyzed by Two-Way ANOVA with Dunnett's multiple comparisons test. Cellular activation of eosinophil and basophil cell lines, proliferation data for T and B cells, IgE, leukotriene, histamine, and cytokine production were all analyzed using Ordinary One-Way ANOVA with Dunnett's multiple comparisons test. P values indicated by asterisks in graphs are as follows: * P<0.05, ** P<0.005, *** P<0.0005, **** P<0.0001.

3 Results

3.1 Immediate cellular responses

To determine if *in vitro* exposure to lunar dust resulted in immediate mitogenic activation of any subset of human peripheral blood immune cells, both PBMC and whole blood from healthy human test subjects were cultured with mitogens SEB or αCD3/αCD28 (positive controls), Der P1 (common recall antigen), or silica (lunar dust simulant control) in parallel to lunar dust.

Flow cytometric analysis of unstained lunar dust or fine ground silica was first conducted to confirm these particles had unique forward- and side scatter properties and would not interfere with our cellular analysis (Supplementary Figure S2). In comparison to whole blood cellular populations this study will focus on (granulocytes, monocytes and lymphocytes), the scatter properties of silica and lunar dust were below the size seen in the cell population gates to be analyzed.

Cellular activation is vital in the immune response against a foreign invader. It is a cascade of events that leads to the formation of appropriate immune cell responses. Whole blood and PBMC cultures were set up to determine immediate cellular responses including cellular activation of T cells, B cells, monocytes, eosinophils and basophils. Representative flow cytometry plots to show gating strategy of the T cell (CD45+CD3+CD25+CD69+), B cell (CD45+CD19+CD25+), and monocyte (CD45+CD14+MHCII+CD69+) populations in PBMC cultures are displayed in Figure 1 while activated eosinophil (CD45+CD11b+CCR3+CD125+CD69+) and activated basophil (CD45+CCR3+CD123+CD63+CD203c+) populations in whole blood are displayed in Figure 2.

The percentage of T cells in whole blood and PBMC cultures after 48 hours did not change compared to baseline collection and no treatments/stimulations induced any significant changes. The percentage of B cells did significantly decrease in whole blood and PBMC cultures from baseline with the decrease being slightly more in PBMC cultures. However, there were no significant differences among treatment groups compared to untreated control 48 hour culture. The decrease in B cells from baseline after 48 hour culture is expected without specific B cell stimulation and growth factors added (data not shown). It takes over 48 hours for B cells to recover and adapt to culture conditions using the T cell dependent factors in untreated cultures to maintain survival and cell growth (10–12). Relatively little alteration in the relative percentages of these cells was expected given the short-term duration of the cultures. After 48 hours of culture, significant T cell and B cell activation was only seen in the positive control stimuli in comparison to untreated control group (Figures 3A, B). These results were expected for the positive controls, and not for the recall antigen, positive simulant silica, or lunar dust, as we hypothesized an allergic response requiring different cell population responses, specifically basophils, mast cells and eosinophils. After 48 hours of culture, there was a significant decrease in the percentage of monocytes in both whole blood and PBMC cultures with αCD3/αCD28, SEB, and silica stimuli, but not with Derp1 or lunar dust indicating cell death in response to those specific stimuli (data not shown). There was no monocyte activation seen in any stimuli group compared to untreated control (Figure 3C). These results would suggest monocytes do not play a significant role in the immune response to Derp1, silica or lunar dust stimuli in this model.

Eosinophils and basophils are white blood cells found in the granulocyte cell population (Supplementary Figure S2). They are

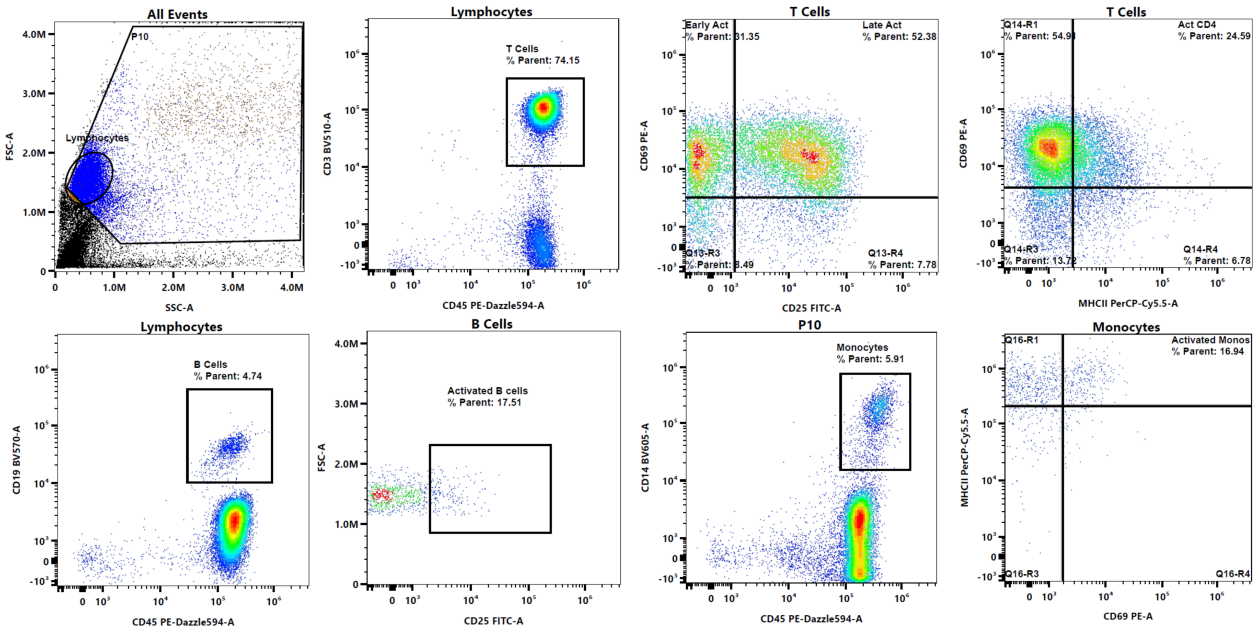

FIGURE 1
Representative flow plots to depict gating strategy to identify T cells, B cells, and monocytes, and their activation.

involved in immune cell responses to inflammation, parasitic infections, and allergic responses. The roles of eosinophils and basophils includes enzymatic granule production, reactive oxygen species production, antigen presentation, among others (13–16). We focused on these cell populations from primary human donors and cell lines for the potential roles they can play in allergic reactions. We did not see any significant changes in the activation of eosinophils (CD69+) in response to any stimuli in whole blood cultures after 48 hours (Figure 4A). Similarly, the activation of basophils (CD203c+CD63+) showed no changes (Figure 4B). This could be explained by the diminishment of the CD45+CCR3 +CD123+ cell population with the presence of silica most likely due to an exhaustive basophil response.

The same experimental setup was conducted using eosinophil (EOL-1) and basophil (KU812) cell lines. Silica and lunar dust significantly induced eosinophil activation in the cell line cultures

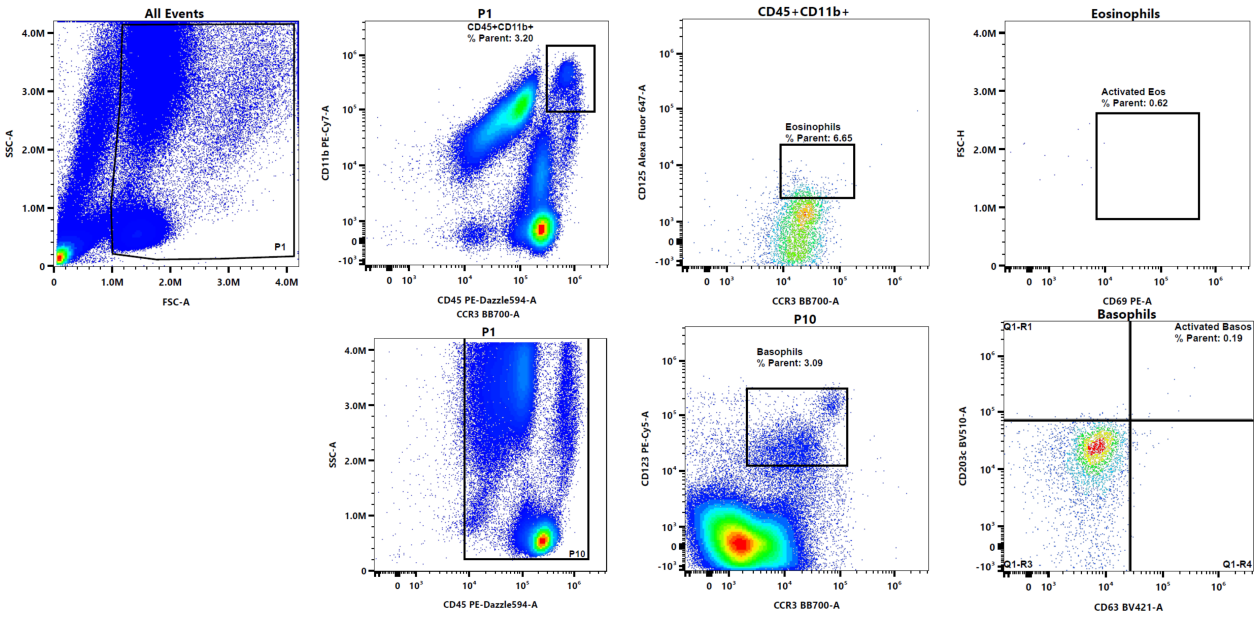

FIGURE 2
Representative flow plots to depict gating strategy to identify eosinophils and basophils, and their activation.

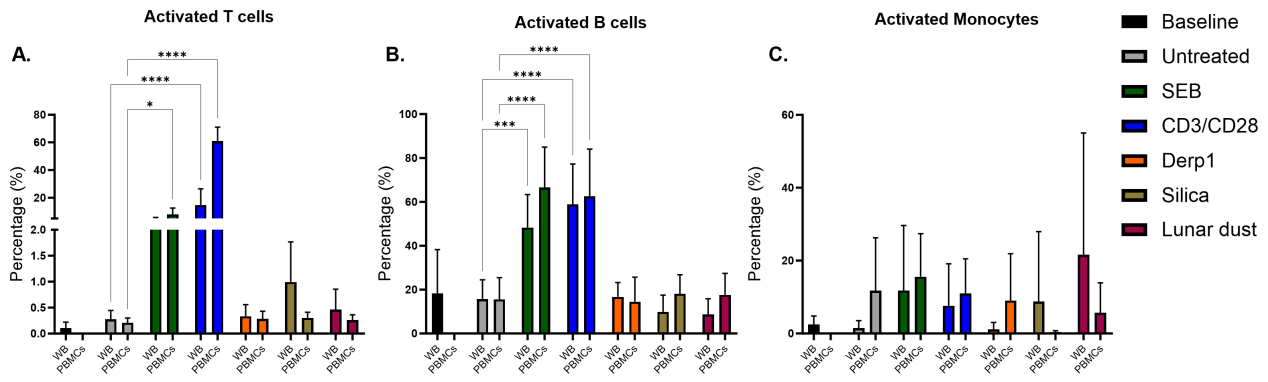

FIGURE 3
Percentage of **(A)** activated T cells **(B)** activated B cells and **(C)** activated monocytes in whole blood (WB) and PBMC cultures at baseline collection, and after 48 hour stimulation. * P<0.05, *** P<0.0005, **** P<0.0001.

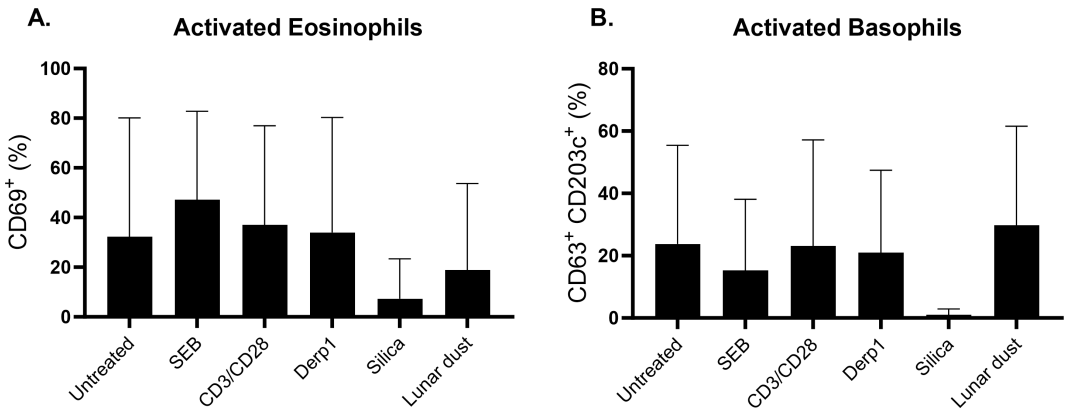

FIGURE 4
Percentage of **(A)** activated eosinophils and **(B)** activated basophils after 48 hour culture stimulation compared to untreated control.

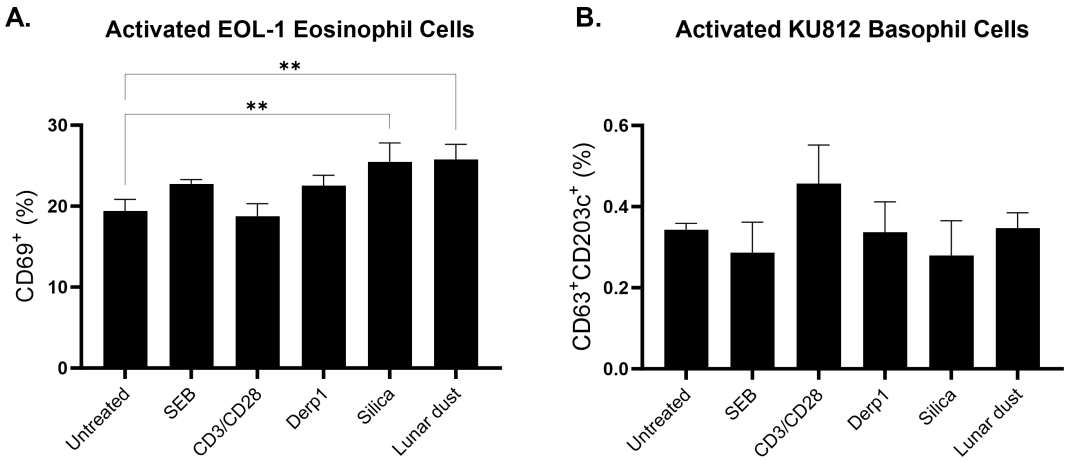

FIGURE 5
Percentage of activated **(A)** EOL-1 cell line eosinophils and **(B)** KU812 cell line basophils after 48 hour culture stimulation in comparison to untreated control. ** P<0.005.

after 48 hours of stimulation whereas no stimuli induced a change in the basophil cell line cultures in comparison to the untreated control (Figures 5A, B).

To fully understand the responses seen when lunar dust is introduced to immune cells, this study looked at supernatant derived cytokine production in whole blood cultures after 48 hour stimulation (Figure 6). As expected, we saw a significant increase in pro-inflammatory cytokines in response to the positive control mitogens, SEB (GM-CSF, IFNγ, IL-12, IL-2, TNFα, IL-7, IL-8) and the T cell stimuli αCD3/αCD28 (GM-CSF, IL-12). There were also increases seen in some cytokines in response to SEB and αCD3/αCD28 (IL-10, IL-13, IL-4). As expected, silica induced significant increases only in proinflammatory cytokines (IL-1, IL-6, IL-7, IL-8) while lunar dust did not elicit any significant cytokine response.

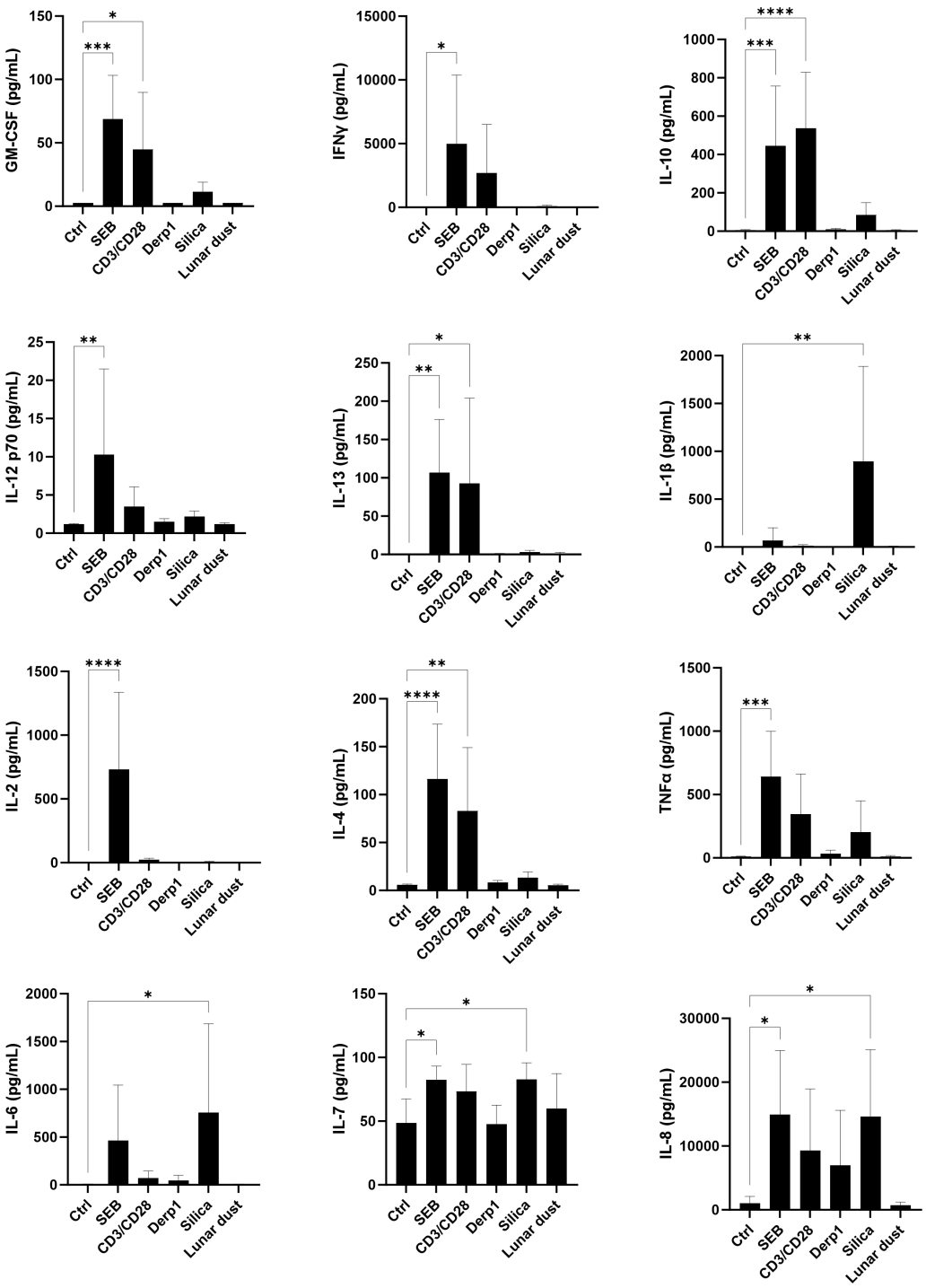

FIGURE 6
Supernatant cytokine concentration (pg/mL) in whole blood cultures after 48 hour stimulation. * P<0.05, ** P<0.005, *** P<0.0005, **** P<0.0001.

This suggests silica is inducing an innate immune response, but not lunar dust and this could be explained by the small particulate size of silica in comparison to the lunar dust sample used allowing the cell-particulate interaction needed to induce such a response.

Our study focused on whole blood cultures to capture the entire cellular population dynamic during an immune reaction in response to our specific stimuli. The inherent benefits of a whole blood culture system were previously discussed. The limitations of this include interpretation of specific cell types producing these cytokines. However, assumptions can be made on which cell types are producing cytokines based on cell activation data shown earlier. As expected, there were significant increases in cytokines in response to our positive mitogenic control. The absence of cytokine production in response to lunar dust is similar to what was seen in our inhalation study whole blood cultures (17).

This study also looked at eosinophil cell line cultures (EOL-1) and basophil cell line cultures (KU812) for direct cell specific cytokine responses after 48 hours of culture stimulation as these cell types are key players in allergic nasal reactions. There was only a significant decrease in the anti-inflammatory cytokine IL-10 in response to lunar dust in the eosinophil cells, although eosinophils are not a major source of IL-10 in allergic pathophysiology (Figure 7). In the basophil cell line, we detected mostly decreases in cytokines in response to SEB, αCD3/αCD28, and silica (IL-10), Derp1 (IL-1β), and lunar dust (IL-8). Increases were also seen in response to αCD3/αCD28 and silica (IL-8) (Figure 8).

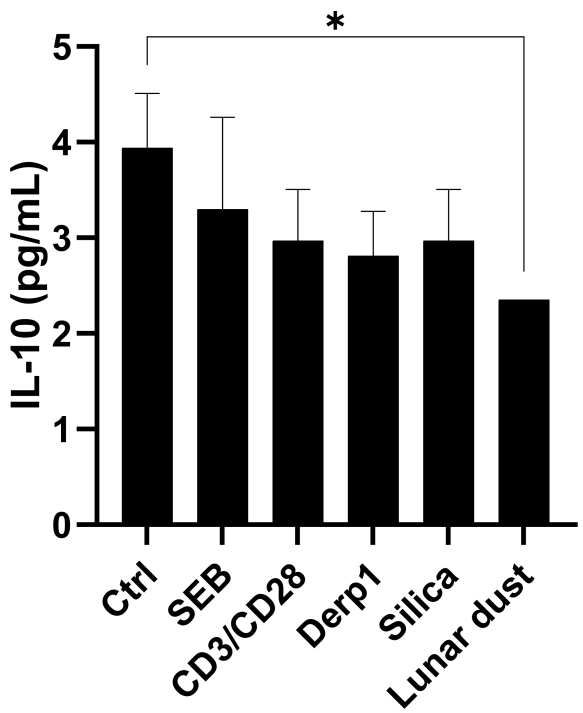

FIGURE 7
Supernatant cytokine concentration (pg/mL) in EOL-1 eosinophil cell line cultures after 48 hour stimulation. * P<0.05.

Elevated levels of IgE in whole blood can be indicative of allergies. To determine if subjects responded to lunar dust, *in vitro* IgE response using whole blood was utilized. This study investigated the allergic responses to lunar dust specifically in supernatant derived histamine, leukotriene B4 and IgE from 48 hour stimulated cultures of whole blood, eosinophil cell line and basophil cell line. Leukotriene B4 production was significantly increased by the basophil cell line in response to lunar dust (Figure 9). Furthermore, lunar dust exposure induced histamine production in the eosinophil cell line (Figure 10). As eosinophils are not producers of histamine, this could be attributed to a percentage of undifferentiated myeloblasts in the EOL-1 cell suspension. Interestingly, there was no significant response to any stimuli, including lunar dust, in total IgE production in whole blood, eosinophil, or basophil cultures (data not shown). This data suggests lunar dust can induce a potentially proallergic milieu in specific purified artificial cell lines representing human basophils and eosinophils. Although, no responses were seen in primary whole blood cultures, this could be explained by the counteractive responses of other immune cells in these cocultures. The human whole blood cultures presented a wide range of IgE concentration per subject which is well known regardless of the atopic status on the individual. There were no significant changes in total IgE production in response to any stimuli, but data is graphed per subject to reveal the extent of the breadth of data collected and the necessity for an increase in human subject enrollment with specific medical history information such as allergies and antihistamine use documented (Figure 11).

3.2 Cell proliferation

In experimental setup, dying PBMCs with CFSE and culturing for 6 days, indicated that cell proliferation of T and B cells was not induced by Der p1, silica, or lunar dust, only the positive mitogenic controls, αCD3/αCD28 and SEB (Supplementary Figure S3). The percentage of T and B cells that proliferated were similarly significant (P>0.0001) for the positive controls (Figure 12). T cells are commonly induced for cell division during an immune response that leads to their activation (Figure 3), and B cells can be induced to proliferate as well in response to activated T cells producing the cytokine IL-4, which we confirmed is occurring in response to the mitogenic positive controls in our cytokine assay (Figure 6). T cell or B cell activation does not occur in response to Der p1, silica or lunar dust (Figure 3), which explains why proliferation does not occur either. This suggests that any irritation seen in crew in response to lunar dust is not a result of T or B cell immunoreactivity.

3.3 Microscopy analysis of cell-dust interactions

To determine if *in vitro* exposure to lunar dust and silica (lunar dust simulant control) resulted in direct interaction of human peripheral blood immune cells, environmental scanning electron

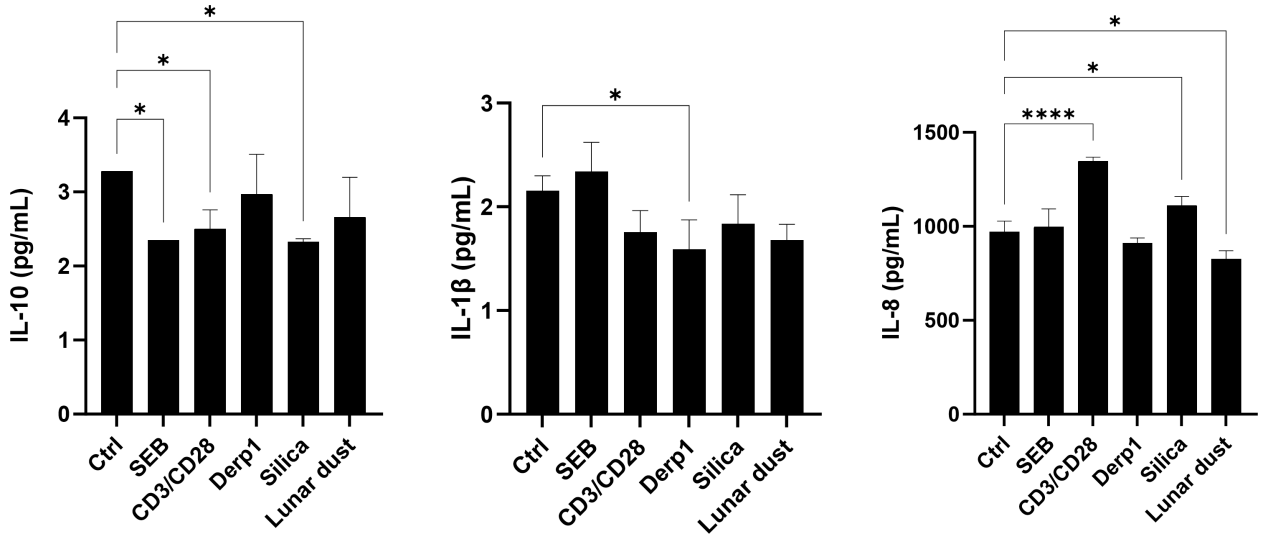

FIGURE 8
Supernatant cytokine concentration (pg/mL) in KU812 basophil cell line cultures after 48 hour stimulation. * P<0.05, **** P<0.0001.

microscopy (ESEM) analysis was carried out on PBMCs from healthy human test subjects cultured with control media, media with silica and media with lunar dust. Figure 13 shows representative images of PBMCs fixed following 48hr of culture with control media (Figure 13A), media with silica (Figure 13B) and media with lunar dust (Figure 13C). Image analysis was acquired using the environmental with a backscatter detector, which enables the detection of high energy particles such as silica and lunar dust, against the lower energy carbon-based cells. Figure 13B, left panel, shows silica sitting on top of the cell as depicted by the bright small material located at the center of the cells in the image while the right panel shows both a cluster of silica particles as well as an adjacent cell interacting with the silica. Figure 13C shows cells with a tiny lunar dust particle on their surface (left panel) which was the more common finding, while the right panel shows a representative cell that has ingested the lunar dust.

To better understand the size distribution of the specific lunar dust (sample ID 68501) that was used for coculture with the PBMCs, samples of the media with lunar dust that was utilized in the cell cocultures, was fixed for ESEM analysis then run through a particle size distribution macro using Image J. Supplementary Figure S4A shows a backscatter image of the lunar dust particles distributed through the sample while Supplementary Figure S4B shows the representative particle ID by number with the matching size distribution on the adjacent chart. Size distribution varied greatly with the smallest particle size at a surface area of 0.323µm2 (width and height of 0.744µm and 0.709µm) and the largest particle in this sample at a surface area of 60.3µm2 (width and height of 8.56µm and 10.4µm). Supplementary Figures S4C, D represent an even larger lunar dust particle isolated from the lunar dust-PBMC coculture sample that had a surface area measurement of 5760µm2 (width and height of 75.8µm and 111µm). Information

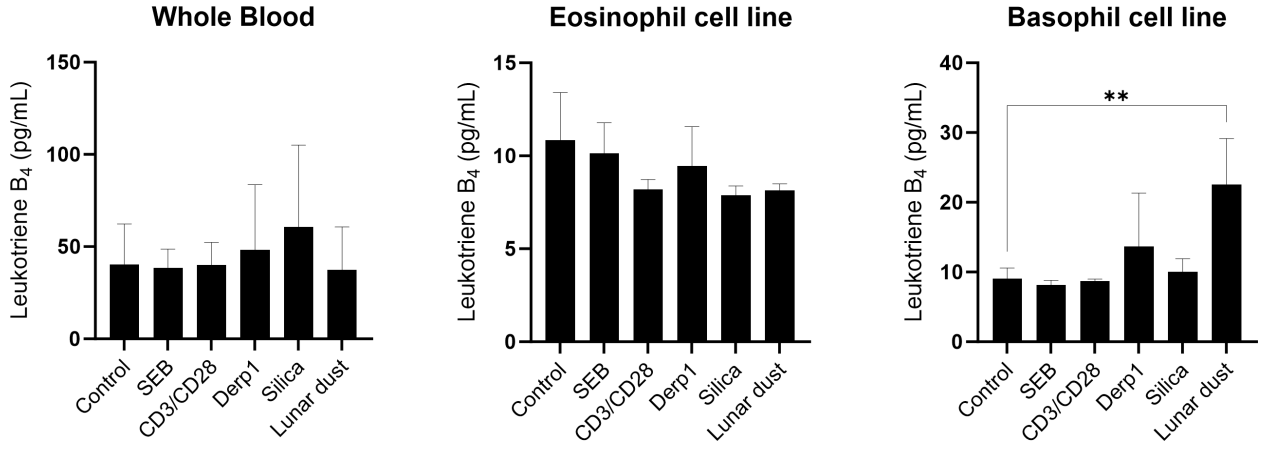

FIGURE 9
Leukotriene B4 concentration (pg/mL) in whole blood, eosinophil, or basophil cultures after 48 hours stimulation. ** P<0.005.

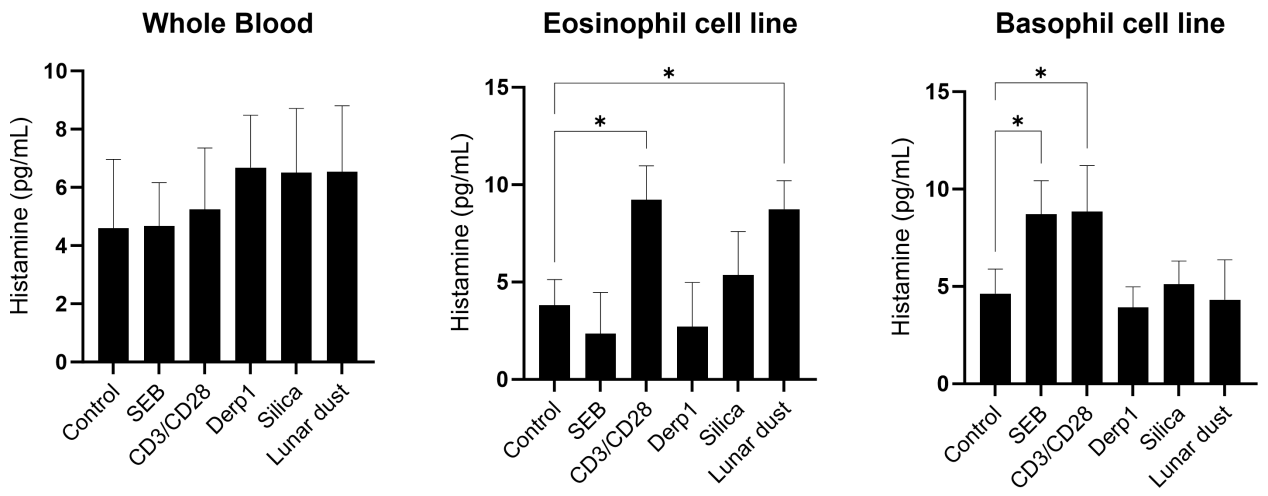

FIGURE 10
Histamine concentration (pg/mL) in whole blood, eosinophil, or basophil cultures after 48 hours stimulation. * P<0.05.

on the Lunar Sample Compendium, show that lunar dust ID 68501 (https://curator.jsc.nasa.gov/lunar/lsc/68501.pdf) is a soil and rake sample collected from surface regolith of the ejector blanket of South Ray Crater at Station 8, with an average coarse grain size of 84µm – 115µm range. Although the size distribution varied greatly of the specific sample set we obtained, smaller grain sizes were detected which are more optimal for cell-particle interactions. For the subjects tested, there were limited cell-lunar dust interactions throughout the samples analyzed by ESEM. These results are similar to those described in the flow cytometry assessments. Despite limited cell-lunar dust interactions, Supplementary Figure S5 shows a PBMC that has ingested a lunar dust particle (bright particle in cell detected by back scatter imaging). This confirms that for this lunar dust sample type, there is the occasional cell-lunar dust interaction when particulate size is optimal.

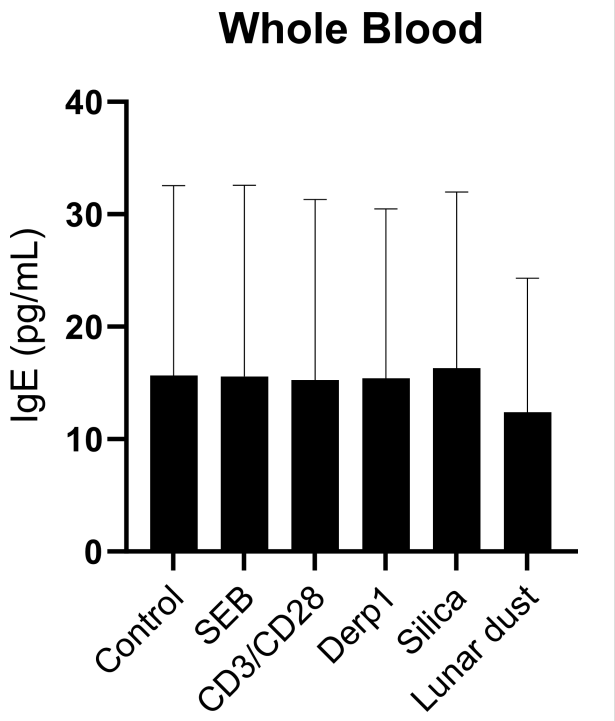

FIGURE 11
IgE concentration (pg/mL) in whole blood cultures after 48 hours stimulation per subject.

In addition to the imaging, energy-dispersive X-ray spectroscopy (EDS) analysis was carried out on the lunar dust and silica particles. It should be noted that due to the cellular composition of the samples, analysis could not be conducted above 10 KV in order to minimize destruction of the cells. This lower energy level was not sufficient to allow the detection of iron which is a classic hallmark for lunar dust. However, EDS analysis of lunar dust (Supplementary Figure S6, top panel) confirms that the particle present in the cell-lunar dust coculture was lunar dust. Similarly, EDS analysis of the cell-silica coculture also confirms the presence of silica. Last, EDS analysis of the bright spot detected on the cell of the lunar dust coculture sample confirms that the particulate ingested by the cell is lunar dust (Supplementary Figure S6, middle panel). This finding confirms that cells are able to ingest lunar dust.

4 Discussion

This study aimed to investigate the potential of immune reactions that are associated with clinical allergy to lunar dust primarily looking at the key immune cell responsiveness to lunar dust itself, a simulant, and other common recall antigens or polyclonal mitogens serving as positive controls. Human primary leukocytes isolated from blood were primarily used in this investigation. Eosinophils and basophils are known mediators of nasal allergic disease and make up less than 10% of the peripheral blood of healthy individuals so we also utilized two cell lines representing those populations. Cellular responsiveness to coculture in the presence of lunar dust was evaluated in several

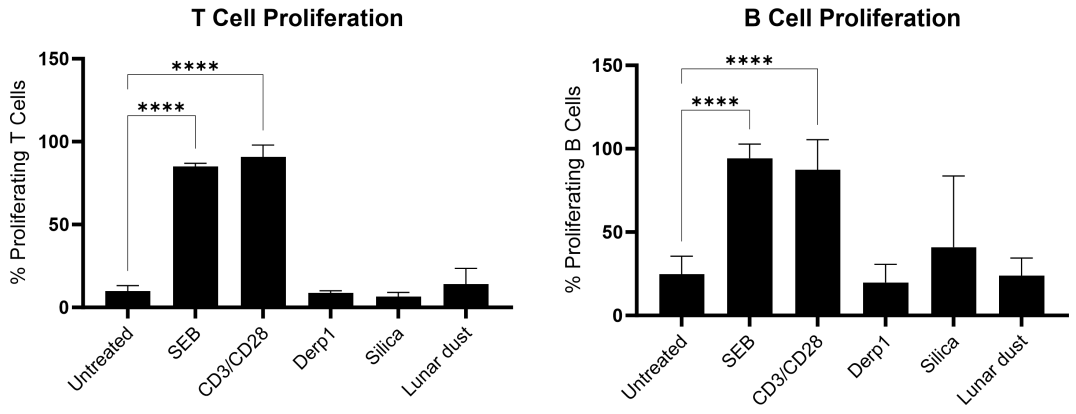

FIGURE 12
Percentage of **(A)** T cell and **(B)** B cell proliferation in 6 day cultures for each stimulation/treatment in comparison to untreated control cultures. **** P<0.0001.

different ways. Our investigation assessed the bulk levels of key immune cells before and after culture by flow cytometry. The induction of cell surface activation markers was also determined by flow cytometry. Cytokines are small proteins produced by several cell types with many different functions. Some roles cytokines play is in cell signaling during an immune response to communicate to other immune cells for recruitment, expansion, activation or to produce more antigen specific cytokines. Not relying on cellular assessments, which can be difficult for activated cells, assaying supernatant cytokine profiles is an extremely sensitive and reliable indicator of both cellular activation and the specific nature of the response (inflammatory, Th1, Th2, etc.). There were no significant changes in cytokine production in response to the allergen, Derp1, or lunar dust. This indicates Derp1 and lunar dust do not induce an immediate and inflammatory immune response in this model. Allergic reactions are triggered by exposure to allergens, or usually harmless substances, such as dust, pollen, pet hair, etc., that induce the immune system into an immediate overactive Th2 inflammatory response by recruitment and expansion of cells, and production of cytokines, histamine, IgE, leukotrienes, etc. We measured soluble cytokines in culture supernatants by multiplex array and the production of allergy-specific products IgE, leukotriene B4, and histamine by ELISA. In any immune response to a foreign invader, the cascade of events for immune cells to respond after activation include rapid cell growth, or proliferation. T cells are a proliferating cell population in response to a foreign antigen or pathogen and this study used a cellular proliferation assay to determine if lunar dust induced this response. Flow cytometry was also applied to evaluate proliferative/blastogenesis responses of the T and B cell populations. Lastly, we employed microscopy to examine cell-lunar dust interactions.

Regarding the healthy subject primary immune cells, we did not find any significant changes in cellular activation or cytokine production in the human whole blood cultures in response to lunar dust. Allergy specific reactions indicated by increased histamine, leukotrienes, or IgE, were also not detected in subject whole blood cultures. Proliferative responses of any whole blood populations to lunar dust were not detected in any subjects.

For the cell line assessments, we did see direct activation of the eosinophils cell line (EOL-1) in response to lunar dust, however activation was also detected in response to silica (Figure 5). The response to silica and lunar dust in the eosinophil cell line cultures, but not in the primary whole blood cultures are likely due to a direct eosinophil response. Whole blood cultures have the benefits of all responding cell populations (not culturing artificially purified cells), and retaining soluble factors, resulting in a more *in-vivo*-like system. However, the other immune cells present that could mitigate responses from the eosinophil population, or more likely, the very low percentages of basophils and eosinophils in peripheral blood may have blunted any responsiveness. The basophil cell line (KU812) responded to lunar dust exposure by increased leukotriene B4 production (Figure 9) and the eosinophil cell line increased histamine after culture with lunar dust (Figure 10). No similar leukotriene or histamine responses were observed, in either cell line, to silica.

In short, assessments in primary human subject blood immune cells indicated no evidence whatsoever for sensitization, cellular responsiveness, nor 'allergy' to lunar dust. Possible caveats include the limited number of subjects used, the wide range of atopy seen in generally healthy individuals (the subjects were not known to be atopic) and a lack of previous sensitization (the subjects had not visited the lunar surface). During the Apollo reports of 'allergy' responses, those individuals similarly could not have been pre-sensitized, so we assume that any sensitization would have been via cross reactivity to some terrestrial product that induced cross reactivity to elicit an allergy-like response. Therefore, monitoring future Artemis crewmembers that will participate in lunar surface extravehicular activities for reactivity to lunar dust is appropriate to rule out some inherent existing reactivity to lunar dust.

Interestingly, assessments using purified 'allergic' cell lines, did yield some unique but mild responsiveness to lunar dust. At least for monitoring activation for the eosinophil cell line, responsiveness was observed to both lunar dust and silica. For leukotriene B4 and histamine, responses were seen that seem to be lunar dust specific. The eosinophil responsiveness to silica could indicate a manifestation of some sort of particulate response, however the

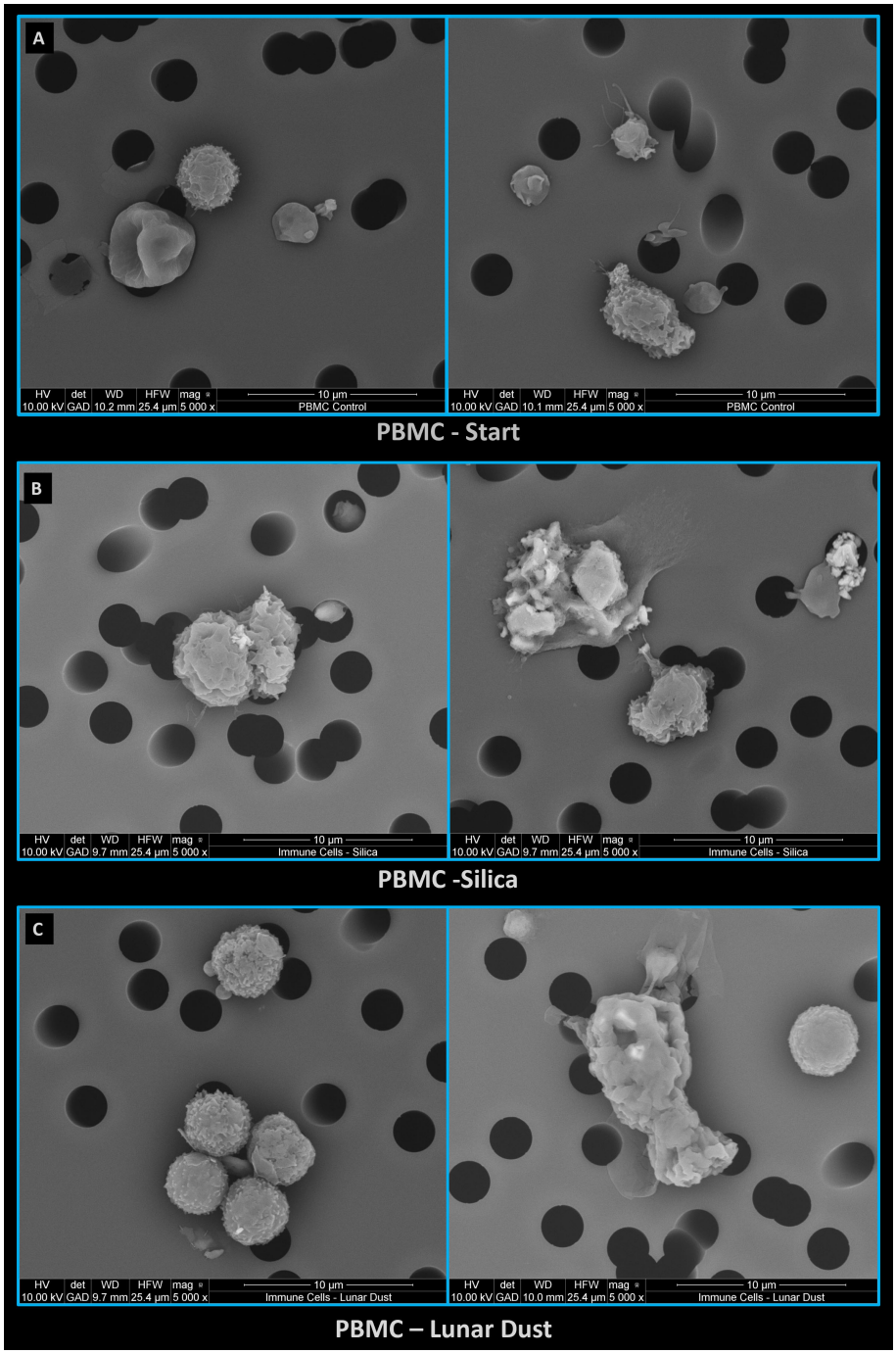

FIGURE 13
Representative images of PBMCs fixed following 48hr of culture with **(A)** control media, **(B)** media with silica, and **(C)** media with lunar dust.

leukotriene and histamine responses were more specific. While these results may seem disparate, for clinical interpretation we would prioritize the findings from the primary subject donor cell populations.

While no responses were observed from the test subjects, it should be disclosed that it is possible that these subjects, lacking prior sensitization to whatever terrestrial product that may induce immunogenic responses similar to lunar dust, were simply 'not allergic' to the product that lunar dust represents. The findings from the cell lines however, may represent the possibility that human allergenic cell sensitivity/reactivity to lunar dust is conceptually possible.

Future investigations could expand on this study. Certainly, an assessment of more human subjects with complete medical history data would allow a better determination of population sensitivity. More refined lunar dust with similar consistency in texture, size and granularity would also benefit the study. Lunar dust exposure is inevitable for future lunar exploration missions and efforts to

reduce the amount of lunar dust exposure and countermeasures for addressing irritation will need to be put in to place. Our previous studies looking at the inhalation toxicity of lunar dust in rats (7), the immunoreactivity data of lung inflammation in response to inhalation of fine lunar dust particles and increased immune cell migration (17), and this study determining the allergy specific immune responses, will help guide NASA to develop mitigation techniques and potential countermeasures necessary in the event of excessive exposure to lunar dust during lunar surface EVAs.

Data availability statement

The original contributions presented in the study are included in the article/Supplementary Material. Further inquiries can be directed to the corresponding author.

Ethics statement

The studies involving humans were approved by NASA Institutional Review Board. The studies were conducted in accordance with the local legislation and institutional requirements. The participants provided their written informed consent to participate in this study.

Author contributions

AC: Conceptualization, Data curation, Formal analysis, Investigation, Methodology, Project administration, Validation, Visualization, Writing – original draft, Writing – review & editing. CG: Data curation, Formal Analysis, Investigation, Methodology, Software, Writing – review & editing. MN: Data curation, Formal analysis, Investigation, Methodology, Project administration, Supervision, Validation, Writing – review & editing. GM: Conceptualization, Resources, Visualization, Writing – review & editing. JM: Conceptualization, Funding acquisition, Project administration, Resources, Supervision, Visualization, Writing – review & editing. BC: Conceptualization, Funding acquisition, Methodology, Project administration, Resources, Supervision, Visualization, Writing – review & editing.

Funding

The author(s) declare that financial support was received for the research and/or publication of this article. This work was supported by 2019 HERO 80JSC019N0001-FLAGSHIP & OMNIBUS: Human Research Program Crew Health. Appendix A&B.

Conflict of interest

The authors declare that the research was conducted in the absence of any commercial or financial relationships that could be construed as a potential conflict of interest.

Generative AI statement

The author(s) declare that no Generative AI was used in the creation of this manuscript.

Publisher's note

All claims expressed in this article are solely those of the authors and do not necessarily represent those of their affiliated organizations, or those of the publisher, the editors and the reviewers. Any product that may be evaluated in this article, or claim that may be made by its manufacturer, is not guaranteed or endorsed by the publisher.

Supplementary material

The Supplementary Material for this article can be found online at: https://www.frontiersin.org/articles/10.3389/fimmu.2025.1539163/full#supplementary-material

References

1. Loftus DJ, Rask JC, McCrossin C, Tranfield EM. The Chemical Reactivity of Lunar Dust: From Toxicity to Astrobiology. *Earth Moon Planets*. (2010) 107:95–105. doi: 10.1007/s11038-010-9376-x

2. Scheuring RA, Jones JA, Novak JD, Polk JD, Gillis DB, Schmid J, et al. The Apollo Medical Operations Project: Recommendations to improve crew health and performance for future exploration missions and lunar surface operations. *Acta Astronaut*. (2008) 63:980–7. doi: 10.1016/j.actaastro.2007.12.065

3. Crucian B, Stowe RP, Mehta S, Quiriarte H, Pierson D, Sams C. Alterations in adaptive immunity persist during long-duration spaceflight. *NPJ Microgravity*. (2015) 1:15013. doi: 10.1038/npjmgrav.2015.13

4. Mehta SK, Laudenslager ML, Stowe RP, Crucian BE, Feiveson AH, Sams CF, et al. Latent virus reactivation in astronauts on the international space station. *NPJ Microgravity*. (2017) 3:11. doi: 10.1038/s41526-017-0015-y

5. Crucian B, Johnston S, Mehta S, Stowe R, Uchakin P, Quiriarte H, et al. A case of persistent skin rash and rhinitis with immune system dysregulation onboard the International Space Station. *J Allergy Clin Immunol Pract*. (2016) 4:759–762 e8. doi: 10.1016/j.jaip.2015.12.021

6. Meyer C. (2010). Lunar sample compendium, in: *The 41st Lunar Planetary Science Conference*. TX, United States: The Woodlands. Available online at: https://ntrs.nasa.gov/api/citations/20090041867/downloads/20090041867.pdf.

7. Lam CW, Scully RR, Zhang Y, Renne RA, Hunter RL, McCluskey RA, et al. Toxicity of lunar dust assessed in inhalation-exposed rats. *Inhal Toxicol*. (2013) 25:661–78. doi: 10.3109/08958378.2013.833660

8. IARC Working Group on the Evaluation of Carcinogenic Risks to Humans. Arsenic, Metals, Fibres and Dusts. Lyon (FR): International Agency for Research on Cancer; 2012. (IARC Monographs on the Evaluation of Carcinogenic Risks to Humans, No. 100C.)

SILICA DUST, CRYSTALLINE, IN THE FORM OF QUARTZ OR CRISTOBALITE (2012). Available online at: https://www.ncbi.nlm.nih.gov/books/NBK304370/.

9. Marshall GD Jr., Davis F. Dusting off recombinant allergens. *Nat Biotechnol*. (1997) 15:718–9. doi: 10.1038/nbt0897-718

10. Marsman C, Verhoeven D, Koers J, Rispens T, Ten Brinke A, et al. Optimized protocols for in-vitro T-cell-dependent and T-cell-independent activation for B-cell differentiation studies using limited cells. *Front Immunol*. (2022) 13:815449. doi: 10.3389/fimmu.2022.815449

11. Thyagarajan B, Barcelo H, Crimmins E, Weir D, Minnerath S, Vivek S, et al. Effect of delayed cell processing and cryopreservation on immunophenotyping in multicenter population studies. *J Immunol Methods*. (2018) 463:61–70. doi: 10.1016/j.jim.2018.09.007

12. Su KY, Watanabe A, Yeh CH, Kelsoe G, Kuraoka M. Efficient culture of human naive and memory B cells for use as APCs. *J Immunol*. (2016) 197:4163–76. doi: 10.4049/jimmunol.1502193

13. Bochner BS. Systemic activation of basophils and eosinophils: markers and consequences. *J Allergy Clin Immunol*. (2000) 106:S292–302. doi: 10.1067/mai.2000.110164

14. Hirai K, Miyamasu M, Takaishi T, Morita Y. Regulation of the function of eosinophils and basophils. *Crit Rev Immunol*. (1997) 17:325–52. doi: 10.1615/CritRevImmunol.v17.i3-4.40

15. Yang S, Chen L, Zhang H, Song Y, Wang W, Hu Z, et al. Beyond the itch: the complex interplay of immune, neurological, and psychological factors in chronic urticaria. *J Neuroinflammation*. (2025) 22:75. doi: 10.1186/s12974-025-03397-4

16. Ogulur I, Mitamura Y, Yazici D, Pat Y, Ardicli S, Li M, et al. Type 2 immunity in allergic diseases. *Cell Mol Immunol*. (2025) 22:211–42. doi: 10.1038/s41423-025-01261-2

17. Crucian BE, Quiriarte H, Lam CW, Nelman M, Colorado AA, Diak DM, et al. Pulmonary and systemic immune alterations in rats exposed to airborne lunar dust. *Front Immunol*. (2025) 16:1538421. doi: 10.3389/fimmu.2025.1538421

frontiers | Frontiers in Physiology

TYPE Review
PUBLISHED 13 May 2025
DOI 10.3389/fphys.2025.1558711

OPEN ACCESS

EDITED BY
Christopher D. Porada,
Wake Forest University, United States

REVIEWED BY
Marta Gimunová,
Masaryk University, Czechia
Jonathan Steller,
UC Irvine Medical Center, United States

*CORRESPONDENCE
Mariano Bizzarri,
mariano.bizzarri@uniroma1.it

RECEIVED 10 January 2025
ACCEPTED 28 April 2025
PUBLISHED 13 May 2025

CITATION
Cutigni M, Cucina G, Galante E, Cerri M and Bizzarri M (2025) Microgravity impairs endocrine signaling and reproductive health of women. A narrative review.
Front. Physiol. 16:1558711.
doi: 10.3389/fphys.2025.1558711

Microgravity impairs endocrine signaling and reproductive health of women. A narrative review

Michela Cutigni[1], Giorgia Cucina[1], Emanuele Galante[1], Matteo Cerri[2] and Mariano Bizzarri[1]*

[1]Department of Experimental Medicine, Space Biomedicine Laboratory, University Sapienza, Rome, Italy, [2]Department of Biomedical and NeuroMotor Sciences, University of Bologna, Bologna, Italy

During space exploration missions the organism is subjected to several challenges. Most of the studies have been performed on male health in space, leaving the focus on sex differences behind. With the development of new biological technologies, attention is now being paid more to how spaceflight conditions affect human reproductive health. In this review, the focus is on how weightlessness disrupts ovarian function and endocrine signaling by affecting the hypothalamic-pituitary-gonadal axis. Emerging evidence suggests that microgravity can impair estrogen production through the suppression of aromatase expression in granulosa cells. This condition leads to a hypo-estrogenic condition that harms the ovulation and the menstrual cycle. Likely, due to reduced estrogen availability, bone density, and cardiovascular health can consequently be severely involved. New studies focus on how space-related deregulation involving ovarian steroidogenesis look like the picture observed in the Polycystic Ovary Syndrome. These similarities open the perspective to counteract pharmacologically the observed abnormalities. However, our knowledge is severely constrained by the limited data available as well by the lack of proper experimental models of investigation. Indeed, much is required in order to acquire a full understanding of endocrine and functional changes occurring during microgravity exposure, including the joint effect of radiation and weightlessness that deserve to be thoroughly investigated to recognize the respective contribution of each one as well as the eventual synergies.

KEYWORDS

weightlessness, steroidogenesis, aromatase, female fertility, ovarian function

Introduction: The importance of assessing the gonadal hormones in space

To undertake prolonged missions in deep space, and in the perspective for stable settlements on the Lunar or Mars surface, it is mandatory to assess how spaceflight conditions–radiation and microgravity exposure–interfere with gonadal functions and affect the reproductive capabilities. By February 2024, a total of 681 individuals have reached the altitude of space according to the USAF definition, with 610 achieving Earth orbit. Among them, 155 (22.7%) have been women.

The overall physiological and psychological adaptation to the spaceflight environment is similar for male and female astronauts. However, there are critical differences in physiological functioning related to sex (Ronca et al., 2014).

Noticeably, besides the well-known effects of radiation on the reproductive system (Ogilvy-Stuart and Shalet, 1993), microgravity can also modify the endocrine control of both male and female gonads (Mathyk B. et al., 2024).

Male and female reproductive systems are different and therefore deserve independent focus and research to understand the short and long-term impacts of the spaceflight environment. The female reproductive system presents a significant challenge for scientific investigation, as its endocrine regulation involves multiple interconnected levels—including the central nervous system, adrenal glands, and gonads—functioning according to a highly orchestrated timing.

Furthermore, throughout all its phases, female sexual and reproductive function is highly sensitive to a wide range of physical, chemical, and psychological stressors.

Therefore, understanding whether and how ovarian endocrine function is conserved in space conditions is mandatory to preserve the integrity of other systems, which are frequently hindered in space, especially due to weightlessness (Aydogan et al., 2024). Although pregnancy is contraindicated during spaceflight, in the forecast of permanent off-Earth human settlements, this aspect of human life in space should be considered. Indeed, female sex steroid hormones (estrogen, progesterone) have an impact on multiple body apparatuses, and they play a special role in modulating bone, muscle and cardiovascular functions, making a clear difference in respect to males. As we said above, certain conditions exhibit significant differences based on sex (Chromiak et al., 2003). However, no increase in gynecologic cancer risk has yet been revealed in the female astronaut population (Barr et al., 2007) but, as exploration missions will be outside of low Earth orbit and for increasingly long durations, concern remains regarding the effects related to prolonged exposure to both microgravity and even a low-dose rate of radiation accumulating over time (Drago-Ferrante et al., 2022).

Sadly, the distinctive features of the female endocrine system, which is more intricately connected to a periodic endocrine regulation of the organism, have been ignored for decades in biomedical space research, considering that the space community considered males a sufficient/appropriate proxy for all humans (Simon, 2005).

Lately, however, the overall impact of spaceflight weightlessness on reproductive function has been investigated in several studies and reviews (Gimunová et al., 2024), (Strock et al., 2023).

Recently, the ESA *SciSpacE* white papers set out the research needed to advance our knowledge in this field of space physiology and identified eight key knowledge gaps (ESA SciSpacE White Papers, 2021). Namely, the white paper recognizes that there is limited knowledge available on the systemic effects of spaceflight stressors upon the general endocrine control on both females and males. However, due to the small numbers of female astronauts who have undertaken long-duration spaceflight it was not possible to perform a direct assessment of the impact of space conditions upon female fertility. Therefore, it is required to deepen our understanding on how increased and prolonged spaceflight affect the functionality of reproductive organs, as well as the conceivable risk of cancer for offspring due to the exposure of germ cells to space stressors. To achieve such objectives, it is essential to identify appropriate experimental models both encompassing simulated weightlessness and experiments conducted aboard the International Space Station involving cells, tissues and organs as well as living animals. Reproductive capabilities of living organisms are challenged by both radiation exposure and microgravity, and these stressor factors can eventually synergize. We are aware of the impact of radiation on endocrine and reproductive apparatus, whereas microgravity consequences have been underestimated for a long time; given that, the mechanisms elicited by weightlessness are still a matter of research and deserve an appropriate investigation.

Therefore this review aims to examine the effects of microgravity on gonadal function and reproductive health, with a focus on female fertility. It wants to highlight the existing knowledge gaps, regarding endocrine regulation and long-term fertility risks in space, remarking the need for experimental models to ensure the feasibility of prolonged human space missions and future space settlements.

For the bibliography research, we began by defining the main research question to establish clear guidelines for selecting relevant sources. We then explored various academic databases, library catalogs, and reliable online repositories to gather books, journal articles, and other materials related to the topic. Once we identified the most suitable references, we organized them systematically and formatted them according to the appropriate citation style, ensuring accuracy and consistency throughout the bibliography.

Assessing the reproductive function: main challenges

The female reproductive system consists of internal and external organs that are modulated by several nutritional, biophysical, endocrine and psychological factors, interacting across different and intertwined levels of organization. This apparatus is involved in regulating sex hormones (participating in several critical physiological functions), producing gametes and ensuring their subsequent maturation. This process is instrumental in the development of the zygote and subsequent fetus, ensuring the functional environment necessary for fetal growth and preparation for delivery. The female reproductive interval spans between menarche (the first occurrence of menstruation) and menopause (cessation of menses for 12 consecutive months): the interconnected endocrine network encompasses critical changes during the lifespan, also undergoing sophisticated modifications across time - the menstrual cycle. Noticeably, reproduction-associated processes entail several organs and tissues, not limited to sexual organs as other apparatus–including bone and cardiovascular systems–are tightly dependent from the endocrine ovarian control acting mostly through the release of the main steroid hormones 17β-estradiol (E2) and Progesterone (P4) (Figure 1).

Upstream of this process, ovarian steroidogenesis is extremely sensitive to the influence exerted by systemic neuroendocrine regulatory factors–including gonadotropin-releasing hormone (GnRH) and Kisspeptin, produced by the hypothalamic–pituitary–adrenal axis (HPA), as well as by paracrine cues, which include a plethora of signaling

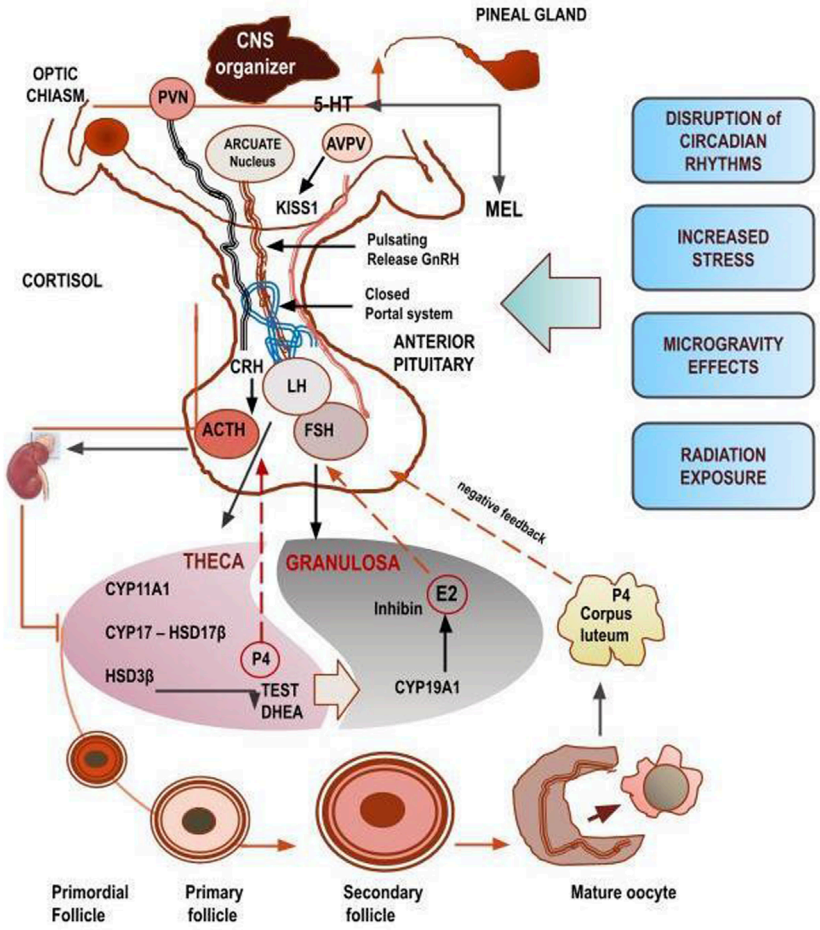

FIGURE 1
Regulatory tree of steroidogenesis distributed along a hierarchical axis. The diagram illustrates the main hubs that environmental space-related stressors can affect.

factors (Bone Morphogenetic Protein, Activin, Inhibin, Melatonin) (Zavala et al., 2020).

Kisspeptin encoded by the KiSS-1 gene plays a pivotal role in gametogenesis and endocrine regulation by modulating the HPA axis, inducing the release of GnRH and being inhibited, in a negative feedback cycle, by sex hormones such as testosterone and 17β-estradiol (Smith et al., 2005). A preliminary study performed on a rodent model of tail-suspension hindlimb unloading to simulate the microgravity condition has demonstrated that Kisspeptin significantly decreases after 30 days of exposure (Moustafa, 2021). Albeit the study was carried out on male rats, results showed that the simulated weightlessness was able to also downregulate pituitary expression levels of FSH and LH, ultimately impairing spermatogenesis, suggesting the possibility of an influence on female steroidogenesis as well.

GnRH is released in a pulsatile manner by the hypothalamus and acts on the anterior pituitary lobe (Adeno-Hypophysis), modulating the synthesis and subsequent secretion of follicle-stimulating hormone (FSH) and luteinizing hormone (LH) into the bloodstream. In the follicle, downstream of the Hypothalamic-Pituitary-Gonadal axis (HPG), FSH and LH activate the steroidogenic pathway by promoting in the Theca cells the synthesis of androgens that are further converted in estrogens in Granulosa cells. Steroidogenesis operates according to the two-compartment model, whose effectiveness depends primarily on the activity of Aromatase (Cyp19A1), the enzyme responsible for the aromatization of androgens into estrogens (Estrone and 17β-Estradiol) (Stocco, 2012). Specifically, FSH induces the upregulation of aromatase in Granulosa cells, while LH stimulates the production of androgens in theca cells.

Estrogens and Progesterone are released in a cyclic manner under the influence of LH/FSH and, in turn, they exert negative feedback onto the hypothalamus and anterior pituitary. A relevant exception is the positive feedback deployed by E2 during the ovulation, thus increasing the GnRH pulse frequency and stimulating the LH surge.

Additionally, female behavior during mating shows variable sexual susceptibility depending on endocrine inputs (Yin and Lin, 2023). Several hypothalamic areas, located especially in ventrolateral and ventromedial hypothalamus, display a specific distribution of estrogen receptors (ER) type 1, which are involved in controlling mating receptivity (Liu et al., 2022), according to a complex dynamic (Liu et al., 2024).

Overall, the menstrual dynamics reflect many underlying complex interactions, involving ovarian steroidogenesis, scheduled recruitment of follicles ending with the maturation of the oocyte, and contemporary changes in the endometrium, which are driven by central hormones (release by HPG axis), triggering many feedback loops encompassing molecular and biophysical factors. Noteworthy, the entire system is tightly synchronized with the circadian rhythm, alongside with both central and peripheral clock genes.

Spaceflight conditions likely may disrupt this delicate control, by acting through different and convergent mechanisms. Alteration of the sleep-wake rhythm and alteration of circadian rhythms impair the physiological release of melatonin and other several neurotransmitters. It is worth mentioning that several hypothalamic neurohormones (including serotonin, catecholamines, and oxytocin) are modified after exposure to microgravity (Blanc et al., 1998), (Kastello and Sothmann, 1999), (García-Ovejero et al., 2001), although the mechanisms responsible for these changes are not yet known. Circadian rhythm disruption is one of the main causes of fewer chances for reproductive success, given that some critical functions, such as body temperature, heart rate, and hormone secretion are tuned and regulated according to the chronobiological rhythm (Sciarra et al., 2020). Specifically, loss of rhythm in the suprachiasmatic nuclei–tightly modulated by the alternate cycle of appropriate dark/light periods - can affect the pulsatile sexual hormones release (Dickmeis et al., 2013).

Glucocorticoids produced by adrenal glands function according to a circadian rhythm and participate in the synchronization of the endogenous clocks. Stress conditions and disruption of circadian rhythms steadily increase cortisol levels and impair many functions, including the reproductive system (Domes et al., 2024). Noticeably, cortisol inhibits GnRH release upon the hypothalamus and influences gonadotropins synthesis and release on the pituitary (Vitellius et al., 2018). Consequently, glucocorticoids can cause alteration of ovarian cyclicity, by either inhibiting Kisspeptin neurons or stimulating the release of gonadotropin-inhibitory hormone (Michael et al., 1993). As expected, both salivary and blood/urine levels of cortisol show a significant increase during spaceflight missions (Zangheri et al., 2019), (Benjamin et al., 2016), and it is tempting to speculate that this effect can impair the reproductive function.

Physical exercise is a further confounding issue. On Earth, HPG axis activation is tightly dependent upon both the extent and intensity of exercise (Tremblay et al., 1985) and can even lead to amenorrhea/anovulation (Hakimi and Cameron, 2017). Nutritional deficits can worsen the HPG response further (Williams et al., 2015), eventually leading to a relevant disruption of reproductive hormones balance. Therefore, as women in space undergo a stressful program of physical exercise–required to counteract the negative impact of weightlessness on bone and muscle–it is possible that intense physical exercise in space could alter the HPG response, though there is no evidence of exercise in space leading to amenorrhea/anovulation to date.

Thus, it is conceivable that exposure to microgravity, as well to other harmful spaceflight conditions, can significantly interfere with proper reproductive function and steroidogenesis. Noticeably, modifications of reproductive capabilities can occur at multiple levels and do not involve only endocrine organs (ovaries, testis), but may happen at the hypothalamus or pituitary.

Due to the complexity of the system under scrutiny, as well as the different mechanisms of action triggered by spaceflight, investigating this intricate question is arduous and requires the use of several and appropriate experimental models.

Models

Until now, limited research has focused on the effect of space travel on the reproductive system and its function, along with endocrine regulation of reproduction or prenatal development (Jain et al., 2023). A fundamental preliminary issue lies in establishing a proper model of investigation, a task essential for identifying the impact of specific stressors. Indeed, it is problematic to distinguish whether reproductive changes are due either to modified gravity or to radiation–the two most relevant threats–or should also be ascribed to other factors, such as noise, isolation, disrupted circadian rhythms, and stress (Monga and Gorwill, 1990). It is worth remembering that ovarian steroidogenesis undergoes modifications throughout a woman's lifespan. Therefore, it is imperative to correlate experimental data to women's age, and with the concomitant hormonal changes, especially those occurring during critical periods (perimenopausal and postmenopausal periods).

In addition, the short duration of spaceflights, and the small number of women who have participated in at least one space mission, limits the statistical validity of such studies. Moreover, it can be reliably assumed that short and long exposure to space conditions may have different (and eventually unexpected) effects on reproductive health. Indeed, in both male animals and astronauts, microgravity showed to influence the HPG axis response only during exposure for short periods. In rodents, plasma and tissue testosterone decreased after 2 weeks of spaceflight (Amann et al., 1985), (Grindeland et al., 1990). Similarly, testosterone decreased in astronauts after 12 days of weightlessness. In contrast, quite paradoxically, testosterone did not change during prolonged stay in space, while, after landing, it decreased up to 50% of basal values (Smith et al., 2012).

By no doubt, the simultaneous exposure to multiple environmental hazards complicates the assessment of the relative weight of each risk factor and their mutual synergy. It is worth mentioning that studies conducted during spaceflights have been performed in Low Earth Orbit (LEO), where radiation exposure is lower compared to that in outer space.

Therefore, various ground-based models involving either animals or *in vitro* cells are frequently used for investigating the bone and musculoskeletal systems (Emily, 1979); they also have been employed to assess the adaptive and pathological response to microgravity of the reproductive apparatus. Using these models offers several advantages, including practical feasibility, the possibility to control environmental factors in a more precise manner, as well as the possibility to conduct experiments repeatedly at minimal cost. However, these opportunities present a double-edged nature, as animals adapt rapidly to these stressing conditions, thereby dabbing the physiological stress response in short times (Ortiz et al., 1999). Therefore, ground-based models could be questionable as simulated microgravity models are bias-affected by considering gravity a force rather than a field.

Moreover, astronauts are vulnerable to both reduced and increased gravity exposures, and this could represent an additional source of uncertainty in identifying exactly the impact of weightlessness upon the reproductive system. In addition, different microgravity values are expected when different space environments are considered: on the surfaces of the Moon and Mars, and on the ISS, the intensity of the gravitational field varies and is lower compared to Earth, tending towards zero in the latter case, due to the free fall regime (Williams, 2015). It is therefore conceivable that organisms, in their macroscopic complexity, and cells, locally, would respond in a very different manner in those different circumstances. (Wolfe and Rummel, 1992).

Female reproductive effects

Animal data

The first studies focusing on mammalian reproduction were performed on unmanned satellites. A pool of male and female rats experienced 19 days onboard of the COSMOS-1129 biosatellite, in which the sexual encounters were allowed after removing a physical barrier. Once back on land, they guessed that two out of five females underwent pregnancy with resorption, while the remaining three rats showed signs of estrus disturbance, lack of ovulation and other problems related to fertilization (Serova and Denisova, 1982).

In a subsequent, similar study pregnant rats were sent during the COSMOS-1514 biosatellite mission for some days in space. On the re-entry, they showed reduced fetal weight and skeletal development when compared to ground controls (Serova et al., 1984). In addition, litter from flight mothers showed increased mortality during the first postnatal week. Two experimental investigations (study NIH. R1 and NIH. R2) focused on the pregnancy outcome of Sprague–Dawley rats that spent 2 weeks in space. After landing, animals were sacrificed, whereas the pups were assigned to on ground-raised dams. Spaceflight did not alter main pregnancy (maternal weight gain during pregnancy, duration of pregnancy, duration of parturition, litter size) and hormonal parameters (serum LH, FSH, and P4), when compared to either synchronous flight or unilateral hysterectomy vivarium controls, albeit pituitary LH content decreased (Burden et al., 1997). Some other interesting modifications were recorded in myometrium structure, given that the major gap junction protein (connexin 43) – required for enabling the electrical coupling of myometrial cells - was decreased in the flight group *postpartum* compared to controls (Burden et al., 1998). Tissue estrogen and progesterone receptor expression were both lower than that assessed in animals in ground controls. However, by examining in detail the experimental plan of the aforementioned studies we can detect many potential factors of bias. First animals had a laparotomy before (to make sure they had enough developing embryos) and post-flight, before being allowed to labor. This complicated procedure may have significantly altered the results, not to mention the stress the animals had to undergo.

Further studies performed during sequential missions (STS-131, 133, and 135/BSP) showed that female mice had reduced ovary weights than controls (Ronca et al., 2014). The ovaries were significantly smaller in flight (4.04 + 1.53 mg) compared to ground controls (5.52 + 0.89 mg), with fewer corpora lutea in the flight ovaries. Moreover, several growing follicles were atretic, indicating blocked estrous cycle. Similar results have been recorded during three subsequent missions (STS-131, STS-133, STS-135), confirming a serious impairment of the corpora lutea and the significant reduction of estrogen receptors in the uterus (Holets et al., 2015). Remarkably, expression of estrogen receptors ERα and ERβ were significantly lower (>20-fold) in the uteri of animals exposed to spaceflight. Similarly, progesterone receptor Pgr-AB expression was downregulated (3–4 fold) in flight ovaries. Reduced expression of estrogen receptors was further confirmed by the recorded downregulation of lactoferrin expression, as both ERα and ERβ are known positive regulators of lactoferrin (Teng et al., 2002).

Intriguingly, some precursors of the tryptophan-melatonin pathways (5-Hydroxy-Indoloacetic acid and 5-Hydroxy-Tryptamine) were found increased in mice during Cosmos1887-Bion eight and the Cosmos 2044-Bion nine spaceflight missions (Charles et al., 2015), (Holley et al., 1991). The overall results of the latter study indicate that animals experienced a significant stress as witnessed by adrenal hypertrophy and depletion of pineal melatonin stores, associated with an increased turnover of several intermediate metabolites of the serotoninergic pathway. According to the author's conclusions, melatonin may have been released in large quantities due to spaceflight-related stress, resulting in pineal depletion of the neurohormones. In turn, increased release of melatonin could exert negative effects upon steroidogenesis, namely by inhibiting the hypothalamic release of GnRH, with a consequent alteration of FSH and LH levels (Basini and Grasselli, 2024).

Taken together, data provided by experimentation on mice suggest that the spaceflight environment may affect the reproductive system, by interfering with several hormone signaling. However, the reduction in estrogen availability could be an underlying mechanism explaining changes on wider physiological systems occurring during spaceflight (Tash et al., 2011). Moreover, changes in estrogen availability might likely influence sexual arousal and, ultimately, pregnancy potentialities.

Overall, the studies performed in the years 1965–2000 with animal models demonstrated potentially serious implications for human reproductive capability in microgravity conditions. Namely, investigations utilizing mammalian species concordantly reported significant alterations in morphology and development of both male and female germ cells (Keefe et al., 1981), (Plakhuta-Plakutina et al., 1976). These findings could have significant implications for embryogenesis, potentially leading to a significant number of abnormalities and/or aborted fetuses. The preliminary conclusions were rather pessimistic, stating, «The problems of embryogenesis or later child development may prove to be insurmountable in a zero—gravity environment due to the significant contribution of gravity to the normal development of bone and muscle. Planetary surfaces with higher or lower levels of gravity compared to Earth may also result in developmental abnormalities *in utero* or after birth» (Santy and Jennings, 1992). However, the modulation of endocrine pathways and the regulation of embryogenesis under gravity regimes distinct from Earth's gravity or microgravity remain a largely unexplored area of research.

Intrinsic, methodological limits of experiments carried out in this period were unsurmountable and, as highlighted by many

scientists, asked for a more appropriate investigation model in which the entire cycle of mammalian development could be studied in the space environment (Serova et al., 1982).

A highly used device for investigating microgravity effects on rodents is the Morey-Holton hindlimb suspension (HLS) model. This model–first described in the 1970s - involves suspending rats by the tail base to produce a 30° head-down position, a condition comparable to the human 6° head-down tilt utilized in bed-rest studies (Morey-Holton and Globus, 1985). This position results in a cephalic fluid shift and musculoskeletal unloading, which also occur during spaceflight. The intent of developing a hindlimb unloading model is to provide a ground-based system that simulates certain aspects of spaceflight in animals. The first model did not allow for ambulatory activity and provoked a significant stress response in the animals. To overcome this important limitation, HLS models continue to be modified in order to minimize stress and to allow either horizontal or head-down unloading to investigate the consequences of fluid shifts (Musacchia, 1985).

The HLS model was used to simulate the major physiological effects of hypo gravity on pregnancy. Exposure of rats to HLS during the early phases of pregnancy reduces implantation (Gharbi et al., 1996). Intriguingly, in this condition rats did not experience a significant distress, as documented by the lack of elevated plasma or adrenal corticosterone, suggesting that the impaired reproductive capabilities were due to microgravity effects only, rather than to secondary effects of stress (Kinoue, 1996).

In female Sprague-Dawley rats, the simulated weightlessness prolonged the diestrus and lengthened estrous cycles, suggesting that animals experienced hypoestrogenism (Tou et al., 2004). Remarkably, the length of these cycle's phases resulted significantly modulated by diet, given that commercial chow showed to attenuate hypoestrogenism (likely by providing an exogenous source of estrogens). Simulated weightlessness is reputed to «activate» the HPA axis, as confirmed by increased urinary cortisol levels during the first experimental days, thus suggesting that the response to acute stress constitute a feasible mechanism explaining the disruption of estrous cycles. It is worth noting that in chow-fed rats, the increase in urinary cortisol resulted unaffected, thus suggesting that estrogens in chow-diet do not antagonize the stress response.

Hormonal data collected after spaceflight have provided controversial results, with reduced hypophysis content of LH, while serum LH concentrations resulted in normal range (Burden et al., 1997). Similarly, FSH in the pituitary showed a significant reduction whereas the plasma content steadily increases. Likely, a more realistic analysis would benefit from a sequential blood sampling as both LH and FSH display a pulsatile secretion, imposing to reconstruct a circadian profile for an appropriate assessment. Indeed, some reports showed that rats mated during spaceflight ovulated and cycled normally; however, in that study mating did not give rise to birth (Serova and Denisova, 1982). Autoptic examination performed post flight evidenced that fetuses could be resorbed, without clear proof of whether conception or implantation could have occurred in space. Therefore, there is still a lack of scientific evidence regarding conception and implantation mechanisms under stress conditions, such as microgravity, suggesting that this represents a significant issue that still requires many answers.

Studies performed to assess the consequences of spaceflight on pregnancy provided inconclusive results. Some spaceflight missions have included rat dams for different times between days 9–19 of the 22-day gestation period (Amann et al., 1985), (Ronca and Alberts, 2000), (Wong and DeSantis, 1997). Overall, these studies recorded minor changes in respect to control dams, besides a reduction in offspring weight gain, prolonged parturition, lower birth weights, and increased perinatal mortality were recorded in just one study (Jain et al., 2023). In this case, the environmental stress may have contributed to the increased natal mortality, a finding that persisted in the F2 generation, as evidenced by several publications (Herrenkohl and Gala, 1979).

Microgravity may also interfere with oocyte maturation throughout the ovarian folliculogenesis, although this issue has attracted scarce attention. Mammal females have a limited number of oocytes throughout their life span, and the count steadily decreases as age advances. Oocytes are actively nurtured during folliculogenesis, a complex process involving systemic endocrine and intra-ovarian control, displaying gonadotropin-independent and gonadotropin-dependent phases, regulated by hormones (LH, FSH, ACTH), intra-ovarian endocrine factors (melatonin, AMH, Activin, Inhibin), cytokines (growth differentiation factor-9 - GDF-9 – and bone-morphogenetic protein-15 - BMP-15), inositol, growth factors, calcium fluxes, gap-junction proteins and cytoskeleton components (Orisaka et al., 2021). This complex framework undergoes time-dependent changes according to a non-linear dynamic, which cannot be described by reductionist models since they fail to capture sophisticated phenomena like those following the removal of the gravitational constraint (Echenim et al., 2005).

Simulated weightlessness reproduced using rotating wall vessels showed that proliferation of granulosa cells obtained from porcine ovaries was severely inhibited, with consequent arrest of the cell cycle (Dai et al., 2021). This effect is associated with other abnormalities related to cell-to-cell communication, resulting in the disruption of intercellular communications. Deregulation among theca and granulosa cells therefore impair the folliculogenesis, as witnessed by the increased rate of atresia in ovaries flown in space (Holets et al., 2015).

In mice exposed to simulated weightlessness, the rate of oocyte maturation significantly dropped (from 8.94% *versus* 73.0% in controls), probably because of a disruption of the meiotic spindle organization (Wu et al., 2011). This study - specifically designed to minimize shear stress (a frequently overlooked factor that can lead to biased results for on ground-based models) - showed delayed maturation of oocytes harvested at the first meiotic division from immature mice exposed to weightlessness, albeit oocytes were properly stimulated with FSH, LH and 17β-estradiol for 16 h. In addition, since the intercellular communications (GCs transzonal projections and oocyte microvilli) were found severely disrupted in microgravity, it was hypothesized that these abnormalities may decrease oocyte quality due to the lack of morphogenetic factors (Cheng et al., 2023). Those findings have been vindicated by an investigation showing that the ultrastructural morphology of mitochondria, endoplasmic reticulum, and cortical granules of human oocytes exposed to simulated weightlessness are severely disrupted, probably because a rewiring of the cytoskeleton (Miglietta et al., 2023). Additionally, using a rotatory system device to reproduce simulated weightlessness, several ultrastructural abnormalities of the oocyte, reduced follicle survival and downregulation of GDF-9 expression were found

(Zhang et al., 2016). It is worth mentioning that the study highlighted that follicles embedded in a three-dimensional microenvironment (alginate) survived significantly longer, showing a behavior superimposable to follicles growing on normal gravity. This finding suggests that the impairment of mechanotransduction–apparently « restored » by enabling cells to interact with a solid, surrounding environment–could be considered a primary causative factor in weightlessness-related effects on living organisms (Bizzarri et al., 2022). It is worth of mention that the Rotary Cell Culture System (RCCS) is a bioreactor designed to simulate microgravity conditions for cell culture. (Mitteregger et al., 1999). The system uses gentle fluid dynamics to maintain cells in a dynamic suspension, promoting spheroid formation while minimizing shear stress. However, this device has relevant limitations. These include potential for cell sedimentation at high speeds, requires a dynamic fluid suspension for cell culture (promoting hence some hydrodynamic forces), limited velocity ranges, and challenges with large cell aggregates and mass transfer (Talukdar et al., 2014).

The involvement of GDF-9 it is worth of interest given that–in association with IGF-1–it stimulates the replication of theca cells in small follicles (3–6 mm) from bovine ovaries, while depressing steroidogenesis (by reducing androstenedione and progesterone availability) (Spicer et al., 2008). Consequently, in theca cells from developing follicles, mRNA expression related to LH receptors and CYP11A1 was significantly downregulated by GDF-9, which is synthesized by granulosa cells. In addition, GDF-9 (associated with BMP-4) promotes granulosa cell proliferation and prevents premature differentiation of the granulosa cells during growth of follicles (Spicer et al., 2006). Reduced synthesis of GDF-9 in microgravity may therefore impair the cross talk between theca and granulosa cells, leading to disruption of both the steroidogenic pathway and the morpho-functional relationship inherent in the follicle's two-compartment structure.

Until now, the effects of the space environment on the ovaries of non-pregnant animal females have not received the attention they deserve. The analysis of the ovaries of *postpartum* rats flown in space do not report significant changes regarding macroscopic parameters of ovarian function (weight, number of atretic or preovulatory follicles) (Ying et al., 1973).

Limited data are available regarding the HPA axis activity during spaceflight. A single study reported several disturbances and a clear reduction in serum GnRH, FSH, LH and testosterone in male rats exposed to weightlessness (Yin and Lin, 2023). Unfortunately, female rats were excluded from this experiment. These findings have been ascribed to an imbalance in cephalad-fluid shift occurring in microgravity, as the fluid redistribution probably induces pituitary deformation, as documented by MRI investigation performed during a spaceflight (Kramer et al., 2020).

Female data

There is limited knowledge available on the systemic effects of spaceflight stressors, e.g. a wide range of diverse factors acting through different mechanisms - including altered gravity (micro-, hypo-as well as hyper-gravity), exposure to space radiation, confinement, disruption of chronobiological rhythms, changes in diet and physical activity. Overall, those leads can affect the HPG axis and significantly impair the functionality of the reproductive system. The limited available data related to women that experienced spaceflight represents a severe hurdle in assessing whether the space environment could compromise the fertility potential, albeit indirect information of female astronauts who flew during the Shuttle era evidence that the reproductive capabilities do not seem to be impaired by spaceflight.

Extreme states of stress can affect the menstrual cycle on Earth, and it is unknown if this would have the same impact on natural menstrual cycles in space. Data from female astronauts who flew during the Shuttle era suggest that pregnancy rates, including complication rates, are equivalent to ground-based, age-matched controls.

Indeed, after spaceflight some women were able to conceive (with or without the support of assisted reproductive technology), albeit several unsuccessful attempts have been recorded. Overall, data are scarce and do not allow for assessment of the real impact of microgravity and radiation exposure on the female reproductive capabilities. However, menstrual cycle irregularities have been reported in female flight attendants (Lauria et al., 2006), (Radowicka et al., 2013) - with an incidence ranging from 20% to 30%.

Considering that on board of the ISS the alternation of sunlight and darkness consists of ~90-min intervals due to the orbital journey around the Earth, changes in the circadian rhythm interfere with GnRH signaling and can impair HPG control upon ovarian steroidogenesis. This unusual condition disrupts the sleep module (frequency/duration/quality), with consequent effects on the reproductive axis, as confirmed by studies performed on ground in which menstrual irregularities, as well as many other dysregulations (miscarriage, preeclampsia, preterm birth), are associated with sleep disturbances (Baker and Driver, 2007), (Caetano et al., 2021). Deregulation of circadian clock involves also specific genes at cellular levels, as exposure to microgravity modifies the expression of several clock genes (Bmal1 and Rev-erba among others), thus highlighting the existence of an integrated signaling network between the gravitational field and the circadian gene regulation (Ranieri et al., 2015). Clock genes are expressed in many tissues and organs, including ovaries where they participate in the regulation of key steroidogenic genes, including Cyp19A1 (Fujita et al., 2020).

Furthermore, female astronauts during space missions use contraceptives to suppress menstruation, thus preventing in assessing ovarian function and the consequent effects upon the endometrium. The combined oral contraceptive (COC) pill is one medication usually used by female astronauts, though there is no official requirement for using contraceptives. Although we have extensive knowledge about the physiological effects of the COC on Earth, there has been no extensive investigation regarding benefits/disadvantages in space. Use of COC would not only avoid unwarranted pregnancy but are instrumental to prevent menstrual problems that could be unmanageable during spaceflight missions (Grandi et al., 2012). Young women frequently suffer from menstrual pain and dysmenorrhea, affecting more than 50% of women (Proctor et al., 2001). The combined oral contraceptive pill, norgestrel and ethinyl estradiol, are recommended in the dose of 30–35 mcg COCs (taken continuously) to provide better

suppression of the ovary (less chance for cysts and breakthrough bleeding, depending upon OC formulation) (Murad, 2008).

Noticeably, we should keep caution with contraceptives that suppress ovarian function for extended periods (like contraceptives containing medroxyprogesterone acetate, Depo-Provera or norethisterone enanthate), given that they have been shown to adversely affect women's bone density and cardiovascular risk on Earth (Nappi et al., 2012). Therefore, as continuous use of COCs may inhibit ovulation, and reduce estrogens, it is tempting to speculate if COCs treatment for very lingering periods could be a suitable strategy for long-duration missions.

However, as assumption of COC inhibits ovulation, assessment of steroidogenesis would likely be biased by the concomitant hormonal treatment.

Since spaceflight is associated with reduced hemoglobin levels, menstrual irregularities may likely predispose astronauts to developing anemia (Jennings and Baker, 2000). However, while utilization of COCs to suppress menses may decrease the risk of inflight anemia, use of COCs have now been found to increase the risk of venous thrombosis, particularly amongst women with a genetic predisposition (Sehovic and Smith, 2010), (Lo et al., 2024). This problem deserves special attention: given that the first episode of venous thromboembolism (VTE) occurred in space in 2019, it is critical to investigate those factors which may further increase the risk associated with coagulation. Indeed, a recent study focused on venous thromboembolism events in female astronauts, showing an association between oral contraceptive use and serum albumin, among other factors, which potentially increase the risk of venous thromboembolism in astronauts (Zwart et al., 1985). Oxytocin can influence coagulation, potentially affecting venous thromboembolism (VTE) risk, also by increasing the probability of clot formation (Golparvar et al., 2014).

It is worth mentioning that oxytocin–a hormone involved in the modulation of HPA axis response to chemical and environmental stresses (Suh et al., 1986) – is reduced during spaceflight (Uno et al., 1997) and after COC assumption (Salonia et al., 2005). The two factors can likely synergize in reducing oxytocin in women involved in spaceflight missions and thus can further impair the adaptive response to stress and, consequently, reproductive fitness. Furthermore, considering that some contraceptives (like injectable depot medroxyprogesterone acetate) can reduce bone mass and impair calcium metabolism (Ampatzis et al., 2022), they are no longer prescribed to female astronauts. The impact of COC upon bone is currently an open issue, complicated by several concurring characteristics (posology, concentration of estrogen, and age of user) (Prior et al., 2001). To our knowledge, only a single study has examined the impact of spaceflight on bone structural qualities in female astronauts, showing that after prolonged space missions (49–215 days), male and female crew members displayed no relevant differences in bone density decrease, accounting −1.5% in Bone Mineral Density per months, regardless of sex and exercise modality (Smith et al., 2014).

Historically, fertility outcomes following space travel have been relatively poor. Success rates for assisted reproductive technology (ART) in female astronauts have been markedly low, when compared to age-matched controls (Ampatzis et al., 2022), albeit such results have been critically revised (and mitigated) by the same authors in a more recent update, in which it is concluded that « Long-duration exploration spaceflight will introduce new challenges for maintenance of gynecological and reproductive health. The impact of the space environment outside of LEO on gynecological concerns remains unknown, with factors such as increased radiation exposure adding complexity and potential risk» (Steller et al., 2020).

These findings reinforce the need for a specific women's health database reporting clinical and biochemical data related to spaceflight.

Difficulties in obtaining evidence from women flying in space have prompted the use of models based on simulated weightlessness, including the six-head-down-tilt bed-rest model.

This approach has been employed in several studies, but the results gathered up to now are scarce and biased by the lack of a clear methodological rationale (Tou et al., 2002). The first study using the bed-rest model was unable to evidence any significant change, evidencing only minor modifications related to the secretion of Progesterone during the luteal phase (Sandler and Winters, 1978). The study, performed with an on-ground model, is unfortunately affected by an evident bias, as the observational period was restricted to only 17 days. This fails to account for the entire menstrual cycle and thus makes it difficult to provide a more complete interpretation of physiological changes experienced by women during this timeframe.

A further study reported that women exposed to weightlessness according to the bed-rest model showed luteal phase deficiency, interpreted as caused by HPA axis dysfunction (Rock and Fortney, 1984).

Another model that is gaining momentum is the «dry immersion» approach (Navasiolava et al., 2011), (Watenpaugh, 2016). However, as already noticed for other experimental models, the primary focus of these studies was to assess the musculoskeletal, nervous, and cardiovascular systems, and information about reproductive function was practically incidental (Robin et al., 2022), (Linossier et al., 2022).

Some recent reports based on different study designs have investigated the impact of simulated weightlessness performed by dry immersion. The experimental plan greatly differs among these studies, as the dry immersion period ranged from three to 5 days, occurring either between day 7 and 10 or between day 10 and 15 of subject's menstrual cycles (Gorbacheva et al., 2023), (Tomilovskaya et al., 2019). Noticeably, the paper from Gorbacheva et al. observed increased Inhibin-B (that selectively suppresses the secretion of pituitary FSH) (Luisi et al., 2005) levels and decreased LH and P4 at day 9 of the menstrual cycle after the immersion. Unfortunately, Estrogen levels were not evaluated by the study. Remarkably, the ovarian volume after prolonged immersion decreased significantly (−22%), while an increase in dominant follicle diameter was reported.

Effects of simulated microgravity on ovarian function in space

Ovaries play a central role in the control of female fertility: namely, the delicate balance between ovarian steroid hormones reflects the underlying driving influence of many systems and environmental factors–psycho-physical stresses, nutritional changes, drugs and immune stimuli - mostly acting through the

apical endocrine control exercised by the HPG axis (Toufexis et al., 2014). Moreover, intrinsic and systemic endocrine and paracrine cues orchestrate menstruation in a cyclical manner, according to a complex mechanism involving several hormones, like Insulin (Ins), Luteinizing hormone (LH), Gonadotropin Releasing Hormone (GnRH), Follicle Stimulating Hormone (FSH), which dynamically interact with ovarian signaling pathways, involving Progesterone (P4) and 17β-Estradiol among others. The menstrual cycle travels through distinctive phases - proliferation, decidualization, inflammation, apoptosis, hemostasis, vasoconstriction, hypoxia, repair, and regeneration–that are instrumental in shaping the endometrium according to the aims required. This is why the ovarian cycle runs in parallel to the menstrual cycle, involving endocrine and structural changes for facilitating the maturation of a single oocyte. Once the oocyte has been released, corpus luteum emerges from the follicle and secrete P4 to support endometrial growth and maintenance of an eventual pregnancy. In the absence of fertilization, estrogens and P4 downfall and menstruation occurs.

Ovarian steroidogenesis is the main source of sex steroid hormones, produced through the interacting cooperativity between two distinct compartments: theca (TC) and granulosa cells (GC). Steroidogenesis begins with cholesterol as substrate for a number of subsequent transformations, catalyzed by specific enzymes and constrained by several factors belonging to both the internal and the external milieu, including hormonal mediators released by the HPG and the HPA (Figure 2). According to the two-cell two-gonadotropin theory (Armstrong et al., 1979), stimulation exerted by LH promotes the biosynthesis of androgens (DHEA, Androstenedione, and Testosterone) from cholesterol in Theca cells. Androgens then shuttle to GCs where, under the enzymatic activity of aromatase (CYP19A1), they are transformed into Estrogens (Estrone and 17β-Estradiol).

FSH is required to increase aromatase synthesis and activity. Estrogens produced by the ovary are needed to support the reproductive apparatus, but their role is not limited to the fertility field, as they are involved in maintaining cardiovascular efficiency, bone homeostasis, metabolism and immune functions (Davis et al., 2015). Particularly, available data suggest that weightlessness could impair estrogen synthesis and, for this reason, it is clear that estrogen deficiency may be a contributing factor to the worsening of the decrease in bone mineral density recorded during spaceflight (Stavnichuk et al., 2020).

Albeit no data (except from some anecdotal cases) (Kikina et al., 2024) are available about the steroidogenesis occurring in women ovaries during spaceflight, indirect data have shown that estrogen receptors–in different tissues - are modulated by the microgravity regimen (Mathyk BA. et al., 2024). This investigation evidenced significant changes in insulin as well estrogen signaling in murine and human cells exposed to microgravity. Noticeably, estrogen (including the CYP17A1 gene) and insulin-related genes were upregulated post-flight. An indirect confirmation of the disruption of estrogen signaling has been provided by an extensive study performed on rodents flown in space, in which transcriptomic analysis was carried out on OSD-511 dataset from NASA's Open Science Data (Arnold et al., 2024). This study was able to evidence that microgravity severely downregulates Greb-1 - a gene regulated by estrogens and regulating cytoplasmic glycosyl-transferase that post-translationally stabilizes Erα (Shin et al., 2021).

These findings are intriguing, given that a correlation has been already suggested between dysregulated insulin signaling and ovarian steroidogenic function, namely in Polycystic Ovary Syndrome (PCOS) (Fedeli et al., 2023).

Polycystic ovary syndrome is the most common endocrine disease in women of reproductive age, and the principal cause of infertility (Yu et al., 2023). PCOS recognizes four distinct phenotypes, although the most frequent characteristics include hyperandrogenism with ovarian dysfunction, chronic oligo-anovulation, and/or polycystic morphology of the ovary. Noticeably, evidence shows that the reproductive function is severely impaired in ovaries from PCOS women, given that androgens (and related enzymes) increase, altogether with AMH (anti-Müllerian hormone), while estrogens and CYP19A1(aromatase) are significantly downregulated. As a consequence, granulosa cells are unable to efficiently transform the intra-ovarian androgen excess into estrogens *via* aromatase, thus leading to the arrest in follicular growth and anovulation (Fedeli et al., 2024). Given that aromatase function is highly sensitive to a number of environmental and psychological stresses, it is worth remembering that by this way the HPA axis can transduce negative inputs to the ovarian function (Fedeli et al., 2023), although a direct microgravity effect cannot be discarded, as exposure of granulosa cells in both real and simulated weightlessness showed a significant downregulation of CYP19A1.

Alteration of estrogen receptors were most prominent in the liver, where it resulted associated with a concomitant hepatic insulin resistance and steatosis. Hepatic steatosis can be ascribed to insulin resistance, which can worsen the transduction of insulin (Fabbrini and Magkos, 2015). Indeed, in the mentioned report it was shown that lipids accumulated into the liver, thus reinforcing the pathogenetic hypothesis. Even older studies showed higher plasma glucose and insulin levels after the oral glucose tolerance test in astronauts during short-lived spaceflight mission (Macho et al., 2003).

However, as estrogen receptors knockout is associated with the emergence of insulin resistance (Allard et al., 2019), it is tempting to speculate that estrogen deficiency may play a causative primary role in inducing insulin resistance. In any case, both insulin resistance and estrogen deficiency can impair the mitochondrial function. Interestingly, mitochondria activity is critically impaired during spaceflight (Tocci et al., 2024). Furthermore, Insulin resistance is associated with circadian rhythm changes and was recorded in both astronauts and animals flying in space (Aydogan Mathyk et al., 2021), (Hughson et al., 2016). Insulin signaling regulation is sensitive to many stressors, and its dysregulation affects folliculogenesis homeostasis. Impaired insulin transduction is recognized as a major factor in female infertility, as it can disrupt menstrual cyclicity and also lead to complications in pregnancy, leading to gestational diabetes (Lei et al., 2024).

The integrity of this complex system is mandatory not only to support a pregnancy but providing a balanced input of estrogens and progesterone, it ensures other relevant physiological tasks, belonging to the cardio-vascular and musculoskeletal system (den Ruijter and Kararigas, 2022), (Chidi-Ogbolu and Baar, 2019). Indeed, the most relevant homeostatic processes occurring within mammals–especially in females - are intensely influenced by gonadal hormones and this explains why fitness of the reproductive system

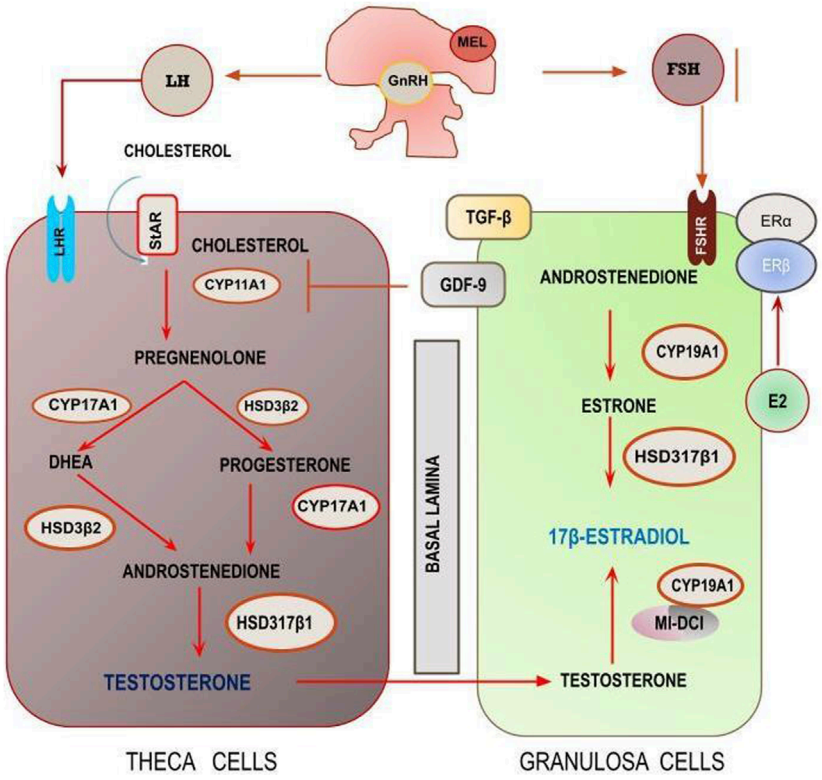

FIGURE 2
The steroidogenic pathway according to the two-compartment model. Theca cells synthetize androgens that, subsequently, are converted into estrogens. The entire process is under the regulatory control of both systemic (mediated by the activation of HPG) and local, chemical and biophysical factors.

is often considered a marker of overall health (Rajkovic and Pangas, 2017). Noticeably, steroid hormones play an indispensable support in modulating several physiological functions, including bone and cardiovascular homeostasis that are specifically affected by weightlessness. Unfortunately, research is still limited regarding the impact that microgravity could have on reproductive capabilities and its consequences upon other physiological functions (Mishra and Luderer, 2019).

Recently, NASA's Rodent Research Hardware System (Rodent Research Habitat System) has been built to be used as a research platform aboard the ISS for long-duration rodent experiments in space. The platform hosted the Rodent Research-1, flown on the SpaceX-4 CRS-4 Dragon cargo spacecraft. This validation mission was the first to transport animals aboard the ISS in an unmanned vehicle (Hong et al., 2021). The experiment, lasting 37 days in microgravity, was the longest space rodent study conducted by NASA. Estrogen and progesterone - analyzed in the ovarian tissue and in serum - did not show significant modification among the different experimental arms. However, mice in flight had more animals in metestrus and diestrus, two stages in which the ovary usually displays reduced steroidogenic activity; whereas in control groups (vivarium and baseline control groups), all animals were found in proestrus and estrus, two stages associated with increased ovarian steroidogenesis due to the concomitant LH surge. It should be noted that the rodent estrous cycle lasts 4–5 days and it is divided into the aforementioned four phases, each lasting 1–2 days (Nowak et al., 2018). The overall analysis performed to investigate the gene expression pattern was unfortunately biased by the inclusion of stromal tissue and smaller follicles, which predominate over the selected follicles that become highly steroidogenic during the maturation process. Thereby, as stated by the authors, «when whole ovarian RNA is used, it was not surprising to see no major differences in ovarian gene expression across the treatment groups or even during different stages of the cycle».

The coordinated steroidogenic activity occurring between theca and granulosa cells is the ultimate process regulating reproduction as well as the release of relevant hormones, including estrogens and progesterone. TCs produce androgens then converted into estrogens in the GCs. Aromatase (encoded by CYP19A1) is the key enzyme in estrogen production by GCs.

Theca and granulosa cells capabilities and morphology in microgravity have not been specifically addressed, with the exception of the Ovospace experiment, flown in space during the 2022 Minerva mission, and the Orion experiment flown in 2024 as part of the AX-3 human mission by Axiom. The investigation focused on theca and granulosa cells growing into a minilab for 9 days (including the docking period). Preliminary results (Roiati et al., 2023), obtained from both in space experiments and in RPM-simulated microgravity, showed that steroidogenic enzymes belonging to GCs undergo a dramatic downregulation. Aromatase activity was almost completely suppressed, whereas CYP19A1 methylation (assessed either at CpG and non-CpG moieties) significantly increased. Overall, these findings indicate that aromatase activity–and consequently estrogen

release–is severely downregulated, thus impairing the ovarian steroidogenic competency.

Noticeably, weightlessness seems to suppress aromatase activity, thus leading to a hypo-estrogenic condition. Reduction in estrogen synthesis not only impair ovulation and menstrual cycle, but also can likely affect bone and cardiovascular homeostasis. In this way, ovarian insufficiency can affect the functioning of many other systems, ultimately compromising health and performances of astronauts. Namely, evidence from three space shuttle missions (STS-131, STS-133, and STS-135) demonstrated that ovarian function is severely impaired in female animals. Ovarian folliculogenesis and luteal function were disrupted, as well as the uterine structure, likely because of dysregulated endocrine support (Ronca et al., 2014), (Holets et al., 2015). These findings derived from the spaceflight experiments raise questions as to whether pregnancy can be sustained in a reduced gravitational field (they want it in the discussion section).

The ovarian endocrine profile - so far underrated–deserves a proper assessment, by planning a well-designed experimental strategy. It is worthy of interest that the space-related deregulation involving ovarian steroidogenesis looks like the picture observed in the PCOS (Fedeli et al., 2024). These hints suggest that–as for PCOS–specific pharmaceutical countermeasures support could be envisaged to mitigate weightlessness-induced steroidogenic alteration (they want it in the discussion section).

Conclusion

The primary challenge with any voyage or mission into space or to other planets is undoubtedly survival. The moment we leave our planet, we find ourselves in hostile territory: space is a dangerous field for human beings. At the very beginning of the Apollo program (1967), NASA operated without the concept of "permissible doses" of hazards–primarily focusing upon radiation–with the aim to prioritize success of the mission. This is no longer the case, as we now have tools and technologies to make space travel safer. Yet, several concerns arise as we are planning for a return to the Moon (Artemis program), and eventually to travel to Mars (Bizzarri et al., 2023). Protecting human reproduction capabilities belongs to these worries.

There is a severe paucity of data: preliminary results gathered during the last 50 years–in both animal and human studies - reveal that the space environment may have a significant impact on the reproductive cycle. Therefore, they ask for a confirmation. Indeed, much is required in order to acquire a full understanding of endocrine and functional changes occurring during microgravity exposure. Moreover, the joint effect of radiation and weightlessness deserve to be thoroughly investigated to recognize the respective contribution of each one as well as the eventual synergies. This implies that we have to design specific models–on ground as well as in flight–to perform extensive studies. Noticeably, how different gravitational regimens (like Moon and Mars where gravity account for 0.16 and 0.38 g, respectively) can affect reproduction needs to be specifically addressed and compared to results obtained on board of the ISS (in which the free-fall condition with less than 0.01 g is actually experienced by crew members). In this context, advancing technological efforts to establish facilities dedicated to long-term animal studies in orbit or on the Moon could significantly enhance our understanding of the effects of space adaptation on mammalian reproductive physiology.

Changes in gene expression, proteomic pattern, metabolomic analyses, as well as miRNAs release are required to fully attain an understandable picture of the whole (Corti et al., 2024). Moreover, studies involving both animals and 3D-cell models would require longer exposure either in space or in simulated conditions. In addition, novel modeling would benefit from the collection of biological samples in-flight to avoid the confounding effects due to several physical stresses related to the reentry. In particular, investigation should explore to what extent gravity-related changes can be considered an «acute transition state», anticipating an eventual «steady-state» that still has to be unveiled. Furthermore, it is still a matter of inquiry if the observed dysregulation in steroidogenic function is reversible and can finally allow recovery of normal reproductive function after prolonged exposure to microgravity.

Consequently, research into the reproductive function in space can provide useful important data regarding the properties of the reproductive process by highlighting critical targets and pathways, which are specifically affected by microgravity conditions. Furthermore, this field of research can potentially open new perspectives of investigation, including those aimed at improving fertilization assisted technologies, stem and germ cells management, oocyte maturation and detoxification from toxicant harmful for reproduction.

Author contributions

MC: Supervision, Writing – review and editing. GC: Supervision, Writing – review and editing. EG: Supervision, Writing – review and editing. MC: Supervision, Validation, Writing – review and editing. MB: Conceptualization, Investigation, Methodology, Visualization, Writing – original draft.

Funding

The author(s) declare that financial support was received for the research and/or publication of this article. The author(s) declare that this research was partly supported by ASI Grant "Ovospace" - DC-DSR-UVS-2022-2.

Conflict of interest

The authors declare that the research was conducted in the absence of any commercial or financial relationships that could be construed as a potential conflict of interest.

Generative AI statement

The author(s) declare that no Generative AI was used in the creation of this manuscript.

Publisher's note

References

Allard, C., Morford, J. J., Xu, B., Salwen, B., Xu, W., Desmoulins, L., et al. (2019). Loss of nuclear and membrane estrogen receptor-α differentially impairs insulin secretion and action in male and female mice. *Diabetes* 68 (3), 490–501. doi:10.2337/db18-0293

Amann, R. P., Deaver, D. R., Zirkin, B. R., Grills, G. S., Sapp, W. J., Veeramachaneni, D. N., et al. (1985)1992). Effects of microgravity or simulated launch on testicular function in rats. *J. Appl. Physiol.* 73 (2 Suppl. l), 174S–185S. doi:10.1152/jappl.1992.73.2.S174

Ampatzis, C., Zervoudis, S., Iatrakis, G., and Mastorakos, G. (2022). Effect of oral contraceptives on bone mineral density. *Acta Endocrinol. (Buchar)* 18 (3), 355–360. doi:10.4183/aeb.2022.355

Armstrong, D. T., Goff, A. K., and Dorrington, J. H. (1979). *Ovarian follicular development and function* (Midgley, A. R., and Sadler W. A., eds.), New York: Raven Press, 169–182.

Arnold, C., Casaletto, J., and Heller, P. (2024). Spaceflight disrupts gene expression of estrogen signaling in rodent mammary tissue. *Med. Res. Archives* 12 (3). doi:10.18103/mra.v12i3.5220

Aydogan, M., Imudia, A., Quaas, A., Halicigil, C., Karouia, F., Avci, P., et al. (2024). Understanding how space travel affects the female reproductive system. *NPJ Women's Health* 2 (20). doi:10.1038/s44294-024-00009-z

Aydogan Mathyk, B., Alvarado, F., Young, S., Quaas, A., and Beheshti, A. (2021). Expression of insulin resistance related genes during spaceflight. *Fertil. Steril.* 116, E107. doi:10.1016/j.fertnstert.2021.07.299

Baker, F. C., and Driver, H. S. (2007). Circadian rhythms, sleep, and the menstrual cycle. *Sleep. Med.* 8 (6), 613–622. doi:10.1016/j.sleep.2006.09.011

Barr, Y. R., Bacal, K., Jones, J. A., and Hamilton, D. R. (2007). Breast cancer and spaceflight: risk and management. *Aviat. Space Environ. Med.* 78 (4 Suppl. l), A26–A37.

Basini, G., and Grasselli, F. (2024). Role of melatonin in ovarian function. *Anim. (Basel)* 14 (4), 644. doi:10.3390/ani14040644

Benjamin, C. L., Stowe, R. P., St John, L., Sams, C. F., Mehta, S. K., Crucian, B. E., et al. (2016). Decreases in thymopoiesis of astronauts returning from space flight. *JCI Insight* 1 (12), e88787. doi:10.1172/jci.insight.88787

Bizzarri, M., Fedeli, V., Piombarolo, A., and Angeloni, A. (2022). Space biomedicine: a unique opportunity to rethink the relationships between physics and biology. *Biomedicines* 10 (10), 2633. doi:10.3390/biomedicines10102633

Bizzarri, M., Gaudenzi, P., and Angeloni, A. (2023). The biomedical challenge associated with the artemis space program. *Acta Astronaut.* 212, 14–28. doi:10.1016/j.actaastro.2023.07.021

Blanc, S., Somody, L., Gharib, A., Gauquelin, G., Gharib, C., and Sarda, N. (1998). Counteraction of spaceflight-induced changes in the rat central serotonergic system by adrenalectomy and corticosteroid replacement. *Neurochem. Int.* 33 (4), 375–382. doi:10.1016/s0197-0186(98)00042-4

Burden, H. W., Poole, M. C., Zary, J., Jeansonne, B., and Alberts, J. R. (1998). The effects of space flight during gestation on rat uterine smooth muscle. *J. Gravit. Physiol.* 5 (2), 23–29.

Burden, H. W., Zary, J., Lawrence, I. E., Jonnalagadda, P., Davis, M., and Hodson, C. A. (1997). Effects of space flight on ovarian-hypophyseal function in postpartum rats. *J. Reprod. Fertil.* 109 (2), 193–197. doi:10.1530/jrf.0.1090193

Caetano, G., Bozinovic, I., Dupont, C., Léger, D., Lévy, R., and Sermondade, N. (2021). Impact of sleep on female and male reproductive functions: a systematic review. *Fertil. Steril.* 115 (3), 715–731. doi:10.1016/j.fertnstert.2020.08.1429

Charles, W., and Daniel, C. (2015). "Holley, regulatory physiology introduction," in *translational cell and animal research in space 1965–2011*. Editors E. Ronca, K. A. Souza, and R. C. Mains, 371–381.

Cheng, K., Feng, X., Yang, C., Ma, C., Niu, S., Jia, L., et al. (2023). Simulated microgravity reduces quality of ovarian follicles and oocytes by disrupting communications of follicle cells. *NPJ Microgr.* 9 (1), 7. doi:10.1038/s41526-023-00248-5

Chidi-Ogbolu, N., and Baar, K. (2019). Effect of estrogen on musculoskeletal performance and injury risk. *Front. Physiol.* 9, 1834. doi:10.3389/fphys.2018.01834

Chromiak, J. A., Abadie, B. R., Braswell, R. A., Koh, Y. S., and Chilek, D. R. (2003). Resistance training exercises acutely reduce intraocular pressure in physically active men and women. *J. Strength Cond. Res.* 17 (4), 715–720. doi:10.1519/1533-4287(2003)017<0715:rteari>2.0.co;2

Corti, G., Kim, J., Enguita, F. J., Guarnieri, J. W., Grossman, L. I., Costes, S. V., et al. (2024). To boldly go where no microRNAs have gone before: spaceflight impact on risk for small-for-gestational-age infants. *Commun. Biol.* 7 (1), 1268. Erratum in: Commun Biol. 2024 Oct 16;7(1):1339. 10.1038/s42003-024-07022-7. doi:10.1038/s42003-024-06944-6

Dai, T. X., Son, H. N., Chi, H. N. Q., Huy, H. N. Q., Minh, N. T., Tram, N. T. T., et al. (2021). Simulated microgravity induces the proliferative inhibition and morphological changes in porcine granulosa cells. *Curr. Issues Mol. Biol.* 43 (3), 2210–2219. doi:10.3390/cimb43030155

Davis, S. R., Lambrinoudaki, I., Lumsden, M., Mishra, G. D., Pal, L., Rees, M., et al. (2015). Menopause. *Nat. Rev. Dis. Prim.* 1, 15004. doi:10.1038/nrdp.2015.4

den Ruijter, H. M., and Karalis, G. (2022). Estrogen and cardiovascular health. *Front. Cardiovasc Med.* 9, 886592. doi:10.3389/fcvm.2022.886592

Dickmeis, T., Weger, B. D., and Weger, M. (2013). The circadian clock and glucocorticoids–interactions across many time scales. *Mol. Cell Endocrinol.* 380 (1-2), 2–15. doi:10.1016/j.mce.2013.05.012

Domes, G., Linnig, K., and von Dawans, B. (2024). Gonads under stress: a systematic review and meta-analysis on the effects of acute psychosocial stress on gonadal steroids secretion in humans. *Psychoneuroendocrinology* 164, 107004. doi:10.1016/j.psyneuen.2024.107004

Drago-Ferrante, R., Di Fiore, R., Karouia, F., Subbannayya, Y., Das, S., Aydogan, M. B., et al. (2022). Extraterrestrial gynecology: could spaceflight increase the risk of developing cancer in female astronauts? An updated review. *Int. J. Mol. Sci.* 23 (13), 7465. doi:10.3390/ijms23137465

Echenim, N., Monniaux, D., Sorine, M., and Clément, F. (2005). Multi-scale modeling of the follicle selection process in the ovary. *Math. Biosci.* 198 (1), 57–79. doi:10.1016/j.mbs.2005.05.003

Emily, R. (1979). Morey, spaceflight and bone turnover: correlation with a new rat model of weightlessness. *BioScience* 29 (3), 168–172. doi:10.2307/1307797

ESA SciSpacE white papers (2021). Available online at: https://esamultimedia.esa.int/docs/HRE/12_HumanResearch_HumanPhysiology.pdf.

Fabbrini, E., and Magkos, F. (2015). Hepatic steatosis as a marker of metabolic dysfunction. *Nutrients* 7 (6), 4995–5019. doi:10.3390/nu7064995

Fedeli, V., Catizone, A., Querqui, A., Unfer, V., and Bizzarri, M. (2023). The role of inositols in the hyperandrogenic phenotypes of PCOS: a Re-reading of larner's results. *Int. J. Mol. Sci.* 24 (7), 6296. doi:10.3390/ijms24076296

Fedeli, V., Unfer, V., Dinicola, S., Laganà, A. S., Canipari, R., Monti, N., et al. (2024). Inositol restores appropriate steroidogenesis in PCOS ovaries both *in vitro* and *in vivo* experimental mouse models. *Cells* 13 (14), 1171. doi:10.3390/cells13141171

Fujita, S. I., Rutter, L., Ong, Q., and Muratani, M. (2020). Integrated RNA-seq analysis indicates asynchrony in clock genes between tissues under spaceflight. *Life (Basel)* 10 (9), 196. doi:10.3390/life10090196

García-Ovejero, D., Trejo, J. L., Ciriza, I., Walton, K. D., and García-Segura, L. M. (2001). Space flight affects magnocellular supraoptic neurons of young prepuberal rats: transient and permanent effects. *Brain Res. Dev.* 130 (2), 191–205. doi:10.1016/s0165-3806(01)00236-x

Gharbi, N., El Fazaa, S., Fagette, S., Gauquelin, G., Gharib, C., and Kamoun, A. (1996). Cortico-adrenal function under simulated weightlessness during gestation in the rat–effects on fetal development. *J. Gravit. Physiol.* 3 (1), 63–68.

Gimunová, M., Paludo, A. C., Bernaciková, M., and Bienertova-Vasku, J. (2024). The effect of space travel on human reproductive health: a systematic review. *NPJ Microgr.* 10 (1), 10. doi:10.1038/s41526-024-00351-1

Golparvar, M., Esterabi, M., Talakoub, R., and Saryazdi, H. H. (2014). Evaluation of *in vivo* effects of Oxytocin on coagulation of parturient during cesarean delivery by thromboelastography. *J. Res. Pharm. Pract.* 3 (1), 28–33. doi:10.4103/2279-042X.132707

Gorbacheva, E. Y., Toniyan, K. A., Biriukova, Y. A., Lukicheva, N. A., Orlov, O. I., Boyarintsev, V. V., et al. (2023). The state of the organs of the female reproductive system after a 5-day "dry" immersion. *Int. J. Mol. Sci.* 24 (4), 4160. doi:10.3390/ijms24044160

Grandi, G., Ferrari, S., Xholli, A., Cannoletta, M., Palma, F., Romani, C., et al. (2012). Prevalence of menstrual pain in young women: what is dysmenorrhea? *J. Pain Res.* 5, 169–174. doi:10.2147/JPR.S30602

Grindeland, R. E., Popova, I. A., Vasques, M., and Arnaud, S. B. (1990). Cosmos 1887 mission overview: effects of microgravity on rat body and adrenal weights and plasma constituents. *FASEB J.* 4 (1), 105–109. doi:10.1096/fasebj.4.1.2295371

Hakimi, O., and Cameron, L. C. (2017). Effect of exercise on ovulation: a systematic review. *Sports Med.* 47 (8), 1555–1567. doi:10.1007/s40279-016-0669-8

Herrenkohl, L. R., and Gala, R. R. (1979). Serum prolactin levels and maintenance of progeny by prenatally-stressed female offspring. *Experientia* 35 (5), 702–704. doi:10.1007/BF01960408

Holets, L. M., Gupta, V., Roby, K. F., Prohaska, C., and Tash, J. S. (2015). "Spaceflight disrupts reproductive dynamics, and reduces estrogen receptors gene expression in adult mouse ovary and uterus. Unpublished data, 2013. Quoted in: wade charles and daniel C. Holley, regulatory physiology introduction," in *Translational cell and animal research in space 1965–2011*. Editors E. Ronca, K. A. Souza, and R. C. Mains (New Orleans, Louisiana: American Society for Gravitational and Space Research), 371–381.

Holley, D. C., Soliman, M. R., Kaddis, F., Markley, C. L., and Krasnov, I. (1991). Pineal physiology in microgravity: relation to rat gonadal function aboard Cosmos 1887. *Aviat. Space Environ. Med.* 62 (10), 953–958.

Hong, X., Ratri, A., Choi, S. Y., Tash, J. S., Ronca, A. E., Alwood, J. S., et al. (2021). Effects of spaceflight aboard the International Space Station on mouse estrous cycle and ovarian gene expression. *NPJ Microgr.* 7 (1), 11. doi:10.1038/s41526-021-00139-7

Hughson, R. L., Robertson, A. D., Arbeille, P., Shoemaker, J. K., Rush, J. W., Fraser, K. S., et al. (2016). Increased postflight carotid artery stiffness and inflight insulin resistance resulting from 6-mo spaceflight in male and female astronauts. *Am. J. Physiol. Heart Circ. Physiol.* 310 (5), H628–H638. doi:10.1152/ajpheart.00802.2015

Jain, V., Chuva de Sousa Lopes, S. M., Benotmane, M. A., Verratti, V., Mitchell, R. T., and Stukenborg, J. B. (2023). Human development and reproduction in space-a European perspective. *NPJ Microgr.* 9 (1), 24. doi:10.1038/s41526-023-00272-5

Jennings, R. T., and Baker, E. S. (2000). Gynecological and reproductive issues for women in space: a review. *Obstet. Gynecol. Surv.* 55 (2), 109–116. doi:10.1097/00006254-200002000-00025

Kastello, G. M., and Sothmann, M. S. (1999). Brain norepinephrine changes with simulated weightlessness and relation to exercise training. *Physiol. Behav.* 66 (5), 885–891. doi:10.1016/s0031-9384(99)00030-x

Keefe, J. (1981). "Rat and quail ontogenesis," in *U.S. Rat experiments flown in the soviet Cosmos 1129*. Editors M. R. Heinrich, and B. Souza (California, United States: NASA Ames Research Center, Moffett Field), 325.

Kikina, A. Y., Matrosova, M. S., Gorbacheva, E. Y., Gogichaeva, K. K., Toniyan, K. A., Boyarintsev, V. V., et al. (2024). Weightlessness leads to an increase granulosa cells in the growing follicle. *NPJ Microgr.* 10 (1), 70. doi:10.1038/s41526-024-00413-4

Kinoue, T. (1996). Can a tail-suspension model be applied to simulate the reproduction system under weightlessness? *Nichidai Igaku Zasshi* 55 (10), 549–559.

Kramer, L. A., Hasan, K. M., Stenger, M. B., Sargsyan, A., Laurie, S. S., Otto, C., et al. (2020). Intracranial effects of microgravity: a prospective longitudinal MRI study. *Radiology* 295 (3), 640–648. doi:10.1148/radiol.2020191413

Lauria, L., Ballard, T. J., Caldora, M., Mazzanti, C., and Verdecchia, A. (2006). Reproductive disorders and pregnancy outcomes among female flight attendants. *Aviat. Space Environ. Med.* 77 (5), 533–539.

Lei, R., Chen, S., and Li, W. (2024). Advances in the study of the correlation between insulin resistance and infertility. *Front. Endocrinol. (Lausanne)* 15, 1288326. doi:10.3389/fendo.2024.1288326

Linossier, M. T., Peurière, L., Fernandez, P., Normand, M., Beck, A., Bareille, M. P., et al. (2022). DI-5-Cuffs: bone remodelling and associated metabolism markers in humans after five days of dry immersion to simulate microgravity. *Front. Physiol.* 13, 801448. doi:10.3389/fphys.2022.801448

Liu, M., Kim, D. W., Zeng, H., and Anderson, D. J. (2022). Make war not love: the neural substrate underlying a state-dependent switch in female social behavior. *Neuron* 110 (5), 841–856.e6. doi:10.1016/j.neuron.2021.12.002

Liu, M., Nair, A., Coria, N., Linderman, S. W., and Anderson, D. J. (2024). Encoding of female mating dynamics by a hypothalamic line attractor. *Nature* 634 (8035), 901–909. doi:10.1038/s41586-024-07916-w

Lo, F. V., Johansson, T., and Johansson, Å. (2024). The risk of venous thromboembolism in oral contraceptive users: the role of genetic factors-a prospective cohort study of 240,000 women in the UK Biobank. *Am. J. Obstet. Gynecol.* 230 (3), 360.e1–360.e13. doi:10.1016/j.ajog.2023.09.012

Luisi, S., Florio, P., Reis, F. M., and Petraglia, F. (2005). Inhibins in female and male reproductive physiology: role in gametogenesis, conception, implantation and early pregnancy. *Hum. Reprod. Update* 11 (2), 123–135. doi:10.1093/humupd/dmh057

Macho, L., Koska, J., Ksinantova, L., Pacak, K., Hoff, T., Noskov, V. B., et al. (2003). The response of endocrine system to stress loads during space flight in human subject. *Adv. Space Res.* 31 (6), 1605–1610. doi:10.1016/s0273-1177(03)00097-8

Mathyk, B., Imudia, A. N., Quaas, A. M., Halicigil, C., Karouia, F., Avci, P., et al. (2024a). Understanding how space travel affects the female reproductive system to the Moon and beyond. *npj Womens Health* 2, 20. doi:10.1038/s44294-024-00009-z

Mathyk, B. A., Tabetah, M., Karim, R., Zaksas, V., Kim, J., Anu, R. I., et al. (2024b). Spaceflight induces changes in gene expression profiles linked to insulin and estrogen. *Commun. Biol.* 7 (1), 692. doi:10.1038/s42003-023-05213-2

Michael, A. E., Pester, L. A., Curtis, P., Shaw, R. W., Edwards, C. R., and Cooke, B. A. (1993). Direct inhibition of ovarian steroidogenesis by cortisol and the modulatory role of 11 beta-hydroxysteroid dehydrogenase. *Clin. Endocrinol. (Oxf)* 38 (6), 641–644. doi:10.1111/j.1365-2265.1993.tb02147.x

Miglietta, S., Cristiano, L., Espinola, M. S. B., Masiello, M. G., Micara, G., Battaglione, E., et al. (2023). Effects of simulated microgravity *in vitro* on human metaphase II oocytes: an electron microscopy-based study. *Cells* 12 (10), 1346. doi:10.3390/cells12101346

Mishra, B., and Luderer, U. (2019). Reproductive hazards of space travel in women and men. *Nat. Rev. Endocrinol.* 15 (12), 713–730. doi:10.1038/s41574-019-0267-6

Mitteregger, R., Vogt, G., Rossmanith, E., and Falkenhagen, D. (1999). Rotary cell culture system (RCCS): a new method for cultivating hepatocytes on microcarriers. *Int. J. Artif. Organs* 22 (12), 816–822. doi:10.1177/039139889902201207

Monga, M., and Gorwill, R. (1990). Effects of altitude, flight, and space travel on reproduction. *Semin. Reprod. Med.* 8 (1), 89–93. doi:10.1055/s-2007-1021427

Morey-Holton, E. R., and Globus, R. K. (1985)2002). Hindlimb unloading rodent model: technical aspects. *J. Appl. Physiol.* 92 (4), 1367–1377. doi:10.1152/japplphysiol.00969.2001

Moustafa, A. (2021). Hindlimb unloading-induced reproductive suppression via Downregulation of hypothalamic Kiss-1 expression in adult male rats. *Reprod. Biol. Endocrinol.* 19 (1), 37. doi:10.1186/s12958-021-00694-4

Murad, A. (2008). Contraception in the cosmos: the combined oral contraceptive pill in space. *J. Fam. Plann Reprod. Health Care* 34 (1), 55–59. doi:10.1783/147118908783332159

Musacchia, X. J. (1985). The use of suspension models and comparison with true weightlessness: "a resumé". *Physiologist* 28 (6 Suppl. l), S237–S240.

Nappi, C., Bifulco, G., Tommaselli, G. A., Gargano, V., and Di Carlo, C. (2012). Hormonal contraception and bone metabolism: a systematic review. *Contraception* 86 (6), 606–621. doi:10.1016/j.contraception.2012.04.009

Navasiolava, N. M., Custaud, M. A., Tomilovskaya, E. S., Larina, I. M., Mano, T., Gauquelin-Koch, G., et al. (2011). Long-term dry immersion: review and prospects. *Eur. J. Appl. Physiol.* 111 (7), 1235–1260. doi:10.1007/s00421-010-1750-x

Nowak, R. A., Cycles, M., and Skinner, M. K. (2018). *Encyclopedia of reproduction*. Second Edition. London, United Kingdom: Academic Press, 114–120. doi:10.1016/B978-0-12-801238-3.64631-7

Ogilvy-Stuart, A. L., and Shalet, S. M. (1993). Effect of radiation on the human reproductive system. *Environ. Health Perspect.* 101 (Suppl. 2), 109–116. doi:10.1289/ehp.93101s2109

Orisaka, M., Miyazaki, Y., Shirafuji, A., Tamamura, C., Tsuyoshi, H., Tsang, B. K., et al. (2021). The role of pituitary gonadotropins and intraovarian regulators in follicle development: a mini-review. *Reprod. Med. Biol.* 20 (2), 169–175. doi:10.1002/rmb2.12371

Ortiz, R. M., Wang, T. J., and Wade, C. E. (1999). Influence of centrifugation and hindlimb suspension on testosterone and corticosterone excretion in rats. *Aviat. Space Environ. Med.* 70 (5), 499–504.

Plakhuta-Plakutina, G. I., Serova, L. V., Dreval', A. A., and Tarabrin, S. B. (1976). Effect of 22-day space flight factors on the state of the sex glands and reproductive capacity of rats. *Kosm. Biol. Aviakosm Med.* 10 (5), 40–47.

Prior, J. C., Kirkland, S. A., Joseph, L., Kreiger, N., Murray, T. M., Hanley, D. A., et al. (2001). Oral contraceptive use and bone mineral density in premenopausal women: cross-sectional, population-based data from the Canadian Multicentre Osteoporosis Study. *CMAJ* 165 (8), 1023–1029.

Proctor, M. L., Roberts, H., and Farquhar, C. M. (2001). Combined oral contraceptive pill (OCP) as treatment for primary dysmenorrhoea. *Cochrane Database Syst. Rev.* (4), CD002120. doi:10.1002/14651858.CD002120Update in: Cochrane Database Syst Rev. 2009 Apr 15;(2):CD002120. 10.1002/14651858.CD002120.pub2

Radowicka, M., Pietrzak, B., and Wielgoś, M. (2013). Assessment of the occurrence of menstrual disorders in female flight attendants - preliminary report and literature review. *Neuro Endocrinol. Lett.* 34 (8), 809–813.

Rajkovic, A., and Pangas, S. (2017). Ovary as a biomarker of health and longevity: insights from genetics. *Semin. Reprod. Med.* 35 (3), 231–240. doi:10.1055/s-0037-1603571

Ranieri, D., Cucina, A., Bizzarri, M., Alimandi, M., and Torrisi, M. R. (2015). Microgravity influences circadian clock oscillation in human keratinocytes. *FEBS Open Bio* 5, 717–723. doi:10.1016/j.fob.2015.08.012

Robin, A., Navasiolava, N., Gauquelin-Koch, G., Gharib, C., Custaud, M. A., and Treffel, L. (2022). Spinal changes after 5-day dry immersion as shown by magnetic resonance imaging (DI-5-CUFFS). *Am. J. Physiol. Regul. Integr. Comp. Physiol.* 323 (3), R310–R318. doi:10.1152/ajpregu.00055.2022

Rock, J. A., and Fortney, S. M. (1984). Medical and surgical considerations for women in spaceflight. *Obstet. Gynecol. Surv.* 39 (8), 525–535. doi:10.1097/00006254-198408000-00022

Roiati, M., Raia, T., Fedeli, V., Monti, N., Borges, L. D. F., Parca, L., et al. (2023). The OvoSpace project: simulated microgravity affects epigenetic factors in bovine granulosa and theca cells. in *"Frontiers in epigenetics and epigenomics - abstract book of the 1st epigenetics society international meeting "epigenetics of disease and development"*, Rome, Italy: Frontiers Media SA. 290. doi:10.3389/978-2-8325-1235-7

Ronca, A. E., and Alberts, J. R. (2000). Physiology of a microgravity environment selected contribution: effects of spaceflight during pregnancy on labor and birth at 1 G. *J. Appl. Physiol.* 89 (2), 849–854; discussion 848. doi:10.1152/jappl.2000.89.2.849

Ronca, A. E., Baker, E. S., Bavendam, T. G., Beck, K. D., Miller, V. M., Tash, J. S., et al. (2014). Effects of sex and gender on adaptations to space: reproductive health. *J. Womens Health (Larchmt)* 23 (11), 967–974. doi:10.1089/jwh.2014.4915

Salonia, A., Nappi, R. E., Pontillo, M., Daverio, R., Smeraldi, A., Briganti, A., et al. (2005). Menstrual cycle-related changes in plasma oxytocin are relevant to normal sexual function in healthy women. *Horm. Behav.* 47 (2), 164–169. doi:10.1016/j.yhbeh.2004.10.002

Sandler, H., and Winters, D. (1978) "Physiological responses of women to simulated weightlessness," in *A review of the significant findings of the first female bed rest study NASA SP-340*. California, United States: NASA Ames Research Center, Moffett Field.

Santy, P. A., and Jennings, R. T. (1992). Human reproductive issues in space. *Adv. Space Res.* 12 (2-3), 151–155. doi:10.1016/0273-1177(92)90102-4

Sciarra, F., Franceschini, E., Campolo, F., Gianfrilli, D., Pallotti, F., Paoli, D., et al. (2020). Disruption of circadian rhythms: a crucial factor in the etiology of infertility. *Int. J. Mol. Sci.* 21 (11), 3943. doi:10.3390/ijms21113943

Sehovic, N., and Smith, K. P. (2010). Risk of venous thromboembolism with drospirenone in combined oral contraceptive products. *Ann. Pharmacother.* 44 (5), 898–903. doi:10.1345/aph.1M649

Serova, L. V., and Denisova, L. A. (1982). The effect of weightlessness on the reproductive function of mammals. *Physiologist* 25 (6), S9–S12.

Serova, L. V., Denisova, L. A., Apanasenko, Z. I., Kuznetsova, M. A., Meyzerov, Y. S., and Chelnaya, N. A. (1982). Reproductive function in male rats after flight abourd Cosmos 1129 biosatellite. *Snace Biol. Aviat. Med. (USSR)* 5, 62.

Serova, L. V., Denisova, L. A., Makeeva, V. F., Chelnaya, N. A., and Pustynnikova, A. M. (1984). The effect of microgravity on the prenatal development of mammals. *Physiologist* 27, S107–S110.

Shin, E. M., Huynh, V. T., Neja, S. A., Liu, C. Y., Raju, A., Tan, K., et al. (2021). GREB1: an evolutionarily conserved protein with a glycosyltransferase domain links ERα glycosylation and stability to cancer. *Sci. Adv.* 7 (12), eabe2470. doi:10.1126/sciadv.abe2470

Simon, V. (2005). Wanted: women in clinical trials. *Science* 308 (5728), 1517. doi:10.1126/science.1115616

Smith, J. T., Dungan, H. M., Stoll, E. A., Gottsch, M. L., Braun, R. E., Eacker, S. M., et al. (2005). Differential regulation of KiSS-1 mRNA expression by sex steroids in the brain of the male mouse. *Endocrinology* 146 (7), 2976–2984. doi:10.1210/en.2005-0323

Smith, S. M., Heer, M., Wang, Z., Huntoon, C. L., and Zwart, S. R. (2012). Long-duration space flight and bed rest effects on testosterone and other steroids. *J. Clin. Endocrinol. Metab.* 97 (1), 270–278. doi:10.1210/jc.2011-2233

Smith, S. M., Zwart, S. R., Heer, M., Hudson, E. K., Shackelford, L., and Morgan, J. L. (2014). Men and women in space: bone loss and kidney stone risk after long-duration spaceflight. *J. Bone Min. Res.* 29 (7), 1639–1645. doi:10.1002/jbmr.2185

Spicer, L. J., Aad, P. Y., Allen, D., Mazerbourg, S., and Hsueh, A. J. (2006). Growth differentiation factor-9 has divergent effects on proliferation and steroidogenesis of bovine granulosa cells. *J. Endocrinol.* 189 (2), 329–339. doi:10.1677/joe.1.06503

Spicer, L. J., Aad, P. Y., Allen, D. T., Mazerbourg, S., Payne, A. H., and Hsueh, A. J. (2008). Growth differentiation factor 9 (GDF9) stimulates proliferation and inhibits steroidogenesis by bovine theca cells: influence of follicle size on responses to GDF9. *Biol. Reprod.* 78 (2), 243–253. doi:10.1095/biolreprod.107.063446

Stavnichuk, M., Mikolajewicz, N., Corlett, T., Morris, M., and Komarova, S. V. (2020). A systematic review and meta-analysis of bone loss in space travelers. *NPJ Microgravity* 6, 13. doi:10.1038/s41526-020-0103-2

Steller, J. G., Blue, R. S., Burns, R., Bayuse, T. M., Antonsen, E. L., Jain, V., et al. (2020). Gynecologic risk mitigation considerations for long-duration spaceflight. *Aerosp. Med. Hum. Perform.* 91 (7), 543–564. doi:10.3357/AMHP.5538.2020

Stocco, C. (2012). Tissue physiology and pathology of aromatase. *Steroids* 77 (1-2), 27–35. doi:10.1016/j.steroids.2011.10.013

Strock, N., Rivas, E., and Marshall-Goebel, K. (2023). *Aerospace conference, the effects of space flight and microgravity exposure on female astronaut health and performance*. Big Sky, MT, United States: IEEE (Institute of Electrical and Electronics Engineers) Aerospace Conference. doi:10.1109/AERO55745.2023.10115765

Suh, B. Y., Liu, J. H., Rasmussen, D. D., Gibbs, D. M., Steinberg, J., and Yen, S. S. (1986). Role of oxytocin in the modulation of ACTH release in women. *Neuroendocrinology* 44 (3), 309–313. doi:10.1159/000124661

Talukdar, S., and Kundu, S. C. (2014). "Silk scaffolds for three-dimensional (3D) tumor modeling," in *Silk biomaterials for tissue engineering and regenerative medicine*. Editor S. G. Kundu (Sawston, Cambridge, United Kingdom: Woodhead Publishing), 472–502.

Tash, J. S., Gupta, V., Holets, L., and Roby, K. F. (2011) "STS-131: spaceflight has negative impacts on the morphology, follicle health, and steroid hormone receptors in ovaries and uterine horns in C57Bl/6J mice," in Proceedings of the 18th IAA humans in space symposium, Houston, TX. April 11–15.

Teng, C. T., Gladwell, W., Beard, C., Walmer, D., Teng, C. S., and Brenner, R. (2002). Lactoferrin gene expression is estrogen responsive in human and rhesus monkey endometrium. *Mol. Hum. Reprod.* 8 (1), 58–67. doi:10.1093/molehr/8.1.58

Tocci, D., Ducai, T., Stoute, C. A. B., Hopkins, G., Sabbir, M. G., Beheshti, A., et al. (2024). Monitoring inflammatory, immune system mediators, and mitochondrial changes related to brain metabolism during space flight. *Front. Immunol.* 15, 1422864. doi:10.3389/fimmu.2024.1422864

Tomilovskaya, E., Shigueva, T., Sayenko, D., Rukavishnikov, I., and Kozlovskaya, I. (2019). Dry immersion as a ground-based model of microgravity physiological effects. *Front. Physiol.* 10, 284. doi:10.3389/fphys.2019.00284

Tou, J., Ronca, A., Grindeland, R., and Wade, C. (2002). Models to study gravitational biology of Mammalian reproduction. *Biol. Reprod.* 67 (6), 1681–1687. doi:10.1095/biolreprod.102.007252

Tou, J. C., Grindeland, R. E., and Wade, C. E. (2004). Effects of diet and exposure to hindlimb suspension on estrous cycling in Sprague-Dawley rats. *Am. J. Physiol. Endocrinol. Metab.* 286 (3), E425–E433. doi:10.1152/ajpendo.00287.2003

Toufexis, D., Rivarola, M. A., Lara, H., and Viau, V. (2014). Stress and the reproductive axis. *J. Neuroendocrinol.* 26 (9), 573–586. doi:10.1111/jne.12179

Tremblay, M. S., Copeland, J. L., and Van Helder, W. (1985)2004). Effect of training status and exercise mode on endogenous steroid hormones in men. *J. Appl. Physiol.* 96 (2), 531–539. doi:10.1152/japplphysiol.00656.2003

Uno, A., Takeda, N., Horii, A., Morita, M., Yamamoto, Y., Yamatodani, A., et al. (1997). Histamine release from the hypothalamus induced by gravity change in rats and space motion sickness. *Physiol. Behav.* 61 (6), 883–887. doi:10.1016/s0031-9384(96)00613-0

Vitellius, G., Trabado, S., Bouligand, J., Delemer, B., and Lombès, M. (2018). Pathophysiology of glucocorticoid signaling. *Ann. Endocrinol. Paris.* 79 (3), 98–106. doi:10.1016/j.ando.2018.03.001

Watenpaugh, D. E. (2016). Analogs of microgravity: head-down tilt and water immersion. *J. Appl. Physiol.* 120 (8), 904–914. doi:10.1152/japplphysiol.00986.2015

Williams, D. R. (2015). A crewed mission to Mars. NASA Goddard Space. Flight Center. Available online at: https://nssdc.gsfc.nasa.gov/planetary/mars/marsprof.html.

Williams, N. I., Leidy, H. J., Hill, B. R., Lieberman, J. L., Legro, R. S., and De Souza, M. J. (2015). Magnitude of daily energy deficit predicts frequency but not severity of menstrual disturbances associated with exercise and caloric restriction. *Am. J. Physiol. Endocrinol. Metab.* 308 (1), E29–E39. doi:10.1152/ajpendo.00386.2013

Wolfe, J. W., and Rummel, J. D. (1992). Long-term effects of microgravity and possible countermeasures. *Adv. Space Res.* 12 (1), 281–284. doi:10.1016/0273-1177(92)90296-a

Wong, A. M., and DeSantis, M. (1997). Rat gestation during space flight: outcomes for dams and their offspring born after return to Earth. *Integr. Physiol. Behav. Sci.* 32 (4), 322–342. doi:10.1007/BF02688630

Wu, C., Guo, X., Wang, F., Li, X., Tian, X. C., Li, L., et al. (2011). Simulated microgravity compromises mouse oocyte maturation by disrupting meiotic spindle organization and inducing cytoplasmic blebbing. *PLoS One* 6 (7), e22214. doi:10.1371/journal.pone.0022214

Yin, L., and Lin, D. (2023). Neural control of female sexual behaviors. *Horm. Behav.* 151, 105339. doi:10.1016/j.yhbeh.2023.105339

Ying, S. Y., Gove, S., Fang, V. S., and Greep, R. O. (1973). Ovulation in postpartum rats. *Endocrinology* 92 (1), 108–116. doi:10.1210/endo-92-1-108

Yu, O., Christ, J. P., Schulze-Rath, R., Covey, J., Kelley, A., Grafton, J., et al. (2023). Incidence, prevalence, and trends in polycystic ovary syndrome diagnosis: a United States population-based study from 2006 to 2019. *Am. J. Obstetrics Gynecol.* 229 (1), 39.e1–39.e12. doi:10.1016/j.ajog.2023.04.010

Zangheri, M., Mirasoli, M., Guardigli, M., Di Nardo, F., Anfossi, L., Baggiani, C., et al. (2019). Chemiluminescence-based biosensor for monitoring astronauts' health status during space missions: results from the International Space Station. *Biosens. Bioelectron.* 129, 260–268. doi:10.1016/j.bios.2018.09.059

Zavala, E., Voliotis, M., Zerenner, T., Tabak, J., Walker, J. J., Li, X. F., et al. (2020). Dynamic hormone control of stress and fertility. *Front. Physiol.* 11, 598845. doi:10.3389/fphys.2020.598845

Zhang, S., Zheng, D., Wu, Y., Lin, W., Chen, Z., Meng, L., et al. (2016). Simulated microgravity using a rotary culture system compromises the *in vitro* development of mouse preantral follicles. *PLoS One* 11 (3), e0151062. doi:10.1371/journal.pone.0151062

Zwart, S. R., Auñón-Chancellor, S. M., Heer, M., Melin, M. M., and Smith, S. M. (1985)2022). Albumin, oral contraceptives, and venous thromboembolism risk in astronauts. *J. Appl. Physiol.* 132 (5), 1232–1239. doi:10.1152/japplphysiol.00024.2022

Frontiers in Physiology

Understanding how an organism's components work together to maintain a healthy state

The second most-cited physiology journal, promoting a multidisciplinary approach to the physiology of living systems - from the subcellular and molecular domains to the intact organism and its interaction with the environment.

Discover the latest Research Topics

See more →

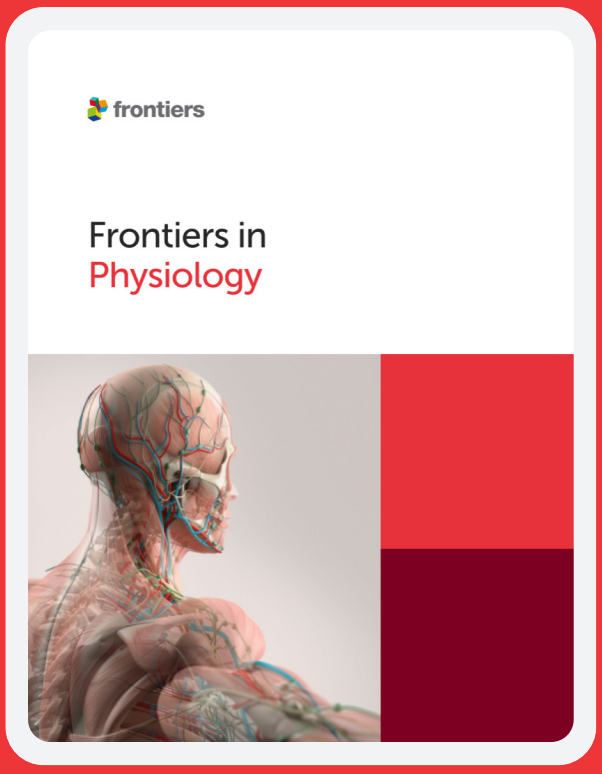

Frontiers

Avenue du Tribunal-Fédéral 34
1005 Lausanne, Switzerland
frontiersin.org

Contact us

+41 (0)21 510 17 00
frontiersin.org/about/contact